Indian Journal of Natural Sciences www.tnsroindia.org.in ©IJONS

Vol.9 /Issue 51 / December / 2018 *International Bimonthly* *ISSN: 0976 – 0997*

RESEARCH ARTICLE

Heavy Minerals Distribution of Peramagroon Alluvial Fans Sulaimaniyah Governorate (Northern Iraq) as Indicator to Tectonic Activity

Sarah K. Mohammed*[1], Manal Sh. Al-Kubaisi[2], Azhar Kh. Bety[3]

[1,2]Department of Geology, Faculty of Science,University of Baghdad,Iraq
[3]Department of Geology, Faculty of Science,University of Sulaimani,Iraq

Received: 04 Aug 2018 Revised: 07 Sep 2018 Accepted: 11 Oct 2018

***Address for Correspondence**
Sarah Kadhim Mohammed
Department of Geology,
Faculty of Science, University of Baghdad,
Baghdad, Iraq.
Email: sarahiraq1982@gmail.com

ABSTRACT

The study area is located within the north- east part of Iraq, covering 958 Km of its area. The aim of this research is to define the heavy mineral composition of alluvial fans of Peramagroon anticline, and try to determine the origin or the source of these alluvial fans. 10 samples were collected from these alluvial fans, the samples were separated into light and heavy fractions by heavy liquids, the rock fragments were composed mainly of carbonate, chert, igneous, and metamorphic rock. The heavy minerals are mostly opaque's, chlorite, pyroxenes, amphiboles, epidotes, garnet, biotitic, kyanite, staurolite, and muscovit. The north east part of Iraq is known to be tectonically an active area due to its position in the north east marginal part of the Arabian Plate, which is in collision with the Eurasian (Iranian) Plate. This area had suffered from Nontectonic movement, which is indicated by the existence of large alluvial fans such the Qara Chattan and Sutuka. The heavy minerals analysis proved that the studied area is characterized by high tectonic activity.

Keywords: Heavy Minerals, Alluvial Fan, Tectonic activity, Peramagroon.

INTRODUCTION

Analysis of the bed thicknesses and clastic sizes within beds can thus be used as a mean of identifying periods of tectonic uplift in the high ground adjacent to the basin. A change in climate can also result in changes in the processes of deposition on a fan[1]. The heavy minerals of detrital sedimentary rocks are a diverse and non genetic mineral

group. Heavy minerals are parent rock remains destruction by weathering, abrasion and have a specific gravity greater than 2.85. The minerals are not necessarily related to each other in any way, it is the operational procedure in their classification that defines them as a group [2].Heavy mineral analysis can play an important part in unraveling the intra-basinal and extra-basinal processes that effect the formation of clastic rocks [3].Faulting and folding resulted from several phases of deformations during the Alpine orogeny. The strike of the strata and trend of the folds are generally in NW_SE direction in accordance with the main trend of Zagros folds. Generally, the area of study lies between High Zagros Reverse Fault and Zagros Mountain Front Fault, which make most of the study area form part of the Zagros High Folded Zone [4].This study area is located within Kurdistan Region, within Sulaimaniyah Governorate, northwest of Sulaimaniyah city is located between longitudes (45° 9′ 00″ and 45° 18′ 00″) and Latitudes (35° 43′ 00″ and 35° 47′ 00″), It is comprises the of Peramagroon anticline.The Peramagroon anticline is located within the north east part of Iraq, it's part of the Outer of the Arabian Plate [5]. There are several major and minor anticlines and thrust faults exist within the High Folded Zone, the Peramagroon anticline located within these zone.These major anticlines are considered as a complex structures due to the deformation, which had caused by the collision of the Arabian Plate with the Iranian Plate that was intermittently uplifted in Cretaceous and Paleocene and strongly deformed in the Late Neocene causing regional compressive horizontal forces in NE – SW direction, leading to folds trending in NW – SE axial direction Figure (1).

MATERIALS AND METHODS

Many field trips were made for general geologic and geomorphic studies of this area. Field work includes samples collection Table - 1 including photography, measuring, check point and describing quaternary cover. Data obtained by the field observation have been largely applied to support this research. After the field working was done, laboratory work included the heavy mineral analysis which begins with disaggregation of grains and sieving to obtain a particular size range, typically in the fine to medium sand size range. Heavy minerals are separated using a heavy liquid with a density of 2.85 g/cm3. In traditional analysis, the separated heavy mineral grains are mounted on a glass slide and then identified and counted using transmitted light microscopy [6].

RESULTS AND DISCUSION

Peramagroon Structure

The Peramagroon anticline is located about 10 km north-west of Sulaimaniyah city, with a width ranging from [2 to 4] km and the length is about [30] km. It is a huge asymmetrical doubly plunging anticline within High Folded Zone of the Zagros Fold Thrust Belt. The trend of the anticline is NW- SE in line with the general Zagros fold trend and this anticlinal fold is bending [7].

The southwestern limb is steeper than northeastern limb, and the southwestern limb in some places as in Zewi Gorge, show vertical to overturned strata. The highest peak is in the Qamchuqa Formation above Zewi village, The fold is bifurcated at the southeastern plunge to form a surface anastomosing pattern represented by small anticline named Yakhiyan anticline plunged parallel to the main plunge of Peramagroon anticline near Qamar-Tali village, [8]. Qamchuqa Formation forms the carapace of the fold and it is overlain by the Kometan, Shiranish and Tanjero formations in both limbs respectively. In the Zewi area the core of the anticline is eroded and other Cretaceous and Jurassic formations are exposed. Qamchuqa Formation overlies with Sarmord Formation (Cretaceous age) which covers Jurassic formations (Chia Gara and Sargelu) respectively Figure (2).

Alluvial fans

Alluvial fans are cone deposits of granular debris that extend from the base of a mountain front to low land. Each fan radiates from a single source channel, has a fan shape in a plain view. The longitudinal profile is slightly concave and transverse profile is arched. Alluvial fans have slopes that are usually less than 10° and best developed in semiarid terrains, whereas, elongate mountain are tectonically active and lack protective vegetation cover, and are subjected to erosion by heavy rain precipitation [9]. Alluvial fans are supposed to act as useful landforms to determine the tectonic activity level [10].

Alluvial fans exist on the foot of anticline. According to their dimensions, two types are developed: Large alluvial fans and small alluvial fans, the latter coincide together to form Bajada .These fans are developed in this study area due to the existence of mountains, which are drained by many valleys [11].Alluvial fans occur in a large size in front of Peramagroon anticline, it exists in different parts and topography, and usually dissected by parallel, sub parallel and dendritic valleys which come down from the mountain. Qara Chatan Fan is located in the southwestern limb of Peramagroon anticline, while Sutuka Alluvial Fan is located within the southwestern limb near the southeastern plunge of Peramagroon anticline. The thickness of sediments on Qara Chattan and Sutuka Fans is between 10 to 20 m, and those sediments include unsorted fragments which are mostly derived from Kometan, Qamchuca and Balambo formations. These fans are classified as multi stage Alluvial Fans.In the field of this study, all alluvial fans occur at mountain fronts. These conditions are controlled by long term landform evolution, including the tectonic setting and erosional history Figure (3).

Mineralogy

The mineralogy of clastic sediment found in sand or sandstone provides important evidence about its origin, including transportation history and source rock lithologies. In addition to the major constituents of sand or sandstones (feldspars, quartz and lithic fragments), sandstones contains minor abundances of other mineral grains, including heavy minerals (densities greater than 2.85 g/cm3). Heavy minerals reflect the source area because different rock types contain different heavy mineral assemblages [12].10 Samples of alluvial fans from two localities were selected for mineralogical study by using the polarizing microscope. Sand samples were taken from the fine sand (2-3phi) and very fine sand (3 - 4phi) fractions to determine the heavy minerals.Each sample were separated into the heavy and light fraction by using Bromoform (Specific Gravity 2.89), [13].. The separated fractions were mounted on glass slide using Canada balsam.

Heavy Minerals analysis

Heavy minerals are defined as minerals having a higher density than quartz, the most common rock forming mineral with a density of (2.65 g/cm3). In practice, only the minerals that are heavier than the dense media are most commonly used in the lab-Bromoform (2.89 g/cm3) or tetrabromomethane (2.94 g/cm3) – i.e. the sink in these media, are included in the group of heavy minerals. In contrast, minerals with a lower density than heavy minerals, e.g. Quartz, Feldspars, calcite, dolomite, aragonite, and evaporates, are called light minerals [14]. Heavy minerals can be very useful, particularly when the interpretation of the major constituent grains is ambiguous [15].Heavy minerals analysis is one of the most sensitive and widely used techniques in the determination of sand and sandstone provenance. The heavy minerals assemblage is not only controlled by the mineralogical composition of the source region but also modified by several other processes that operate during the sedimentation cycle [16].The heavy minerals known in the studied samples were estimated by using point counter mechanical stage following the method of [17], the results are presented in Table - 2 and 3.The characteristics of each of the recognized heavy minerals in the studied samples are summarized below:

1- Opaque's: The opaque minerals have the highest percentages of the heavy minerals in all studied samples, the percentages was observed in Qara Chattan fan ranging between (66.6% – 73.5%), and in Sutuka fan ranging between (64.6% – 70.4%). Opaque minerals are black, dark brown, and variable in shape Figure (4-A).
2- Chlorite: Chlorites have the second highest percentages of heavy minerals, Chlorites observed in all studied samples, the percentages of chlorites observed Qara Chattan fan ranging between (6.7% – 8.5%), while in Sutuka fan ranging between (7.9% – 9%). The types of chlorite that are observed in the studied samples usually green color with no pleochroism Figure (4-B).
3- Garnet: The percentages of garnets observed Qara Chattan fan ranging between (0% - 0.9%), while in Sutuka fan ranging between (0.3% - 0.8%). Garnet grains mainly show high relief. Shapes are equant, to sub equant, occasionally sub angular to sub rounded Figure (4-C).
4- Pyroxene: The percentages of pyroxene observed Qara Chattan fan ranging between (4.6% - 5.5%), while in Sutuka fan ranging between (5.7% - 6.8%). Pyroxenes usually show green to light green color with prismatic habit, two set of cleavage, and subdural Figure (4-D).
5- Amphibole: The percentages of amphiboles observed Qara Chattan fan ranging between (3.1% - 5.9%), while in Sutuka fan ranging between (4.8% - 7.9%). Amphiboles in the studied samples are observed as prismatic and cleaved grains, mostly fresh with some showing some degree of alteration, euhedral to subdural, some grains have cockscomb texture Figure (4-E).
6- Tourmaline: The percentages of Tourmaline observed Qara Chattan fan ranging between (0% - 0.6%), while in Sutuka fan ranging between (0% - 0.5%). Tourmaline grains have brown to honey color with strong pleochroism, sub rounded to well-rounded form, these grains are mostly fresh Figure (4-F).
7- Epidotes: The percentages of Epidotes observed Qara Chattan fan ranging between (3.5% - 5.7%), while in Sutuka fan ranging between (5.4% - 6.4%). Epidote under the polarizing microscope show a high relief, green to pale green color, and rounded, sub angular, and angular shape Figure (5-A).
8- Rutile: The percentages of rutile observed Qara Chattan fan ranging between (0% -0.8%), while in Sutuka fan ranging between (0% - 0.7%). Deep yellow color with black shades, with a very high relief Figure (5-B).
9- Kyanite: The percentages of kyanite observed Qara Chattan fan ranging between (0% - 1.3%), while in Sutuka fan ranging between (0.3% - 1%). Kyanite grains are colorless, high relief, prismatic form, subhedral with elongated habit Figure (5-C).
10- Staurolite: The percentages of staurolite observed Qara Chattan fan, ranging between (0.2% – 0.9%), while in Sutuka fan ranging between (0.6 – 1.3%). Staurolite grains show high relief, yellowish to golden color with pleochroism, sub angular to sub rounded in form Figure (5-D).
11- Biotite: The percentages of Biotite observed Qara Chattan fan ranging between (0.7% - 1.9%), while in Sutuka fan ranging between (0.4% - 1.9%). Biotite under the polarizing microscope is pleochroic brown corroded, mostly irregular to angular in shape, platy grains are common Biotite is usually fresh with some altered grains Figure (5-E).
12- Muscovite: The percentages of muscovite observed Qara Chattan fan ranging between (1.9% - 3.8%), while in Sutuka fan ranging between (1.6% - 3.7%). Muscovite is colorless, basal flakes, with angular to irregular outline. Most of the observed muscovite grains are clear Figure (5-F).

Heavy minerals have been used to determine transport and provenance signature in several depositional environments such as dunes, beach, alluvial deposits, and rivers [17]. Heavy minerals are usually used for source rocks determination [18]. Identifying the provenance of sediments carried by modern rivers can provide information on earth surface processes and help us to interpret geological history more clearly. The types and distribution patterns of surface sediments deposited in river systems are determined mainly by the fluvial flux and weathering of the proximal source rocks [19]. The heavy mineral assemblages determined for Qara Chattan and Sutuka Fans indicates a variety of probable source rock types including igneous, metamorphic, and sedimentary, the possible source of each of the described minerals are given in Table -4. Taking into account the relative abundance and distribution of each minerals, may suggest that the studied heavy mineral assemblages, are primarily derived from sedimentary rocks (single or multi cycles), low and high rank metamorphic rocks, acidic and basic igneous rocks.The

linkage between plate-tectonic setting and sediment composition has been long recognized. Models describing this association have been based largely on chemical compositions and major elastic components of modern sands[2]. (Nechoev & Isphording, 1993) [28] suggested a plate tectonic interpretation of heavy mineral data by comparing the assemblage configuration with the possible sources of clastic sediments resulting from different stages of the plate tectonic cycle. However, recent studies suggest that study of heavy-mineral assemblages might supply information on plate-tectonic settings that may be more understandable and more easily interpreted than results from modal or chemical analysis.Sedimentary assemblages of heavy minerals may serve as relatively reliable and definitive indicators of the major plate-tectonic settings associated with continental margins. Identification of these settings, a quantitative interrelationship between the following mineral suites can be used:

(I) MF (common constituents of marine magmatic rocks) = total content of olivine, all pyroxenes, and brown-green hornblende;
(2) MT (common constituents of basic metamorphic rocks) = total content of pale-colored and blue-green amphiboles, epidote (group), and garnet.
(3) GM (accessory minerals of granites and sialic metamorphic rocks, which are, at the same time, the most resistant mineral phases) = total content of zircon, tourmaline, staurolite, kyanite, andalusite, monazite, and sillimanite.
Plotting of the studied fans samples on the ternary diagram Figure (6), indicate that all samples fill within the field of active continental margins which are characterized by a relatively high percentage of minerals derived from Basic and intermediate igneous rocks. These source rocks represent Zagros Mountains and their derived formations.

CONCLUSION

Heavy minerals composition shows us that these are two major sources in the areas of study. The Qarah Chattan and Sutuka Fans have their source from Zagros Mountains and Peramagroon Anticline indicated by the presence of the metamorphic rocks and carbonate rock fragments. An Opaque heavy mineral represents the major component in all studied alluvial fans samples followed by chlorites, pyroxene, amphibole and Epidote. The abundance of these heavy minerals indicates different source rocks such as igneous, metamorphic, and sedimentary rocks. The sample studied fall with the field of active continental margin that shows by using ternary diagram, which is distinguished by a relatively high percentage of heavy minerals derived from metamorphic rocks and igneous rocks.

REFERENCES

1. Harvey, A.M., "Differential effects of base-level, tectonic setting and climatic change on Quaternary alluvial fans in the northern Great Basin, Nevada", USA Geological Society Special Publication. 2005., No.251 : PP:117–131.
2. Pettijohn, F.J., Porter, P.E., and Siever, R., "Sand and Sandstone", 2nd edition: New York, Springer-Verlag, 553 p.Prentice Hall, 1987., 774 P.
3. Dill, H. G., "Heavy mineral response to the progradation of an alluvial fan: implications concerning unroofing of source area, chemical weathering and palaeo-relief (Upper Cretaceous Parkstein fancomplex, SE Germany)" ,Sedimentary Geology.1995., 95, PP. 39-56.
4. Al-Qayim, B., Ibrahim, A. O., and Koyi, H., "Tectonic Stratigraphic overview of the Zagros Suture Zone, Kurdistan Region, Northeast Iraq". GeoArabia. 2012., V17, No.4, P 109-156.
5. Fouad,S,F., Tectonic map of Iraq,scale1:1000000,3rd,GEOSURV,Iraq, 2010.
6. Carver, R. E. (edit.), Procedures in sedimentary petrology, Wiley inter science,New York. 1971., 653 P.
7. Karim, K.H. and Khanaqa, P., "Geomorphology of the Piramagroon– Kanikhan Valley, Sulaimani Governorate, Kurdistan Region, North Iraq" International Journal of Geography and Geology. 2015.,4(12):PP: 183-195
8. AL-Hakari, S. H., Geometric Analysis and Structural Evolution of NW Sulaimani Area, Kurdistan Region, Iraq. Unpub. PhD. thesis, University of Sulaimani, Iraq. 2011.

9. Sissakian, V.K. and Abdul Jab'bar, M.F., "Classifications of alluvial fans in Iraq". Iraqi Bulletin of Geology and Mining. 2014., 10, 3,PP: 43 – 67.
10. Bahrami, S., "Tectonic controls on the morphometry of alluvial fans around Danehkhoshk anticline, Zagros, Iran, Geomorphology".2013., pp:217–230.
11. Sissakian, V.K. and Fouad, S.F., "Geological Map of Sulaimaniyah Quadrangle, scale 1: 250 000, 2nd edit". Iraq Geological Survey (GEOSURV) Publications, Baghdad, Iraq. 2014.
12. Hubert, J. F., 1971. Procedures in Sedimentary Petrology, Wiley-Inter Science: New York, 478P.
13. Tucker, M. E., "Techniques in Sedimentology". Black Well. Oxford.1977., 394p.
14. Elsner. H., "Heavy minerals of economic important," Germany. 2010., vol. 218.
15. Webster. J. R., Kight. R. P., Winburn.John R. S., and Christopher. A. C., 2003. "Heavy Minerals Analysis of Sandstones by Rietveid Analysis"., International Centre for Diffraction Data., Advances in X-ray Analysis. 2003, V. 46, P.198-203.
16. M. G. Shehata, A. A. E.-H. Abdou, T. M., and A. S. Mousa,"Heavy miner- als: A case study on the gebel ghorabi member; bahariya oasis," Western Desert, Egypt.International Journal of Academic Research. 2010., vol. 2, no. 4, pp. 159–172,.
17. Kasper-Zubillaga, J. J., Dickinson, W. W., Carranza Edwards, A., and Hornelas-Orozco, Y., "Petrography of Quartz Grains in Beach and Dune Sands of Northland, North Island, New Zealand". NZ J. Geol. Geophys. 2008., V.48, P. 649-660.
18. Boggs Jr., S., 2006. "Principles of Sedimentology and Stratigraphy", 4th ed. Prentice Hall, New Jersey.2006., 662p.
19. Meng.Q, Zhang.W, Zhang.J ,Zhang.Z,Wu.T, "Heavy mineral analysis to identify sediment provenance in the Dan River drainage, China ,Geosciences Journal August. 2016., Volume 20, Issue 4, pp 449–462.
20. Hibbard, M. J., "Mineralogy. A geologist point of view". McCraw-Hill. Higher education, New York. 2002., 562 P.
21. Nesse, W. D., Introduction to Mineralogy, Oxford University press, New York. 2000., 442p.
22. Boggs, S. J., "Principle of Sedimentology and Stratigraphy". New Jersy. 1995., pp:676.
23. Tucker, M.E., "Sedimentary petrology an introduction". Blackwell scientific. 1985.
24. Pettijohn, F. J., "Sedimentary Rocks". Harper and Raw Publishers, Inc., New York. 1975.,628p.
25. Folk, R. L., Petrology of sedimentary rocks". Hamphill, Texas. 1974., 182 P.
26. Kerr, P.F., "Optical Mineralogy". Third edition. McGraw-Hill Book. 1959.
27. Krumbein, W.C. and Sloss, L.L., "Stratigraphy and sedimentation", 2nd Ed, W. H. Freeman., San Francisco.1963., 660p.
28. Nechoev, V.P. and Isphording, W.C., "Heavy mineral assemblages of continental margins as indicators of plate-tectonic environments" Jour. Sed. Petrol.1993., V, vol. 63, no. 6, pp. 1110–1117.

Table 1. Coordination of samples at the study area.

Areas	Section No	Sample No	Location	
			Longitude	Latitude
Qara Chatan fan	Section (A)	1- 2 -3	E 45° 13` 39.6″	N 3 5° 43` 49.2″
	Section (B)	4- 5	E 45° 12` 49″	N 35° 43` 50″
	Section (C)	6-7- 8	E 45° 11` 57.6″	N 35° 43` 7.1″
Sutuka fan	Section (D)	10-11-12-13-14-15	E 45° 16` 46″	N 35° 35` 15.3″
	Section (F)	16-17-18	E 45° 18` 29.3″	N 35° 34` 56.6″

Table 2. Percentage of heavy mineral distribution of Qara Chattan fan.

Heavy Minerals	Heavy Minerals				
	1	**4**	**5**	**6**	**7**
Opaques	73.5	66.6	68.2	68.7	68.3
Chlorite Group	6.7	7.6	6.8	7.6	8.5
Garnet Group	0.9	0.4	-	-	0.7
Pyroxene Group	4.8	5.2	5.5	4.6	4.6
Amphibole Group	3.8	5.6	3.1	5.9	4.8
Tourmaline	-	0.2	0.5	-	0.6
Epidote Group	3.5	4.3	5.7	4.8	5.2
Rutile	-	0.6	-	0.8	-
Kyanite	0.5	0.9	2.0	-	1.3
Staurolite	0.9	0.8	0.2	0.9	0.4
Biotite	0.7	1.2	0.7	1.9	1.3
Muscovite	2.5	3.4	3.8	2.5	1.9
Others	2.2	3.2	3.5	2.3	2.4

Table 3. Percentage of heavy mineral distribution of Sutuka Fan.

Heavy Minerals	Heavy Minerals				
	10	**11**	**12**	**13**	**15**
Opaques	70.4	64.6	65.5	68.4	65.6
Chlorite Group	8.4	8.6	7.9	9.0	8.6
Garnet Group	0.6	0.5	0.8	0.3	0.8
Pyroxene Group	5.8	5.7	6.2	6.8	5.9
Amphibole Group	5.2	6.8	4.8	7.9	5.0
Tourmaline	-	0.3	0.5	0.2	0.5
Epidote Group	5.4	6.4	6.0	5.9	5.5
Rutile	-	0.4	0.2	0.7	-
Kyanite	0.3	0.9	0.7	0.3	1.0
Staurolite	0.6	0.8	1.0	1.3	0.8
Biotite	0.4	1.6	1.5	1.7	1.9
Muscovite	1.6	1.7	3.1	3.7	2.7
Others	1.3	1.7	1.8	1.9	1.7

Table 3. Probable source rocks of the heavy minerals of Qara Chattan and Sutuka fans. (X is the probable source rocks), and references are:

1- Hibbard (2002) [20]
2- Neese (2000) [21]
3- Boggs (1995) [22]
4- Tucker (1985) [23]
5- Pettijohn (1975)[24]
6- Folk (1974)[25]
7- Krumbein and Sloss (1963) [26].
8- Kerr (1959) [27].

Table 4. Probable source rocks of the heavy minerals of alluvial Fans.

Source rocks / Heavy minerals	Sedimentary rocks	Acidic igneous rocks	Basic igneous rocks	Metamorphic rocks	Pegmatite rocks	References
Opaque's	X	X	X	X		1, 3, 5, 6, 7, 8
Chlorite Group				X		1, 2, 3, 5, 6, 7
Garnet Group				X	X	1, 2, 3, 4, 5, 6, 7, 8,
Pyroxene Group		X				1, 2, 3, 4, 5, 6, 7, 8
Amphibole			X	X		1, 2, 3, 4, 5, 6, 7
Tourmaline				X		1, 2, 3, 4, 5, 6, 7
Epidote Group		X		X		1, 2, 3, 4, 5, 6, 7
Rutile		X				1, 2, 3, 4, 5, 6, 7
Kyanite		X		X		1, 2, 3, 6, 7, 8
Staurolite		X		X	X	1, 2, 3, 5, 6, 7
Biotite		X		X		1, 2, 3, 5, 6, 7, 8
Muscovite				X		1, 2, 3, 5, 6, 7

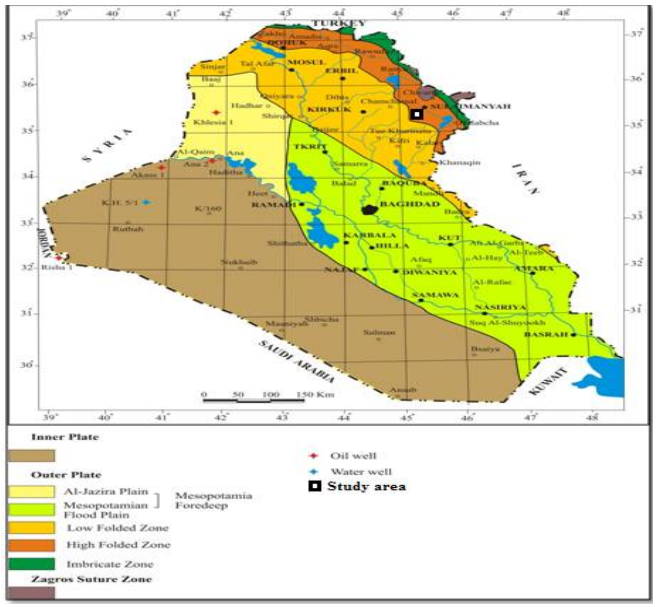

Figure 1. Location of study area within tectonic map (after Fouad, 2010).

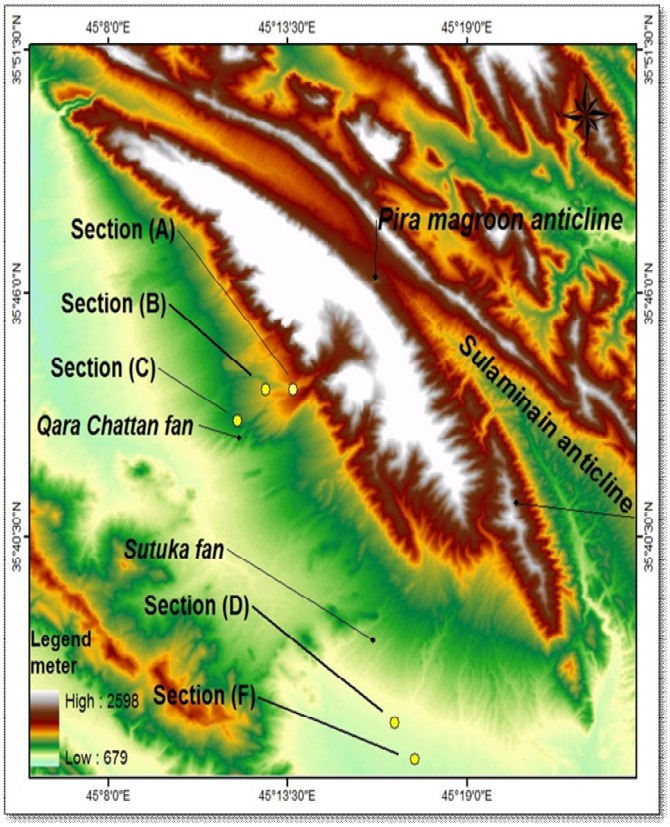

Figure 2. Sampling areas are specific to the DEM of the study Area.

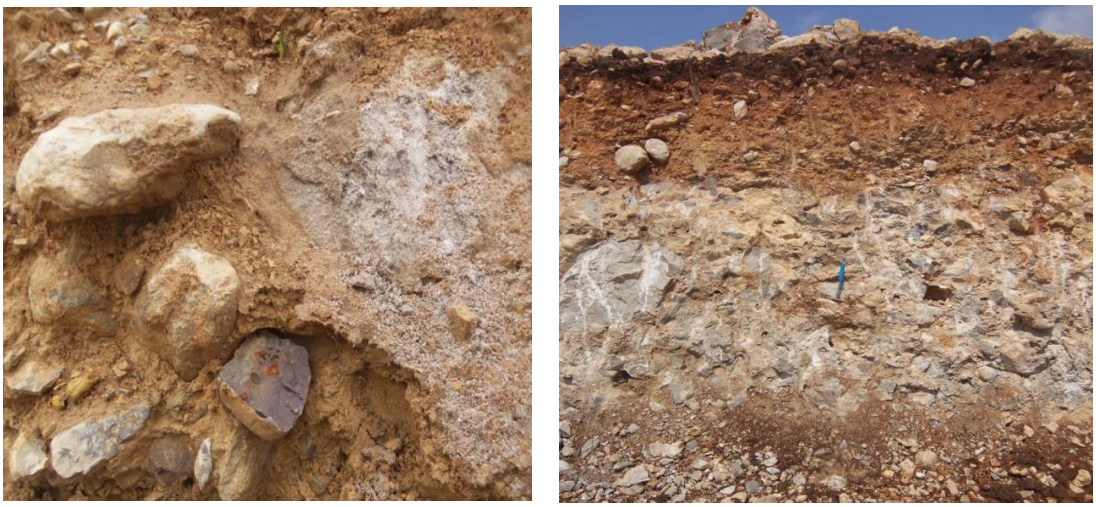

Figure 3. Characteristics of the sediment of alluvial Fans of study area.

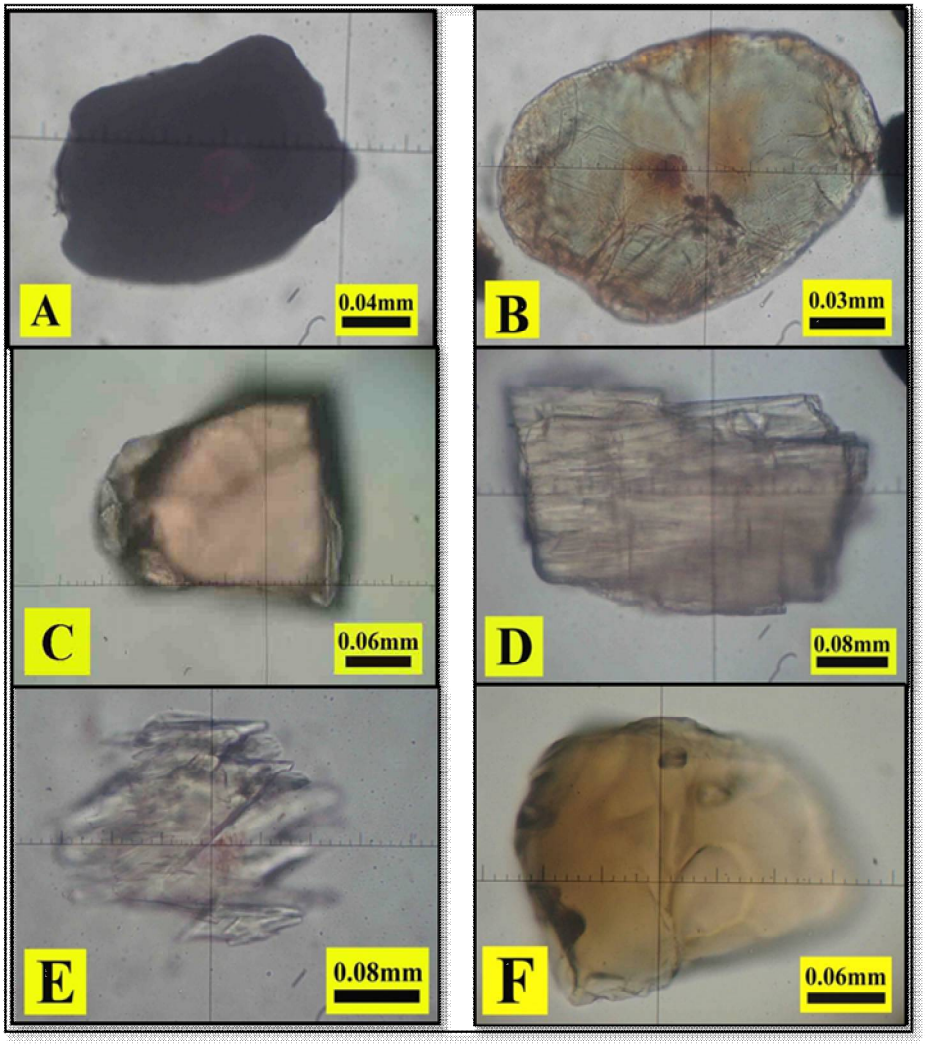

Figure 4-A. Opaque's mineral grain (iron oxides), sample number 4, PPL.

Figure 4-B. Green chlorite, sample number 5, PPL.

Figure 4-C. Light rose, high relief garnet, sample number 10, PPL.

Figure 4-D. High relief, prismatic pyroxene, sample number 12, PPL.

Figure 4-E. Cockscomb amphibole, sample number 6, PPL.

Figure 4-F. Honey color Tourmaline, sample number 6, PPL.

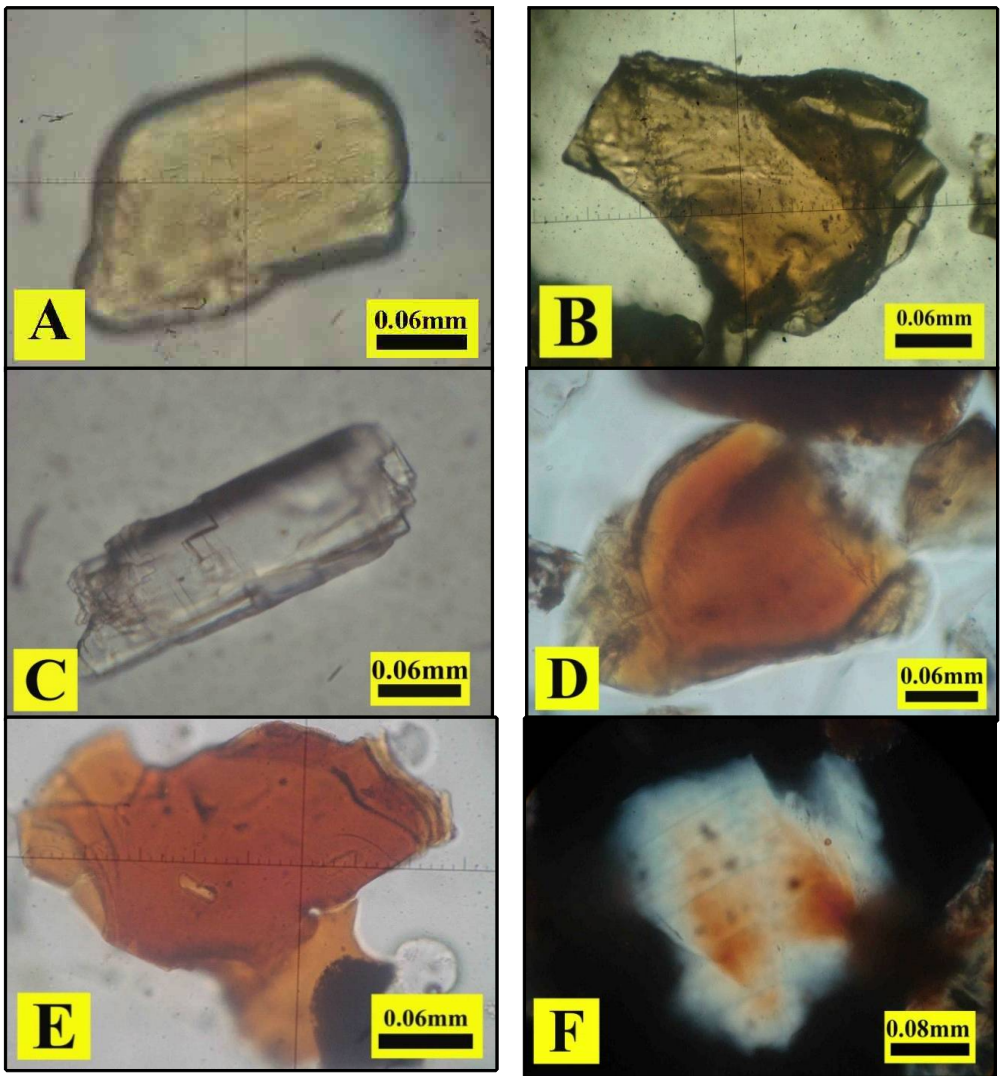

Figure 5-A. brown color, high relief Epidote, sample number 13, PPL.

Figure 5- B. Deep yellow rutile, sample number 15, PPL.

Figure 5- C. Colorless, high relief, prismatic kyanite, sample number 1, PPL.

Figure 5- D. yellowish color, high relief staurolite, sample number 7, PPL.

Figure 5- E. brown color, flaky form Biotite, sample number 5, PPL.

Figure 5- F. flaky form, colorless muscovite, sample number 11, PPL.

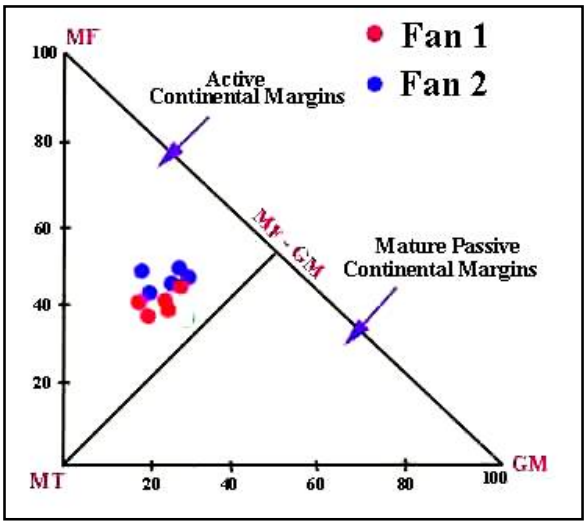

Figure 6. Interrelationship of the MF-MT-GM suits of Fans heavy minerals [28], Where by MF: Pyroxene, Amphibole, Olivine. GM: Zircon, Tourmaline, Staurolite, Andalusite, Kyanite, Monazite, Sillimanite. MT: Epidote, Garnet (Qara Chattan Fan (1), Sutuka Fan (2).

Indian Journal of Natural Sciences www.tnsroindia.org.in ©IJONS

Vol.9 /Issue 51 / December / 2018 *International Bimonthly* *ISSN: 0976 – 0997*

RESEARCH ARTICLE

Sero-Prevalence of Chicken Anemia Virus in Local Fowls and Japanese Quails

Karim Sadun Al-Ajeeli*, Amer Khazaal Al-Azawi and Haneen Ghazwan Al-Rubayee

Department of Microbiology, College of Veterinary Medicine, University of Diyala,Iraq

Received: 14 Aug 2018 Revised: 18 Sep 2018 Accepted: 22 Oct 2018

***Address for Correspondence**
Karim Sadun Al-Ajeeli
Department of Microbiology,
College of Veterinary Medicine,
University of Diyala,Iraq
Email: alajeelikarim@gmail.com

ABSTRACT

Serum samples were collected from local fowls (indigenous) and Japanese quails from different locations of Diyala province for the period of October, 21st 2017 to June 5th 2018. All the birds (local fowls and Japanese quails) were apparently healthy.These samples were 100 from local fowls of four villages, and 100 samples from four quail commercial farms. The samples were collected according to the age and subjected to ELISA test using IDEXX , ELISA Germany commercial kit. The results showed for the first time in Iraq that 87 serum samples of local fowls out of 100 were positive for chicken anemia virus (CAV) antibodies, and 29 serum samples out of 100 samples from quails were positive to CAV antibodies. The ages of local fowls were 12, 24,27, and 30 weeks and the age of birds do not significantly affected the sero-positivity of the result (P=0.211). In contrast the ages of quails were 2, 3, 4 and 5 weeks. The age of birds was significantly correlated to the results (P<0.004), when 13 samples out of 29 positive samples were from young quails of 2 weeks of age. 42.5% of positive samples collected from local fowls appeared with low S/N ratio (0.001-0.199) and high antibody titer, whereas, 20.5% of positive samples from quails showed the same above mentioned S/N ration. It seems that local fowls are highly susceptible to CAV in comparison to quails and might be a source for the infection of other commercial farms.

Keywords:- Local fowls, Japanese Quails, Chicken anemia virus

INTRODUCTION

Chicken anemia virus disease (CAVD) or chicken infectious anemia virus disease (CIAVD), is one of the important viral disease that affect the immune system of susceptible birds of poultry industry worldwide (1,2,3). The disease was circulated in USA since 1959 (4), but it was firstly isolated from infected chicken in Japan 1970 (5).

Chicken anemia virus (CAV) as a contagious and infectious disease was reported to infect young chicken of 1 to 4 weeks of age, causing severe anemia and lymphoid atrophy (6,7).The resulted immunosuppression due to lymphoid atrophy caused by the virus made the infected birds susceptible to secondary bacterial or viral infections (8,9,2,10).Clinically, infected birds showed depression, pale mucous membranes and lethargic. Hemorrhages might be observed under the skin of different parts of the body, included the wings (Blue wing disease).Mortality rates generally were variable and increased with presence of secondary infections due to immune suppression (11).The economic losses in poultry industry due to CAV might be attributed to poor weight gain of infected birds in comparison to uninfected birds, immunosuppression and susceptibility to secondary infection, and losses from mortality due to active infection (12,13).

The causative virus was found to be transmitted horizontally by fecal-oral route (14) or vertically from infected male and female parents (15,16) regardless their immune status or antibody titer (17,18).Chicken anemia virus is a single stranded circular negative sense or ambisense DNA virus. It is the smallest among DNA viruses and classified within the genus *Gyrovirus*. This genus and the genus *Circovirus* were classified with the family *Circoviridae*. The virus DNA was encoded for three proteins VP1, VP2 and VP3 (19).Many studies or authors suggested that chicken was the only bird species to be infected with CAV, whereas, pigeons, pheasant and duck were negative (20,21,22). In contrast many other reports mentioned the CAV infection in other birds like fancy chicken (23), Japanese quail (24,25), rooks and jackdaws(26).In Iraq no data were available on screening of poultry for the presence of CAV infection in broiler, layers and other birds. Furthermore, virus gens were not detected and/or the virus was not isolated. Accordingly, the present study was designed and aimed to screen, local fowls and Japanese quails of Diyala province for CAV antibodies.

MATERIALS AND METHODS

This survey study was conducted in Diyala province. The study was extended over the period from October twenty first 2017 to June 5th, 2018. The main objective is to point out the presence of chicken anemia virus (CAV) antibodies for the first time in local fowls and Japanesequails.

Serum samples

A total of 200 blood samples were collected from 4 commercial quail farms, 4 villages for local fowls (Table 1) in Diayla provincebyveno-puncture of the wing vein using sterile syringes andvacuum blood collection tubes/gel/clot activator (UNIMEDIC, Iraq). Sera were separated and placed in Eppendorf sterile tube, labelled and centrifuged at 1500 rpm for 5 minutes (Cold Eppendorf centrifuge. THERMO FISHER, USA).Supernatant serum was collected from each sample and transferred to another sterile Eppendorf tube labeled and stored at -20°C until used.

Processing of Samples for ELISA Test

The sera were tested using a commercial ELISA kit (IDEXX Lab,Germany) at a 1:10 dilution and the results were expressed as S/N ratios (sample to negative ratio) according to manufacturer's instructions. Processed ELISA sample plate was washed using ELISA washer automatic system ELX 800™,Optical density value was red at 650 nm wave length on an ELX 800™ microplate reader (BIO-TEK Instruments, USA).

Interpretation of the CAV ELISA Results

The negative control index (NCX) must be calculated for both duplicated wells and the same could be applied for the positive control index (PCX) at 650 nm absorption and according to the following:

$$NCX^{-} = \frac{NC1\ A(650) + NC2\ A(650)}{2} \qquad PCX^{-} = \frac{PC1\ A(650) + PC2\ A(650)}{2}$$

Validity criteria

$NCX^{-} \geq 0.600$ $PCX^{-} / NCX^{-} \leq 0.50$

$$S/N = \frac{SAMPLE\ A(650)}{NCX^{-}}$$

The presence or absence of antibodies (Ab) to CAV was determined by the sample to negative (S/N) ratio for each. Accordingly, the 1/10 diluted serum samples that showed S/N > 0.60 were negative for CAV antibodies, whereas samples showed S/N ≤ 0.60 were positive to CAV antibodies.The results were statistically analyzed using IBMSPSS V21 PC 9IBM (statistical package of social science).

RESULTS

All the flocks of both types of birds were positive for CAV antibodies when were tested by ELISA IDEXX kit (Table-2,figure-1).Sero-prevalence of CAV Ab in local fowls showed that 87 out of 100 serum samples were positive to CAV, whereas 29 serum samples out 100 from Japanese quails were positive to CAV. The correlation in the positivity rate between the two groups of different birds was highly significant (P<0.000).In local (indigenous) fowls the sero-prevalence of CAV antibodies showed that 87 out of 100 serum samples were positive for such antibodies. The correlation of age to positivity rate of each four groups of local fowls was not significant (p=0.211) (Table-3, figure-2).

The sero-prevalence of CAV antibodies showed that 29 out of 100 serum samples were positive for such antibodies. The correlation of age to positivity rate of each four groups of quails was highly significant (P≤0.004) (Table-4, figure-3).Serum samples from both birds that were positive for CAV antibodies showed that were 37 serum samples from local fowls out of 87 with high Ab level and low S/N ratio, 30 with moderate Ab level and medium S/N ration and 20 with low Ab level and high S/N ratio (Table-4).In Japanese quails the result showed that 6 out of 29 serum samples were positive with high level of Ab and low S/N ratio, four samples with moderate level of Ab and medium S/N ratio, and 19 with low Ab level and high S/N ration (Table 5, figure-4).The correlation of Ab level between the two groups of bird was highly significant (P≤0.000).

DISCUSSION

It is well known that chicken anemia virus was worldwide in its distribution and was recorded broilers, layers and breeder farms (21,22). In some poor countries backyard (indigenous) chickens were regarded as one of the main economic incomes for such people like African (27).In Iraq there is no data regarding the infection of local fowls with chicken anemia virus.The present study showed that 87 out of 100 samples that were collected from four different locations were positive to CAV antibodies. Similar findings were reported by Hernandes-Divers *et al*. (28), when they reported 90% positivity rates to CAV antibodies in backyard chicken in Ecuador regardless their ages. Emikpe*et al*. (29) reported for the first time CAV antibodies in apparently healthy indigenous chickens of Nigeria from four communities. The sero-prevalence was 88.9%.The local fowls of present study had an age ranged from 12 to 30 weeks and the high level of antibodies might be caused subclinical infections as all samples were collected from apparently healthy birds (7).These local fowls may be play a role of CAV transmission to healthy commercial chicken (29,27), or CAV might be transmitted from adjacent broiler and layer farms to backyard birds or vice versa (30). Bülow and Schat(31) stated that breeders, broilers, and layers were the source of CAV infections in backyard chickens. The same authors added that, contaminated eggs, cells, and vaccines of live type may be the source of CAV dissemination to backyard chickens. In contrast Barrios *et al*. (32) reported that the source of CAV in backyard chickens was unknown,

and not got a concern for study or detection for longtime and might be the source of CAV infection in poultry industry.

In Japanese quails of present study 100 samples were collected from four farms. Seroprevalence of CAV antibodies in such birds showed that 29 (29%) of the serum samples were positive to CAV antibodies (Table 4). Six of them were with low S/N ratio and high Ab level, four with medium S.N and moderate Ab level and 19 of them with high S/N ratio and low Ab level (Table 5). The seropostivity of Japanese quails of present study came in agreement with many other studies. Farkas*et al. (24)* reported the sero-positivity of 103 serum samples of Japanese quails out of 168samples tested for CAV. Furthermore, the same authors added that the titer of CAV Ab in serum samples collected from quails in 1992 was lower than that collected from quails in 1995. The positivity rate of infection was estimated 83.3% when 10 flocks were positive to CAV Ab out of 12. Zia-Jahromi and Gholami-Ahangaran (25) detected CAV infection in 50 flocks of Japanese quails and suggested that quails could be a host for CAV infection. CAV virus was also detected in the thymus samples of 38 quails (15%) out of 250 samples (33).

In the present study all the four farms were positive to CAV Ab (Table 3).In comparison to seropositivity in local fowls, high numbers of indigenous birds were positive to CAV Ab (87%) when compared to 29 (29%) positive of quail samples. It seems that local fowls were highly susceptible to the CAV infection (7).In a final conclusion this study showed for the first times in Iraq that local fowls (indigenous) and Japanese quails were susceptible to CAV infection. As they were apparently healthy birds they might be act as a source of infection to chicken industry (broilers and layers). CAV was reported as an immunosuppressive and its infection might predispose the poultry farms to the complicated infections with other bacterial and viral agents, or causing vaccine failures.

It is recommended firstly to isolate the virus from clinically infected birds and subjected the isolated virus to molecular study to compare its genomic structure from different isolates to point out the possibility of strain variation, secondly to subjects all the Iraqi poultry farms and local fowls to wide scale of vaccination program with local isolate of CAV.

REFERENCES

1. Hagood, L.T., Kelly, T.F., Wright, J.C. and Hoerr, F.J. (2000). Evaluation of chicken infectious anaemia virus and associated risk factors with disease and production losses in broilers. *Avian Dis. 44: 803-808.*
2. Schat, K.A. (2009). Chicken infectious anaemia. Curr. Top. Microbiol. *Immunol. 331: 151-183.*
3. Bhatt, P., Shukla, S. K., Mahendran, M., Dhama, K., Chawak, M. M., &Kataria, J. M. (2011). Prevalence of Chicken Infectious Anaemia Virus (CIAV) in commercial poultry flocks of Northern India: a serological survey. *Transboundary and emerging diseases*. *58*(5): 458-460.
4. Toro, H., Ewald, S., &Hoerr, F. J. (2006). Serological evidence of chicken infectious anemia virus in the United States at least since 1959. *Avian diseases*, *50*(1), 124-126.
5. Yuasa, N., Taniguchi, T. and Yoshida, I. (1979). Isolation and some characteristics of an agent inducing anemia in chicks. *Avian Dis. 23: 366-385.*
6. Dhama, K., Mahendran, M., Somvanshi, R. and Chawak, M.M. (2008). Chicken infectious anaemia virus: an immunosuppressive pathogen of poultry - A review. *Indian J. Vet. Pathol. 32(2): 158-167.*
7. Oluwayelu, D.O.(2010). Diagnosis and epidemiology of chicken infectious anemia in Africa. *African Journal of Biotechnology. 9(14):2043-2049.*
8. Todd, D. (2000). Circoviruses: immunosuppressive threats to avian species: a review. *Avian Pathol. 29: 373-394.*
9. De Herdt, P., Van Den Bosch, G., Ducatelle, R., Uyttebroek, E. and Schrier C (2001). Epidemiology and signifcance of chicken infectious anemia virus infections in broilers and broiler parents under nonvaccinated European circumstances. *Avian Dis.* 45: 706-708.
10. Hoerr, F. J. (2010). Clinical aspects of immunosuppression in poultry. *Avian Diseases*. *54*(1): 2-15.

11. Toro, H., Gonzalez, C., Creda, L., Hess, M., Reyes, E. and Geisse, C. (2000). Chicken anaemia virus and fowl adenoviruses: association to induce the inclusion body hepatitis/hydropericardium syndrome. *Avian Dis. 44: 51-58.*

12. Adair, B.M. (2000). Immunopathogenesis of chicken anaemia virus infection. *Dev. Comp. Immunol.* 24: 247-255.

13. Dhama, K., Mahendran, M., Somvanshi, R. and Chawak, M.M. (2008). Chicken infectious anaemia virus: an immunosuppressive pathogen of poultry - A review. *Indian J. Vet. Pathol. 32(2): 158-167.*

14. Yuasa, N., Taniguchi, T., Goda, M., Shibatani, M., Imada, T. and Hihara, H. (1983).Isolation of chicken anemia agent with MDCC-MSB1 cells fromchickens in the field. *Natl. Inst. Anim. Health Q. Jpn. 23: 75-77.*

15. Hoop, R.K. (1992). Persistence of vertical transmission of chicken anemia agent in experimentally infected laying hens. *Avian Pathology. 21:493-501.*

16. Cardona, C., B. Lucio, P. Oconnell, J. Jagne, and K. Schat. 2000. Humoral immune responses to chicken infectious anaemia virus in three strains of chickens in a closed flock. *Avian Dis.* 44:661–667.

17. Miller, M.M., Katie, A.E., Oswald, W.B. and Schat, K.A.(2003). Detection of chicken anemia virus DNA in embryonal tissues and eggshell membranes. *Avian Dis 2003, 47:662-671.*

18. Brentano, L., Lazzarin, S., Bassi, S.S., Klein, T.A. and Schat, K.A.(2005). Detection of chicken anemia virus in the gonads and in the progeny of broiler breeder hens with high neutralizing antibody titers. *Veterinary Microbiology.* 105:65-72.

19. Ducatez, M. F., Owoade, A. A., Abiola, J. O., and Muller, C. P. (2005). Molecular epidemiology of chicken anemia virus in Nigeria. *Arch. Virol.* 151:97–111.

20. Schat, K.A. (2003). Chicken infectious anemia. In Saif, Y.M., Barnes, H.J., Glisson, J.R., Fadly, A.M., McDougald, L.R.and Swayne, D.E. (eds) Diseases of Poultry (11th Ed.), Iowa State Press, Ames, Iowa, pp. 182-202.

21. MaLachan, N.J. and Dubovi, E.J. (2011). Fenner's Veterinary Virology. 4th ed. Pp:237-242.

22. Quinn,P.J., Markey, B.K., Leonard,F.C.,Fitzpatrick, E.S., Fanning, S. and Hartigan, P.J. (2011). Veterinary Microbiolgy and Microbial Diseases. Willey-Blackwell. A John Willey and Sons, Ltd Publication. 2nd ed. Pp:615-617.

23. Crooijmans, R. P., &Pijpers, A. (2004). A serological survey for pathogens in old fancy chicken breeds in central and eastern part of The Netherlands. *Tijdschriftvoordiergeneeskunde*, *129*(10): 324-327.

24. Farkas, T., Maeda, K., Sugiura, H., Kai, K., Hirai, K., Otsuki, K. and Hayashi, T. (1998). A serological survey of chickens, Japanese quail, pigeons, ducks and crows for antibodies to chicken anaemia virus (CIAV) in Japan. *Avian Pathol. 27: 316-320.*

25. Zia-Jahromi, N. and Gholami-Ahangaran, M. (2014). Molecular detection of infectious anaemia virus in quail, in Iran. *Journal of Pure and Applied Microbiology.* 8(1):623-626.

26. Campbell, G. (2001). Investigation into evidence of exposure to infectious bursaldisease virus (IBDV) and chick infectious anaemia virus (CIAV) in wild birds in Ireland. Pages 230–233 in Proc. 2nd Int. Symp. Infectious Bursal Disease and Chicken Infectious Anaemia, Rauischholzhausen, Germany. InstitutfürGeflügelkrankheiten, Justus Liebig University, Giessen, Germany.

27. Oluwayelu, D.O., Todd, D., Ohore, G., Emikpe, B., Oladele, O. and Olaleye, O.D. (2009). A monoclonal blocking ELISA to detect chicken anaemia virus antibodies in Nigerian poultry. *Bull. Anim. Health Prod. Afr. 57:131-141.*

28. Hernandez-Divers, S.M., Villegas, P., Prieto, F., Unda, J.C., Stedman, N., Ritchie, B., Carroll, R. and Hernandez-Divers, S.J. (2006). A survey of selected avian pathogens of backyard poultry in northwestern Ecuador. *Journal of Avian Medicine and Surgery. 20:147-158.*

29. Emikpe, B.O.,Oluwayelo. D.O.,Ohore, O.G. and Oladokun, A.T. (2005). Serological evidence of chicken anemia virus infection in Nigerian indigenous chickens. *Onderstepoort Journal of Veterinary Research. 72:101-103.*

30. Oluwayelu,D.O.,Todd,D.andOlaleye,O.D (2008). Sequence and phylogenetic analysis of chicken anemia virus obtained from backyard and commercial chickens in Nigeria. *Onderstepoort Journal of Veterinary Research.75:353-357.*

31. Von Bülow, V. and K. A. Schat. (1997). Chicken infectious Anemia. In B. W. Calnek, H. J. Barnes, C. W. Beard, L. R. McDougald, and Y. M. Saif (eds.). Diseases of Poultry, 10th edition, State University Press: Ames, Iowa, 739—756.

32. Barrios, P. R., Marín, S. Y., Resende, M., Rios, R. L., Resende, J. S., Horta, R. S., Costa, M.P., & Martins, N. R. S. (2009). Occurrence of chicken anemia virus in backyard chickens of the metropolitan region of Belo Horizonte, Minas Gerais. *RevistaBrasileira de CiênciaAvícola*, *11*(2), 135-138.

33. Gholami-Ahangaran, M. (2015). Serological and molecular detection of chicken anemia virus in Iranian poultry frocks. *Veterinariaitaliana.51(3): 211-215.*

Table 1.Serum samples collected from birds according to kind of birds and locality of farms

No.	Number of samples	Age	Location	Kind of bird
1	25	12 weeks	C1/Mindily	Local hens
2	25	24 weeks	C2/Al-Huayder	Local hens
3	25	27 weeks	C3/Al-Mokdadia	Local hens
4	25	30 weeks	C4/Al-Shaab	Local hens
5	25	2 Weeks	Q1/ Al-Khalis	Quails
6	25	3 weeks	Q2/ Buhris	Quails
7	25	4 weeks	Q3/ Al-Mokdadia	Quails
8	25	5 weeks	Q4/Baquba	Quails
Total	200			

Table 2. Sero-prevalence of CAV antibodies in Japanese quails and local fowls

Type of Birds	Antibody positivity to CAV		Total
	CAV-Ab +ve	CAV-Ab-ve	
Local Fowls	87 (87%) 75%	13(13%) 15.5%	100
Japanese Quails	29(29%)* 25%**	71(71%) 84.5%	100
Total	116(52%)	84(42%)	200

*****Percent among the total group of samples for each type of birds

**Percent among the total samples of positive/negative samples for CAV antibodies birds.

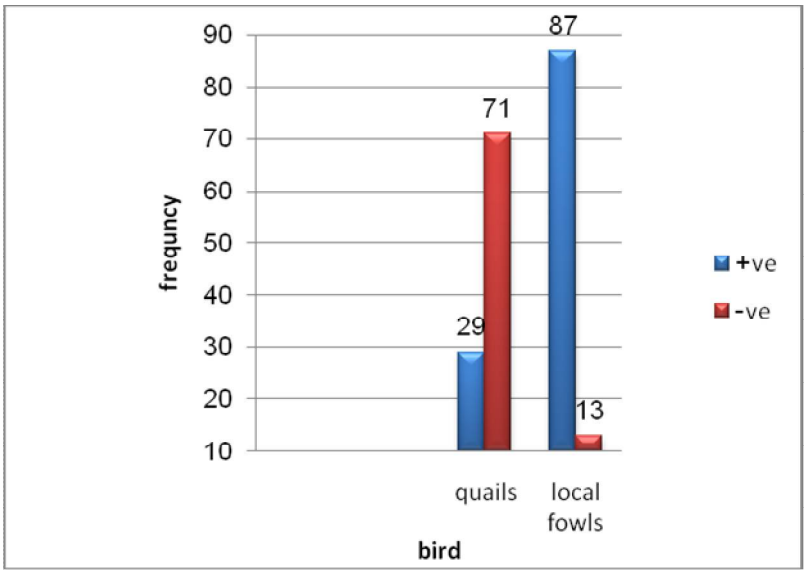

Figure 1. Descriptions of CAV serum positive and negative samples according to bird species

Table 3. Sero-prevalence of CAV antibodies in local fowls

Age	Antibody positivity to CAV		Total
	CAV-Ab +ve	CAV-Ab-ve	
12 weeks	24 (96.0%)	1 (4.0%)	25 (100.0%)
24 weeks	20 (80.0%)	5 (20.0%)	25 (100.0%)
27 weeks	20 (80.0%)	5 (20.0%)	25 (100.0%)
30 weeks	23 (92.0%)	2 (8.0%)	25 (100.0%)

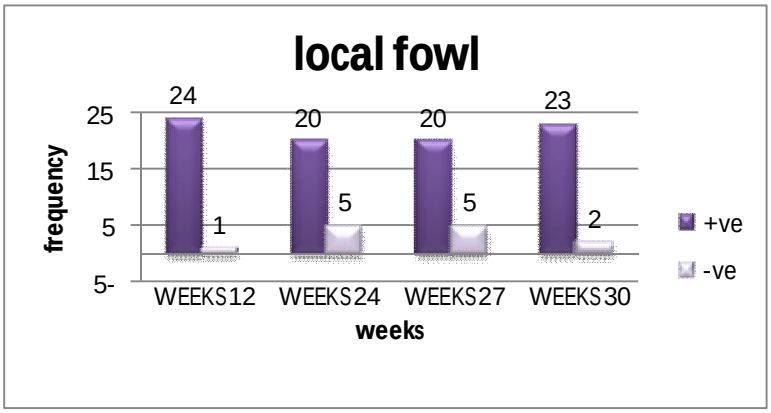

Figure 2. Descriptions of CAV serum positive and negative samples of local fowls according to age groups

Table 4.Sero-prevalence of CAV antibodies in Quails

Age	Antibody positivity to CAV		Total
	CAV-Ab +ve	CAV-Ab-ve	
Two weeks	13(52.0%)	12(48.0%)	25(100.0%)
Three weeks	9 (36.0%)	16(64.0%)	25(100.0%)
Four weeks	5 (20.0%)	20(80.0%)	25(100.0%)
Five weeks	2 (08.0%)	23(92.0%)	25(100.0%)

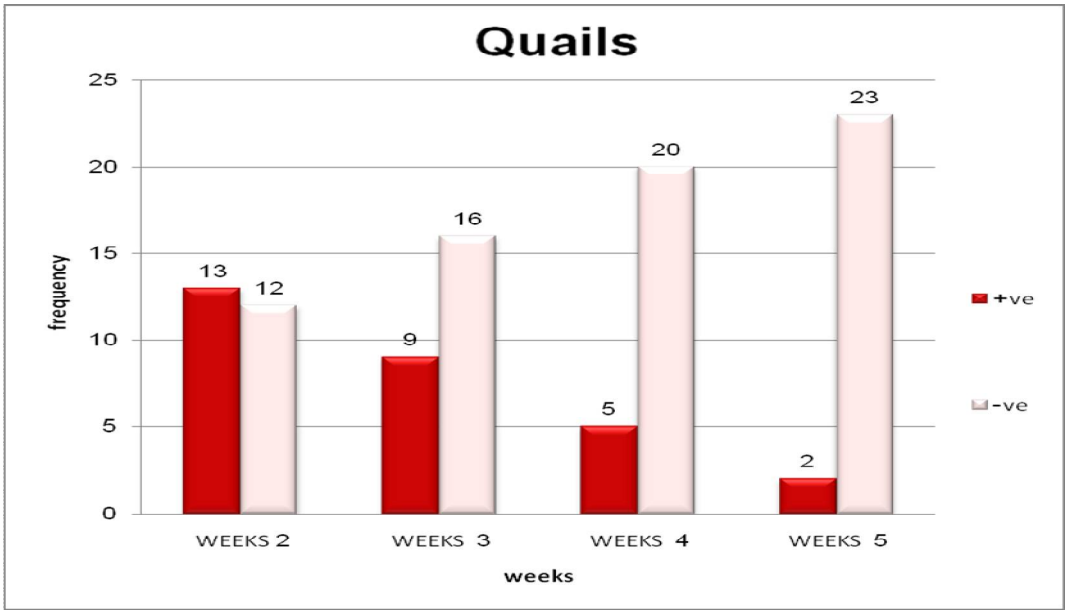

Figure 3. Descriptions of CAV serum positive and negative samples of Japanese quails according to age groups

Table 5.Antibody levels according to S/N ratio in local fowls and Japanese quails

S/N ratio *	Antibody level	Type of Birds		Total
		Local Fowls	Japanese Quails	
Low (0.001 to 0.199)	High	37(86%) 42.5%	6 (14.0%)** 20.7%***	43(100%) 37.1%
Medium (0.200 to 0.399	Moderate	30(88.0%) 34.5%	4 (12.0%) 13.8%	34(100%) 29.3%
High (0.400 to 0.599)	Low	20(51.3%) 23%	19(48.7%) 65.5%	39(100%) 33.6%
Total		87(81%) 100%	29(25%) 100%	116(100%)

*Serum samples with S/N > 0.60 were negative for CAV antibodies, whereas samples showed S/N ≤ 0.60 were positive to CAV antibodies

**Percent among total group of each S/N ration

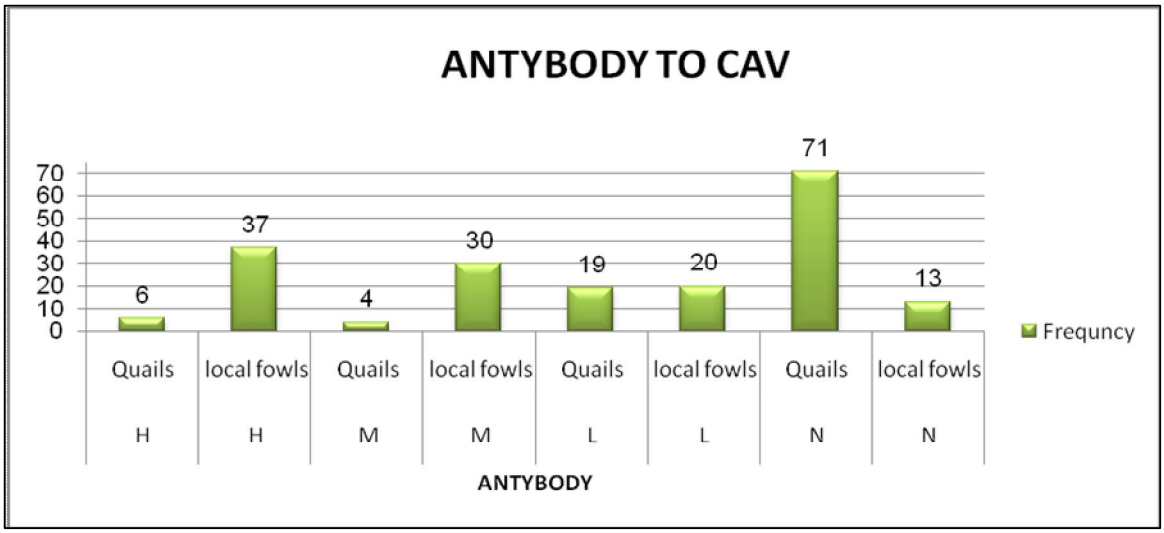

***Percent among the total group of positive samples

Figure 4.Shows the descriptions of CAV serum positive and negative samples according to bird species. Bars are the number of samples, H, M and L (high, medium and low) levels of CAV antibodies respectively, N (negative) for CAV antibodies.

Indian Journal of Natural Sciences www.tnsroindia.org.in ©IJONS

Vol.9 /Issue 51 / December / 2018 *International Bimonthly* *ISSN: 0976 – 0997*

RESEARCH ARTICLE

Characterization of Titania Thin Film Behavior Preparation by Spray Pyrolysis

Nagham Abdulameer Yasir*, Alzubaidy Muneer Hlail and Ali Kamel Mohsin

Department of Physics, University of Wasit, College Of Science, Wasit, Iraq

Received: 18 Aug 2018 Revised: 23 Sep 2018 Accepted: 24 Oct 2018

***Address for Correspondence**
Nagham Abdulameer Yasir
Department of Physics,
College of Science, University of Wasit,
Wasit, Iraq.
E-mail:naghama224@uowasit.edu.iq

ABSTRACT

Controlling condition of spray deposition of TiO_2 film from titanium trichloride solution as a titanium source is a key for important applications. Three types of specimens were prepared depending on the number of sprinklers; 20, 40, and 60 sprays with thin films thicknesses; 42.32nm, 211.64nm, and 423.28nm respectively. The titanium dioxide thin film was deposited on glasses substrate at 300 °C temperature. After that, titanium dioxide thin film annealed at 400 °C in order to form the crystalline anatase phase.The manufactured TiO_2 thin films were studied and characterized by X-Ray Diffraction (XRD), Fourier transform infrared spectroscopy (FTIR), and Atomic Force Microscopy (AFM). XRD analysis confirms the tetragonal single-crystalline nature of the deposited thin films with a preferred orientation along (101) plane. The crystallite size suggests the formation of the nanostructure of the deposited films. The average particle size obtained by AFM assure the existence of nanostructure. The FTIR spectra analysis assure the existence of the Ti-O-Ti chemical bond indicates the formation of a titanium dioxide network observed at the fingerprint region in the mid-infrared spectrum.

Key words: Thin films, Titanium dioxide, Spray pyrolysis, Crystallite size.

INTRODUCTION

Titanium dioxide, as well known as (Titania) and its chemical formula is TiO_2 (1). TiO_2 is generally considered to be the best semiconductor photocatalyst available at present due to its strong oxidizing power at ambient temperature and pressure, stable, non-toxic, cheap and readily available (2). Nanostructured titanium dioxide (TiO_2) has been of significant research interests in the past decades, due to its unique physical and chemical properties as well as the great potential applications in a wide range of fields including catalysis, photocatalysis, photoluminescence, solar

cells, fuel cell, and gas sensor (3-4). The unique physical and chemical properties of TiO_2 depend on the crystal phase, particle size, and also on the particle shape. For example, crystalline TiO_2 have different crystalline structures that rutile, anatase, and brookite, which determine the photocatalytic performance of TiO_2. On the other hand, particle size plays an important role in Nanocrystalline TiO_2 based catalysts. Small particles offer a large surface area and exhibit high photocatalytic activity mostly by influencing the dynamics of $e^-/h+$ recombination and the adsorption rate and adsorbed amount of reaction species (5-6). Thin film processing routes based on spray pyrolysis, sol-gel dip-coating, and spin-coating are attractive because they are versatile and cost-effective. Among very interesting thin film materials processed in this way are TiO_2 films which have been deposited by spray pyrolysis for different applications. The formation and composition of TiO_2 films using Ti Alkoxide as precursors have been studied extensively (7-8-9). This research reports on crystal structure and surface morphological properties of TiO_2 thin films prepared by the spray pyrolysis processing. Particular attention was paid to the effects of preparation conditions such as deposition and annealing temperature.

MATERIALS AND METHODS

Preparation of Titanium Dioxide thin film

TiO_2 thin films were prepared from Titanium Trichloride ($TiCl_3$) (99.9% Sigma Aldrich) and utilized as the Titanium dioxide procedure. 10 ml of Titanium Trichloride ($TiCl_3$) solution were diluted in 66.5 ml of distilled water by a magnetic stirrer, in order to utilize as a source of Titanium dioxide. TiO_2 thin films were synthesis on glass substrates utilizing chemical spray pyrolysis technique. The substrate was cleaned more than once with rinsing ultrasonically in distilled water, absolute ethanol and acetone. Finally, clean with distilled water, and dried by nitrogen.

The films were prepared at a substrate temperature (300 °C), distance between the nozzle and substrate was kept at 30 cm, spray rate was 5 ml/min, spray time was fixed at 6 seconds followed by 2 seconds waiting to avoid excessive cooling and to prevent glass cracking, during waiting the samples were rotated at the heater in order to obtain a homogeneous films. There are three types of specimens were prepared depending on the number of sprinklers; 20,40, and 60 sprays with thin films thicknesses; 42.32nm, 211.64nm, and 423.28nm respectively. The thin film thicknesses were obtained by the gravimetric method. The final thin films were annealed at (400°C) temperatures for 2 hours in an ambient atmosphere, in order to obtain TiO_2 thin film in the anatase phase.

Characterization

The crystalline structure of TiO_2 thin film examined by X-Ray Diffraction device model (Shimadzu-6000-XRD) manufactured in Japan records the intensity as a function of Braggs angle, with the following Specifications: Target is copper (Cu) with wavelength (λ=1.5418 °A), voltage (40 kV) and current (30mA). The scanning angle 2theta is changed in the range of (10-80) degree with a speed of 8.0000 (deg/min). The FTIR measurements were performed with a SHIMADZU spectrometer model (IR Prestige-21) with resolution 4 (1/cm) and the number of scans 10. The topography surface study was conducted out using an atomic force microscope (SPM Ntegra NT – MDT) made in Russia.

RESULTS AND DISCUSSION

X-Ray Diffraction (XRD) analysis

X-Ray Diffraction (XRD) analysis has been done to study the crystal structures, the crystallite size, the dislocation density, and the number of crystallites per unit area of the TiO_2 thin film prepared at different thin film thicknesses

(42.32, 211.64, and 423.28nm). The XRD patterns showed that all specimens have a single crystalline structure of TiO_2 in anatase phase. As well as, the XRD pattern showed that these specimens have single sharp peak 2Θ angle at 25.2506°, 25.2107°, and 25.1957° with (101) diffraction plane, as shown in fig.1.The crystalline size of the prepared thin film was determined by Debye Scherrer equation 1.

$$D = \frac{k\lambda}{\beta \cos \theta_B} \quad \ldots\ldots 1$$

Where, (D) is the crystallite size, (k) is the Scherrer constant = 0.94 assuming that the particles are spherical, (λ) is the X-ray wavelength, (θ) is the Bragg diffraction angle, and (β) is the full width at half maximum (FWHM) (10). The numbers of the dislocations lines which cut the crystal per unit area represent dislocation density, can be obtained by using the following relationship 2.

$$\delta = \frac{1}{D^2} \quad \ldots\ldots 2$$

Where, (δ) is the dislocation density,and (D) is the crystallite size (11).The number of crystallites per unit area, can be obtained using the following relationship3.

$$N_\circ = \frac{t}{D^3} \quad \ldots\ldots 3$$

Where, (N_0) is the number of crystallites per unit area and (t) is the thickness of the film(12). The stacking fault (SF) values for the preferred orientation of (101) plane of the TiO_2 thin films are calculated utilizing equation 4.

$$SF = \left[\frac{2\pi^2}{45(3tan\theta)^{\frac{1}{2}}}\right]\beta \quad \ldots\ldots 4$$

Where, (SF) is the stacking fault, (β) is the full width at half maximum (FWHM), and (Θ) is the Bragg diffraction angle (12).According to the results, it is found that as the thin film thickness increased, the full width at half maximum (FWHM) increased, the crystallite size decreased, the numbers of the dislocations lines (dislocation density) increased, and the number of crystallites per unit area increased. This outcome was also in good synchronized with the previous work (13-14-15). Table 1. Summarizes the structural properties of all specimens with different TiO_2 thin film thicknesses (42.32, 211.64, and 423.28 nm).

Fourier Transform Infrared Spectroscopy (FTIR) analysis

The FTIR spectra of the synthesized Titanium dioxide thin film in the wavenumber range of 400-4000 cm^{-1} which identifies the chemical bonds and functional groups in the compound. Fig.2, fig.3, and fig.4. Shows FTIR spectra of the Titanium dioxide thin film with a different thin film thickness (42.32, 211.64, and 423.28 nm), respectively. Table 2. Give the chemical bonds and functional groups of FTIR spectra of the Titanium dioxide thin film with a different thin film thickness (42.32, 211.64, and 423.28 nm). The results showed that the Titanium dioxide thin film thicknesses didn't affect by the chemical bonds. It is found that all specimens have a strong and sharp peak of the chemical bond (Ti-O-Ti) indicates the formation of a titanium oxide network observed at the fingerprint region in the mid-infrared spectrum. As well as, the medium and sharp peaks of the chemical bonds; O-H stretching, O=C=O stretching, C-H bending, O-H bending, and C=C bending observed at the functional group region in the mid-infrared spectrum.

Atomic Force Microscope (AFM) analysis

The surface topography, surface roughness parameters, and an average grain size of all specimens with different TiO_2 thin film thicknesses (42.32, 211.64, and 423.28 nm) were studied using Atomic Force Microscope (AFM).Average surface roughness, root mean square, surface skewness, surface kurtosis, and the average grain size for all specimens that are included in the investigation are summarized in Table 3. Fig. 5. Shows 2D and 3D AFM images of the TiO_2 thin films presentation a smooth surface with uniform grains. In Fig. 5, the surface topography discovers the Nano-crystalline TiO_2 grains, which rise to make intensive films significantly with the increased thickness. From the images, it was observed that the surface of the films exhibited a confirmed degree of coarseness and the thin films surface became rougher when the thickness increases. Fig. 6. Shows the average particle size range distribution for the TiO_2 thin film with different thin film thicknesses (42.32, 211.64, and 423.28 nm).

CONCLUSION

TiO_2 thin films were fabricated successfully utilizing chemical spray pyrolysis method. XRD patterns reveal that all the deposited films were single-crystalline having a preferred orientation along (101). It is found that as the thin film thickness increased, the full width at half maximum (FWHM) increased, the crystallite size decreased, the numbers of the dislocations lines (dislocation density) increased, the stacking fault (SF) increased, and the number of crystallites per unit area increased. AFM 2D and 3D images confirm the presence of nanostructured thin films. From the determination of AFM, concluded that an increment in thin film thickness offset it, an increment in average surface roughness, root mean square, surface skewness, and surface kurtosis. As well as, the average grain size decreases.The FTIR spectra showed that all the deposited films have a strong and sharp peak of the chemical bond (Ti-O-Ti) indicates the formation of a Titanium dioxide network observed at the fingerprint region in the mid-infrared spectrum. As well as, the medium and sharp peaks of the chemical bonds; O-H stretching, O=C=O stretching, C-H bending, O-H bending, and C=C bending observed at the functional group region in the mid-infrared spectrum.

ACKNOWLEDGEMENTS

This work was supported by thin film laboratory in Wasit University, college of science, physics department.

REFERENCES

1.Zakarya SA, Kassim A, Lim HN, Anwar NS, Huang NM. Synthesis of titanium dioxide microstructures via sucrose ester microemulsion-mediated hydrothermal method. Sains Malaysiana. 2010; 39(6):975-9.
2.Mills A, Lee SK. A web-based overview of semiconductor photochemistry-based current commercial applications. Journal of Photochemistry and Photobiology A: Chemistry. 2002; 152(1-3):233-247.
3.Fujishima A, Honda K. Electrochemical photolysis of water at a semiconductor electrode. nature. 1972; 238(5358):37-38.
4.Chen X, Mao SS. Titanium dioxide nanomaterials: synthesis, properties, modifications, and applications. Chemical reviews. 2007; 107(7):2891-2959.
5.Zhang Z, Wang CC, Zakaria R, Ying JY. Role of particle size in nanocrystalline TiO_2-based photocatalysts. The Journal of Physical Chemistry B. 1998; 102(52):10871-10878.
6.Tan Z, Sato K, Takami S, Numako C, Umetsu M, Soga K, Nakayama M, Sasaki R, Tanaka T, Ogino C, Kondo A. Particle size for photocatalytic activity of anatase TiO_2 nanosheets with highly exposed {001} facets. RSC Advances. 2013; 3(42):19268-19271.
7.Oja I, Mere A, Krunks M, Solterbeck CH, Es-Souni M. Properties of TiO_2 films prepared by the spray pyrolysis method. In Solid State Phenomena 2004; 99: 259-264.

8.Alam MJ, Cameron DC. Investigation of annealing effects on sol–gel deposited indium tin oxide thin films in different atmospheres. Thin Solid Films. 2002; 420:76-82.

9.Djaoued Y, Taj R, Brüning R, Badilescu S, Ashrit PV, Bader G, Vo-Van T. Study of the phase transition and the thermal nitridation of nanocrystalline sol–gel titania films. Journal of non-crystalline solids. 2002; 297(1):55-66.

10.Wang H, Wu G, Cai XP, Zhao Y, Shi ZF, Wang J, Xia XC, Dong X, Zhang BL, Ma Y, Du GT. Effect of growth temperature on structure and optical characters of NiO films fabricated by PA-MOCVD. Vacuum. 2012; 86(12):2044-2047.

11.Maji SK, Dutta AK, Biswas P, Karmakar B, Mondal A, Adhikary B. Nanocrystalline FeS thin film used as an anode in photo-electrochemical solar cell and as hydrogen peroxide sensor. Sensors and Actuators B: Chemical. 2012 May 20; 166:726-732.

12.Balaji M, Chandrasekaran J, Raja M. Characterization of $WMoO_3$ Thin Films and its n-$WMoO_3$/p-Si Junction Diodes via JNS Pyrolysis Technique. Zeitschrift für Physikalische Chemie. 2017; 231(5):1017-1037.

13.Mechiakh R, Bensaha R. Analysis of Optical and Structural Properties of Sol–Gel TiO_2 Thin Films. Moroccan Journal of Condensed Matter. 2006; 7.

14.Negishi N, Takeuchi K, Ibusuki T. Surface structure of the TiO_2 thin film photocatalyst. Journal of materials science. 1998; 33(24):5789-5794.

15.Jung SC, Kim SJ, Imaishi N, Cho YI. Effect of TiO_2 thin film thickness and specific surface area by low-pressure metal–organic chemical vapor deposition on photocatalytic activities. Applied Catalysis B: Environmental. 2005; 55(4):253-257.

Table 1. Structural properties of the TiO_2 thin films.

TiO_2 thin filmthickness (nm)	42.32	211.64	423.28
2Θ (Deg.)	25.1957	25.2107	25.2506
hkl	Anatase (101)	Anatase (101)	Anatase (101)
FWHM(Deg.)	0.5900	0.7600	0.8000
Crystalline size (nm)	14.42	11.19	10.63
d_{hkl} (Å)	3.53176	3.52969	3.52420
Strain (ε)	0.0817	0.0850	0.0591
Dislocation Density δ (nm^{-2})	$4.809x10^{-3}$	$7.986x10^{-3}$	$8.849x10^{-3}$
Number of Crystals N_o (nm^{-2})	0.0141	0.151	0.352
stacking fault (SF)	$5.516x10^{-3}$	$7.103x10^{-3}$	$7.471x10^{-3}$
Card Data	00-021-1272	00-021-1272	00-021-1272

Table 2. Chemical bonds and functional groups of the TiO_2 thin films.

TiO_2 thin filmthickness (nm)	Absorption peak (1/cm)	Appearance	Group	Compound Class
42.32	3527.921-3394.828	Medium, Sharp	O-H Stretching	alcohol
	2366.735	Medium, Sharp	O=C=O Stretching	Carbon dioxide
	1649.192	Medium, Sharp	C-H Bending	alkane
	1276.918	Medium, Sharp	O-H Bending	phenol
	844.849	Medium, Sharp	C=C Bending	alkene
	661.605-615.312	Strong, Sharp	Ti-O-Ti	Titanium dioxide
211.64	3401.274-3614.721	Medium, Sharp	O-H Stretching	alcohol
	2320.442	Medium, Sharp	O=C=O Stretching	Carbon dioxide
	1655.089	Medium, Sharp	C-H Bending	alkane
	1273.060	Medium, Sharp	O-H Bending	phenol
	844.849	Medium, Sharp	C=C Bending	alkene
	662.898-615.312	Strong, Sharp	Ti-O-Ti	Titanium dioxide
423.28	3608.9344-3527.921	Medium, Sharp	O-H Stretching	alcohol
	2332.015-2362.878	Strong, Sharp	O=C=O Stretching	Carbon dioxide
	1512.241-1654.979	Medium, Sharp	C-H Bending	alkane
	1282.705	Medium, Sharp	O-H Bending	phenol
	966.368	Medium, Sharp	C=C Bending	alkene
	611.454	Strong, Sharp	Ti-O-Ti	Titanium dioxide

Table 3. Surface roughness parametersand Average GrainSize measurements for TiO_2 thin films.

TiO_2 Thin Film Thickness (nm)	Surface roughness parameters					Average GrainSize(nm)
	Average Surface Roughness (nm)	Surface Skewness (dimensionless)	Surface Kurtosis (dimensionless)	Root Mean Square RMS(nm)	Peak-Peak (nm)	
42.32	0.909	-1.08×10^{-5}	1.8	1.05	3.63	88.42
211.64	3.16	-0.00773	1.79	3.63	12.6	67.70
423.28	3.22	-0.375	2.05	3.67	13.5	57.62

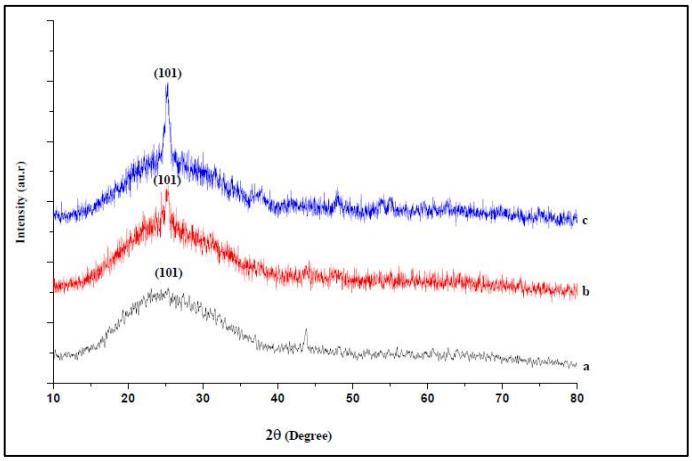

Fig.1. XRD analysis of the TiO_2 thin film synthesized with different thin film thicknesses: (a) 42.32 nm, (b) 211.64 nm, and (c) 423.28 nm.

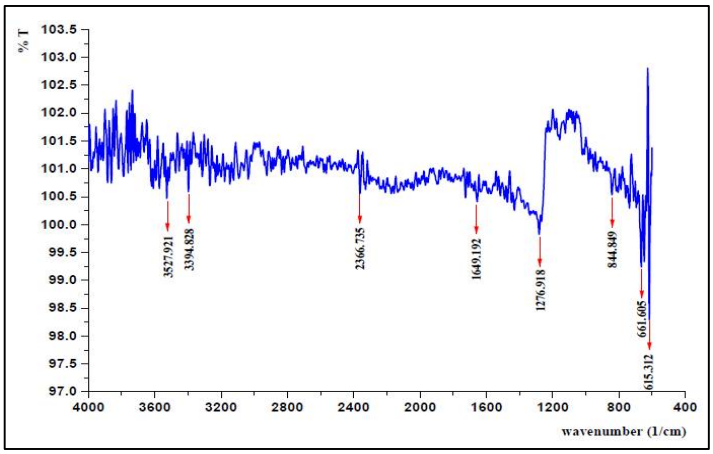

Fig. 2. FTIR spectra of the TiO_2 thin film with thin film thickness 42.32 nm.

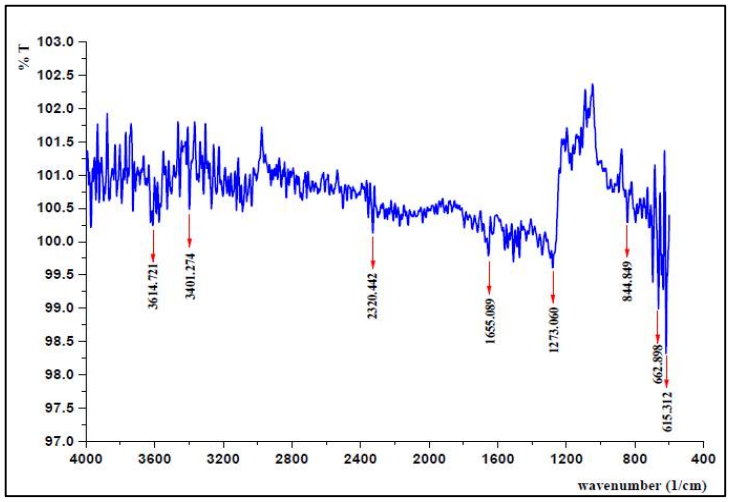

Fig. 3. FTIR spectra of the TiO_2 thin film with thin film thickness 211.64 nm.

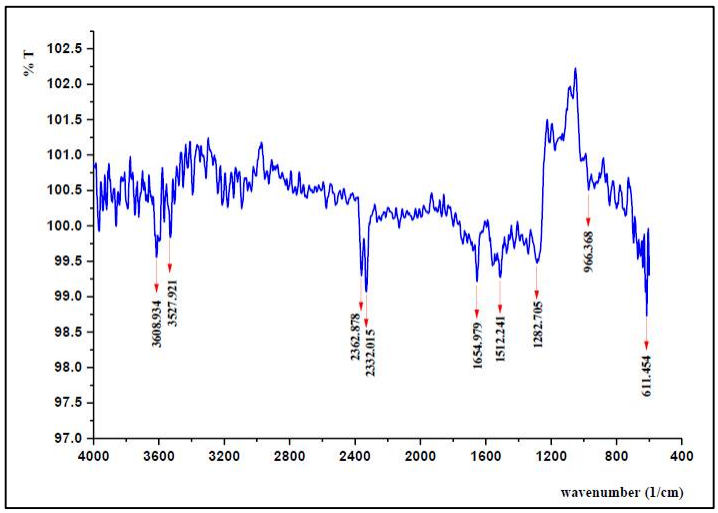

Fig. 4. FTIR spectra of the TiO_2 thin film with thin film thickness 423.28 nm.

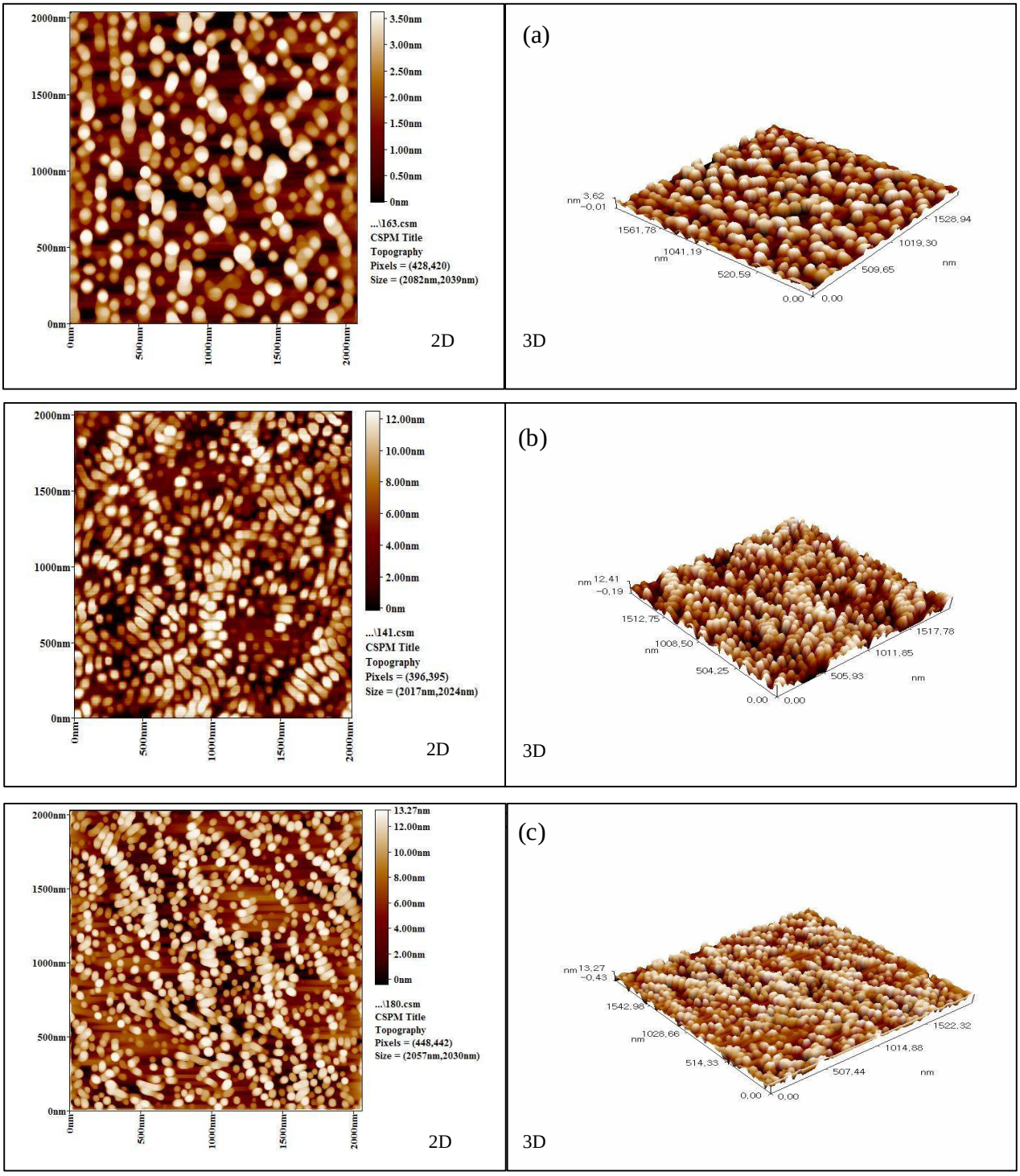

Fig. 5. AFM 2D and 3D images: (a) TiO_2 thin film thickness 42.32 nm, (b) TiO_2 thin film thickness 211.64 nm, and (c) TiO_2 thin film thickness 423.28 nm.

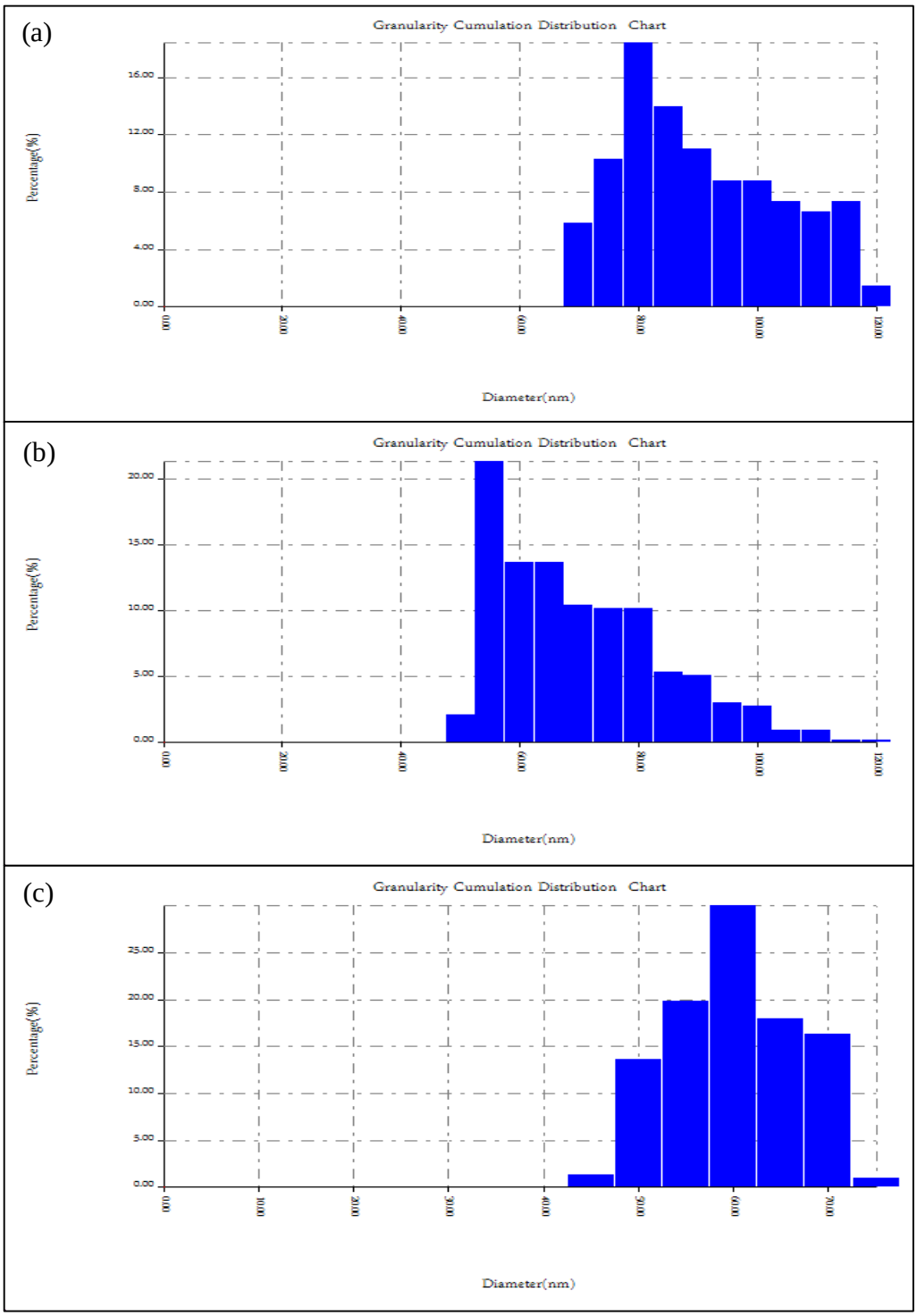

Fig. 6. Average grain size distribution in nanometer scale histogram for (a) TiO_2 thin film thickness 42.32 nm, (b) TiO_2 thin film thickness 211.64 nm, and (c) TiO_2 thin film thickness 423.28 nm.

Indian Journal of Natural Sciences www.tnsroindia.org.in ©IJONS

Vol.9 /Issue 51 / December / 2018 *International Bimonthly* *ISSN: 0976 – 0997*

RESEARCH ARTICLE

The Relationship between Type 2 Diabetes Mellitus and Thyroid Dysfunction

Lubna F. Hussain[1]*, Jabbar H. Yenzeel[2] and Essam N. Salman[3]

[1]Department of Biology, College of Science, University of Baghdad, Baghdad, Iraq.
[2]Department of Biology, College of Science, University of Baghdad, Baghdad, Iraq.
[3]Specialist Center for Endocrine and Diabetes Diseases, AL Mustansiriya University, Iraq .

Received: 18 Aug 2018 Revised: 21 Sep 2018 Accepted: 25 Oct 2018

***Address for Correspondence**
Lubna F. Hussain
Department of Biology,
College of Science, University of Baghdad,
Baghdad, Iraq.
E-mail: Lubnaaljanabi93@gmail.com

ABSTRACT

Diabetes mellitus and thyroid diseasesare themost common endocrine disorders. Action of thyroid hormone has long been recognized as an important factor of glucose homeostasis.60 menwith age ranged from (35-65) years were involved in this study during their attendance at the National Diabetes Center through the period from October 2017 to April 2018. Men were selected as four groups: G1 (10) healthy individuals as control group, G2 (10) patients with type2 diabetes mellitus, G3 (20) patients with type2 diabetes mellitus and hypothyroidism, and G4 (20) patients with type2 diabetes mellitus and hyperthyroidism.Serum samples were collected from each subject for determination the level of Fasting Blood Glucose (FBG), Thyroid Stimulating Hormone (TSH), Thyroxine (T4), and Triiodothyronine (T3). and whole blood to determination the level of HbA1c.The results revealed a highly significant (P<0.01) increase in the level of FBS in G2 (164.86 ± 4.87mg/dl), G3 (163.50 ± 4.23 mg/dl) and G4 (177.16 ± 4.72 mg/dl) when compared with G1 (86.46 ± 1.78 mg/dl). Alsothe HbA1c showed highly significant (P <0.01) increase in G2 (8.31 ± 0.38 %), G3 (8.56 ± 0.24 %) and G4 (9.35 ± 0.35 %) when compared with G1 (4.70 ± 0.09 %). TSH level was highly significant (P <0.01) increase in G3 (35.01 ± 2.53 µmol/L) when compared with G1 (2.40 ± 0.26 µmol/L), G2 (2.73 ± 0.28 µmol/L) and G4 (0.021 ± 0.004 µmol/L). T4 and T3 levels was highly significant (P <0.01) decrease in G3 (39.02 ± 1.99 nmol/L) (0.50 ± 0.03 nmol/L) when compared with G1 (99.97 ± 5.68 nmol/L) (1.20 ± 0.06 nmol/L) G2 (111.09 ± 6.00 nmol/L) (1.60 ± 0.11 nmol/L), and G4 (201.03 ± 4.37 nmol/L) (6.11 ± 0.35 nmol/L), respectively.This study shows the prevalence of abnormal thyroid hormones levels in type 2 diabetic patients as compared to control.

Keywords: Diabetes mellitus, Thyroid disease, hyperthyroidism, hypothyroidism, TSH, HbA1c, FBG.

INTRODUCTION

Diabetes mellitus (DM) is one of the important health problem worldwide. Is the most common endocrine disorder, described by a chronic hyperglycemia resulting from defects in insulin secretion, insulin action, or both.Development of diabetes mellitus involves several pathogenic processes ranging from autoimmune destruction of the pancreatic β-cells with consequent deficiency of insulin to abnormalities that result in resistance to action of insulin. Type 2 diabetes mellitus is described by combination of defective insulin secretion and peripheral insulin resistance [1]. Thyroid disorders are also common within the general population and it's the second most common endocrine disorder. Thyroid hormones contribute to the regulation of carbohydrate metabolism and function of the pancreas. on the other hand, diabetes mellitus also affects thyroid function tests to a variable extent. As a result, it is common for an individual to be affected by both diabetes mellitus and thyroid disease .Thyroid hormones are involved in cellular functions, deficit or excess of these hormones can produce in functional derangement of cell [2].Thyroid disorder is a pathological state that adversely impacts diabetic control and commonly found in most forms of diabetes mellitus which is associated with advanced age in type 2 DM and autoimmune diseases in type 1 DM. However, thyroid disorders were found to be more common in subjects with type 1 DM compared to those with type 2 DM [3] .

In the NHANES III study, observed that there was an elevated frequency of thyroid disease with advancing age and a higher prevalence of thyroid dysfunction in women compared to men and in diabetic subjects in comparison to non-diabetic [4].Diabetes mellitus appears to influence thyroid function in two sites; firstly at the level of hypothalamic control of thyroid stimulating hormone release and secondly at the conversion of thyroxine to triiodothyronine in the peripheral tissue [5].Underlying thyroid disorders in diabetic patients may go undiagnosed because the common signs and symptoms of thyroid disorders are similar to those for diabetes mellitus and can be overlooked or attributed to other medical disorders. Associations of thyroid disorders in type 2 diabetic patients are common [6]. Since, findings from the different study reports were differed, the prevalence rates of thyroid disorders in diabetic patients still stay debatable. Furthermore, not many studies had been pronounced in thyroid disorders in type 2 diabetes [7]. Therefore, the aim of the present study was to investigate the relationship between type 2 diabetes mellitus and thyroid dysfunction.

MATERIALS AND METHODS

Participants

Sixtyparticipant menwith age ranged from (35-65) years were involved in this study during their attendance at the National Diabetes Center (AL Mustansiriya University)in Baghdad through the period from October 2017 to April 2018. Men were selected as four groups: G1 ten healthy individuals as control group, G2 ten patients with type2 diabetes mellitus, G3 twenty patients with type2 diabetes mellitus and untreated newly diagnosed hypothyroidism, and G4 twenty patients with type2 diabetes mellitus and untreated newly diagnosed hyperthyroidism.

Blood samples collection

Blood samples were collected from each individual after (8-12) hour fasting, 5 milliliters of venous blood has been collected. One milliliters was immediately transferred into tube containing EthylenDiamine Tetra Acetic Acid (EDTA),to estimate hemoglobin A1C (HbA1C) by a sandwich immunodetection method by using ichroma. While the other were dropped into clean disposable tubes, and allowable to clot at room temperature for 15 minutes. Then it has been centrifuged for 10 minutes at 3000 run per minute until serum separated. FBS, T3, T4 and TSH were measured by using Enzyme Linked Fluorescent Assay using minividas (Biomerieux).

Statistical Analysis

The Statistical Analysis System- SAS (2012) program was used to effect of difference factors in study parameters. Least significant difference –LSD test (ANOVA) was used to significant compare between means.

RESULTS AND DISCUSSION

Determination levels of FBG and HbA1c

The level of FBG showed a highly significant ($p < 0.01$) increase in three patients groups when compared to healthy control group. While there was non-significant difference between three patients groups.Also level of HbAlc showed highly significant ($p < 0.01$) increase in three patients groups when compared to healthy control group, while there was non-significant difference between G3 and G4 and between G2 and G3.as shown in (Table 1 and Figure 1, 2).

From the result of this study, although there was not a statistically significant difference between patients groups in FBG, but it was highest in diabetes with hyperthyroidism group and the lowest in diabetes with hypothyroid group compared to healthy control group in agreement with [8]. The elevation level of FBG could also be resulting from defects in insulin secretion, insulin action or both. In hypothyroid with diabetes patients group, low FBG may be attributed to decreased metabolic rate and in hyperthyroid with diabetes patients group, increased level of FBG may be due to increased metabolic rate [9]. This study is agreed with a study by [10] the levels of HbA1c were significantly higher in patients with diabetes having thyroid disorders. Could be explained by increased insulin resistance, due to reduced rate of insulin degradation, which leads to lower the exogenous insulin requirement. The increasing of HbA1c levels in this study suggests that people with diabetes have poor control of blood glucose levels. With the increase in the duration of diabetes, the HbA1c values increase. The serum glucose is unstable in patients with diabetes mellitus and one effective way to monitor it by measured HbA1c, that provide the average blood glucose level of preceding three months [11].

Determination levels of TSH, T4 and T3

Level of TSH show highly significant ($p < 0.01$) increase in G3when compared to G1,G2, and G4. While there was highly significant ($p < 0.01$) decrease in G4 when compared to G1 and G2.Levels of T4 and T3 show highly significant ($p < 0.01$) increase in G4 when compared to G1,G2 and G3. While there was highly significant ($p < 0.01$) decrease in G3 when compared to G1 and G2. In addition, there was non-significant difference in the levels of TSH, T4, and T3 between G1 and G2. As shown in (Table 2 and Figure 3,4,5).

This result showed altered of thyroid hormone in diabetic patients was agreed with other study achieved by [12] who mentioned that altered thyroid hormone level of different magnitude (both low and high) in diabetic patients. The abnormal hormone level in diabetes may be due to the presence of thyroid hormone binding inhibitor, inhibitor of T4 toT3 conversion, dysfunction hypothalamopituitary-thyroid axisand the influence of poorly controlled diabetes on thyroid hormone concentration [13]. The presence of both high and low levels of thyroid hormones in diabetics in this study may be due to modified TRH synthesis and release, and may depend on the glycemic status of the diabetics studied. Glycemic status is influenced by insulin, which is known to modulate TRH and TSH levels [14].A variety of thyroid abnormalities may coexist and interact with diabetes mellitus. The hypo- and hyper-functioning thyroid gland influences carbohydrate metabolism at the levels of pancreatic islets and glucose-utilizing target tissues, posing important therapeutic and diagnostic questions. Moreover, thyroidal and islet cells are affected by diseases that are clinically and genetically associated, and where parallel autoimmune pathogenesis is very highly suspected. Uncontrolled hyperthyroidism in diabetic patients might trigger hyperglycaemic emergencies whereas

recurrent hypoglycaemic episodes have been reported in diabetic patients with hypothyroidism. Moreover, thyroid disorders may amplify cardiovascular disease risk in diabetic patients through inter- relationships with insulin resistance, dyslipidemia and vascular endothelial dysfunction [15].

Thyroid disorder is a biologic state and the target cell fails to respond to ordinary levels of circulating insulin resulting in failure to maintain normal glucose. Furthermore, In hypothyroidism T4 is low and TSH is high. Means the pituitary is sending more TSH to stimulate the thyroid, but the thyroid does not respond. Insufficient in thyroid hormones production and function, while elevated level of TSH resulting from lack negative-feedback stimulation to the hypothalamus and pituitary. Thyroid insufficiency leads to generalized slowing of calorigenic metabolism, including over all decreases in daily energy intake, thermogenesis, and oxygen consumption. The abnormal thyroid hormones levels may be due to various medication the diabetics were receiving, like phenylthiourea which suppress the level of T4 while causing raised levels of TSH [16].

Hyperthyroidism may result from increased synthesis and secretion of thyroxine and triiodothyronine from the thyroid, caused by thyroid stimulators in the blood or by autonomous thyroid hyperfunction. It can also result from excessive release of thyroid hormone from the thyroid without increased synthesis. Such release is commonly caused by the destructive changes of various types of thyroiditis. Various clinical syndromes also cause hyperthyroidism [19]. Hyperthyroidism causes a reduced rate of liver glucose production and this account for the decreased insulin demand in hyperthyroid diabetic patients [17].The exact explanation for the increased prevalence of autoimmune thyroid disease in T2DM is still not known. It is believed to be due to genetic and environmental factors, infections, and psychological stress. Autoimmune aspects in T2DM could be a possible link. It is believed thatinsulin resistance arises when β-cells and other immune cells react against the self-antigens. β-cells have been found to accumulate in the visceral fat of obese mice. The resulting self-antigens can trigger an autoimmune response, which in turn accelerates β-cell death [18].

CONCLUSION

This study shows the prevalence of abnormal thyroid hormones levels in type 2 diabetic patientsas compared to control. The relationship between thyroid disorders and diabetes is described by a complex interdependent interaction. Failure to recognize the presence of abnormal thyroid hormones levels in diabetic patients may be a primary cause of poor management often encountered in some treated diabetics.

REFERENCES

1. Sachin, B., Mahesh, M., Sachin, S., Vaishali, G.2013. Evaluation of thyroid hormones in patients with type II diabetes mellitus. J Med Educ Res. 3(2):9-33.
2. Singh, G., Gupta, V., Sharma AK., et al. 2011. Evaluation of thyroid dysfunction among type 2 diabetic Punjabi population. Advbiores. 2:3-9.
3. Kordonouri, O., Charpentier, N., Hartmann, R. 2011.GADA positivity at onset of type 1 diabetes is a risk factor for the development of autoimmune thyroiditis. Pediatr Diabetes.12: 31-33.
4. Hollowell, J.G., Staehling, N.W., Flanders, W.D., Hannon, W.H., Gunter, E.W., et al. 2002. Serum TSH, T(4), and thyroid antibodies in the United States population (1988 to 1994): National Health and Nutrition Examination Survey (NHANES III). J ClinEndocrinolMetab. 87: 489-499.
5. Mukherjee, S., Datta, S., Datta, P., Mukherjee, A.K., Maisnam, I. 2015. A study of prevalence of primary hypothyroidism in recently diagnosed type 2 diabetes mellitus in a tertiary care hospital. Int J Sci Rep.1(2):105-112.
6. Wu, P. 2000. Thyroid disease and diabetes. Clin diabetes. 18: 38-39.

7. Devi, M.A., Singh, L.S., Singh, N.S. 2013. Association of Thyroid Disorder in Type 2 Diabetic Patient.9(3): 23-24.
8. Dogantekin, A., Gurel, A., Ozkan, Y. 2015. Fasting Blood Glucose Levels and Lipid Profile in Patients with Thyroid Dysfunction. Sch. J. App. Med. Sci. 3(3F):1447-1449.
9. Kadiyala, R., Peter, R., Okosieme, O. 2010. Thyroid dysfunction in patients with diabetes: clinical implications and screening strategies. Int. J. Clin. Pract. 64(8): 1130-1139.
10. Khurana, A., Dhoat, P., Jain, G. 2016. Prevalence of thyroid disorders in patients of type 2 diabetes mellitus. JIACM. 17(1):12-15.
11. d'Emden, M. 2016.Glycatedhaemoglobin for the diagnosis of diabetes. Australian Prescriber. 37(3): 98-100
12. Islam, S., Yesmine, S., Khan, S.A.,Alam, N.H., Islam, S. 2008. A comparative study of thyroid hormone levels in diabetic and non-diabetic patients. Southeast Asian J. Trop. Med. Public Health. 39(5): 913-916.
13. Chen, H.S., Wu, T.E., Jap, T.S., Lu, R.A., Wang, M.L., Chen, R. L., Lin, H.D. 2007. Subclinical hypothyroidism is a risk factor for nephropathy and cardiovascular diseases in Type 2 diabetic patients. Diabet. Med. 24(12): 1336-1344.
14. Kitahara, C.M., Platz, E.A., Ladenson, P.W., Mondul, A. M., Menke, A.de., González, A.B. 2012. Body fatness and markers of thyroid function among US men and women. PLoS One. 7(4): 34979.
15. Eckel, R.H., Grundy, S.M., Zimmet, P.Z.,2005. The metabolic syndrome. The lancet. 365(9468): 1415-1428.
16. Carreras-González G, Pérez, A. 2007. Thyroid autoimmunity at onset of type 1 diabetes as a predictor of thyroid dysfunction. Diabetes Care. 30(6): 1611-1612.
17. Mitrou, P., Dimitriadis, G., Raptis, S.A. 2014. Diabetes and hyperthyroidism. Diabetes Secondary to Endocrine and Pancreatic Disorders. 22: 52-63.
18. Witting, V., Bergis, D., Sadet, D., Badenhoop, K. 2014. Thyroid disease in insulin-treated patients with type 2 diabetes: a retrospective study. Thyroid research. 7(1): 2.
19. Tayde, P., Borle, A., Zanwar, Y., Rode, M., Phatak, M. 2013. Glycated hemoglobin pattern andits correlation with lipid profile in type 2 diabetic males in central India. Nat. J. Com. Med. 4 (4): 564-569.

Table 1. Shows FBG and HbA1c levels in study groups

Groups	No. of subject	Mean ± SE	
		FBG (mg/dl)	HbA1c (%)
Healthy control	15	86.46 ± 1.78 b	4.70 ± 0.09 c
Diabetic	15	164.86 ± 4.87 a	8.31 ± 0.38 b
Diabetes with hypothyroidism	30	163.50 ± 4.23 a	8.56 ± 0.24 ab
Diabetes with hyperthyroidism	30	177.16 ± 4.72 a	9.35 ± 0.35 a
LSD value		13.672 **	0.931 **
P-value		0.0001	0.0001
** (P<0.01)Means having with the different letters in same column differed significantly			

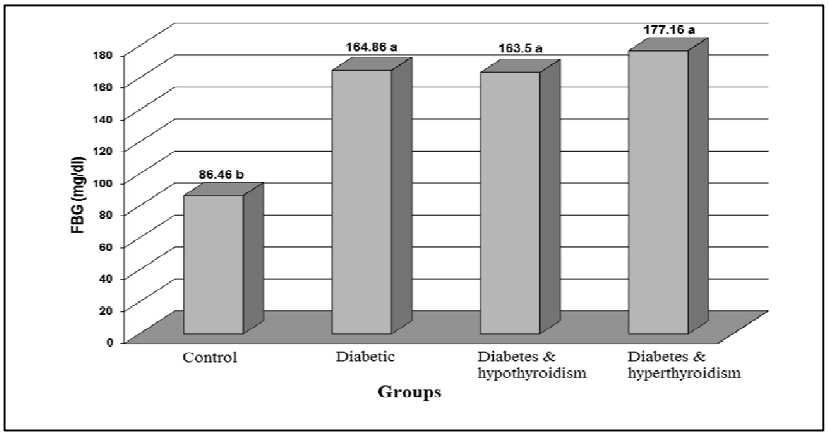

Figure 1: Level of FBG in study groups

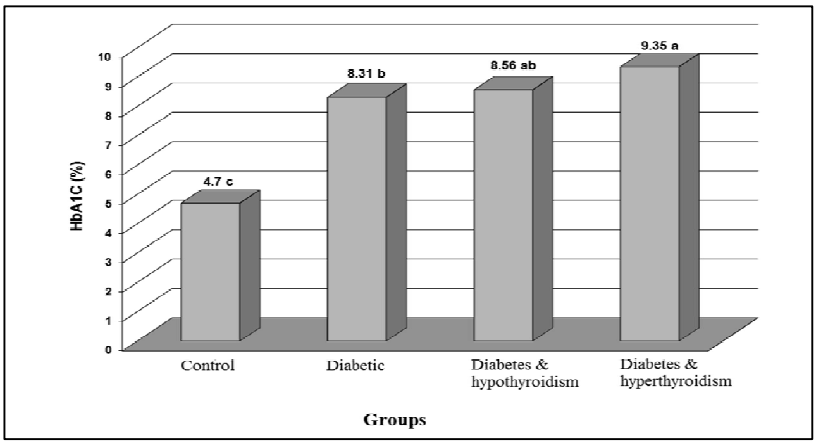

Figure 2: Level of HbA1c in study groups

Table 2.Shows T4, T3 and TSH levels in study groups

Groups	No. of subject	Mean ± SE		
		TSH (µmol/L)	T4 (nmol/L)	T3 (nmol/L)
Healthy control	15	2.40 ± 0.26 b	99.97 ± 5.68 b	1.20 ± 0.06 b
Diabetic	15	2.73 ± 0.28 b	111.09 ± 6.00 b	1.60 ± 0.11 b
Diabetes with hypothyroidism	30	35.01 ± 2.53 a	39.02 ± 1.99 c	0.50 ± 0.03 c
Diabetes with hyperthyroidism	30	0.021 ± 0.004 c	201.03 ± 4.37 a	6.11 ± 0.35 a
LSD value		5.078 **	12.584 **	0.727 **
P-value		0.0001	0.0001	0.0001
** (P<0.01) Means having with the different letters in same column differed significantly				

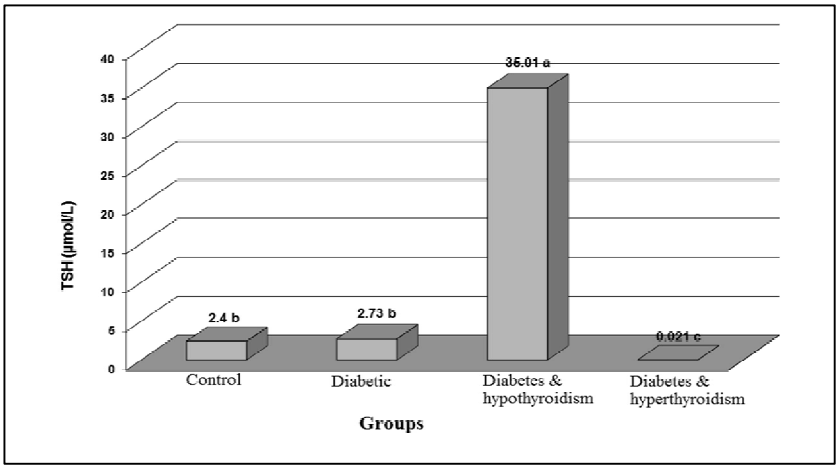

Figure 3: Level of TSH in study groups

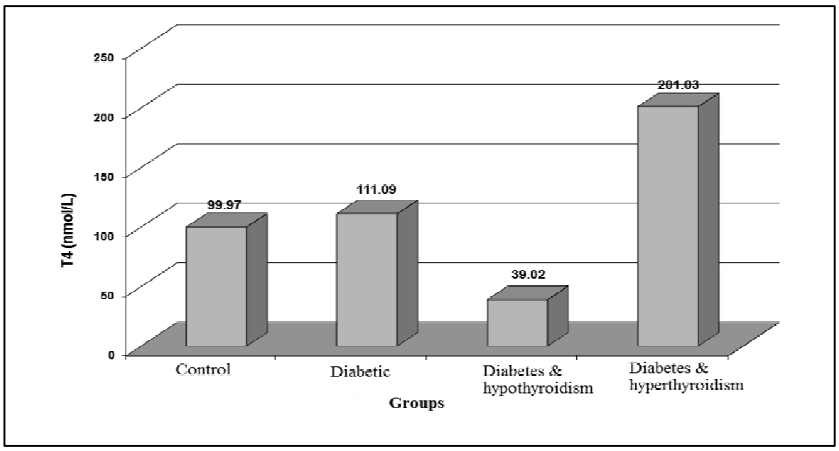

Figure 4: Level of T4 in study groups

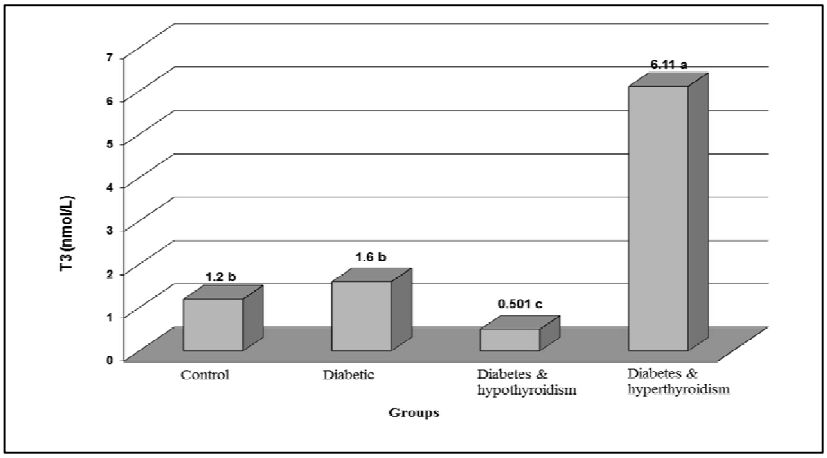

Figure 5: Level of T3 in study groups

Indian Journal of Natural Sciences www.tnsroindia.org.in ©IJONS

Vol.9 /Issue 51 / December / 2018 *International Bimonthly* *ISSN: 0976 – 0997*

REVIEW ARTICLE

The Role of Potassium, Sodium and Chlorides in the Poultry Nutrition

Ahmed M. Al-Nedawi*

Department of Animal Production, College of Agricultural Engineering Science, University of Baghdad, Iraq

Received: 20 Aug 2018 Revised: 23 Sep 2018 Accepted: 26 Oct 2018

***Address for Correspondence**
Ahmed M. Al-Nedawi
Department of Animal Production,
College of Agricultural Engineering Science,
University of Baghdad, Iraq.

ABSTRACT

The broilers represent the most important source of meat for Iraqi consumers, therefore, it is very imperative to know the role of electrolytes (Soduim, Potassium and Clorides) in the poultry nutrition. The mentioned electrolytes play an important role in the maintaining of the body acid-base balance along with the osmotic pressure in body fluids. All three elements act as the synergistic action to product these processes. However, it is so difficult to separate the role of each individual component unless taking into our consideration the other two elements. There are three major factors – balance and ratio of electrolytes in feed, endogenous acid production and level of renal activity- are determined the maintenance of this value. Electrolyte imbalance is quite rare, As the body's buffering system provides maintenance of normal physiological pH value, the electrolyte imbalance is not common to happen. We will try in this article to highlight on the role, importance and needs of poultry for sodium, potassium and chlorides in diet.

Key words: sodium, potassium, chlorides and poultry

INTRODUCTION

Currently there is an understanding of the need to achieve a balance between cation and anion supply, however, the requirements for sodium, potassium and chlorides have been clearly defined (Leeson and Summers, 2001). The formula Na+K-Cl expressed as mEq/kg meal is used to describe the electrolyte balance. The optimal for normal physiological function is 250 mEq/kg. The electrolyte imbalance is not common, because of the body's buffering system act to provide maintenance of normal physiological pH value. The maintenance of this value is determined by three major factors – balance and ratio of electrolytes in feed, endogenous acid production and level of renal ac-tivity. Electrolyte balance formula designated by Mongin (1981) is as following:

Na+K-Cl in feed = feed cations – anions + endogenous acids + excess base Feed anion balance value other than 250 mEq/kg feed results in acidosis or alkalosis, which causes both production and health problems. The adding of Na (without Cl^-) in feed leads to an increase in concentration of HCO3-ions and elevated blood pH, whereas the adding of Cl^- (without Na) will lead to decreases the concentration of HCO3- ions and pH value. The endogenous acid production affects the electrolyte balance. Also it could change according to protein source in feed. In this regards, Mongin, (1981) reported that the replacement of soybean meal with fish meal led to modification of electrolyte balance from17.4 to 12.1 mEq/kg feed. When the anion imbalance occur it can be corrected by bicarbonate supplementation in the diet. Mongin, (1981) recommends to use the fishmeal-based poultry diets with sulfates to get the electrolyte balance. The use of some divalent ions can interfere with electrolyte balance. Thus, supplementation of calcium chloride (CaCl2) in the diet can induce acidosis in poultry, contrary to chloride sources such as NaCl and KCl, as they are associated with acidosis to a much lesser extent because of the calcium absorption from CaCl2 is lower than that of sodium from NaCl. Calcium bounds to carbonates from CaCO3 using up bicarbonates from blood, and excessive unabsorbed chlorine causes acidosis.

Some examples of electrolyte imbalance are tibial dyschondroplasia and respiratory alkalosis. Tibial dyschondroplasia in chicks could be occurred as a result of the consequence of electrolytic misbalance. The condition is associated with a range of factors including administration of NH4Cl in feed production (Leeson and Summers, 2001).Broilers and layers differ in their requirements and reactions to electrolyte therapy in conditions of heat stress. Thus, treatment with aqueous electrolyte solutions positively affects the growth rate and decreases the mortality in broilers. Whiting et al. (1991) confirmed that positive effects of electrolyte supplementation in drinking water for broilers during heat stress are attributed to the increased water intake rather than to anion/cation status

Electrolyte balance can affect the metabolism of numerous amino acids, especially lysine and methionine. It is well established that deficit of potassium in feed induces increased lysine accumulation in tissues (Leeson and Summers, 2001).Electrolyte imbalance can be prevented by balancing anion and cation contents in poultry feed formulations. Thus, wheat has better electrolyte balance than maize, whereas soybean and other protein feeds have very low electrolyte balance due to high potassium content. Electrolyte balance should be considered when changing the protein source in the diet (Baloš et al., 2016).

SODIUM (Na)

Sodium is an essential element for normal life cycle and metabolism of both plants and animals as it is the major cation in extracellular fluid. Sodium makes about 93% of the total cation content in blood plasma (Leeson and Summers, 2001). Its important role has been detected as early as in 1881. Sodium is the basic constituent of salt, and all animals manifest strong need for salt.

Physiological role of sodium

The functions of sodium are the following:

- involvement in the maintenance of acid-base balance and optimal osmotic relationships;
- involvement in the regulation of body fluid volume;
- involvement in muscle cell contractions;

Close relation with adrenal gland functions; has a role in carbohydrate absorption, that is, energy turnover in the body.

Sodium content in poultry ranges from 0.1 to 0.14% of the body mass. About 30-40% of sodium is found in the skeleton, tightly bound to the inorganic part of the bone, thus being hardly available for satisfying animal's needs.

Sodium content in blood plasma of chickens is 8.4 mg/ml (Leeson and Summers, 2001), that is, 122–160 mmol/l in chickens and 145–147 mmol/l in turkey (Puls, 1990).

Sodium absorption and homeostasis

Sodium is readily absorbed from small intestines, while certain amount is absorbed in the stomach. Some 85–90% of dietary sodium is excreted in the urine in the form of phosphates or chlorides (Jovanović et al., 2001).

Sodium metabolism

Active transport of sodium and potassium ions is of vital physiological importance. More than one third of adenosine triphosphate (ATP) consumed by a resting animal is used for active transport of sodium and potassium (Leeson and Summers, 2001). Adenosine triphosphates are enzymes hydrolyzing ATR in the presence of sodium and potassium together with magnesium ions. By breaking ATR, the enzymes provide energy for active ion transport and pump three sodium ions out of the cell (Baloš et al., 2016).

Sodium deficiency

Less pronounced sodium deficiency in chickens causes poor growth, soft bones, corneal keratinization and decreased blood plasma volume. In lay-ing hens, the symptoms mainly include decreased egg production, impaired growth and sometimes even cannibalism. A range of diseases are associated with vast excretion of sodium from the body, diarrhea and other gastrointes-tinal disorders or urinary losses consequent to renal failure or adrenal gland insufficiency. Poultry diet with sodium content below 0.012–0.050% is consid-ered sodium-deficient (Puls, 1990).

Excess of sodium

Sodium content in poultry feed at levels above 0.5% is considered toxic. Even dietary sodium contents of some 0.35% stimulate in-creased water intake in poultry, thus causing electrolyte imbalance, and el-evated sodium levels result in water toxicity. Excess of dietary sodium in laying hens (above 0.19% of feed mix) causes decreased egg fertility (Puls, 1990) and poor quality of the eggshell (Leeson and Summers, 2001).

Sodium requirements in poultry

Sodium requirements for young birds are 0.15% of feed, provided that the level of chlorides is the same. For laying hens, the recommended levels range from 0.17-0.19%. The ratio of sodium and chloride levels in poultry diet should be 1 : 1(Baloš et al., 2016).

Murakami et al. (1997) recommend 0.25% sodium content in formulations for 21-day broilers. Linear relationship between growth rate and dietary sodium level for young poultry has been established, and the limit is commonly deter-mined by manure consistency.

The sources of Sodium

Feeds of animal origin are particularly rich in sodium, as it is present in almost all tissues. Feeds of plant origin contain significantly lower sodium levels, and its content varies depending on numerous factors. Sodium content in grains ranges from 80 mg/kg in maize to over 500 mg/kg in oat grain, the contents in oilseed range 150-170 mg/kg and in wheat bran around 250 mg/kg (Živkov-Baloš et al., 1999).

Ahmed M. Al-Nedawi

POTASSIUM (K)

Potassium is the third most abundant element found in the body of most animals (NRC, 2005). The potassium is found in the body, that is, inside the cell itself. Blood cell level of potassium is about 25 times higher than that of plasma cells. High potassium contents are characteristic for muscle and nerve cells, being some 4 mg/kg in muscles as compared to 0.1 mg/ ml in blood plasma (Leeson and Summers, 2001).

Physiological role of potassium

The most important roles of potassium include:

- participation in the maintenance of acid-base balance and optimal osmotic relationships;
- activation of the range of intracellular enzymes;
- participation in protein and carbohydrate metabolism;
- playing essential role in preserving normal heart function as it decreases the contractility of cardiac musculature and favors heart muscle relaxation;
- increasing the permeability of cell membrane;
- promoting the absorption of free neutral amino acids such as glycine

Potassium metabolism and deficiency

The major manifestation of potassium deficiency (hypokalemia) includes generalized muscle weakness with subsequent limb weakness, decreased intestinal tonus associated with distension cardiac insufficiency as well as respiratory insufficiency and failure. Hypokalemia can occur consequent to severe stress.Low levels of dietary protein combined with low potassium levels or during fasting period result in poor growth of animals. Potassium to nitrogen ratio in muscles and urine is relatively stable, thus, these two elements are released simultaneously during the process of body-tissue decomposition.

Excess of potassium

Potassium toxicities in healthy animals are rare. This is because of the body's ability to readily excrete potassium as well as regulate absorption. The major causes of hyperkalemia are excessive potassium intake, reduced renal losses, and redistribution of potassium (NRC, 2005). Teeter and Smith (1986) found no adverse effects when potassium (as KCl) was supplied in water with corn-soybean base diet containing 7,300 mg K/kg and when fed to week-old chicken pullets for two weeks under near optimal environmental conditions.Smith et al. (2000) reported that the increase in the dietary concentration of potassium from 2,300 to 20,000 mg/kg caused a linear increase in water intake, water to feed ratio, and excreta moisture of layers.

Potassium requirements in poultry

Potassium deficiency is rarely observed in practice since standard poultry feed mixes contain more than 1% K (Puls, 1990). Potassium contents in feed should range between 0.4 and 0.6% of feed mix.Potassium level in the body correlates with muscle mass, so it is used to calculate the body mass in vivo applying radioactive isotope of potassium – K40, since ratio of K40 and total K is constant (Jovanović et al., 2001).

Potassium sources

Feeds of plant origin are rich in potassium, thus, supplementation is not necessary (Živkov-Baloš et al. 1999).

CHLORIDES (Cl^-)

The major part of chlorine is chloride which is found in extracellular fluids and also in red blood cells and other tissues. The elements are absorbed in small intestines; excess chloride is eliminated in the urine and is usually associated with excess sodium and potassium.

Physiological role of chlorides

The chlorides have some distinct independent functions such as:

- Chlorine is major anion of gastric juice and builds up gastric acid together with hydrogen ion;
- It participates in carbon-dioxide transport in the blood thus increasing plasma bicarbonate content

Chloride Metabolism and deficiency

Chloride ions have weak affinity of binding to protein ions, and enter the cell together with potassium. Chlorides are actively transported particularly via the cells of gastric mucosa. Chloride deficiency in chickens is associated with extremely poor growth, limb weak-ness, poor bone mineralization, high mortality rate.

Chloride requirements in poultry

Chloride contents for poultry have to be balanced according to the requirements and/or potassium and sodium levels in the diet. Generally, the concentration of chlorides in the feed should be 10-15% higher than that of sodium (Puls, 1990).

Excess of chloride

Excess salt in drinking water manifests more severe toxic effects as compared with feed (Puls, 1990). In young growing birds, 2.7% salt in the diet, lead to rapid mortality (Morrison et al., 1975).Excess chlorides in poultry feed leads to wet feces, extreme water consumption, ascites, edema, reduced thickness and hardness of the eggshell (Smith et al. (2000).

Chloride sources

Feed formulations based on maize and soybeans are very poor sources of natural sodium chloride. Supplementation of fishmeal into the feed reduces the requirements for salt. Major source of chlorides in animal feed is animal salt or kitchen salt.

CONCLUSION

Sodium, potassium and chlorides play an important role in maintaining body acid-base balance as well as osmotic pressure in body fluids. These processes are the result of synergetic action of all three elements, and the role of each individual component is difficult to define without knowing and taking into consideration the other two elements.

REFERENCES

1. Jovanović R, Dujić D, Glamočić D. Ishrana domaćih životinja, 2. izmen-jeno i dopunjeno izdanje, Stylos-Izdavaštvo, Novi Sad, 2001.

2. Leeson S, Summers JD. Scott's nutrition of the chicken. Chapter 5 – Min-erals. 4th edition. Published by University books, Guelph, Ontario, Canada, 2001, 341-363.
3. Mongin P. Recent advances in dietary anion/cation balance in poultry.Recent Adv. Anim. Nutr.1981, 109-119.
4. Morrison WD, Ferguson AE, Pettit JR, Cunnigham DC. The effects of elevated levels of sodium chloride on ascites and related problems in turkeys. Poult. Sci. 1975, 54. 146-154.
5. National Research Council (NRC). Mineral tolerance of animals. Second revised edition, Committee on minerals and toxic substances in diets and water for animals, Board on agriculture and natural resources, Division on earth and life studies. National Academy Press, Washington D.C., 2005.
6. Puls R. Mineral levels in animal health. Diagnostic data. Published by Sherpa International, Clearbrook, British Columbia, Canada, 1990.
7. Smith AS, Rose RG, Pirgozliev V. Effect of excess dietary sodium, potassium, calcium, and phosphorus on excreta moisture of laying hens. Br. Poult. Sci.,2000, 41, 598-607.
8. Teeter RG, Smith MO. High chronic ambient temperature stress effects on broiler acid-base balance and their response to supplemental ammo-nium chloride, potassium chloride, and potassium carbonate. Poult. Sci.1986, 65, 1777-1781.
9. Whiting TS, Andrews LD, Stamps L. Effects of sodium bicarbonate and potassium chloride drinking water supplementation. Poultry Sci. 1991,70, 53-59.
10. Živkov-Baloš M, Mihaljev Ž, Mašić Z. Količine makro i mikroelemenata u hranivima sa područja Vojvodine. Savremena poljoprivreda, 1999,1-2, 285-288.

Indian Journal of Natural Sciences www.tnsroindia.org.in ©IJONS

Vol.9 /Issue 51 / December / 2018 *International Bimonthly* *ISSN: 0976 – 0997*

RESEARCH ARTICLE

Statistical Study for the Sun's Radio Observation Data Using Noise Elimination Techniques

Mohammed R. Hoobi* and Kamal M.Abood

Department of Astronomy and Space, College of Science, University of Baghdad, Baghdad, Iraq

Received: 17 Aug 2018 Revised: 23 Sep 2018 Accepted: 26 Oct 2018

***Address for Correspondence**
Mohammed R. Hoobi
Department of Astronomy and Space,
College of Science, University of Baghdad,
Baghdad, Iraq
Email.

ABSTRACT

Two statistical method studies for radio observation data files are achieved in this research; First method the noise elimination average technique, and Second method the noise elimination Gaussian function technique. A comparison between the two method is carried out using observed data file for sun in day 3/1/2018, for one hour time interval.

Key words: The Noise Elimination, Average Technique, Gaussian Function Technique, Radio Observations

INTRODUCTION

No matter what the astronomical application, radiofrequency interference (RFI) and other radio noise sources is becoming an increasingproblem in radio astronomy, and many methods forremoving or canceling the RFI are being proposed, evaluated and implemented. In most cases, the astronomer'stargets are the correlations of signals from the antenna, and it is need longer time observationaverages of power that are wanted—there is no requirementto preserve voltage modulation. These applicationsare generally either finding the autocorrelation of signalsfrom a single antenna (to measure the power spectrum of the astronomy signal) [1][2].Suppose that a sampled voltage stream consists ofan additive mixture of components that are uncorrelatedwith each other. Suppose also that each component isstatistically stationary so that if the component happensto be present in more than one voltage stream the phasedifference and the ratio of the sampled amplitudes measured at the receiver are constant [3].

METHODOLOGY

The Noise Elimination by using Average Technique

The sun observation data at date 3/1/2018 and time 9:38:43 AM is stored in the computer, these data are analyzed by using the average technique to eliminate the noise in this data, and this technique is by taking the average of each row in the file and its related on time observation period. For example, by displaying the observation data file with Microsoft Excel for the date 3/1/2018 and starts with time 9:38:43 AM and ends with 10:38:13 AM, found that each row in the file represent a power received at specific time and by plotting the power or the amplitude with frequency at this time 10:00:03 AM, as in figure (1).Figure (1), represent a noisy spectrum at this time 10:00:03 AM. So after applying the average technique on this data file and taking the average for each row for each time and make it one row that represents the whole time observation to give us an accumulation for the received data and plot it with the frequency, as in figure (2).Figure (2), represent a less noisy spectrum and show the difference before and after applying this technique.Then by taking a small part from the spectrum to see the power received at a specific frequency range between (1.39 GHz – 1.43 GHz) to see where the signal is located, as in figure (3).Then by applying the noise elimination average technique on this range of frequencies, the peak will be much clearer and appears at frequency 1402.662000 MHz, as in figure (4).

The Noise Elimination by using Gaussian Function Technique

The sun observation data at date 3/1/2018 and time 09:38:43 AM is carried out, then the observation data is stored in the computer. These data are analyzed by using a program code in (MATLAB R2017a) to eliminate the noise using Gaussian Function Technique.First of all, select the data and take the spectrum at a certain time, then generate a 1-D gaussian function with input multi values of standard deviation $0.1 \leq \sigma \leq 2$, and convolve the selected data with the gaussian function. The result data behavior became smoother; the block diagram is shown in figure (5) explain the technique procedure:Figure (6), represent the relationship between frequency (Hz) and power received (dBm) for three selected times (09:38:43 AM, 10:08:43 AM, 10:38:13 AM) respectively in 3/1/2018, to show the difference of the received power with time. So the figure represents a noisy spectrum.

Then by applying the Gaussian function technique for the same spectrum and for the same time, the spectrum will be clearer and the peaks will appear sharper, as in figure (7).The figure shows the relationship between the frequency and amplitude after applying the gaussian function elimination to eliminate the noise.
Then by taking a small part from the spectrum to see the power received at a specific frequency range between (1.39 GHz – 1.43 GHz) to see where the signal is located, as in figure (8).

Then by applying the noise elimination gaussian technique on this range of frequencies, the peak will be much clearer and appear nearly at frequency 1402.662000 MHz, as in figure (9).

CONCLUSION

From the data analysis by using time interval equal to 1 hour, which is appear that is small enough to effect on the data elimination noise and its prefer that taking longer observation time such as two hours or more.In the Gaussian elimination technique, multi values of standard deviation are applied in Gaussian elimination on the data to test for better results, and we found that when the standard deviation ($\sigma = 1$) gives us the best results.Finally, we conclude that the noise in radio observations datadue to the atmospheric turbulence,the interference noise, and ground stations influence in the telescope location area. The suggested two noise elimination techniques are the best solution to eliminate or reduce this noise.

REFERENCES

1. Thompson, A. R., J. M. Moran, and G. W. Swenson, (1986), "Interferometry and Synthesis in Radio Astronomy", John Wiely, Hoboken, N. J..
2. Taylor, G. B., R. A. Perley, and C. L. Carilli (Eds.), (1999), "Synthesis Imaging in Radio Astronomy II", Astron. Sec. Pac. Conf. Ser., vol. 180, Astron. Soc. Of the Pac., San Francisco, Calif.
3. Barnbaum, C., and R. F. Bradley, (1998), "A New Approach to Interference excision in radio astronomy: Real-time adaptive cancellation", Astron. J., 116, 25598-2614.
4. Mohammed R. Hoobi, Kamal M. Abood, (2018), "The Installation of Three Meter Small Radio Telescope in Baghdad University", Submitted to Iraqi Journal of Science, Baghdad University, Baghdad, Iraq.
5. Mohammed R. Hoobi, Kamal M. Abood, (2018), "Calibration of Three Meter Small Radio Telescope in Baghdad University using the Sun as a Reference Source", Submitted to Iraqi Journal of Science, Baghdad University, Baghdad, Iraq.

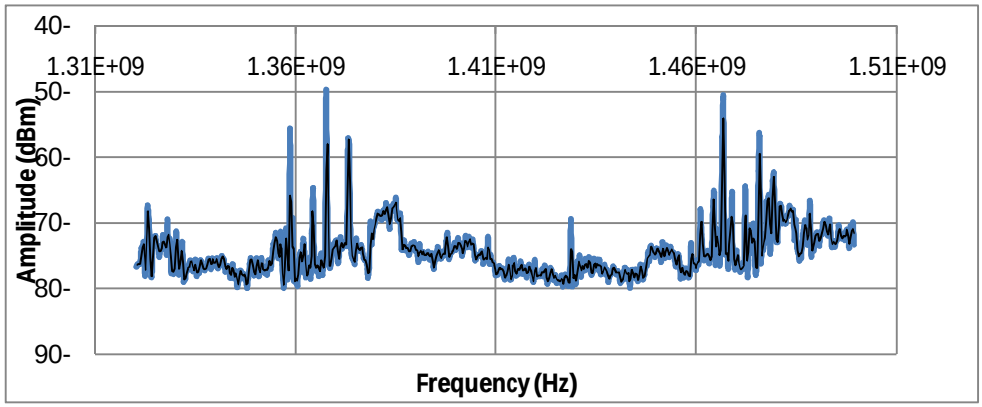

Figure 1: Represent the relationship between Frequency (Hz) and Amplitude (dBm) at time 10:00:03 AM

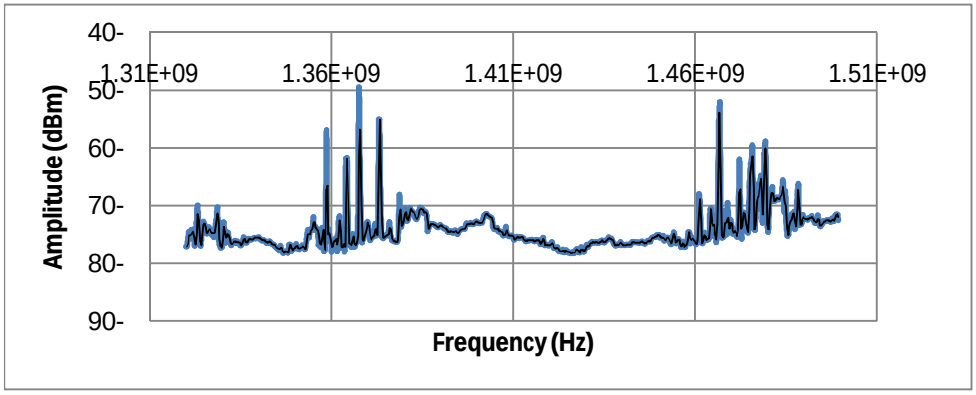

Figure 2: Represent the relationship between Frequency (Hz) and Amplitude (dBm) after applying average technique

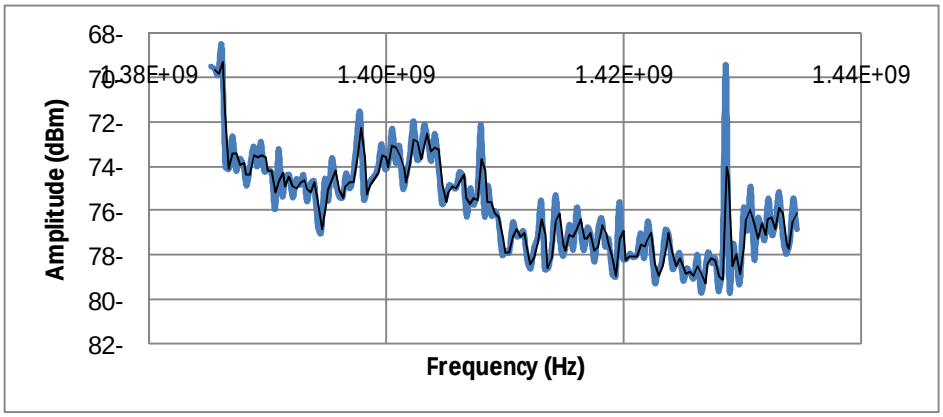

Figure 3: Represent the relationship between Frequency (Hz) and Amplitude (dBm) before applying the noise elimination average technique

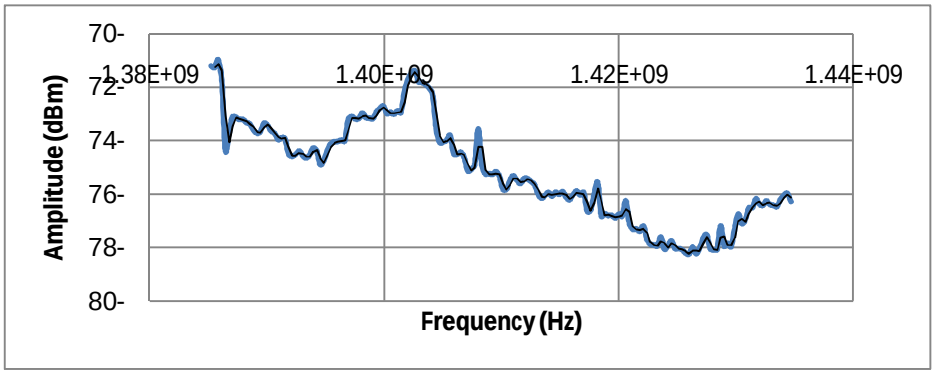

Figure 4 : Represent the relationship between Frequency (Hz) and Amplitude (dBm) after applying the noise elimination average technique

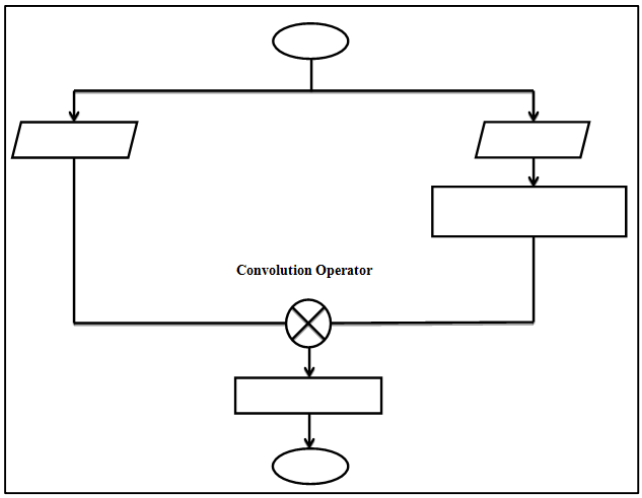

Figure 5 : Gaussian noise elimination technique block diagram

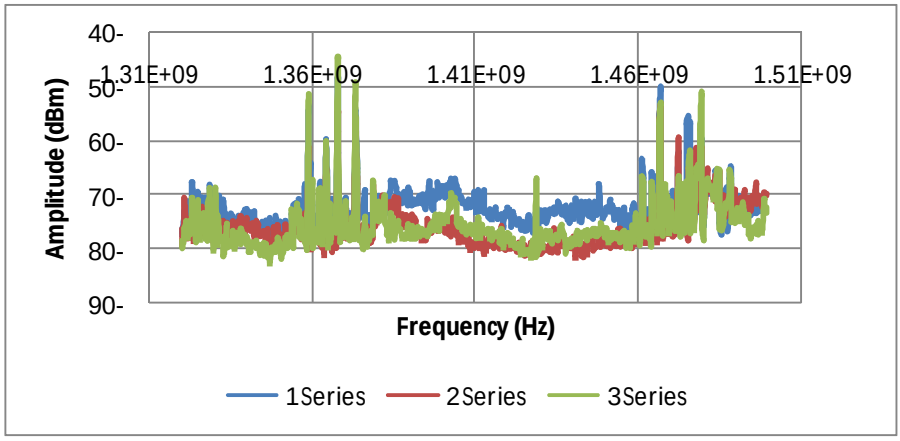

Figure 6: Represent the relationship between Frequency (Hz) and Amplitude (dBm) before applying the Gaussian function technique for different times, Blue for 09:38:43 AM, Red for 10:08:43 AM, Green for 10:38:13 AM

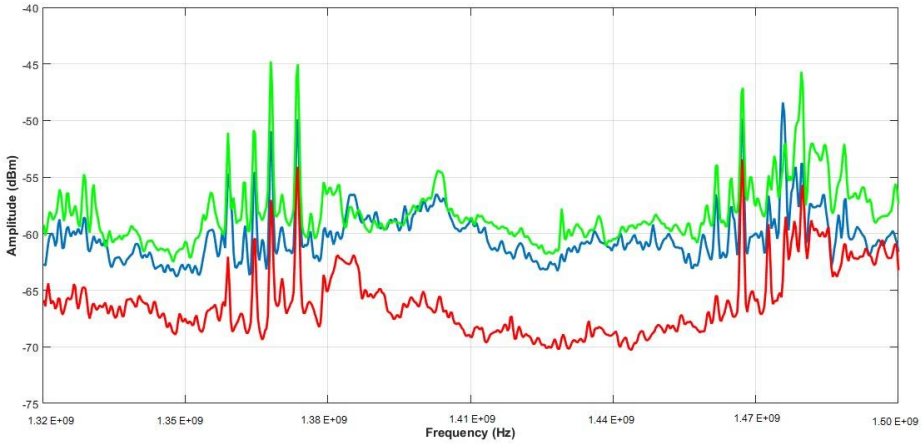

Figure 7 : The relationship between Frequency (Hz) and Amplitude (dBm)

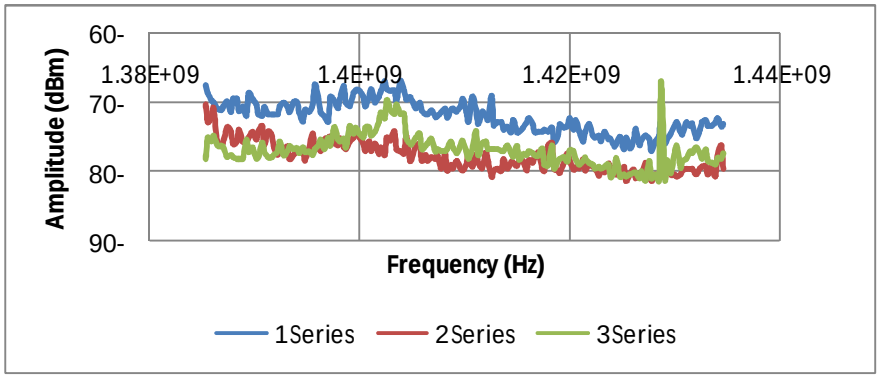

Figure 8: Represent the relationship between Frequency (Hz) and Amplitude (dBm) before applying the noise elimination gaussian technique

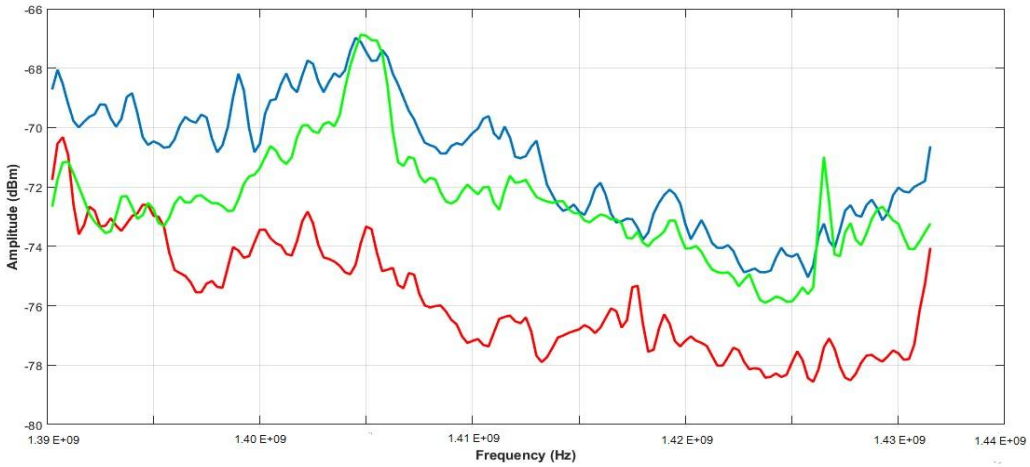

Figure 9: Represent the relationship between Frequency (Hz) and Amplitude (dBm) after applying the noise elimination gaussian technique

Indian Journal of Natural Sciences www.tnsroindia.org.in ©IJONS

Vol.9 /Issue 51 / December / 2018 *International Bimonthly* *ISSN: 0976 – 0997*

REVIEW ARTICLE

Spectral Multi-Wavelength Properties of a RBSC-NVSS Observation for a Sample of Active Galaxies

M. N.Al Najm*, Y.E.Rashed and Hasanain.H. AL-Dahlaky

Department of Astronomy and Space, Collage of Science, University of Baghdad, Baghdad - Aljadirya, Iraq.

Received: 23 Aug 2018 Revised: 25 Sep 2018 Accepted: 27 Oct 2018

***Address for Correspondence**
M. N. Al Najm
Department of Astronomy and Space,
College of Science, University of Baghdad,
Baghdad - Aljadirya, Iraq
Email.: mohalnajm72@yahoo.com

ABSTRACT

We report a statistical analysis of samples of galaxies with active galactic nuclei (Seyferts 1, Seyferts 2, and quasars) taken from ROSAT Bright Source Catalogue (RBSC) and the NRAO VLA Sky Survey (NVSS) of bright X-ray galaxies. We investigate multi-wavelength observations including in the radio (1.4 GHz), the blue optical (4400 A⁰) and the X-ray (0.1-2.4 keV) bands. For Seyfert 1 galaxies the results of a statistical analysis shows that there is a strong correlation between the quantities ($L_{X-ray} - D$ and $L_{1.4} - D$ correlations), and the slopes of the relation($L_B - D$) are flatter than the slope of 0.5 expected for cosmologically nearby objects, while for Seyfert 2 type galaxies, we find that a very strong correlation between relation($L_{X-ray} - D$ and $L_B - D$), which indicates that, the Seyfert 2 have active components unrelated with the radio emission compared to Seyfert 1. We also found that, the Seyfert 1 and 2 galaxies show a strong linear relation between ($L_{X-ray} - D$), which could be related to the presence a very high X-rays emission in broad emission lines in their nucleus. The slopes of the relation between the X-ray emission and distance galaxies for QSO galaxies are significantly steeper than radio continuum, blue emissions and distance (slope ~ 1) with probability of chance correlation, $P < 10^{-7}$. We can conclude that, the presence of a large star formation activity in these galaxies depends linearly on the correlations between galactic luminosities and distance. At large distances this effect may be dominant.

Key words: Galaxies: Nuclei – Radio continuum: galaxies – Techniques: spectroscopy, Active galaxies: Seyfert – Quasars.

INTRODUCTION

In gernral the emission-lines that lay on the spectra of active galaxies can divided into two main types: First type is broad emission-line which can be broad up to ~$10000\ \mathrm{km\ s^{-1}}$, due to the Doppler broading effect, in addition, such an emission-line are mainly related to Seyfert galaxies type 1 and QSOs, or quasistellar objects. Second type is narrow emission-line which has width of ≤ $1000\ \mathrm{kms^{-1}}$, and such an emission-line are mainly related to Seyfert galaxies type 2.

Since the late of the last century till now, many paper had deals with galaxies that has active galactic nuclei host in the center of these objects. Some of those papers studied the nature of these sources via using spectroscopic and photometric data [1-4]. Other projects studied the physical properties of active galaxies by using different wavelength (X-ray, Radio, Infrared, Ultraviolet, and Optical) observations [5-8]. One of these properties is the relation between luminosity (L) and redshift (z). Where in the eighth of the last century some paper have been appeared to clarify this relation (L-z), and find how much these parameters are correlated[9] had studied 273 objects of active galaxies divide to (235 Quasars and 38 Seyfert-1 galaxies) via using X-ray radiation, and they found that there is a linear regression line between the X-ray luminosity $\mathrm{L_{X-ray}}$ an redshift for these samples following this formula: $\log \mathrm{L_{X-ray}} = 41.2 + 1.5 \times \log z$ and the coefficient correlation is R=0.905. Following the last paper [10] studied the extragalactic objects at different redshift and they conclude that there is a linear behavior between the $\mathrm{L_{X-ray}}$ and z for the high redshift sources, except some galaxies clusters. Some authors[11] studied a survey (Spitzer Space Telescope imaging surveys) for a large numbers of AGN sources and they plot between the luminosity at $5\mu m$ and redshift and they confirm the linear correlation between these two parameters.

In this work we plot between the luminosities (Radio, Optical, and X-ray) and distance instead of redshift for Seyfert galaxies (type 1 and 2), becuase these objects are kind of close to us $(0.0024 \le z \le 0.818)$ therefore the relation between the distance and redshift are directly proportional. For the QSOs we plot between the luminosities (Radio, Optical, and X-ray) and distance, as well as, between the luminosities and redshift, becuase for these sources the redshift was increase from low to high values $(0.09 \le z \le 3.27)$, therefore the relation between the distance and redshift are not directly proportional for all QSO galaxies.

The details of the samples that we deals with in this project, as well as, the numbers of these sources has been mentioned in section 2. Furthermore, the mathematical methods that has been used to derive the equations that employed in this paper, in addition to the derivative of the parameters are mentioned in section 2. The statistical analysis of the samples, as well as, the correlation between the luminosities and distance and between luminosities ration and absolute magnitude are present in section 3. Finally, the discussion and conclusions follows in section 5.

THE SAMPLE, DATA USED, AND DERIVATION OF PARAMETERS

In this paper we report on a statistical analysis of a sample of (AGNs) of Seyfert galaxies (Sy1 and Sy2 Seyfert galaxy, emission-line spectra classified from type 1 to 2) and Quasars selected from an RBSC-NVSS sample. [12] have cross-identified the ROSAT Bright Source Catalogue (RBSC) and NRAO VLA Sky Survey (NVSS) to construct an RBSC-NVSS sample. On the basis of the RBSC-NVSS sample [12] , we have selected a sample of number (315) of Seyfert galaxies type (Sy1), number of (32) type (Sy2), and number of (97) Quasars type (QSO).

The luminosity $L[E_1, E_2]$ in the energy bands E_1, E_2 is given by [13,14]:

$$L[E_1, E_2] = 4\pi\, K_{corr}(z)\, D_{bol}^2(z)\, f[E_1, E_2] \qquad (1)$$

where $K_{corr}(z)$ is the K-correction term, $D_{bol}(z)$ is the bolometric luminosity distance term, $f[E_1, E_2]$ is the observed flux density in the energy band $[E_1, E_2]$, and z is the redshift. The $K_{corr}(z)$ are given by [13]:

$$K_{corr}(z) = (1+z)^{-(1+\alpha)} \qquad (2)$$

and the bolometric luminosity distance $D_{bol}(z)$:

$$D_{bol}(z) = \frac{2cz}{H_0\ (G+1)}\ [1+\frac{z}{1+G}]\quad [Mpc] \qquad (3)$$

Where

$$G = \sqrt{1+2q_0} \qquad (4)$$

If density parameters $(\Omega_M, \Omega_\Lambda, \Omega_k)$ = (1, 0, 0), then the deceleration parameter $q_0 = 0.5$ [15].We calculated the optical (L_B), radio ($L_{1.4}$) and X-ray (L_{X-ray}) luminosities from the respective formula:

$$\log L_B = 23.70 + 2\log D_{bol} - (1+\alpha_B)\log(1+z) - 0.4m_B \qquad (5)$$

$$\log L_{1.4} = 17.08 + 2\log D_{bol} - (1+\alpha_{1.4})\log(1+z) + \log f_{1.4} \qquad (6)$$

$$\log L_{X-ray} = 16.50 + 2\log D_{bol} - (1+\alpha_{X-ray})\log(1+z) + \log f_{X-ray} \qquad (7)$$

Where L_B and $L_{1.4}$ in the unit of $[W.Hz^{-1}]$, and L_{X-ray} in unit of $[L_\Theta]$. Futhermore, m_B is represent the blue magnitude at 4400Å blue-band. $f_{1.4}$ and f_{X-ray} are the radio emission flux density at 1.4 GHz in unit (mJy[1]), and X-ray flux density in the soft X-ray band of (0.1 - 2.4 KeV) in units of $[erg\ cm^{-2}\ s^{-1}]$.

We assume energy index for X-ray band $\alpha_{X-ray} = -1.02$, the optical bands $\alpha_B = -0.5$, and for the radio continuum $\alpha_{1.4} = -0.8$ [16] for the Seyfert galaxies types (Sy1 and Sy2). For Quasars type, the energy index α (from optical to X-ray bands) taken to be - 0.5 [13] For Friedman cosmology and assuming the Hubble constant $H_0 = 70\ km\ s^{-1}\ Mpc^{-1}$.

In [12] besides X-ray and radio densities flux data, the blue magnitudes, redshifts, and AGN types are also presented. For statistical investigation of the multi-frequency properties of AGN, specifically Seyfert galaxies (Sy1 and Sy2) and Quasars, the RBSC-NVSS sample provides an exceptional opportunity for a detailed study. According to equations

[1] $1\ Jy = 10^{-23} erg\ cm^{-2}\ s^{-1} Hz^{-1}$

(3,5, 6, and 7), we havecomputed all redshifts, and AGN types are also presented. For statistical investigation of the multi-frequency propertlated average parameters of Seyfert (Sy1 and Sy2) and Quasars galaxies. Table 1 presents the results of these calculations.

STATISTICAL ANALYSIS AND LUMINOSITY-DISTANCE CORRELATIONS

Investigation of an unbiased sample of active galaxies with comprehensive observationaldata on relevant parameters at different wavelengths is essential for a statistically reliable test, for understanding the different physical conditions in these objects, and to test the unification model.

For each sample of AGN galaxies (Sy1, Sy2, and QSOs) we have calculated all correlation coefficients between luminosities from (radio to X-ray) band, including distance. As a result, this procedure significantly reduced the artificial correlations between luminosities and distances caused by the fact that at large distances we observe the more powerful sources. We selected only those pairs of variables that which showed significant correlations $(P < 0.01)$. Then we performed a multiple regression analysis to comprehend more about the relationships between the parameters that involved.

In this paper we used statistical program (statistic-win-program) to find whether there is a correlation relation between many parameters such as luminosities and distance . Also we used various regression to get the graph between these parameters and calculation the significance levels (P) beside the coefficient partial correlation (R). The aim of the linear reduction method is to fit a convenient line out of the points. Precisely, the code will calculate a line so that the deviations squared detected points from that line will be minimized. Generally, this method occasionally referred to as linear least squares approximation. Generally, a various regression procedure will determine the linear formula of the form:

$$Y = a + b_1X_1 + b_2X_2 + ... + b_nX_n \qquad (8)$$

Where Y represent the dependent variable, and the independent variables are represented by X_1, X_2, ..., X_n, as well as, b_1, b_2, ..., b_n represents the slopes that used as retraction coefficients. Finally, a is regarded as the intercept. Note, the dependent variable that predicted by the independent variables are refers to the retraction coefficients that contribute independently in each independent variables. To give an example about what has been mention before or explain in another way: that means the variable Y is correlated with the variable X [16,17]. We have applied this technique for the samples of Sy1, Sy2 and QSOs galaxies.

RESULTS

In this project the investigation of multi-wavelength observational radio, blue and X-ray properties of AGNs (Sy1, Sy2 and QSO) led us to the following results:

$1-$ **For sample of number (315) of Seyfert galaxies (Sy1 types) we have data analysis (see Table2) and relation (Luminosity - Distance)**:

$$\log L_{1.4} = (0.66 \pm 0.05)\log D + (0.20 \pm 0.05)\log L_B + (9.10 \pm 2.10)$$

$$\log L_{X-ray} = (0.78 \pm 0.04)\log D + (0.16 \pm 0.04)\log L_B + (2.00 \pm 1.05)$$

$$\log L_B = (0.35 \pm 0.09)\log D + (0.30 \pm 0.08)\log L_{X-ray} + (0.21 \pm 0.06)\log L_{1.4} + (16.6 \pm 0.60)$$

2 – **For sample of number (32) of Seyfert galaxies (Sy2 types) we have data analysis as shown in Table 3and relation (Luminosity - Distance):**

- $\log L_{X-ray} = (0.78 \pm 0.10)\log D + (0.28 \pm 0.11)\log L_{1.4} + (0.30 \pm 0.10)\log L_B + (12.60 \pm 3.90)$
- $\log L_B = (0.78 \pm 0.28)\log D - (0.79 \pm 0.27)\log L_{X-ray} + (0.70 \pm 0.16)\log L_{1.4} + (15.7 \pm 1.84)$

3 – **For sample of number (97) of Quasar's (QSO types) we have data analysis as present in Table4 and relation (Luminosity - Distance):**

- $\log L_{X-ray} = (0.85 \pm 0.08)\log D + (5.73 \pm 1.16)$
- $\log L_B = (0.65 \pm 0.16)\log D + (16.50 \pm 1.16)$
- $\log L_{1.4} = (0.42 \pm 0.18)\log D + (11.40 \pm 4.03)$

4 – **The relation between luminosities and redshift (z) for QSO active galaxies is given by:**

- $\log L_{X-ray} = (0.682 \pm 0.078)z + (7 \pm 1.43)$, N=95, $R_z \sim 0.67$, $P < 10^{-7}$
- $\log L_B = (0.36 \pm 0.14)z + (0.200 \pm 0.096)\log L_{1.4} + (16.5 \pm 2.10)$, N=95, $R_z = 0.25$, $P \sim 10^{-2}$, $R_{1.4} = 0.21$, $P_{1.4} = 4 \times 10^{-2}$.

DISCUSSION AND CONCLUSIONS

In the present work Multi-wavelength observational properties of a RBSC-NVSS sample for (315) Seyfert type 1 galaxies, (32) Seyfert type 2, and (97) Quasars galaxies are studied by means of the statistical analysis. For this we used complete samples of these galaxies as shown in the Tables (2, 3, and 4). In this research, we studied the relations between blue to X-ray luminosities and distances for a different samples of active galaxies. The results of comparison between distance-luminosity have revealed different effects.

The results of statistical analysis for Seyfert galaxies type (Sy1) shown that, there is a strong relation between $\log L_{X-ray}$ and $\log D$, as well as, between $\log L_{1.4}$ and $\log D$, with a positive and a strong correlation coefficient ($R_{X-ray}, R_{1.4} = 0.75, 0.6$ respectively). Futhermore, this correlation has avery strong probability of ($P \leq 10^{-7}$),and the figures (1 and 3) shows that the slope is nearly linear ($L_{X-ray} \propto D^{0.78 \pm 0.04}$, $L_{1.4} \propto D^{0.66 \pm 0.05}$).In relation ($\log L_B$ - $\log D$) there is a clear relation with a positive and clear correlation coefficient ($R_B \approx 0.22$) and a good probability ($P \sim 10^{-4}$) and the figure 2 shows that the slope is a flat (Slope ~ 0.4).

In the relation ($\log L_{X-ray}$ - $\log D$) for Seyfert galaxies type (Sy2), there is a very strong correlation coefficient ($R \approx 0.9$) and a stronger probability ($P \leq 10^{-7}$), while in ($\log L_B$ - $\log D$) there is a clear correlation coefficient, and there is no relation between (Log L1.4 -LogD). The figures (4 and 5) shows that existence a strong linear relation between luminosities X-ray, blue and distance with slope~ 1.

For Quasars galaxies there is a strong intrinsic correlation coefficient ($R_x \sim 0.75$) of the (L_{X-ray} - D) plot and $R_z \sim 0.67$ for relation ($L_{X-ray} - z$), as well as, a very high probability ($P < 10^{-7}$) and a strong linear ($L_{X-ray} \propto D^{0.85\pm0.08}$), while in the relation between radio ,blue emission and distance there is clear correlation coefficient with a good probability and linear relation of the ($L_B \propto D^{0.65\pm0.16}$), while a flat slope < 0.5 between ($\log L_{1.4}$ - $\log D$) and also there is a positive correlation between blue luminosity L_B and redshift with a slope ~ 0.4 ($L_B \propto z^{0.36\pm0.14}$) . The figures (6 - 10) shows that the slopes of the relations ($\log L_{X-ray}$, $\log L_B$, $\log L_{1.4}$ – $\log D$), for QSO type sample.

The results of multiple regression analysis show apparently many main points:

(1) We have found the luminosities range of the extended radio continuum at 1.4 GHz ($L_{1.4} \sim 1.2 \pm 2 \times 10^{23}$ $W.Hz^{-1}$), blue at 4400Å ($L_B \sim 1.1 \pm 2.5 \times 10^{22}$ $W.Hz^{-1}$) and X-ray emission at energy band (0.1-2.4 KeV) of $L_{X-ray} \sim 1.3 \pm 2.2 \times 10^{10}$ L_Θ for Sy1 galaxies, and ($L_{1.4} \sim 1.4 \pm 10^{23}$ $W.Hz^{-1}$), ($L_B = 1.2 \pm 1.4 \times 10^{22}$ $W.Hz^{-1}$), ($L_{X-ray} \sim 1.5 \pm 5 \times 10^9$ L_Θ) for Sy2 galaxies , while a high luminosities for QSO objects ($L_{1.4} > 10^{26}$ $W.Hz^{-1}$), ($L_B = 1.2 \pm 2.6 \times 10^{23}$ $W.Hz^{-1}$), ($L_{X-ray} \sim 1.2 \pm 5.6 \times 10^{11}$ L_Θ).

(2) The luminosities (L_{X-ray}, L_B, and $L_{1.4}$) for these active galaxies samples (Sy1, Sy2 and QSO) are correlated with the distances of galaxies. The lack of correlation between radio luminosity and distance for type Sy2 perhaps indicates that the association of X-ray, blue emission with a distance is more fundamental, and possibly the weak correlation between radio continuum and a distance may disappear from multiple regression analysis because of the tight correlation between the X-ray and blue emission with distances.

(3) The slope of the correlation between X-ray luminosity and distances of these galaxies is significantly steeper than others with significance levels (probability of chance correlation, $P \sim 10^{-7}$).

(4) In the stronger linear X-ray, blue and radio emission distance correlation, the increases of the slope relation (L_{X-ray}, L_B, $L_{1.4} - D$), believe that with an increase in the star formation, the retention of cosmic-ray electrons within these galaxies (Sy1, Sy2 and QSO) is enhanced. This means that the X-ray, blue and radio luminosities increase on the biggest distance as these active galaxies type Quasars (QSO). Quasar spectra are corrected for the effect of redshift (z). Since many quasars have a high redshift. This means that according to Hubble's law ($V = H_0 \times D$) these active galaxies are very far away, since it must be very luminous, so we can see it. Our results relative to the strong correlation relationship between X-ray luminosity (L_{X-ray}) and redshift (z) for RBSC-NVSS sample selected AGNs for Quasars galaxies consistent compared with the results of [14] for the SPIDERS (RASS and XMMSL sources)-AGN samples. The reason is that both samples have selected surveys for X-ray bright sources.

It can be concluded from the results of statistical analysis of the multi-wavelength radio, blue to X-ray properties of a RBSC-NVSS sample for active galaxies to the following:

I. There are different behaviors of the X-ray, blue and radio luminosities -to- distance relations of sample (Sy1, Sy2 and QSO) galaxies. Statistical analysis showed that we had the presence of a very strong correlation between X-ray emission and distance and a strong linear with slop~ 1.

II. The joint dependence of X-ray, blue and radio luminosities on the distances for (Sy1) type galaxies are strikingly similar to that which was found for Quasars. This similarity of Sy1 and quasars indicates the close link between these two classes of active galaxies (AGNs). The optical spectra of quasars are analogous to the optical spectra of Seyfert 1 galaxies with prominent wide lines, but weaker narrow lines.

III. The X-ray emission of Sy1 and Quasars galaxies is linked with the blue, extended radio emission as well. Moreover, the slopes of the correlations between the X-ray and blue emission are significantly steeper than that for Sy1 and QSO.

IV. The X-ray, blue and extended radio properties are strongly correlated with distances of these galaxies with a higher star formation activity and depend on increasing frequency and on the type of these galaxies. This means that the artificial correlations between these luminosities and distance, caused by the fact that at large distances, we observe the more powerful sources.

V. An analysis of our data shows that the radio, blue and X-ray luminosities ($L_{1.4}, L_B, L_{X-ray}$) does not depend on the morphological of these galaxies (Sy1, Sy2 and QSO).

ACKNOWLEDGEMENTS

The authors would like to thank the anonymous referees for the helpful suggestions and comments that will help to improve this work.

REFERENCES

1-Osterbrock D. E. The nature and structure of active galactic nuclei.Astrophysical Journal. 1993;404(2):551-562.

2-Lipovka A. A., Lipovka N. M.The Nature of Active Radio Galaxies in the Cluster A569. Astronomy Reports. 2002; 46(11):867-870.

3-Loubser S. I., Soechting I. K.The detailed nature of active central cluster galaxies.Monthly Notices of the Royal Astronomical Society. 2013;431(Issue 3):2933-2959.

4- Müller-Sánchez F., Comerford J., Stern D., Harrison F. A. The nature of active galactic nuclei with velocity off set emission lines.Ap.J.2016;830(1):50-65.

5-Vila-Costas M. B., Edmunds M. G.The relation between abundance gradients and the physical properties of spiral galaxies.MNRAS.1992;259(1):121-145.

6-DíazTello J., Donzelli C., Padilla N., Fujishiro N., Hanami H., Yoshikawa T., Hatsukade B.Physical properties, star formation, and active galactic nucleus activity in balmer break galaxies at0 < z < 1.Ap.J.2013;771(1):7-26.

7-Khachikyan E. E., DanelyanM. R.Some physical properties of UV galaxies.Astronomy Reports. 2014;58(Issue 3):516-521.

8-Ucci G., Ferrara A., Gallerani S., Pallottini A. Inferring physical properties of galaxies from their emission-line spectra.MNRAS. 2017;465(Issue 1)::1144-1156.

9-Zhang H., Liu R., Yang H. The Evolution of X-Ray Radiation of Quasars.18thInternational Cosmic Ray Conference. India. 1983;9:14-17.

10-Giovannelli F., Polcaro V. F. A relationship between the X-ray luminosity and redshift of extragalactic objects. MNRAS. 1986;222(Issue 4):619-627.

11-Lacy M., Ridgway S. E., Sajina A., Petric A. O., Gates E. L., Urrutia T., Storrie-Lombardi L. J.The spitzer mid-infrared AGN survey. II. the demographics and cosmic evolution of the AGN population.Ap.J. 2015;802(2):102-115.

12- Bauer F. E., Condon J. J., Thuan T. X., Broderick J. J. RBSC-NVSS Sample. I. Radio and Optical Identifications of a Complete Sample of 1556 Bright X-Ray Sources. Ap.J. 2000;129:547-562.

13-Schmidt M., Green R. F. Counts, evolution, and background contribution of X-ray quasars and other extragalactic X-ray sources.Ap.J.1986;305:68-82.

14-DwellyT., SalvatoM., MerloniA., BrusaM., BuchnerJ., AndersonS. F., et al.SPIDERS: Selection of spectroscopic targets using AGN candidates detected in all-sky X-ray surveys.Monthly Notices of the Royal Astronomical Society.2017;469(Issue 1):1065-1095.

15-Hogg D. W. Distance measures in cosmology.arXiv:astro-ph/9905116.1999.

16-Kandalyan R. A., Al-Naimiy H. M. K. Broad-Band Radio to X-Ray Properties of Seyfert Galaxies. Astrophysics. 2002;45(Issue 3):277-287.

17-Kalloghlian A. T., Kandalyan R. A., Al-Naimiy H. M. K., Khassawneh A. M. Investigation of Barred Galaxies. VII. Comparative Statistics of SB and SA Galaxies. Near and Mid-IR Regions.Astrophysics. 2001;44(Issue 3):292-304.

Table 1: Mean (Average) Variables and Standard Error for Active type Galaxies

Variable	Sy1	Sy1	QSO
Z	0.1268 ± 0.0084 $N = 314$	0.1775 ± 0.0370 $N = 32$	0.6162 ± 0.0523 $N = 97$
$\log D$	2.4978 ± 0.0280 $N = 314$	2.2653 ± 0.0947 $N = 32$	3.3536 ± 0.0337 $N = 97$
$\log L_{X-ray}$	10.3365 ± 0.0524 $N = 314$	9.7320 ± 0.1837 $N = 31$	11.7495 ± 0.0670 $N = 95$
$\log L_{B}$	22.4000 ± 0.0386 $N = 314$	22.1469 ± 0.0840 $N = 32$	23.4220 ± 0.0730 $N = 97$
$\log L_{1.4}$	23.2935 ± 0.0797 $N = 314$	22.9483 ± 0.1586 $N = 32$	26.0470 ± 0.1220 $N = 97$

Notes: Where N is the number of active type galaxies for (Sy1, Sy2 and QSO) used in the sample.

Table 2: Partial correlation coefficients (R) and probability of chance correlation (P) between Various Parameters of Seyfert type 1 (Sy1) galaxies, No. of casess valid (N=309).

Parameters	$\log D$	$\log L_{X-ray}$	$\log L_{B}$	$\log L_{1.4}$
$\log L_{X-ray}$	$R = 0.75$	1	$R = 0.23$	–
	$P < 10^{-7}$	–	$P \sim 10^{-4}$	–
$\log L_{B}$	$R = 0.22$	$R = 0.21$	1	$R = 0.20$
	$P < 10^{-4}$	$P < 3\times10^{-4}$	–	$P \sim 4\times10^{-4}$
$\log L_{1.4}$	$R = 0.60$	–	$R = 0.22$	1
	$P < 10^{-7}$	–	$P \sim 4\times10^{-4}$	–

Table 3: Partial correlation coefficients (R) and probability of chance correlation (P) between Various Parameters of Seyfert type 2 (Sy2) galaxies, (N=31)

Parameters	$\log D$	$\log L_{X-ray}$	$\log L_B$	$\log L_{1.4}$
$\log L_{X-ray}$	R = 0.86	1	R ~ 0.50	R = 0.42
	$P < 10^{-7}$	–	$P \sim 10^{-3}$	$P = 2\times10^{-2}$
$\log L_B$	R = 0.47	R ~ 0.50	1	R = 0.63
	$P < 10^{-2}$	$P \sim 10^{-3}$	–	$P = 2\times10^{-4}$

Table 4: Partial correlation coefficients (R) and probability of chance correlation (P) between Various Parameters of Quasars (QSO types), (N=95).

Parameters	$\log D$	$\log L_{X-ray}$	$\log L_B$	$\log L_{1.4}$
$\log L_{X-ray}$	R = 0.75	1	–	–
	$P < 10^{-7}$	–	–	–
$\log L_B$	R = 0.40	–	1	–
	$P < 10^{-4}$	–	–	–
$\log L_{1.4}$	R = 0.23	–	–	1
	$P < 3\times10^{-2}$	–	–	–

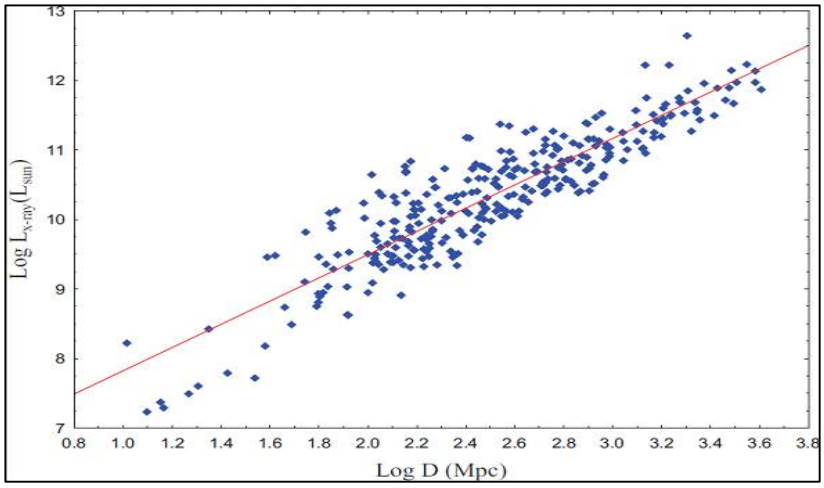

Figure 1: X-ray luminosity as a function of distance for Sy1 galaxies.

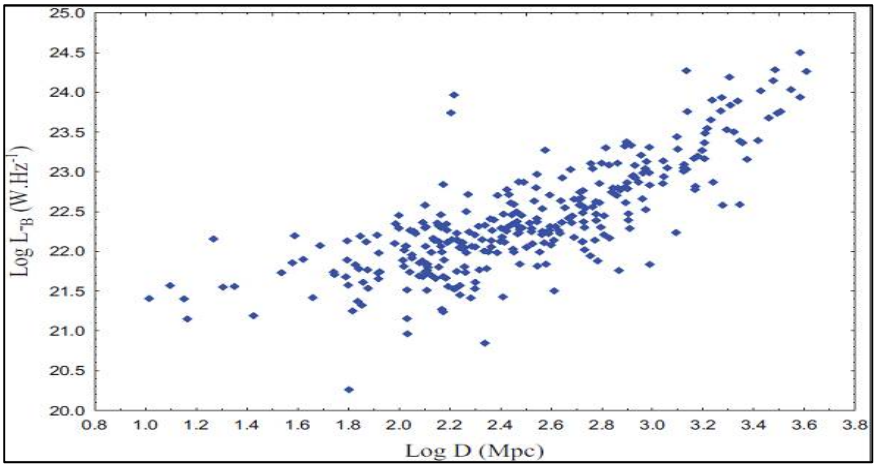

Figure 2: Blue luminosity as a function of distance for Sy1 galaxies.

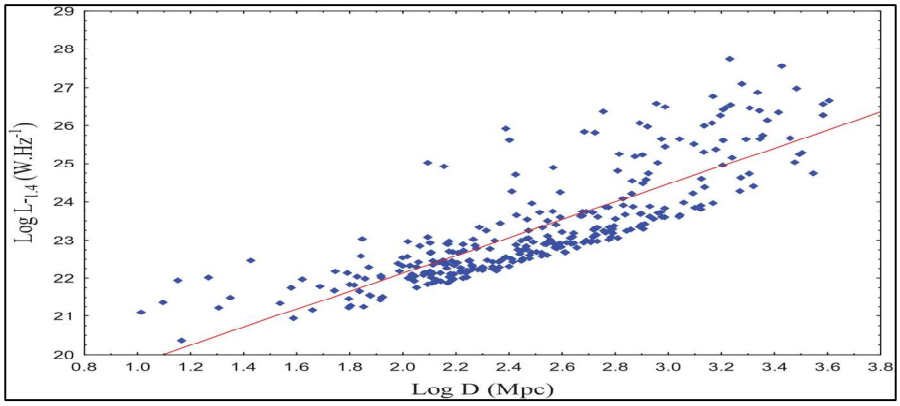

Figure 3: Radio luminosity at 1.4GHz as a function of distance for Sy1 galaxies.

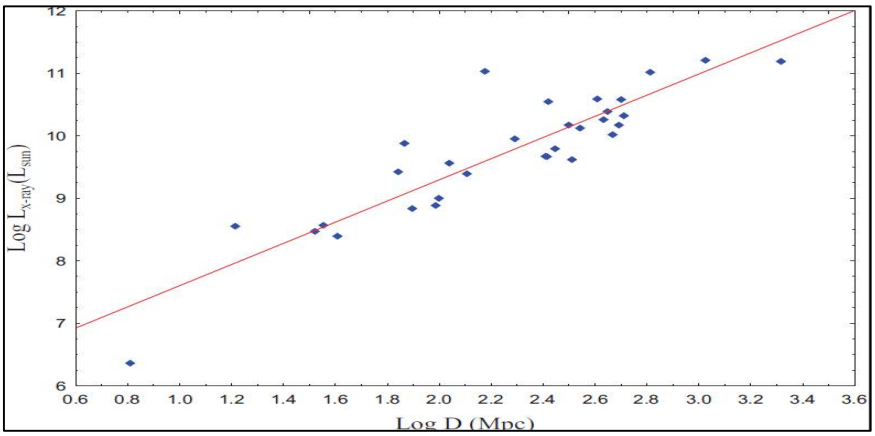

Figure 4: X-ray luminosity as a function of distance for Sy2 galaxies.

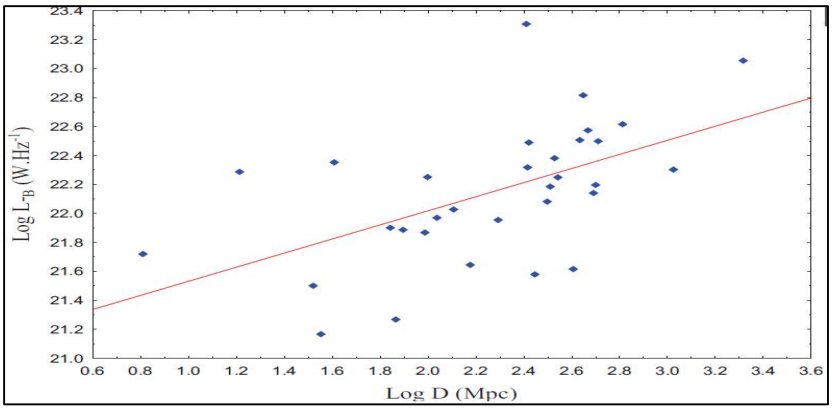

Figure 5: Blue luminosity as a function of distance for Sy2 galaxies.

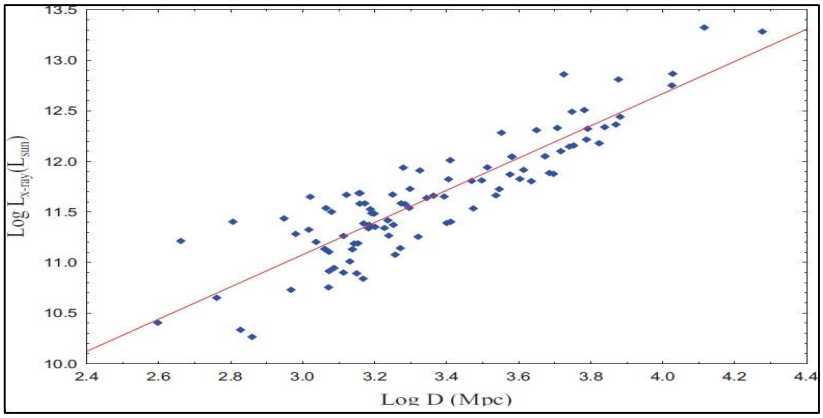

Figure 6: X-ray luminosity as a function of distance for QSO types.

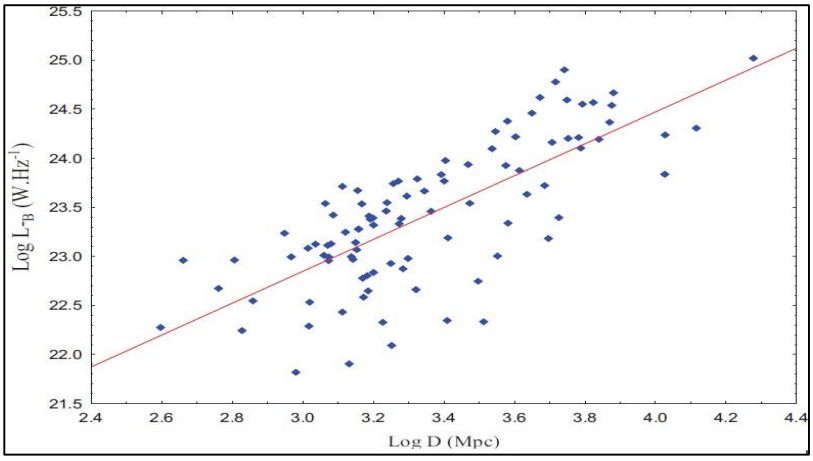

Figure 7: Blue luminosity as a function of distance for QSO types.

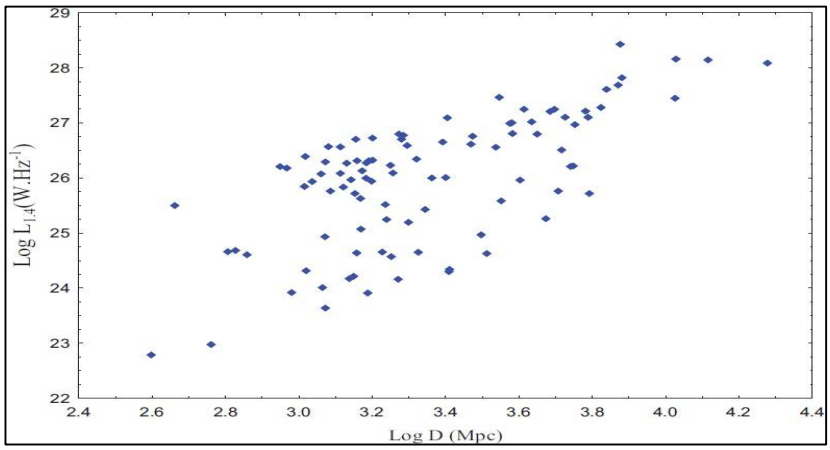

Figure 8: Radio luminosity at 1.4GHz as a function of distance for QSO types.

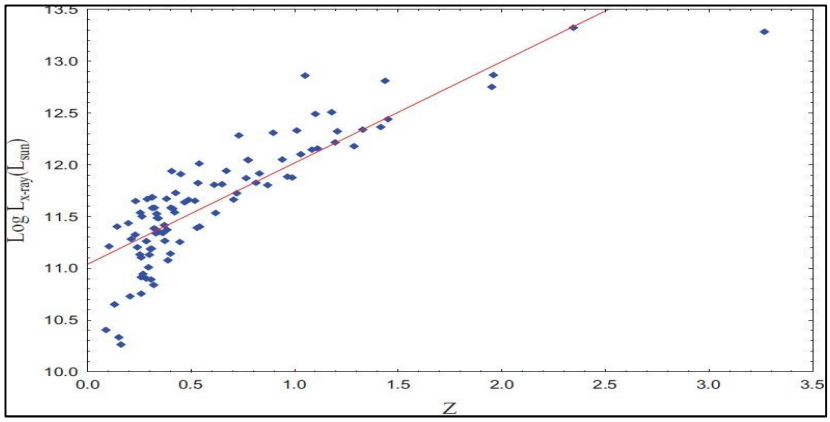

Figure 9: X-ray luminosity as a function of redshift for QSO types.

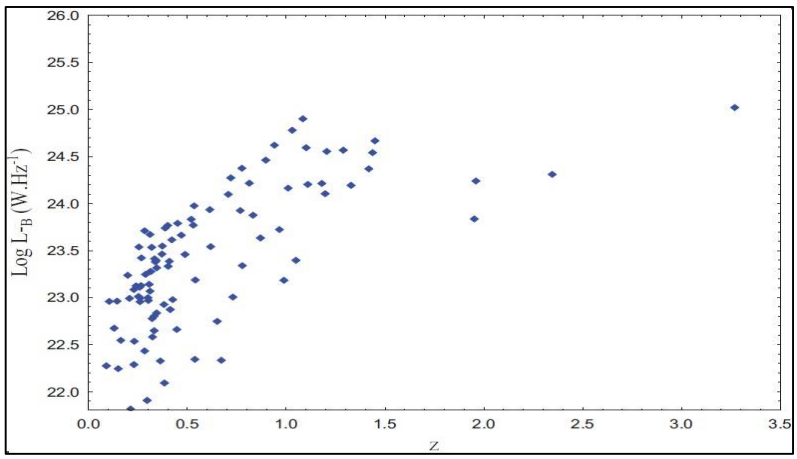

Figure 10: Blue luminosity as a function of redshift for QSO type.

Indian Journal of Natural Sciences www.tnsroindia.org.in ©IJONS

Vol.9 /Issue 51 / December / 2018 *International Bimonthly* *ISSN: 0976 – 0997*

REVIEW ARTICLE

A Review on Arithmetic Modules to Removing Effects of Atmosphere

Salema Sultan Salman[1]*, Wafaa Abdulameer Abbas[1] and Alaa Ali Hussein[2]

[1]Department of Clinical Laboratory of Sciences, College of Pharmacy, University of Baghdad, Baghdad, Iraq
[2]Department of Research and Development, Ministry of higher education and Scientific Research, Iraq

Received: 22 Aug 2018 Revised: 24 Sep 2018 Accepted: 26 Oct 2018

***Address for Correspondence**
Dr.Salemasultan Salman
Leturer, Department of Clinical Laboratory of Sciences,
College of Pharmacy, University of Baghdad,
Baghdad, Iraq
Email: salma3_sultan@yahoo.com

ABSTRACT

Atmospheric correction is the process of removing the effects of the atmosphere from satellite images and to produce surface reflectance values. It can significantly improve the interpretability of an image. While the Radiometric correction is done to reduce or correct errors in the numbers of satellite images. This process improves the interpretability and quality of remote sensed data. Accordingly, these processes are very important to derive exact Earth's surface reflectance data.In the literature, various number of correction algorithms have been proposed to improve the hyperspectral satellite image data. The hyperspectral imaging collects and processes information from across the electromagnetic spectrum, to obtain the spectrum for each pixel in the image of a scene, with the purpose of finding objects, identifying materials, or detecting processes. In this paper, five of the most well-known correction algorithms will be adopted and use to correct the selected hyperspectral scenes; these are: ATCOR2, COST, FLAASH, 6S, and DOS1.

Keywords: Atmospheric Correction, FLAASH, DOSI, ATCOR2, 6S, DOS1.

INTRODUCTION

Satellite images are very beneficial to study changes in land cover and land use, where periodic observation of a specific area over time yield to possibility of many analysis forms to detect changes, But there is a big problem with distortion error of image due to Earth's atmosphere, land, and water, which is a major problem with visible band of remote sensing imagery. Particularly for non-stationary satellite [1]. The electromagnetic radiation emanating from the sun illuminates the Earth's surface, gets back-scattered and will be sensed by satellite-borne remote sensor.

In this process, the radiation travels through the Earth's atmosphere twice – once as it travels from the sun to the Earth's surface, and secondly, after reflection from the Earth's surface on its way to the sensor (Figure 1) [2] .

The radiation received by the satellite sensor that reflected from the earth surface hardly affected by interaction with the atmosphere, which is more strength for the non-bright objects, such as vegetation or water bodies. This problem is significant specifically in multi-spectral satellite data for monitoring aims, such as land use or agricultural studies [3]..Image distortion was made by two error sources, internal and external errors. Internal errors are generating by the remote sensing system, which could be confined and then corrected based on calibration measurements prelaunch or in-flight while External errors produced by varying in surrounding natural phenomena like space and time. External variables cause to expose radiometric and geometric errors include the atmosphere in remote sensor data [4].

The atmospheric errors effect on the goodness of the information taken away from the satellite, such as vegetation indices, thus lead to distortion and increase the uncertainty in image According to the spectral band [3].The satellite images data must correction before using in the geographical information system, (GIS), some techniques of error correction inclusive geometric correction and radiometric correction. The geometric corrections will be made to not exactness correct between coordinates of the objects in the image data and coordinates of real place of objects on the ground, The radiometric corrections of digital image data would be made for the brightness values correction of the elements on the ground, because of problems in sensor calibration or a failure in the sensor function. Image distortion is due to the scattering of reflected electromagnetic energy caused by a permanently changing atmosphere [5].

This review discusses of radiometric correction of remotely sensed imagery to minimize the errors, where, absolute and relative corrections can be applied to satellite images.Radiometric correction methods of remotely sensed images will be categories in two major types: absolute correction and relative correction, which used to normalized satellite images for intercomparison with time- series [6,7].Absolute radiometric correction is extracted the absolute reflectance of targets at the surface of the earth by converts the digital of satellite image data, to at-sensor radiance and then, through atmospheric correction, to the reflectance of the earth [7]. Sensor calibration and the synchronous atmospheric properties must input in this method, hard to get it in many cases, specifically in historical data. Relative radiometric correction is adjusting the radiometric properties by minimizing atmospheric and other variation between several target images to be agreeing with the base image, it is also called relative radiometric normalization. The method based on setting the multi-temporal images into a prevalent scale without more parameters from another measurement. where, "reflectance of invariant targets within multiple scenes can be used to render the scenes to appear as if they were acquired with the same sensor, with the same calibration, and under identical atmospheric conditions" [6].Absolute methods model cut the absorption and scattering process due to gases and aerosols in the atmosphere [8].Absolute radiometric correction is a two-step process. The first step is to convert the digital number (DN) of the sensor measurements to spectral radiance measured by satellite sensors using equation (1).

$$L_{sat} = DN x Gain + Offset \quad (1)$$

Where Lsat is spectral radiance detected by a satellite sensor; DN is the digital number of the sensor measurement, and Gain and Offset represents sensor-specific calibration parameters determined before sensor launch. While these parameters are usually assumed as stable, they can change due to long-time service or accidents [9]. The second step of absolute radiometric correction is to transfer the sensor detected radiance into ground surface reflectance using equation (2)

$$\text{qsurface} = {(L_{sat} - L_{path})\pi}/{E_r} \quad (2)$$

Here qsurface is the ground surface reflectance of the target. Lpath is the path radiance, E is the irradiance on the ground target, and s is the transmission of the atmosphere. Absolute radiometric models use in situ measurements or reasonable estimation of 64 X. Chen et al. Remote Sensing of environment 98 (2005) 63– 79 atmospheric optical depth, solar zenith angle and satellite status to input parameters for calculating the ground surface reflectance [10,11].

Where qsurface is the ground surface reflectance of the target. Lpath is the path radiance, E is the irradiance on the ground target, and is atmosphere transmission. Absolute radiometric models use in its original place measurements or reasonable estimation of 64X, for calculating the ground surface reflectance using atmospheric optical depth, solar zenith angle and satellite status to input parameters [10,11].Relative radiometric normalization is a method of correction that applies one image as a reference and adjusts the radiometric properties of subject images to match the reference [1]. Relative methods reduce the atmospheric effects and the surface directionality effects that are the result of sun angle effects, reducing the noise (residual scatter) and other eventual effects from deterioration in sensor response over the time [8]. The relative atmospheric correction methods generally include the following:

a) Dark-Object Subtraction Method: Several variations of this method exist but the basic concept is the same that the least DN value in a spectral band image that may be occurring over a deep clear water body or deep shadows or dense vegetation deemed as arising due to atmospheric path radiance; this DN value is subtracted from every pixel of the spectral band to generate a new corrected image [6]. This is a simple and fast method to make and has also been the most extensively used one. After making a comparative study of the effectiveness of various methods, [7] found that this method is very good and enough if quantitative estimates of ground reflectance data are not required [10, 3].

b) Histogram Matching Method: This could be implemented if in a given scene where there are clear areas and hazy areas; assuming that surface reflectance characteristics of hazy as well as clear areas are the same, the histograms of hazy regions are displaced to match the histograms of their reference clear regions.

c) Invariant-Object Method: This method assumes that in any given scene there are some pixels whose reflectance values are quite stable (invariant); based on the reflectance of these "invariant objects", a linear relation for each band could be used to normalize images acquired at different times [2].

RADIOMETRIC CORRECTION ALGORITHMS

A useful prior step to interpretation of satellite images is converting the digital numbers (DNs) stored in the original image into biophysical variables (reflectance). These variables are comparable in the same sensor over time and over scenes, as well as between different sensors and between remote sensing and other methods of detecting electromagnetic energy. Correction is also advisable in the case of unevenly distributed atmospheric effects in the image and also when vegetation indexes based on band ratios included in the analyses [12–17]. In order to calculate surface reflectance, the atmospheric effects should be removed. This involves estimating the atmospheric transmissivity (both up and downwelling), diffuse irradiance and atmospheric radiance due to scattering [18]. In the survey, we evaluated six different radiometric correction methods: the first five methods (ATCOR2, COST, FLAASH, 6S, and DOS1) including atmospheric corrections (surface absolute reflectance), while the sixth (TOA) without considering atmospheric effects (remarkable reflectance at the sensor).

Atmospheric Correction for Flat Terrain (ATCOR2)

The aim of ATCOR2 correction [19] is to eliminate the atmospheric effects to recover the physical parameters of the Earth's surface, including the surface reflectance, soil visibility, and temperature. The correction would be made with the ATCOR module [20] included in **ERDAS IMAGINE** software, Version 2014 [21].The main characteristics of ATCOR2 are: a preliminary classification of the scene (soil, water, fog, and clouds), recovery of atmospheric

parameters (aerosol optical thickness, water vapour) and surface reflectance recovery [22]. Surface reflectance (ρ_{SUP}) is obtained by equation (3).

$$\rho_{SUP} = \frac{1}{a_1}\left(\frac{d^2 \pi L_{TOA}}{E_{TOA}\cos\theta_i} - a_0\right) \quad (3)$$

Where d is the direct distance to the sun, LTOA is the spectral radiance of the satellite, ETOA is the solar spectral radiance on a surface perpendicular to the rays of the sun outside the atmosphere, and qi is the solar zenith angle. To get the coefficients. and, the standard atmospheric parameters (aerosol type, visibility or optical thickness, and water vapor column) are must. Such parameters are available in the Software ERDAS IMAGINE, Version 2014.ATCOR was originally developed at DLR, the German Aerospace Centre. Ecosystem's Gmbh, the German Intergraph Distributor,and integrated ATCOR into Imagine.ATCOR supported Sensors: IKONOS 2, IKONOS 2 PAN, Landsat-4/5 MSS, Landsat-4/5 TM, Landsat-7 ETM+, Landsat-7 PAN, QuickBird, SPOT-4 MS, SPOT-5 MS, SPOT-5 PAN, Landsat-8 OLI etc[23, 24].

ATCOR2 for IMAGINE represents several processing options: a haze removal algorithm, atmospheric correction with constant atmospheric conditions and capability of viewing reference spectra of selected target areas. They can be displayed as a function of chosen atmospheric parameters to estimate the appropriate atmosphere if no measured information for the atmospheric conditions is available.

Although ATCOR is developed with an emphasis on small field-of-view (FOV) sensors a limited number of wide FOV satellite sensors are also supported such as IRS-1C/1D WiFS. A second ATCOR module exists for satellite imagery acquired over rugged terrain. It is called ATCOR3 and compensates additionally to the atmospheric effects introduced by topography (3rd dimension). Both ATCOR modules include an option to derive value-adding products (VAP) such as leaf area index (LAI), absorbed photo-synthetically active radiation (FPAR), and surface energy balance components (absorbed solar radiation flux, net radiation, etc.)[23-26].

ATCOR2 Program Modules

Clicking on the **ATCOR** icon from the **ERDAS IMAGINE /Toolbox /GEOSYSTEMS icon panel** will open the **ATCOR Menu**(Figure 2).

The **ATCOR selection menu** displays four different options:

(1) **Sun Position Calculator** A tool to calculate the sun place (sun azimuth and zenith) from the acquisition time/date and place of the image.
(2) **ATCOR2 Workstation** Thisstarts the ATCOR2 main menu.
(3) **ATCOR3 Derive Terrain Files** A tool to calculate the necessary I/P DEM- derivatives for ATCOR3. This will be discussed in the ATCOR3 manual.
(4) **ATCOR3 Workstation** Thisstarts the ATCOR3 main menu.

Sun-position Calculator

This option calculates the solar zenith (degrees) and the solar azimuth (degrees) for your image (Figure 3).

ATCOR2 Workstation Menu

ATCOR Project File(. rep): Before the ATCOR main menu opens you will be asked to enter either a previously existing ATCOR project file or create a new one. After naming and saving the project file the ATCOR2 Main Menu opens, the ATCOR2 main menu contains the necessary options to define the ATCOR2 input parameters (Figure 4).

SPECTRA module

The purpose of the SPECTRA module is the determination of an appropriate atmosphere (aerosol and humidity) and the decision on the selected visibility (ground meteorological range). The selected values will later be used in the atmospheric correction module. SPECTRA Main Display Setup appears (figure 5).

Functional flowchart of the SPECTRA Module

Functional flowchart of the SPECTRA Module for ATCOR2 shown in figure (6).

Haze Removal and Atmospheric Correction Menu

The Haze removal is an independent process of ATCOR and would be used standalone without the following Atmospheric Correction. For the option **Perform Haze Removal before Correction? YES** option means that "Haze Correction" on the right will become active. **NO** option means that "Atmospheric Correction" will become active (Figure 7).Figures (8) shows corrected **ATCOR** images, in terms radiometric, for Baghdad of Iraq (2014 Landast TM+7).

Cosine of the Sun Zenith Angle (COST)

This is a radiometric calibration method, based entirely on characteristics of the satellite image, that considers the atmospheric effect, in contrast with other methods of atmospheric correction, like ATCOR2, FLAASH or 6S, requiring some extra parameters, such as atmospheric profiles, aerosol models or visibility [27,28].Chavez [1996] improved the DOS method by considering the effect of atmospheric multiplicative transmittance. Atmospheric transmittance in the illumination direction ($T_{\lambda z}$) is approximately equal to the cosine of solar zenith angle for Landsat TM bands 1 to 4. Atmospheric transmittance in the viewing direction ($T_{\lambda v}$), Downwelling diffuse irradiance (E_{down}) are equal to unity and zero, respectively.

Chavez [1996] determined two processes approximate estimate atmospheric transmittance. First process involves utilizing solar zenith angle cosine, while the second one adopts the average value of each spectral band derived from the radiative transfer model. Values of the three parameters ($T_{\lambda z}$, $T_{\lambda v}$ and E_{down}) is from Chavez [1996]. Land surface reflectance could be estimated by the following equation:

$$R_\lambda = \pi \times D^2 \times (L_{\lambda sat} - L_{\lambda p}) / (Esun_\lambda \times \cos(\theta_z) \times T_{\lambda z}) \quad (4)$$

where R_λ is surface reflectance , D is Distance between earth and sun (unit: AU), $L_{\lambda sat}$ and $L_{\lambda p}$ is spectral radiance at the sensor's aperture and path radiance respectively ,$Esun_\lambda$ is Exo-atmospheric solar spectral irradiance , $\cos(\theta_z)$ is cosine solar zenith angle . This correction was carried out by implementing the algorithm in the Model Maker ® module of ERDAS IMAGINE software, Version 2014[21].

Fast Line-of-sight Atmospheric Analysis of Spectral Hypercubes (FLAASH)

This is an advanced atmospheric correction module based on the MODTRAN4 algorithm of radiative transfer developed by Spectral Sciences Inc. (Burlington, MA, USA) under the sponsorship of the U.S. Air Force Research Laboratory [29,30].

The FLAASH algorithm is modified to remove atmospheric effects caused by the molecular dispersion of particles in the atmosphere. It will be found by Equation (5). [31, 32].

$$L_{TOA} = \left(\frac{A_{\rho SUP}}{1-\rho_e S}\right)\left(\frac{B_{\rho e}}{1-\rho_e S}\right) + L_0 \quad (5)$$

where L_{TOA} is the spectral radiance reached by the satellite, ρ_{SUP} is the reflectance of the pixel surface, ρ_e is the reflectance of the average surface of the pixel of the surrounding region, S is the sphericalalbedo of the atmosphere, L_0 is the radiance backscattered by the atmosphere, and A as well as **B** arecoefficients that depend on the atmosphere and geometric conditions.The first term of the equation corresponds to the reflectance of the surface that travels directly into the sensor while the second term corresponds to the luminosity of the surface that is dispersed by the environment. The distinction between ρ_{SUP} and ρ_e explains the "adjacency effect" (spatial blending of radiation between nearby pixels) caused by the atmospheric dispersion. The values of **A, B, S,** and L_0 can be determined empirically from the MODTRAN4 standards. The vision and the solar angles of the measurement and the nominal values for the surface elevation, aerosol shape, and visible range of the scene must be specified [33].

FLAASH supports hyperspectral sensors (such as HyMAP, AVIRIS, HYDICE, HYPERION,Probe-1, CASI, and AISA) and multispectral sensors (such as ASTER, IRS, Landsat, RapidEye, and SPOT). Water vapor and aerosol retrieval are only possible when the image contains bands in appropriate wavelength positions. In addition, FLAASH can correct images collected in either vertical (nadir) or slant-viewing geometries [34 – 37]. The correction was carried out with the FLAASH module in ENVI software, Version 5.2.

Algorithm FLAASH in ENVI

- **Input Data Requirements**

  I/P image forFLAASH should be, in terms of radiometric, calibrated radiance image in band interleaved-by-line (BIL) or band-interleaved-by-pixel (BIP) format. The data type would be floating-point, 4-byte signed integers, 2-byte signed integers, or 2-byte unsigned integers. To perform water retrieval, the image bands must span at least one of the following ranges at 15 nm spectral resolution or better:
  - 1050-1210 nm
  - 770-870 nm
  - 870-1020 nm

- **Standard FLAASH Input Parameters**

  Parameters of ENVI FLAASH include selecting an input radiance image, setting output file defaults, entering data of sensor and scene, selecting an atmosphere and aerosol model, and setting options of atmosphere correction model.

  1. From the ENVI Toolbox menu bar, select the following:

  Radiometric Correction →Atmospheric Correction Module→FLAASH Atmospheric Correction.

  The FLAASH Atmospheric Correction Model Input Parameters dialog appears (Figure 9).

  2. Set I/P parameters as described in the following sections.

- **Specifying Input and Output File Information**
  1. In the FLAASH Atmospheric Corrections Model Input Parameters dialog, click ***Input*** → ***Radiance Image*** to open the FLAASH Input File dialog. The I/P radiance image should contain calibrated radiance data in a floating-point, and interleave should be BIL or BIP. To convert between different interleaves, select the following
     - **Radiometric Correction →Radiometric Calibration.**

     Input Parameters of Radiometric Calibration Model dialog appears (figure 10).
  2. Select I/P file and any spatial sub-setting, then click **OK**. The Radiance Scale Factors dialog appears (Figure 11).
  3. Select whether to enter a single scale factor (a constant) for all bands or to read an array of scale factors (one per band) from an ASCII file.
     - By selecting **Read array of scale factors (1 per band) from ASCII file**, a file selection dialog appears. Select I/P ASCII file.
     - By selecting **Use single scale factor for all bands**, the **Single scale factor** text box appears. Enter a scale factor

Output Filename

For changing output filename, in the FLAASH Atmospheric Corrections Model Input Parameters dialog, click **Output Reflectance File**. The Select Output File dialog appears.

Output Directory

To change the output directory, click **Output Directory for FLAASH Files**. The Browse for Folder dialog appears. This setting is the place where all FLAASH files (except the output reflectance file) are written. FLAASH files that are output of this directory include column water vapour and cloud map images, journal file, and optionally the template file.

Root Name

In the **Rootname for FLAASH Files** text box, enter the prefix to add to each FLAASH file produced during a FLAASH session. Do not include a directory path. The root name is the prefix that is appended of the output FLAASH filenames.

Entering Scene and Sensor Information

Scene and sensor data includes the scene center place (lat. / long.), the average ground elevation of the scene, the sensor type, the sensor altitude, and the flight date and time. These data let FLAASH find where the sun was in the sky and the path of sunlight through the atmosphere to the ground and back to the sensor.

Selecting Atmospheric Model Settings

Use the **Atmospheric Model** drop-down list to choose one of the standard MODTRANmodel atmospheres.

Using Water Retrieval

To solve the radiative transfer equations that allow determination of plain surface reflectance, the column water vapor amount for each pixel in the image must be determined. FLAASH contains a method for retrieving water

amount for each pixel. This technique produces a more exact correction than using a constant water amount for the entire scene. To use water retrieval method, the image should have bands that span at least one of the following ranges at a spectral resolution of 15 nm or better:

- 1050-1210 nm (for the 1135 nm water feature)
- 870-1020 nm (for the 940 nm water feature)
- 770-870 nm (for the 820 nm water feature)

For most of multispectral sensor types, the **Water Retrieval** setting is **No** because these sensors do not have proper bands to perform the retrieval.

Selecting an Aerosol Model

Click the **Aerosol Model** drop-down list and select one of the standard MODTRANAerosol /haze types.

Using Aerosol Retrieval

FLAASH includes a method for retrieving aerosol amount and estimating a scene average visibility using a dark pixel reflectance ratio method based on work by Kaufman et al. (1997). Click the **Aerosol *Retrieva*l** drop-down list: then select an option:

- **None**: by selecting this option, the value in the **Initial Visibility (TM)** field would be used for aerosol model (described in the following section).
- **Band (K-T)**: Use aerosol retrieval method. If no suitable dark pixels are found, then the value in **Initial Visibility** field would be used.

Entering an Initial Visibility Value

In **Initial Visibility** field, enter an estimate of the scene visibility in kilometers. The initial visibility value is assumed for the atmospheric correction if aerosol is not being retrieved. Table (2) lists approximate values based on weather conditions

Multispectral Settings

The Multispectral Settings button appears at the bottom of FLAASH Atmospheric Correction Model Input Parameters dialog when you select a multispectral sensor from the Sensor Type button menu. When applying the FLAASH atmospheric correction model to a multispectral dataset, it would be critical to choose the proper the bands used before for water vapor and/or aerosol retrieval. Then, if input data is from an unknown multispectral sensor, it is necessary to define the sensor's spectral response functions.

1. Use the FLAASH Multispectral Settings dialog to define the bands for water vapor and aerosol retrieval.Click **Multispectral Settings**. The Multispectral Settings dialog appears (figure 12).

Starting the Processing

After setting all FLAASH parameters, click **Apply** in FLAASH Atmospheric Model Input Parameters dialog to begin processing.

Saving the Template

To save the FLAASH run settings to a template file at any time, click **Save** in the FLAASH Atmospheric Model Input Parameters dialog.

Restoring a Template File

To restore a FLAASH template file, click **Restore**.Thetemplate files stores the full path names of the input and output files (that is, the file namesinclude the directory names). Figures (13) shows corrected false-color images, in terms radiometric, for Baghdad of Iraq (2014 Landsat TM+7)

Second Simulation of Satellite Signal in the Solar (6S)

This procedure eliminates atmospheric effects on the reflectance values in images captured by sensors onboard satellite or aircraft platforms [18, 38]. The 6S code is a basic RT code used for calculation of lookup tables in the MODIS (Moderate Resolution Imaging Spectroradiometer) atmospheric correction algorithm. It enables correct simulations of satellite and plane observations, accounting for higher targets, use of anisotropic and Lambertian surfaces, and calculation of gaseous absorption. The 6S code based on the method of successive orders of scattering (SOS) approximations. Within this method, the atmosphere will be divided into a number of layers and the RT equation would be solved numerically for each layer with the help of iterations. The intensity is successively computed for photons scattered one, two, three times, etc. with the total intensity obtained as the sum of all orders. Numerical integration would be made using the decomposition in Fourier series for the azimuth angle and Gaussian quadrature for the zenith angle [18, 38, 39].

Dark Object Subtract 1 (DOS1)

The ideal atmospheric correction algorithm is one based solely on the image itself, requiring no in-situ field measurements at the time of satellite passage. The DOS approach, a strictly image-based technique, is an attempt to achieve this goal. It assumes the existence of dark objects (zero surface reflectance) in the remotely sensed image, and the non-zero digital number (DN) value in the histogram from the entire scene is thus attributed to the effect of the atmosphere and is subtracted from all the pixels. The relationship between at-satellite radiance and ground reflectance for a uniform Lambertian surface and horizontally homogeneous atmosphere can be written as [40].

$$L_{sat} = L_p + {\rho F_d T_v}/{\pi(1 - s_\rho)d^2} \qquad (6)$$

where L_{sat} is the at-satellite radiance, L_p is the path radiance, ρ is the land surface reflectance, F_d is the irradiance received at the surface, $T_v$is the atmospheric transmittance in the viewing direction, s_ρ is the fraction of the upward radiation backscattered by the atmosphere to the surface, and d is the Earth–Sun distance in astronomical units.

DOS1 method depends on the properties of the image. This correction method is the most widely used to detect land-use changes. Elements such as water, forests, and shadows deemed as dark objects when their values of reflectance are close to zero. Dark objects would be detected automatically when the pixel reflectance value is less than or equal to 1.0%. The assumption is that some pixels within the image receive 0% of the solar radiation (100% of shade), mainly due to the effect of topography, and the values of radiance corresponding to these pixels registered by the satellite correspond to atmospheric dispersion [28]. If a dark object is found in the image, least reflectance value in the histogram is assigned to such an object. From this least, it is possible to correct the entire scene by the effects of the atmospheric dispersion [41, 42]. To get the surface reflectance, Equation (7) would be used

$$\rho_{SUP} = {d^2\pi(L_{TOA} - L_o)}/{E_{TOA}COS\theta_i} \quad (7)$$

where d is the direct distance to the sun, L_{TOA} is the spectral radiance to the satellite, L_o is the backscatter glow through the atmosphere, E_{TOA} is the solar spectral radiance on a surface perpendicular to the sun's rays outside the atmosphere, and $COS\theta_i$ is the solar zenith angle. The radiometric correction was carried out with the Semi-Automatic Classification plugin developed by Congedo [43] and included in the software QGIS (v.2.18).

Apparent Reflectance at the Top of Atmosphere (TOA)

The value recorded for a given pixel includes not only the reflected or emitted radiation from the surface, but also the radiation scattered and emitted by the atmosphere. In most cases were interested in the real surface values. This technique enables calculation of the plain reflectance in a satellite image and consists of converting the DNS to radiance values and then to reflectance values. The word "apparent" means that reflectance has not been corrected for atmospheric effects and represents an initial normalization of image [18].

To achieve these values radiometric calibration and correction should be applied show in figure (14).

REFERENCES

1. Biday SG,Bhosle U.Radiometric Correction of Multitemporal Satellite Imagery. Journal of Computer Science. 2010; 6 (9): 1027-1036.
2. Saini V, Tiwari RK, Gupta RP.Comparison of FLAASH and QUAC atmospheric correction methods for Resourcesat-2 LISS-IV data. Earth Observing Missions and Sensors. Development, Implementation, and Characterization IV. 2016; Vol. 9881 98811V:1-9.
3. Hadjimitsis DG, Papadavid G,Agapiou A, Themistocleous K, Hadjimitsis MG, Retalis A, Michaelides S, Chrysoulakis N, Toulios L, Clayton CRI. Atmospheric correction for satellite remotely sensed data intended for agricultural applications: impact on vegetation indices. Nat. Hazards Earth Syst. Sci. 2010; 10: 89–95.
4. Devangi BT, Amit VP, Mayur P. Geometric Distortion and Correction Methods for Finding Key Points:ASurvey.IJSRD - International Journal for Scientific Research & Development. 2016;4(2).
5. Venkatesan E, Selvaragini S.A Study on The Geometric Correction Using Satellite Images.International Journal of Pure and Applied Mathematics. 2017; 116 (16): 471-477.
6. Chen X, Vierling L, Deering D. A simple and effective radiometric correction method to improve landscape change detection across sensors and across time. Remote Sensing of Environment. 2005;98:63-79.
7. Paolini L, Grings F, Sobrino JA, Jime´nez mun˜ ozJC, KarszenbaumH. Radiometric correction effects in Landsat multi-date/multi-sensor change detection studies. International Journal of Remote Sensing. February 2006; 27(4): 685-704.
8. Bernardo N,WatanabeF,RodriguesT, Alcaˆntara E. An investigation into the effectiveness of relative and absolute atmospheric correction for retrieval the TSM concentration in inland waters. Model. Earth Syst. Environ. DOI 10.1007/s40808-016-0176-9. 21 June 2016; 2:114.
9. Schowengerdt RA. Remote sensing models and methods for image processing. 3rd edition. San Diego, Academic Press is an imprint of Elsevier. 2007.
10. Chavez PS. Image-based atmospheric corrections—Revisited and improved. Photogrammetric Engineering and Remote Sensing.1996; 62(9):1025-1036.
11. Song C, Woodcock CE, Seto KC,Lenney MP,Macomber SA. Classification and change detection using Landsat TM data:When and how to correct atmospheric effects?. Remote Sensing of Environment. 2001; 75: 230– 244.
12. Lavreau J. De-hazing Landsat thematic mapper images. Photogramm Eng Remote Sens. 1991; 57: 1297–1302.

13. Guyot G, Gu XF. Effect of radiometric corrections on NDVI-determined from SPOT-HRV and Landsat-TM data. Remote Sens. Environ. 1994; 49: 169-180.
14. Richter R. Atmospheric correction of satellite data with haze removal including a haze/clear transition region. Comput. Geosci. 1996; 22: 675–681.
15. Carlotto MJ. Reducing the effects of space-varying, wavelength-dependent scattering in multispectral imagery. Int. J. Remote Sens. 1999; 20: 3333–3344.
16. Song C, Woodcock CE, SetoKC, Lenney MP, Macomber SA. Classification and change detection using Landsat TM data: When and how to correct atmospheric effects?. Remote Sens. Environ. 2001; 75: 230–244.
17. Liang S, Fang H, Morisette JT, ChenM, Shuey CJ, Walthall CL, Daughtry CST. Atmospheric correction of Landsat ETM+ land surface imagery. II. Validation and applications. IEEE Trans. Geosci.Remote Sens. 2002; 40: 2736–2746.
18. Pablito M LS, José J CR, Ramon ADV, Juan GAG, Carlos ALS. Evaluation of Radiometric and Atmospheric Correction Algorithms for Aboveground Forest Biomass Estimation Using Landsat 5 TM Data. Remote Sens. 2016; 8:369.doi:10.3390/rs8050369.
19. Richter RA. spatially adaptive fast atmospheric correction algorithm. Int. J. Remote Sens. 1996; 17: 1201–1214.
20. Geosystems. Haze Reduction, Atmospheric and Topographic Correction. User Manual ATCOR2 and ATCOR3.Geosystems GmbH: Geneva, Switzerland, 2016.
21. ERDAS Inc. Erdas Imagine. Available online: http: //www. hexagongeospatial. com /products/ERDAS-IMAGINE/details.aspx (accessed on 6 October2014).
22. Chavez PS. An improved dark-object subtraction technique for atmospheric scattering correction of Friedman, J.H. Multivariate adaptive regression spline. Ann. Stat. 1991; 19: 1–141.
23. Adler-Golden SM, Matthew MW, Anderson GP, Felde GW,Gardner JA. An algorithm for de-shadowing spectral imagery. Proc. 11th JPL Airborne Earth Science Workshop, JPL-Publication.5-8 March 2002; 03-04: Pasadena, U.S.A.
24. Asrar, G, Fuchs M, Kanemasu ET, Hatfield JL. Estimating absorbed photosynthetically active radiation and leaf area index from spectral reflectance in wheat. AgronJ. 1984; 76: 300-306.
25. Asrar G.Theory and Applications of Optical. Remote Sensing J. Wiley. New York. 1989.
26. Baret F, Guyot G.Potentials and limits of vegetation indices for LAI and APAR assessment. Remote Sensing of Environment. 1991; 35: 161-173.
27. ChavezPS. Image-based atmospheric corrections-revisited and improved. Photogramm. Eng. Remote Sens.1996; 62: 1025–1036.
28. Chavez PS. An improved dark-object subtraction technique for atmospheric scattering correction of multispectral data. Remote Sens. Environ.1988; 24: 459-479.
29. Adler-GoldenS,BerkA, Bernstein LS, Richtsmeier S, Acharya PK, Matthew MW, Anderson GP, Allred CL, Jeong LS, Chetwynd JH. FLAASH, a MODTRAN4 atmospheric correction package for hyperspectral data retrievals and simulations.In Proceedings of the 7th Annual JPL Airborne Earth Science Workshop. Pasadena. CA, USA. 12–16 January 1998; Green, R.O., Ed.: 9–14.
30. Anderson, GP, FeldeGW, Hoke ML, Ratkowski AJ, Cooley TW, Chetwynd JH, Jr, Gardner JA, Adler-Golden SM, Matthew MW, Berk A, et al. MODTRAN4-based atmospheric correction algorithm: FLAASH (fast line-of-sight atmospheric analysis of spectral hypercubes). In Algorithms and Technologies for Multispectral, Hyperspectral, and Ultraspectral Imagery VIII (Proceedings of SPIE); Shen, S.S., Lewis, P.E., Eds.; Society of Photo Optics: Orlando, FL, USA. 2002;65–71.
31. Milborrow S. Earth: Multivariate Adaptive Regression Splines. R Package Version 4.2.0. Available online: http://CRAN.R-project.org/package=earth (accessed on 6 October 2015).
32. Myers RH.Classical and Modern Regression with Applications. PWS-Kent Publishing Company: Belmont, CA,USA, 1990.
33. MarcelloJ, Eugenio F, Perdomo U, Medina A. Assessment of atmospheric algorithms to retrieve vegetation in natural protected areas using multispectral high resolution imagery. Sensors. 2016; 16: 1624.

34. Adler-Golden SM, Matthew MW, Bernstein LS, Levine RY, Berk A, Richtsmeier S C, Acharya PK, Anderson GP, Felde G, Gardner J, Hoke M, Jeong LS, Pukall B, Ratkowski A, BurkeHH. Atmospheric Correction for Short-wave Spectral Imagery Based on MODTRAN4. SPIE Proceedings on Imaging Spectrometry. 1999; 3753: 61-69.
35. Berk A, Bernstein LS, Anderson GP, Acharya PK, Robertson DC, Chetwynd JH, Adler-Golden SM. MODTRAN Cloud and Multiple Scattering Upgrades with Application to AVIRIS. Remote Sensing of the Environment.1998;65: 367-375.
36. Berk A, Bernstein LS, Robertson DC. MODTRAN: a moderate resolution model for LOWTRAN7. GL-TR-89-0122. Air Force Geophysical Laboratory. Hanscom AFB, MA. 1989; p. 38.
37. Matthew MW, Adler-Golden SM, Berk A, Richtsmeier SC, Levine RY, Bernstein LS, Acharya PK, Anderson GP, Felde GW, Hoke MP, Ratkowski A, Burke HH, Kaiser RD, Miller DP. Status of Atmospheric Correction Using a MODTRAN4-based Algorithm. SPIE Proceedings, Algorithms for Multispectral, Hyperspectral, and Ultraspectral ImageryVI.2000;4049: 199-207.
38. Vermote EF, Tanre D, Deuze JL, Herman M, MorcetteJJ. Second simulation of the satellite signal in the solar spectrum, 6S: An overview. IEEE Trans. Geosci. Remote. 1997; 35: 675–686.
39. Svetlana YK, Eric FV, Raffaella M, Frank JK, Jr. Validation of a vector version of the 6S radiative transfer code for atmospheric correction of satellite data.Part I: Path radiance. APPLIED OPTICS, 10 September 2006; 45: No. 26.
40. Zhaoming Z, Guojin H, Xiaoqin W. A Practical DOS model-based atmospheric correction algorithm. International Journal of Remote Sensing. 10 June 2010; 31: No. 11. 2837–2852.
41. Paolini L, Grings F, Sobrino JA, Jiménez Muñoz JC, Karszenbaum H. Radiometric correction effects in Landsat multi-date/multi-sensor change detection studies. Int. J. Remote Sens. 2006; 27: 685–704.
42. CuiQY, Gaillard MJ, Lemdahl G, Stenberg L, Sugita S, Zernova G. Historical land-use and landscape change in Southern Sweden and implications for present and future biodiversity. Ecol. Evol. 2014; 4: 3555-3570.
43. Congedo L. Semi-Automatic Classification Plugin for QGIS. Technical Report. Sapienza University, ACC Dar Project: Rome, Italy. 2013; 64. Lu, D.; Mausel, P.; Brondizio, E.; Moran.

Data Meta Information to run an ATCOR2 session

Table1.The parameters listed below are necessary to run an ATCOR2 session.

ATCOR2 Input Parameters	Source
Acquisition Date (Day and Month)	Available in the Meta-Data of the Satellite Scene.
The sequence of Input Bands (Layers)	Available in the Meta-Data of the Satellite Scene or set individually.
Sensor type	All Sensors supported can be selected.
Gain Settings of the Sensor (menu pops up if the sensor has variable Gain Setting)	Available in the Meta-Data of the Satellite Scene or already included in the Calibration-File.
Calibration-File	Examples to start from are available in the ATCOR2 menu. Detailed values can be extracted from the meta-data of the satellite scene or the data provider.
Solar Zenith Angle	Available in the Meta-Data of the Satellite Scene.
Model for Aerosol	The library is available from ATCOR2 Menu. External Models cannot be incorporated. If unavailable parameters can be assumed and checked with SPECTRA Module.
Model for Solar	Region Library is available from ATCOR2 Menu. External Models cannot be incorporated. If unavailable parameters can be assumed and checked with SPECTRA Module.

Model for Thermal Region (if thermal Band is included)	The library is available from ATCOR2 Menu. External Models cannot be incorporated. If unavailable parameters can be assumed and checked with SPECTRA Module.
Ground Visibility	Available from local Meteorological-Data. Parameters can be assumed and checked with SPECTRA Module.
Ground Elevation	Average elevation available from Ground Truth / topographic map.

Table 2. Approximate scene visibility values

Weather Condition	Scene Visibility
Clear	40 to 100 km
Moderate Haze	20 to 30 km
Thick Haze	15 km or less

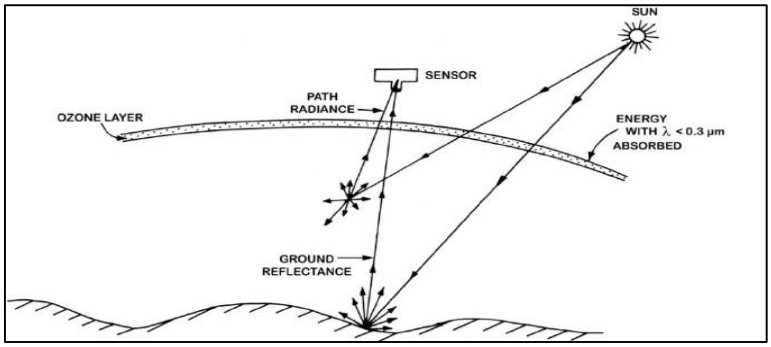

Figure 1 . Schematic showing atmospheric path radiance due to scattering[2].

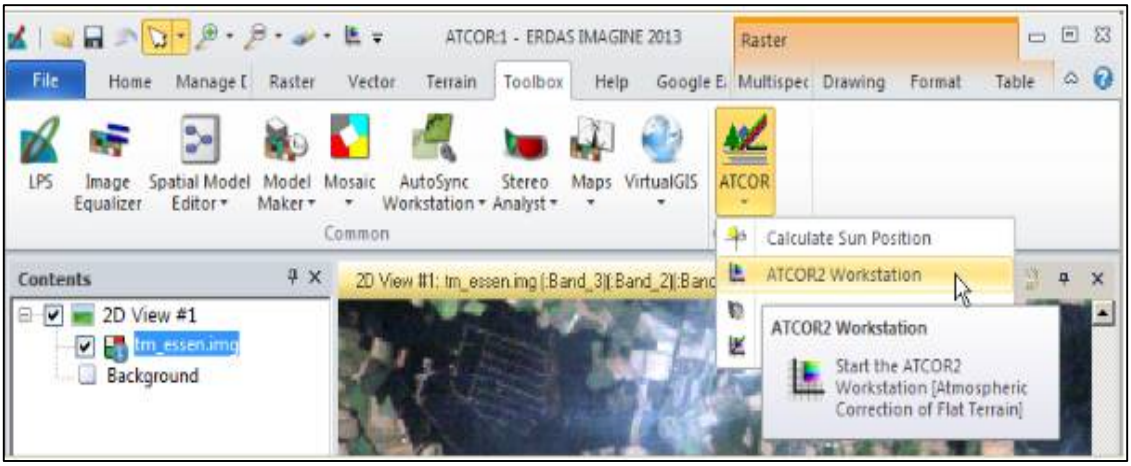

Figure 2. The ATCOR Menu

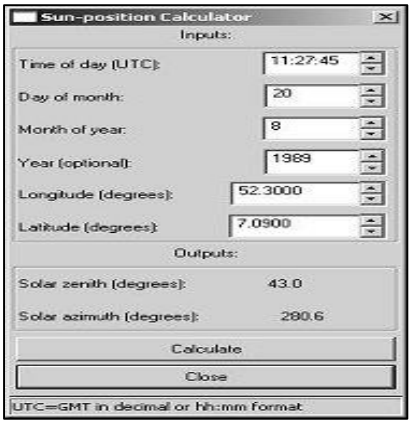

Figure 3. Sun-position Calculator menu

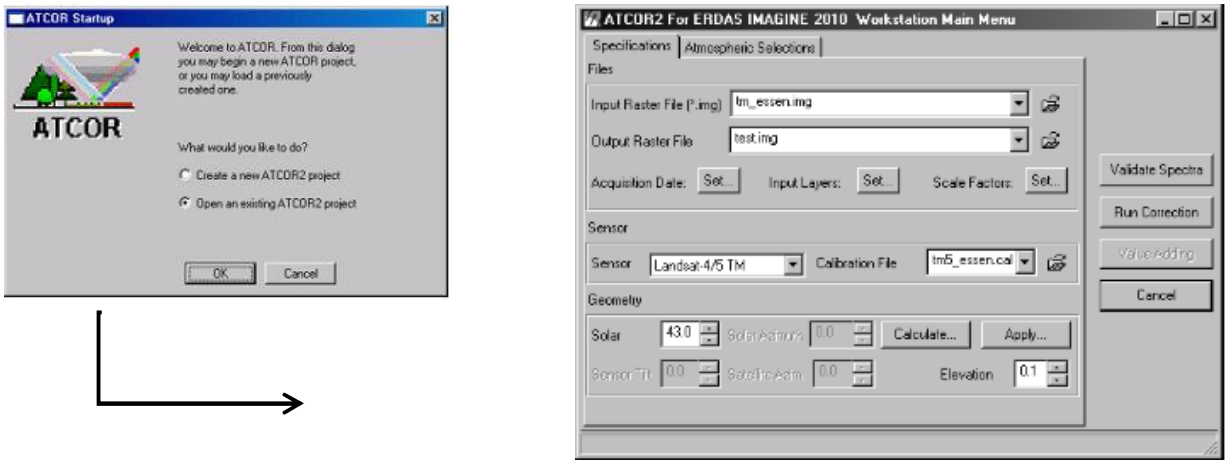

Figure 4. Workstation Menu

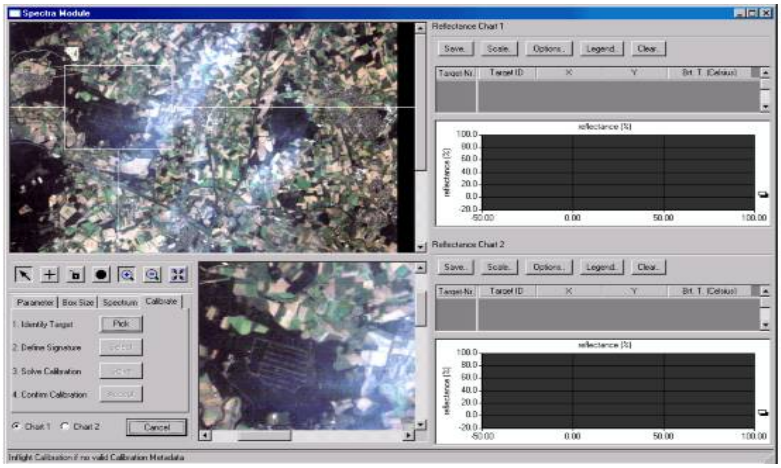

Figure 5. SPECTRA Main Display Setup

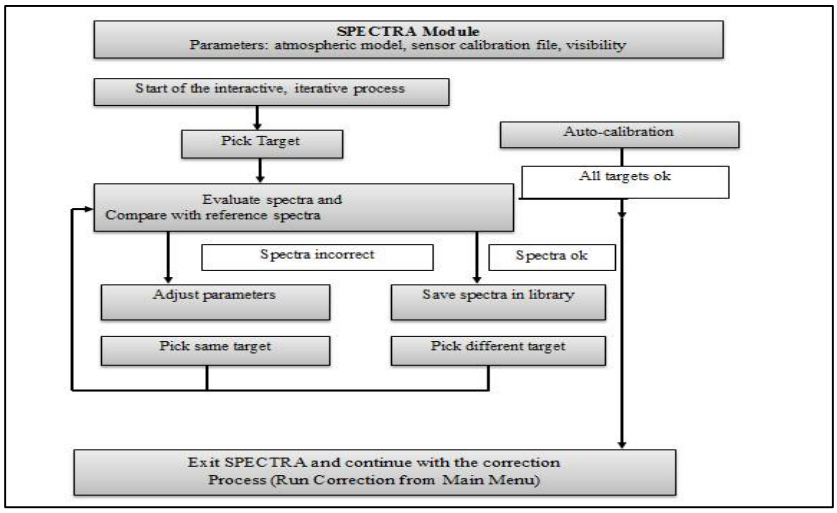

Figure 6. Functional flowchart of the SPECTRA Module for ATCOR2.

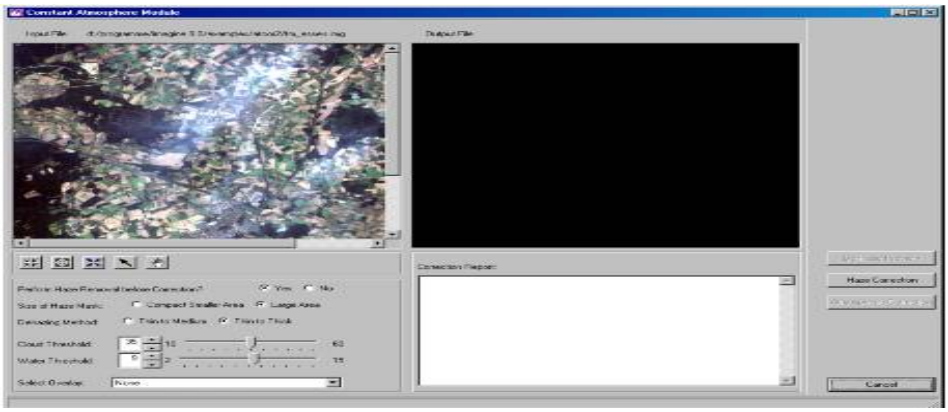

Figure7. Correction Menu of Haze Removal and Atmospheric

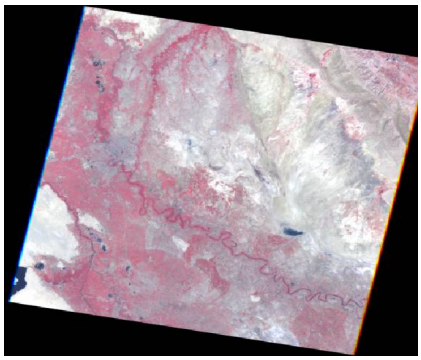

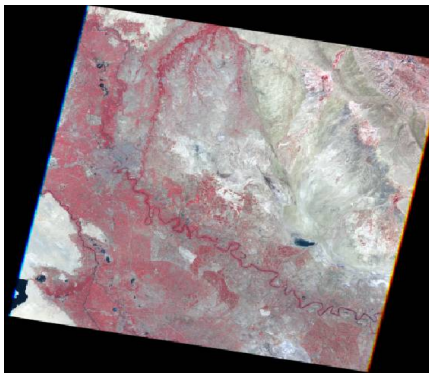

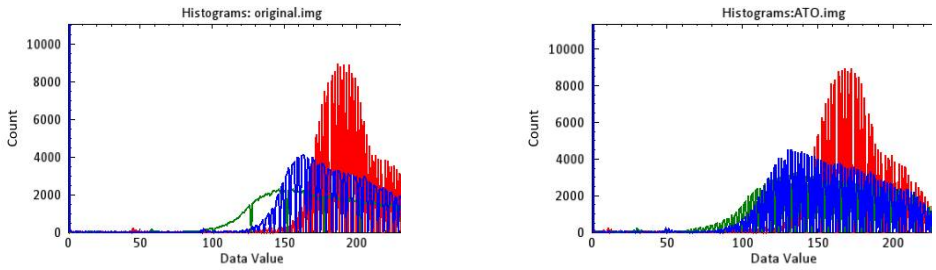

Original image **ATCOR image**

Figure 8 . The radiometrically corrected false-color images using (ATCOR)

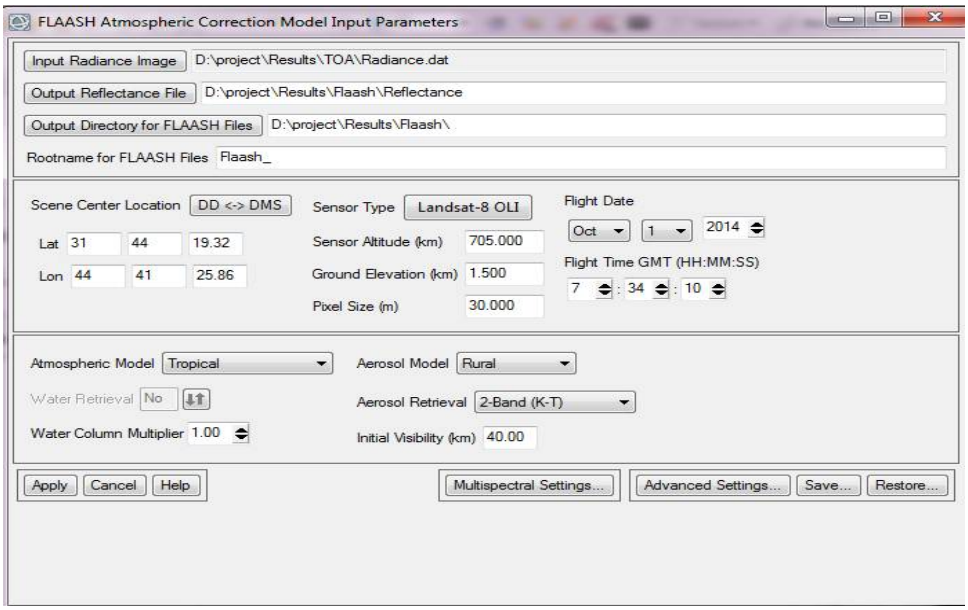

Figure 9 . FLAASH Atmospheric Corrections Model Input Parameters Dialog

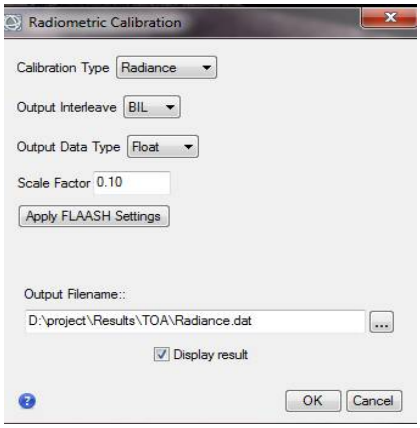

Figure 10. The Radiometric Calibration Model Input Parameters dialog

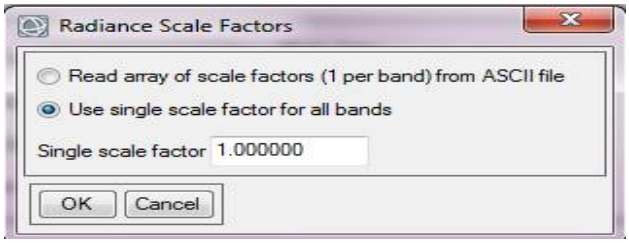

Figure11. Radiance Scale Factors Dialog

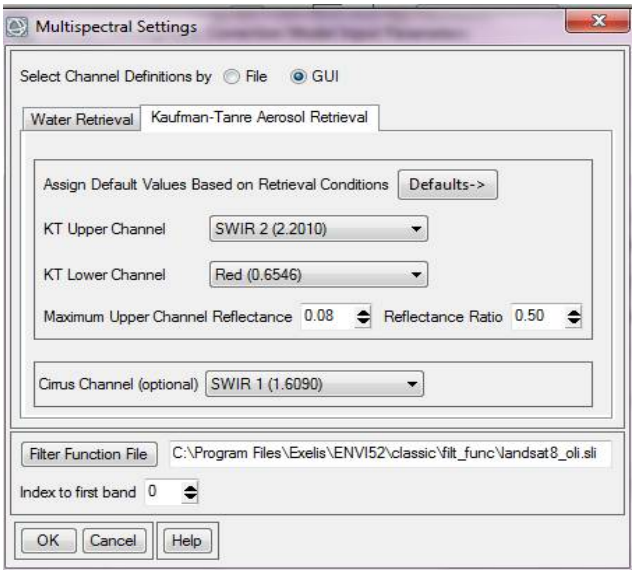

Figure 12. Multispectral Settings Dialog

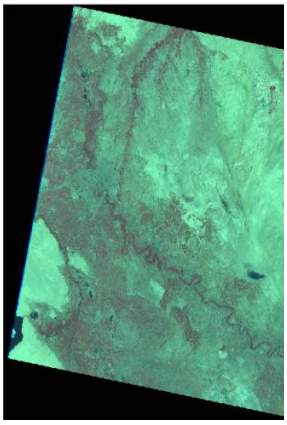

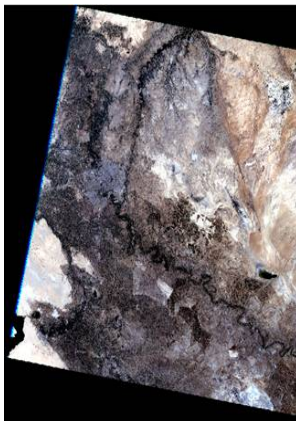

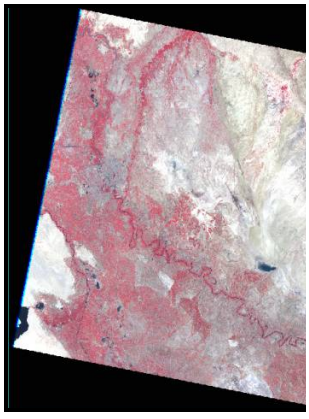

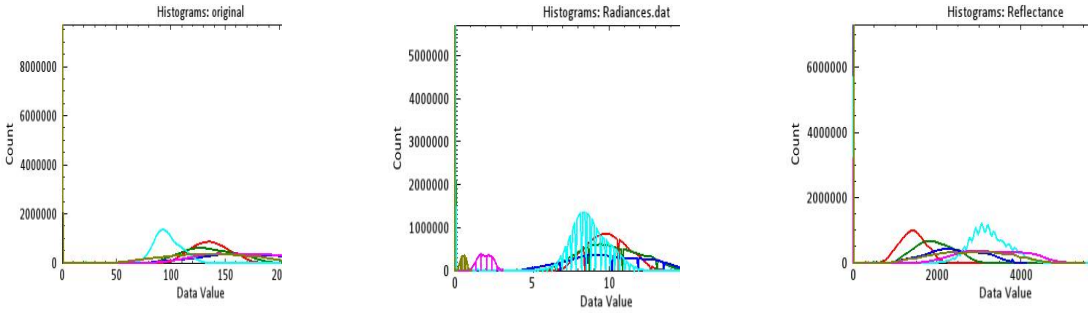

Original image **Radiance _ correct** **Reflectance_ correct**

Figure 13. The radiometrically corrected false-color images using FLAASH

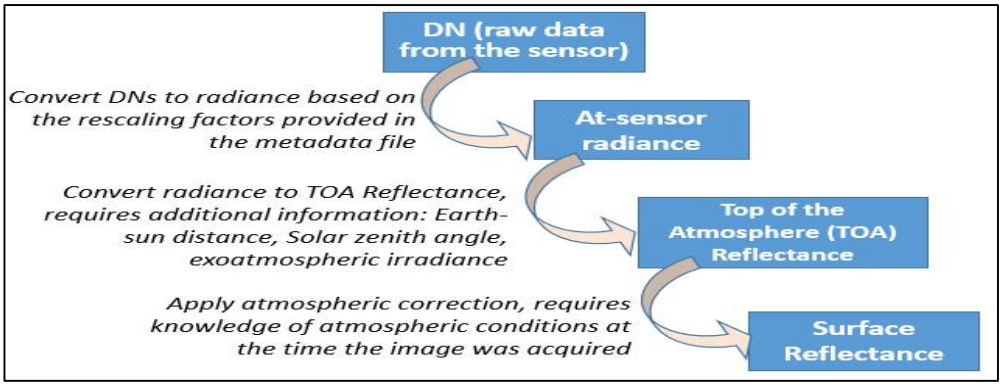

Figure 14. Radiometric Calibration and Correction Process

Indian Journal of Natural Sciences www.tnsroindia.org.in ©IJONS

Vol.9 /Issue 51 / December / 2018 *International Bimonthly* *ISSN: 0976 – 0997*

REVIEW ARTICLE

Evaluation of Discharge Coefficient in Hilla Head Regulator by Using Multi Parameters

Ali Hassan Hommadi[1]*, Fadhil M. Dahir[2] and Oday Tamween Al-Heetimi[3]

[1]M.Sc.in Water Resource, Ministry of Water Resources, Iraq,
[2]Kerbala Technical Institute, AL-Furat Al-Awsat Technical University, 56001 Kerbala, Iraq.
[3]M.Sc.in Hydraulics, Ministry of Water Resources, Iraq,

Received: 19 Aug 2018 Revised: 21 Sep 2018 Accepted: 23 Oct 2018

***Address for Correspondence**
Ali Hassan Hommadi
M.Sc.in water resource,
Ministry of Water Resources, Iraq,
E-mail:alihassan197949@yahoo.com/ inkr.fdl@atu.edu.iq/ oday.alheetimi@gmail.com

ABSTRACT

Water lacks problemand increasing water shortageare became an issuesthreatens the world. These issuescaused by heat retention and reduce river discharges by upstream countries.Therefore;an accurate discharge calculation for each river and water canal branches from dams, barragesand regulators built on main river became urgent need. In this research calculating the accurate discharge relay onestimating precise discharge coefficient with respect to some parameters as height of gate, daily discharge of river, upstream water level ,downstream level and case of flux (free or submerge). Result shows there are a relationship between discharge coefficient (Cd) and multi parameters (height opening gate (W), upstream head (hu), downstream head (hd), height of crest in upstream (p), height of crest in downstream (B)..Results bring to light the relationship between discharge cofficent and those parameter was strong when the flow submerge . Correlation values R^2 ranged between 0.86 to 0.88. In contrast the relationship was weakness when free flow conditions with correlation values ranged 0.37 to 0.69.Average discharge coefficients in submerged flow and free flow were 0.88 and 0.57,respectively.

Keywords: Hilla regulator, discharge coefficient, upstream and downstream water level of regulator.

INTRODUCTION

River discharge effected by several factors cause to reduce amount of discharge and increase the losses same as friction, minor losses, contraction, velocity losses and energy. These losses consequence on discharge by reducing the amount of discharge (Q) via multiply value of ideal Q by coefficient of discharge (Cd). Cd affected by energy, contraction of flux and velocity losses.Thair and Tahssen, (2006) state the hydraulic properties of a combined crested

sloped weir that contain on roundcrest with sharp below freeconditions. Theirexperimental study investigated discharge coefficient (Cd) and discharge of weirs. Theirstudyconducted on a model of weir made of roundcrest with sharp fixedperpendicular and slopedby angles 35°,45° and 60° in fluxdirection in the empirical channel. The model have angle of weir 35°with the channel center had best than 45° ,60° and 90°). The discharge coefficient raising as the ratio (h/P) raising for whole the testing angle.Thedischarge coefficient raising with the reduction of the weir sloped angle.Dabral et al., (2014) mentioned A channel have sidesglass sloping flow on experimental workconducted to limit the Cd and head-dischargerating curve for irrigation structures for example weir have broad edge also other havecrump, sluice andradial gate as well as Spillway of dam. The average Cd for broad edgeweirwas 0.44 andcrump weirwas0.85 also average sluice andradial Gate was0.76, 0.82, respectively.As well asthe average Cd of dam spillway was 1.03.In addition the Cdrelationship with h/a was linearly in whole cases with R2 ranged 0.8 to 0.99.Cd values increased with h/a in all cases.All hydraulic structures which were selected in study shown powerrelationship between head and discharge.Eman et al.,(2013)studied applications of weir in the measuringthe discharge in big and small channels were infree field orthe lab.

The weirs sharp was widespread with rectangular and triangular opening.Cd values raged between 0.55 for rectangular and 0.59 for triangular opening respectively and changing of notchinfluenceon viscosity also on surface tension and roughness.Models with half of circle opening in three various models have diameters 6cm, 8cm and 10cm.The models have same conditions as temperature and for multi times and the models havehalf circle, v-openingalso rectangular opening. The values of Cd of the rectangular opening range 0.73- 0.71, in the other hand V opening ranged 0.85- 0.78 .Nevertheless Cd of semi-circular openingranged 0.93- 0.88. In conclusion half-circular openingwas best in measuring of hydraulicdischarge fromother opening.Anees (2013)utilizingweirs and gates to control and adjust the flux in channel. Some gates have possibility of retention materials floating .Indecate this issue can be solved if the floating combined near weirs. As well as the sediment problem in weir can be also solve bycombining of weirs with sluice gates. Research was conducted in the fluid laboratory of civil engineering in Babylon University .Results showed that theexperiments erected on the notches were obtained for discharge coefficient Cd as follows:rectangular weir have discharge coefficientequal to 0.607 , V_ openingCd = 0.630 , Semicircular weir Cd = 0.693,Combined V-opening weir and Rectangular gate Cd = 0.779 , Combined rectangular weirand Rectangular gate Cd = 0.751 , Combined half circle weir and rectangular gate Cd= 0.781 and Combined half circle weir and half circle gate Cd = 0.797 . Cd in the Compound half circle weir and half circle gate are better than other opening.Riyadh, (2013) calculate Cd of flux over rectangular weir with 1/4 circlenotch crested extending through the all width of the channel was suspending to calculateCd of the flux.

Threeweirs were built and checked for various discharges. The information whichgot from lab provide on head - discharge relation for three samples with various height and curvetingin weir. Each sample has an experimental head – discharge formula.The Cd measured flow rate and the derived flow rateformula. In this study estimated the Cd forrectangular weir. Cd reduction with head upstream the weir crest raised.The height and degree of curveting has a significant effecting on Cdand Cd raised if thestreamlines curvetingraising. Thus the discharge coefficient is depending on shape and type ofthe measuring structure.Safaa, (2013)examinethe influence of variousquantity of total solids (TS) on the discharge pattern and Cd in channels and station of water treatment for ogee spillway, broadand crumpweir. 10testing were conducted on each kind of weir.First one testused tap water but others had various values of TS changing from 620 to 1121 ppm. Each test has 8 values of discharges. The Cd changes with respect of value total solids TS. The Cd values werelarger than the tap watervalue. Results showsdischarge coefficient values decresed when TS values were increasing .Emad, (2012)presents an experimental study and analysis for influence of the geometrical properties, of the oblique cylindrical weir on Cd with three sizes utilized for the weir and 2 angles for the perversion.the Cd is influenceviaengineeringproperties represented via radius of the weir and the angle of sloping with wall of channel.

The raising in the radius of the weir willreduceCd cylindrical weir. Cd of the oblique weir is greater than the Cd of the classic weir. The Cd is immediately proportional with the weir inclining.The oblique weir is higherinfluence than

the normal the raising in the inclining angle willraise in the Cd values. The Cd is moreinfluencedvia the upstream head over the crest. the Cd redused as the radius of weir raised.Ghania et al.,(2012)investigate the Cd for labyrinthine side weir which constructing and building in upstream of side channel of width,depth and long 15,30 and 200cm, respectively with constant horizontal bed. The weir height were changes to 3 types as 9, 12 and 15 cm, respectively and each 8 tested for 4various angels of the weir crest 45º,60º,75º,90º. The weirs utilized with direction and opposite direction of flux with various discharges.The labyrinthine side weir with the less height and the less angle is greater efficient when lay down in the direction of flux. The Cd in direction and opposite direction of flow was affectedby length of weir to the depth of flux.Ghania et al., (2005)study empirically the water surfaceprofiles and to get convenient expressions for calculation Cdfor open flow over the type weir named chimney weir and the discharge factor (q/q1) forsubmerged flux. Four chimney weir models with varioustop angles were built and lab orating, the surface of the water profiles of whole models were soft upstreamand the water fall suddenly on downstream the model and at a maximumflow ratethe water surface profile was concave but at minimumflow rate the water surface profile was convex. The Cd for open flow increased when the upstream head increased and half top angle decresed. While q/q1for submerged flux increased with the decreased of the submergence ratio (h2/h1). Cd calculated with respect of (h/p),(w/p) and half top angle for open flow conditions ; also, calculate q/q1 with respectto the submergence ratio(h2/h1) and (h1/p).The study shows q/q1 incresed when h2/h1 decresed for submerged fluxcases.h1= upstream head, h2= downstream head, q=discharge, q1= discharge due to effect upstream head ,p= height of weir and w= width of crest weir.

MATERIALS AND METHODS

In this research operating condition and required discharge in downstream were the constrain for number of gate opened; so number of gate were open and other were closed Work is carried out for one month for Hilla head regulator with different reguired discharges and different gate opening Hilla head regulator one of new Hindiya barrage in Sadat Al -hindiya city of Babil province in Iraq as shown in Fig. (1) New Hindiya barrage located on latitude ◌32 43' N and longitude ◌4416'E . Elevation of ground level barrage 29m above sea level . Fig. (2) shown radial gate of hilla head regulator with two cases partially gate opening free flow condition shown in (a) and submerged in (b). In this work the Cd of two cases were examine (submerged and free).

Determining the cases of free flow and submerge in downstream of gate by downstream water level of river and crest level of foundation and open gate heightby calculating the difference between open gate water level and downstream water level. The radius of gate(r) was 6.8m and crest level was 27.4m also shift level of gate was 32.60m therefore a= 32.60-27.4 = 5.2m and subtract with height of opening gate to obtain on vertical height dividing on r=6.8m get on cos(Ɵ) after than obtain on angle of open gate as shown in table (2).If the free flow the downstream water level (hd) ≤ crest level under gate + height opening of gate(a). The velocity of Euphrates was ranged from 0.8 to 1 m/s near the Hilla regulators take as average 0.9 m/s. ha= approach velocity head = 0.04m. bed level in U/S = 25.30 and in D/S = 26.10

Field work calculations and Equations

The work conductedin Hilla head regulator which located on left side of Euphratesriver with multi regulators (Hilla-Kifil canal regulator, Husienia regulator, Beni hassan regulator and Al-Hindyia barrage). Hilla head regulator is a hydraulic structure constructed from reinforced concrete material contain on six slots with six radial gates managed hydraulically .These gatesoperates automatically via central control room in hydro-electric station. Design discharge of Hilla head regulator was 326 m^3/s with upstream normal water level 32.55 above sea level while the operation discharge of it was 200m^3/s but in shortage season reached to 100 m^3/s as average discharge and normal water level 31.90m also upstream floor level (crest level) was 27.40m and downstream floor level was 26.10m. The dimension of steel plates gate were 5.4m height and 6m width. The gate can be making to rotate about fixed horizontal axis. The

length of floor regulator in upstream was 10.8m and 13.2m in downstream. The hilla head regulator regulate and gave water from Euphrates river to Shat-Alhilla river which in turn irrigate the farms have area 420000 hector. The approach velocity(va) ranged from 0.8 to 1 m/s as average 0.9 m/s.two state of study to calculate discharge coefficient(Cd)value when free flow in downstream and submerged flow of downstream.
The discharge is determined by the orifice equation

Q= C*A$\sqrt{2gh}$ .....(1)

A= Area of water way through the regulator= S* W
W = actual height of gate above sill in partially closed opening
D/S W.L-Sill level under gate if fully open gate
C = Coefficient of discharge without unit
Q= discharge m^3/s
H = difference in U/S and D/S water level if fully open gate and submerge partially open gate but equal U/S and level of sill if free flow.

If inter velocity of approach Va as head ha = $Va^2/2g$ the eq.(1) become

Q= C*S*W*$\sqrt{2gh + ha}$ .....(2)

Cd = α * Cc *Cv.....(3)

Cv = $\frac{V\ actual\ velocity\ at\ vena-contracta}{V\ theoretical\ or\ ideal\ velocity}$.....(4)

Cc = contraction coefficient = $\frac{area\ of\ jet\ at\ vena-contracta}{the\ area\ of\ the\ orfice}$.....(5)

A = energy coefficient = actual energy head / theoreticalenergy head.

CONCLUSION

- Average value of discharge coefficient of submerged flow in downstream near gate was 0.88 while in free flow was o.57.
- The Cd value increase when the ratio of hu/p, hu/B, hd/hu and Q/Q1 increase but the Cd decrease if height of opening gate (W) increase.
- The R^2 was high in submerged flow ranged between 0.88- 0.86 while in free flow was ranged between 0.37 to 0.69.

RECOMMENDATIONS

- Calculate the Cd to Al Hindiya barrage gates, Beni Hissan regulator gates, alhuseinia regulators gates (old regulator and new regulator).
- Calculate the accumulated sediment in downstream and upstream and effecting on discharge in water shortage season.
- Calculate uplift pressure under regulators and barrage in water shortage season.

REFERENCES

1- Thair Mahmood Al-Taiee Tahssen Ali Hassan Chilmeran, 2006"Hydraulic Characteristics of Flow Over Compound Crested Weir" Al-Rafidain Engineering Vol.14, No.2, pp.81-87.
2- P. P. Dabral, P. K. Pandey, Tushar Kumar and Sourav Chakraborty 2014 "Determination of Discharge Coefficient And Head-Discharge Relationships of Different Hydraulic Structures "Journal of Indian Water Resources Society, Vol 34, No.1, January.
3- Eman Mehdi Al-Mousawi Udai Adnain Jahad Anees Kadhum Idrees AL-Saadi, 2013 "Evaluate the Discharge Cofficient of Semi Circular Weir (notch)" Journal of Babylon University/Engineering Sciences/ No.(5)/ Vol.(21): 1568
4- Anees Kadhum Idrees AL-Saadi "Study Coefficient of Discharge for a Combined Free Flow over Weir and under Gate for Multi Cases" Euphrates Journal of Agriculture Science-5 (4): 26-35 , (2013) AL-Saadi 62, ISSN 2072 3875
5- Eman Mehdi Al-Mousawi Udai Adnain Jahad Anees Kadhum Idrees AL-Saadi, 2013 "Evaluate the Discharge Cofficient of Semi Circular Weir (notch)" Journal of Babylon University/Engineering Sciences/ No.(5)/ Vol.(21): 1568
6- Riyadh Hamad Mohammed, 2013 "Calibrating the Discharge Coefficient of Rectangular with Quarter Circular Edge Crested Weir" Journal of KerbalaUniversity , Vol. 11 No.2 Scientific . 64
7- Safaa Nasser Hassan,2013"The Effect of Total Solids on the Discharge Coefficient of Spillway, Broad crested weir and Crump weir" Journal of Engineering and Development, Vol. 17, No.2, 2013, ISSN 1813- 7822
8- Emad Abdul Gabbar Al Babely,2012"Behavior of the Discharge Coefficient for the Overflow Characteristics of Oblique Circular Weirs" Tikrit Journal of Engineering S ciences/Vol.19/No.4/December, (55-64)
9- Ghania Hayawi, Azza Al-Talib and Mena Al-Sawaf,2012 "Coefficient of Discharge for Labyrinthine Side Weir" Al-Rafidain Engineering Vol.20 No. 4 August, pp.38-48.
10- Ghania A.M.Hayawi, Hanaa A .M.Hayawi Amal A.G.Yahya, 2005 "Coefficient of Discharge of Chimney Weir Under Free and Submerged Flow Conditions" Al_Rafidain engineering Vol.13 No.1,62.

Table 1. Shown U/S and D/S Water level Number of Gate openedand Total Discharge

Hilla Regulator Gates Discharge										
Date	Up Stream Gage Height	Down Stream Gage Height	Discharge	No of Gate Opened	Gate 1	Gate 2	Gate 3	Gate 4	Gate 5	Gate 6
08-Mar-18	31.55	29.4	90	3	1.4	closed	0.8	closed	closed	1.25
09-Mar-18	31.6	29.5	100	3	1.4	closed	1.1	closed	closed	1.25
10-Mar-18	31.6	29.5	100	3	1.4	closed	1.1	closed	closed	1.25
11-Mar-18	31.6	29.5	100	3	1.4	closed	1.1	closed	closed	1.25
12-Mar-18	31.6	29.7	120	3	1.4	closed	1.2	closed	closed	1.25
13-Mar-18	31.6	29.7	120	4	1.4	closed	0.6	0.6	closed	1.25
14-Mar-18	31.70	29.8	130	4	1.4	closed	0.6	1.1	closed	1.25
15-Mar-18	31.70	29.9	140	4	1.4	closed	1.2	1.2	closed	1.25
16-Mar-18	31.70	30.00	140	4	1.4	closed	1.2	1.2	closed	1.25
17-Mar-18	31.70	30.00	140	4	1.4	closed	1.2	1.2	closed	1.25
18-Mar-18	31.70	30.00	140	4	1.4	closed	1.2	1.2	closed	1.25
19-Mar-18	31.70	30.00	140	4	1.4	closed	1.2	1.2	closed	1.25
20-Mar-18	31.70	30.00	140	4	1.4	closed	1.2	1.2	closed	1.25
21-Mar-18	31.70	30.00	140	4	1.4	closed	1.2	1.2	closed	1.25
22-Mar-18	31.70	30.00	140	4	1.4	closed	1.2	1.2	closed	1.25
23-Mar-18	31.80	30.00	140	4	1.4	closed	1.2	1.2	closed	1.25
24-Mar-18	31.80	30.00	140	4	1.4	closed	1.2	1.2	closed	1.25
25-Mar-18	31.80	29.90	130	4	1.4	closed	1	1	closed	1.25
26-Mar-18	31.80	29.90	130	4	1.4	closed	1	1	closed	1.25
27-Mar-18	31.75	30.00	140	4	1.4	closed	1.05	1.05	closed	1.25
28-Mar-18	31.75	30.00	140	4	1.4	closed	1.05	1.05	closed	1.25
29-Mar-18	31.75	30.00	140	4	1.4	closed	1.05	1.05	closed	1.25
30-Mar-18	31.75	30.00	140	4	1.4	closed	1.05	1.05	closed	1.25
31-Mar-18	31.80	30.10	150	4	1.4	closed	1.30	1.30	closed	1.30
01-Apr-18	31.80	30.10	150	4	1.4	closed	1.30	1.30	closed	1.30
02-Apr-18	31.80	30.10	150	4	1.4	closed	1.30	1.30	closed	1.30
03-Apr-18	31.80	30.00	140	4	1.4	closed	0.90	0.90	closed	1.30
04-Apr-18	31.80	30.00	140	4	1.4	closed	0.90	0.90	closed	1.30
05-Apr-18	31.80	30.00	140	4	1.4	closed	0.90	0.90	closed	1.30
06-Apr-18	31.80	30.00	140	4	1.4	closed	0.90	0.90	closed	1.30
07-Apr-18	31.70	30.00	140	4	1.00	closed	1.00	1.00	closed	1.60

Nomenclature

Q1 = discharge of Euphrates riverQ = discharge of Hill canal , hu = upstream water level – crest level hd = downstream water level – crest level, w = height of opening gate r = radius gate,a = shift gate level – crest levelp = crest level – upstream bed level ,B = crest level - downstream bed level,Θ = angle opening of gateS = width opening gate

Table 2. Shown the Open Gateswith Angle of Gate

Radius of shift gate	Deference crest level and shift level	cosΘ1	cosΘ3	cosΘ4	cosΘ6	Θ1	Θ3	Θ4	Θ6
6.8	5.2	0.56	0.65	-	0.58	56.05	49.70	-	54.52
6.8	5.2	0.56	0.60	-	0.58	56.05	52.95	-	54.52
6.8	5.2	0.56	0.60	-	0.58	56.05	52.95	-	54.52
6.8	5.2	0.56	0.60	-	0.58	56.05	52.95	-	54.52
6.8	5.2	0.56	0.59	-	0.58	56.05	54.00	-	54.52
6.8	5.2	0.56	0.68	0.68	0.58	56.05	47.46	47.46	54.52
6.8	5.2	0.56	0.68	0.60	0.58	56.05	47.46	52.95	54.52
6.8	5.2	0.56	0.59	0.59	0.58	56.05	54.00	54.00	54.52
6.8	5.2	0.56	0.59	0.59	0.58	56.05	54.00	54.00	54.52
6.8	5.2	0.56	0.59	0.59	0.58	56.05	54.00	54.00	54.52
6.8	5.2	0.56	0.59	0.59	0.58	56.05	54.00	54.00	54.52
6.8	5.2	0.56	0.59	0.59	0.58	56.05	54.00	54.00	54.52
6.8	5.2	0.56	0.59	0.59	0.58	56.05	54.00	54.00	54.52
6.8	5.2	0.56	0.59	0.59	0.58	56.05	54.00	54.00	54.52
6.8	5.2	0.56	0.59	0.59	0.58	56.05	54.00	54.00	54.52
6.8	5.2	0.56	0.59	0.59	0.58	56.05	54.00	54.00	54.52
6.8	5.2	0.56	0.59	0.59	0.58	56.05	54.00	54.00	54.52
6.8	5.2	0.56	0.62	0.62	0.58	56.05	51.88	51.88	54.52
6.8	5.2	0.56	0.62	0.62	0.58	56.05	51.88	51.88	54.52
6.8	5.2	0.56	0.61	0.61	0.58	56.05	52.42	52.42	54.52
6.8	5.2	0.56	0.61	0.61	0.58	56.05	52.42	52.42	54.52
6.8	5.2	0.56	0.61	0.61	0.58	56.05	52.42	52.42	54.52
6.8	5.2	0.56	0.61	0.61	0.58	56.05	52.42	52.42	54.52
6.8	5.2	0.56	0.57	0.57	0.57	56.05	55.03	55.03	55.03
6.8	5.2	0.56	0.57	0.57	0.57	56.05	55.03	55.03	55.03
6.8	5.2	0.56	0.57	0.57	0.57	56.05	55.03	55.03	55.03
6.8	5.2	0.56	0.63	0.63	0.57	56.05	50.80	50.80	55.03
6.8	5.2	0.56	0.63	0.63	0.57	56.05	50.80	50.80	55.03
6.8	5.2	0.56	0.63	0.63	0.57	56.05	50.80	50.80	55.03
6.8	5.2	0.56	0.63	0.63	0.57	56.05	50.80	50.80	55.03

6.8	**5.2**	**0.62**	**0.62**	**0.62**	**0.53**	**51.88**	**51.88**	**51.88**	**58.06**

Table 3.Shown Discharge Coefficient (Cd) at submerged and free in partially open gate with Velocity Approached Head.

Average open gate	H submerge	H free	Q(m^3/s)	Total Area (AT)(	ha	2gh	$(2gh)^{0.5}$*AT	Cd Submerge	Cd Free
1.15	2.15	4.19	90	18.63	0.04	42.97	122.12	0.74	0.53
1.25	2.1	4.24	100	20.25	0.04	41.99	131.21	0.76	0.54
1.25	2.1	4.24	100	20.25	0.04	41.99	131.21	0.76	0.54
1.25	2.1	4.24	100	20.25	0.04	41.99	131.21	0.76	0.54
1.28	1.9	4.24	120	20.79	0.04	38.06	128.26	0.94	0.63
0.96	1.9	4.24	120	20.79	0.04	38.06	128.26	0.94	0.63
1.09	1.9	4.34	130	23.49	0.04	38.06	144.92	0.90	0.60
1.26	1.8	4.34	140	27.27	0.04	36.10	163.85	0.85	0.56
1.26	1.7	4.34	140	27.27	0.04	34.14	159.33	0.88	0.56
1.26	1.7	4.34	140	27.27	0.04	34.14	159.33	0.88	0.56
1.26	1.7	4.34	140	27.27	0.04	34.14	159.33	0.88	0.56
1.26	1.7	4.34	140	27.27	0.04	34.14	159.33	0.88	0.56
1.26	1.7	4.34	140	27.27	0.04	34.14	159.33	0.88	0.56
1.26	1.7	4.34	140	27.27	0.04	34.14	159.33	0.88	0.56
1.26	1.8	4.44	140	27.27	0.04	36.10	163.85	0.85	0.55
1.26	1.8	4.44	140	27.27	0.04	36.10	163.85	0.85	0.55
1.16	1.9	4.44	130	25.11	0.04	38.06	154.92	0.84	0.55
1.16	1.9	4.44	130	25.11	0.04	38.06	154.92	0.84	0.55
1.19	1.75	4.39	140	25.65	0.04	35.12	152.01	0.92	0.59
1.19	1.75	4.39	140	25.65	0.04	35.12	152.01	0.92	0.59
1.19	1.75	4.39	140	25.65	0.04	35.12	152.01	0.92	0.59
1.19	1.75	4.39	140	25.65	0.04	35.12	152.01	0.92	0.59
1.33	1.7	4.44	150	28.62	0.04	34.14	167.22	0.90	0.56
1.33	1.7	4.44	150	28.62	0.04	34.14	167.22	0.90	0.56
1.33	1.7	4.44	150	28.62	0.04	34.14	167.22	0.90	0.56
1.13	1.8	4.44	140	24.3	0.04	36.10	146.00	0.96	0.62
1.13	1.8	4.44	140	24.3	0.04	36.10	146.00	0.96	0.62
1.13	1.8	4.44	140	24.3	0.04	36.10	146.00	0.96	0.62
1.13	1.8	4.44	140	24.3	0.04	36.10	146.00	0.96	0.62
1.15	1.7	4.34	140	24.84	0.04	34.14	145.14	0.96	0.61
							Average Cd	0.88	0.57

Table 4 .Shown The Relationship Between Cd and Hd (water level in D/S – crest level)

Hd	hd/w *	Cd Submerge	Cd Free	Cd sub. (w/hd)	Cd fr. (w/hd)
2	1.74	0.74	0.53	0.43	0.30
2.1	1.68	0.76	0.54	0.45	0.32
2.1	1.68	0.76	0.54	0.45	0.32
2.1	1.68	0.76	0.54	0.45	0.32
2.3	1.79	0.94	0.63	0.52	0.35
2.3	2.39	0.94	0.63	0.39	0.26
2.4	2.21	0.9	0.6	0.41	0.27
2.5	1.98	0.85	0.56	0.43	0.28
2.6	2.06	0.88	0.56	0.43	0.27
2.6	2.06	0.88	0.56	0.43	0.27
2.6	2.06	0.88	0.56	0.43	0.27
2.6	2.06	0.88	0.56	0.43	0.27
2.6	2.06	0.88	0.56	0.43	0.27
2.6	2.06	0.88	0.56	0.43	0.27
2.6	2.06	0.88	0.56	0.43	0.27
2.6	2.06	0.85	0.55	0.41	0.27
2.6	2.06	0.85	0.55	0.41	0.27
2.5	2.15	0.84	0.55	0.39	0.26
2.5	2.15	0.84	0.55	0.39	0.26
2.6	2.19	0.92	0.59	0.42	0.27
2.6	2.19	0.92	0.59	0.42	0.27
2.6	2.19	0.92	0.59	0.42	0.27
2.6	2.19	0.92	0.59	0.42	0.27
2.7	2.04	0.9	0.56	0.44	0.27
2.7	2.04	0.9	0.56	0.44	0.27
2.7	2.04	0.9	0.56	0.44	0.27
2.6	2.31	0.96	0.62	0.42	0.27
2.6	2.31	0.96	0.62	0.42	0.27
2.6	2.31	0.96	0.62	0.42	0.27
2.6	2.31	0.96	0.62	0.42	0.27
2.6	2.26	0.96	0.61	0.42	0.27

- W= height Opening gate , sub = submerge flow in D/S and fr.= free flow in D/S

Figure 1. Illustreate Google Map For.New Hindya BarrageSystem

(a) Partially Free Flow **(b) Partially Submerged Flow**

Figure 2.Illustreate Radial Gate of Hilla Head Regulator

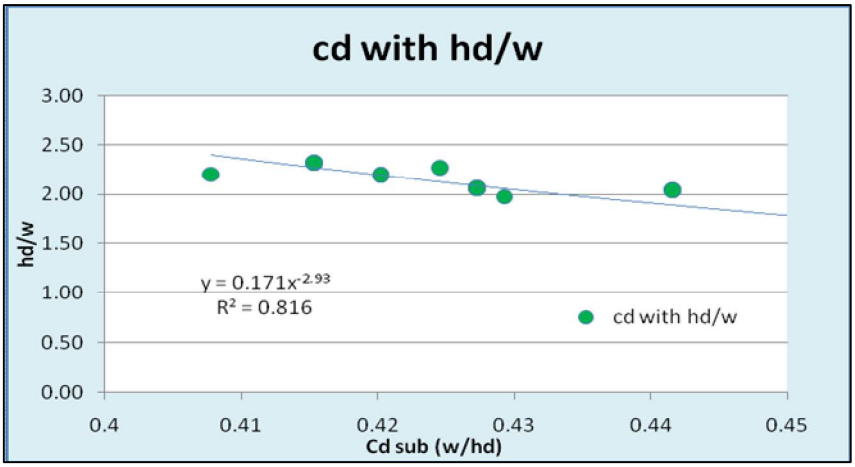

Figure 3. shown the relationship (hd/w) with Cd sub (w/hd)

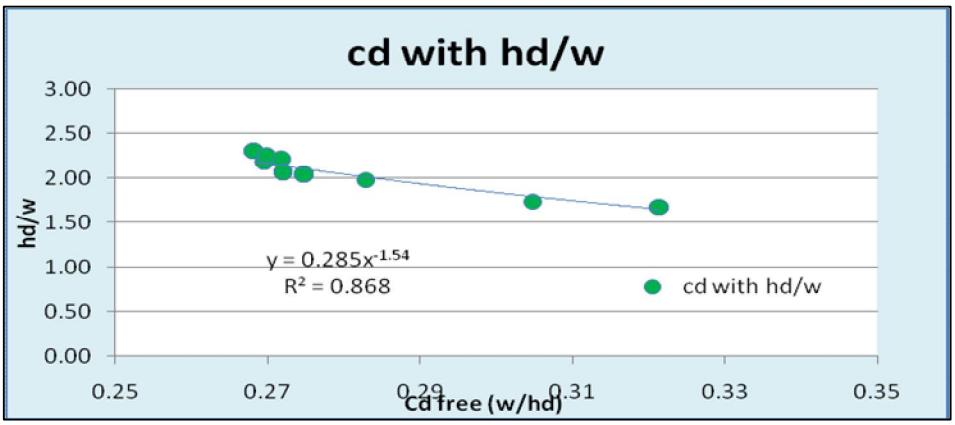

Figure 4. shown the relationship (hd/w) with Cd free (w/hd)

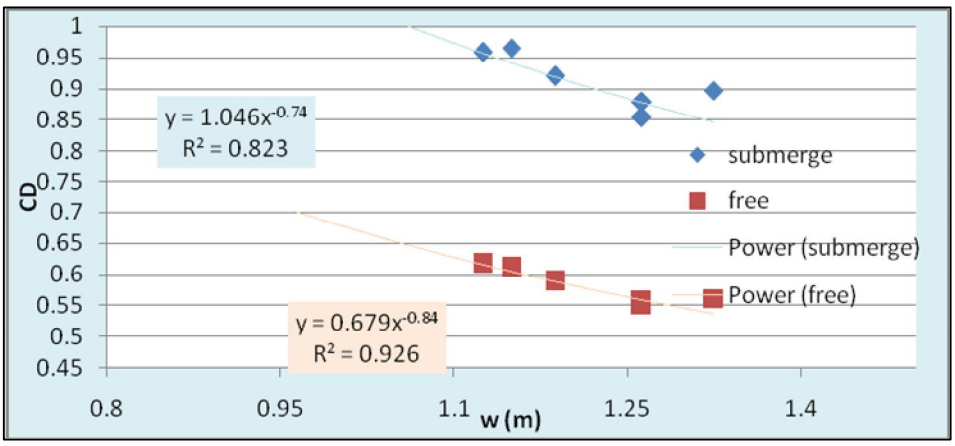

Figure 5. shown the relationship discharge coefficient (Cd) with height opining of gate (w)

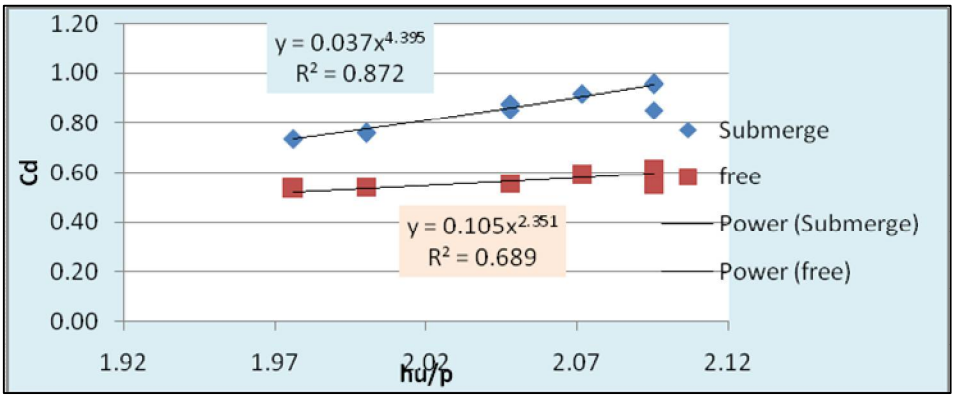

Figure 6.shown the relationship discharge coefficient (Cd) with ratio hu/P

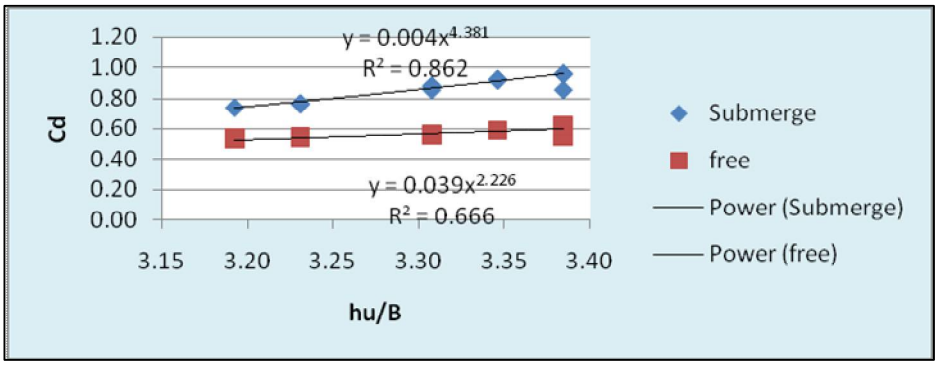

Figure 7. shown the relationship discharge coefficient (Cd) with ratio hu/B

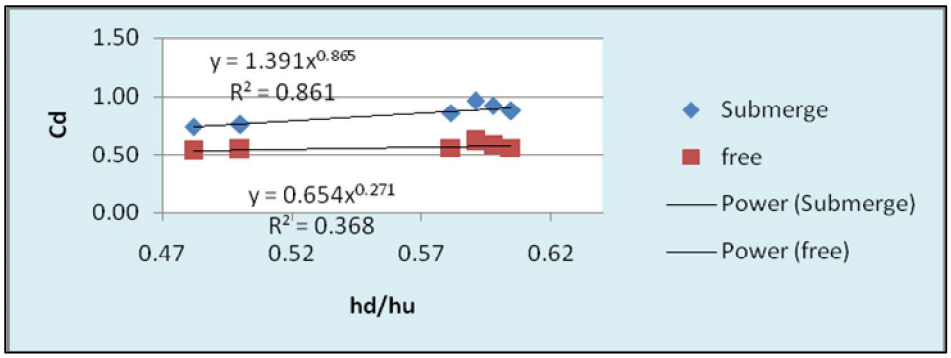

Figure 8.shown the relationship discharge coefficient (Cd) with ratio hd/hu

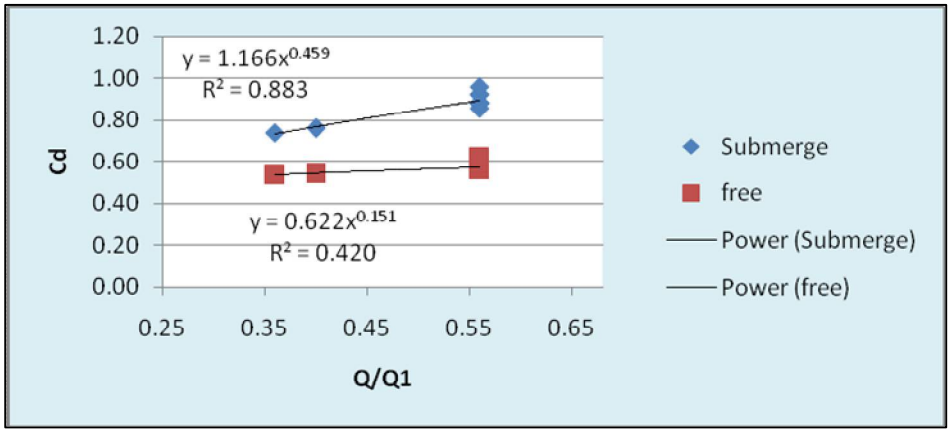

Figure 9.shown the relationship discharge coefficient (Cd) with ratio Q/Q1

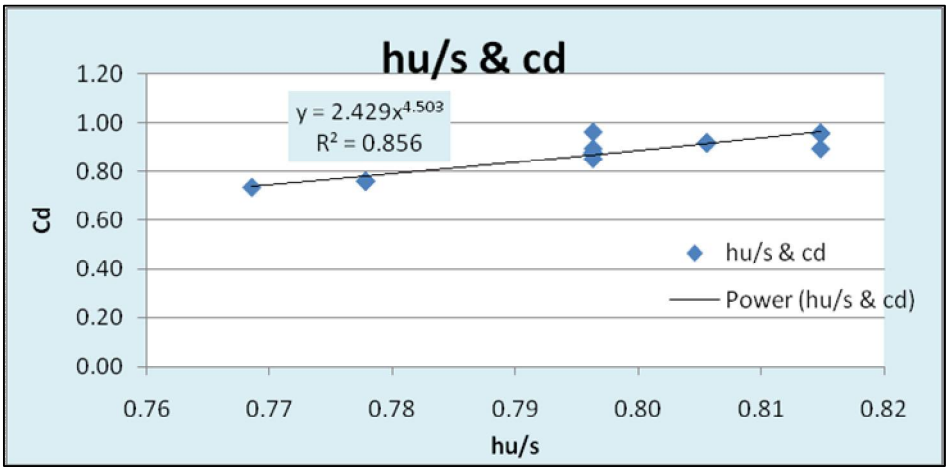

Figure 10. shown the relationship discharge coefficient (Cd) with ratio hu/s

Indian Journal of Natural Sciences www.tnsroindia.org.in ©IJONS

Vol.9 /Issue 51 / December / 2018 *International Bimonthly* *ISSN: 0976 – 0997*

RESEARCH ARTICLE

Expression of CCK, GIP and GLP-2 Immunoreactive Cells in the Small Intestine of the Adult Guinea Fowl (*Numida meleagris*): Frequency and Distribution an Immunohistochemistry Study

Fatimah Swadi Zghair[1]* and Iman Mousa Khaleel[2*]

[1]Department of Anatomy and Histology, College of Veterinary Medicine, University of AL-Qadisiyah, Iraq.
[2]Department of Anatomy, College of Veterinary Medicine, University of Baghdad, Iraq

Received: 23 Sep 2018 Revised: 25 Oct 2018 Accepted: 28 Nov 2018

***Address for Correspondence**
Fatimah Swadi Zghair
Department of Anatomy and Histology,
College of Veterinary Medicine,
University of AL-Qadisiyah, Iraq.
Email: fatima.alrakabi@qu.edu.iq

ABSTRACT

In some parts of small intestinal tract, enteroendocrine cells (EEC)act as the endocrine parts by secretion of hormones. They play important roles in the regulation of secretions of some important organs. For the importance of these hormones in the preservation of the internal environment of the body,we needed to study the proliferation and distribution of these cells in the small intestine using adult guinea fowl (*Numida meleagris*). The regional localization of immunoreactive endocrine cells (IRC) in some parts of small intestine tract of the adult guinea fowls was inspected using immunohistochemistry techniques. Specimens from ten the adult guinea fowls from both sexes,1-3 years old, were explored. Thoroughly, chromogranin A (ChA), a specific marker for the EECs, and 3 hormones (glucose-dependent insulinotropic peptide (GIP), glucagon-like peptide-2 (GLP-2), and cholecystokinin (CCK)) were employed in an immunohistochemistry method. The results revealed subset-epithelial-cell-based expression of GIP, GLP-2, and CCK along the crypt villus axis. Moreover, flask or triangular-shaped hormonal cells were noticed in the gut of these birds. ChA was noticed to be expressed with the GIP, GLP-2, and CCK confirming the specific expression in the EECs. The entire small intestine showed decreases in the K- and I-immunoreactive cells. On the other hands, increases in the L-immunoreactive cells were recorded in the ileum only.

Keywords: Endocrine cells, intestinal tract, immunohistochemistry, hormones, Guinea fowl.

INTRODUCTION

Small intestine (SI) is the place where digestion and absorption of nutrients are performed. Early growth in birds shows some changes in the physiology and morphology in the SI (1). Some active amines and peptides are synthetized and secreted by certain immunoreactive-endocrine cells (IREC) located in the gastrointestinal tract (GIT) (2). Some of these molecules are GIP, GLP-2, and CCK. In mammals and birds, the well-studied GIPis one of the incretin hormonessecreted after food intake augmenting insulin secretion (3; 4). The EECs are differently distributed in the GIT of birds from that in mammals due to differences in maturation in the GIT depending on thegestational period durations (5). Gastrin, 5-hydroxtryptamine, gluagan, andsomatostatine are some of the major hormones related to the GIT (6). Cholecystokininare (K-immunoreactive-cells), as EECs,are mentioned to be located in certain GIT segments storing and releasing some single-precursor-dependent peptides (7).

Moreover, GIP-immunoreactive cells (GIP-IRC) were reported for their presence in mammal SI (8;9); however, these cells were not recorded in some birds (10;11;12). On the other hands, these GIPs were shown in the GIT of chickens (13). A large precursor is related to the production of GIP, a member of glucagon/secretin hormone family (14; 15) and bound to G-protein-coupled receptors (16). There is a relationship between the GIP receptor the proglucagon-derived peptide receptors (glucagon, GLP-2, and GLP-1) (17;18; 19). According to the presence of the enteropancreatic axis, effects of entero-peptideson the pancreas (20), we investigated the distribution of the GIP, GLP-2, and CCK immunoreactive cells in the SI of adult guinea fowl.

MATERIALS AND METHODS

Slide preparations of the SI samples were performed using a wax-embedded-tissue method. Dewaxing processes were generated in 100% xylene for 3x10min each. After that, two-times-100%-ethanol-based steps were performed for 10min each. An air-dry step for 10min was induced preceded withan ImmEdge-Hydrophobic-Pen-dependent circling step. Later, two-times-7%-ethanol soaking steps of the tissues were made for 5min each. Then, two-times-rehydration steps were induced in distilled water (DW) for 5min each. Later, an antigenic-retrieval buffering was performed using (10 mMTris/HCl pH 10.0) followed by autoclavingfor 2 times/15min each at 121°C and 15psi. After that, a cooling-down process was generated within the latest buffer for 30-60min at room temperature followed by washing steps for 3 times/5min each in PBS. Blocking of certain non-specific antibody binding sites were induced by placing the tissues in 10% donkey serum incubated for 1hr using certain humidity at room temperature. Primary polyclonal antibodies, (Santa Cruse Biotechnology, USA) at 1:100 dilutions against GIP, GLP-2, and ChA, with these sections were incubated overnight at 4°C. The buffers of antibodies regarding the primary or the secondary ones contained 2.5% (v/v) donkey serum, 0.25% (w/v) Na azide and 0.2% (v/v) triton X-100 in PBS. Washing of these slides was made in PBS for 5 times/5min each for each slide. Moreover, 1:500 dilutions of FITC-conjugated IgG/IgY and Cy3-conjugated IgG/IgY (Stratech, Scientific Limited, Suffolk, UK) were used. Finally, washing of these slides was performed in PBS for 5 times/5min each followed by mounting them in Vectashield Hard Set Mounting Media with DAPI (Vector Laboratories Ltd, Peterborough, UK). An epifluorescence microscope was used to visualize these sections and imaged using a Hamamatsu digital camera. The control was the omission of the primary antibody. The positive control was mice (Swiss albino)sacrificed usingthe cervical dislocation methodfollowed by dissecting out of the intestines immediately. Five centimeter/specimen from the middle part of duodenum, jejunum, and ileum were employed for the study. After that, the specimens were longitudinally opened, rinsed in ice-cold 0.9% (w/v) NaCl (pH=7.4), and cleaned up from excess mucus using paper towels. Then, the sections were subsequently fixed in 10% formalin for 48hrs for the immunohistochemical investigation (21).

Readings for the IRC frequency were categorized as follows: not detected (-), rare (+; mean values were below 2/filed), a few (±; mean values were below 5/ filed); moderate (++; mean values were below 10/filed) and numerous (+++; mean numbers as seen under one filed of epifluorescence microscope

RESULTS

GIP, GLP-2, and CCK expression in the SI of mice

Using an immunehistochemistry method, the SI tissue sections from mice were used as an indicator, positive control, for the expression of the GIP, GLP-2, and CCK. Theresults identified the expression of the GIP, GLP-2, and CCK(Fig. 1). In the control section, when the primary antibodies were omitted, no staining was recorded (Fig. 1). The typical image means that the gut hormone was expressed.

GIP, GLP-2, and CCK expression and distribution in the SI of the adult guinea fowl

Sections from small intestine (duodenum, jejunum and ileum) of the adult guinea fowl were used to indicate the expression of the GIP, GLP-2, and CCKin the SI of the adult guinea fowl(Fig. 2).

Localisation of Enteroendocrine Cells Using Chromogranin A.

The presence of the gut hormones was demonstrated in small intestine of guinea fowl. Moreover, flask or triangular-shaped hormonal cells were noticed in the gut of these birds (Fig. 2). The shape of these cells suggested that they may have beenEECs. Therefore, ChA was used to investigate the cell type expressing gut hormones using immunohistochemistry method.

GIP, GLP-2, and CCK expression and distribution in the SI of the adult guinea fowl

Sections from small intestine parts of duodenum, jejunum, and ileum of the adult guinea fowls were used to indicate the expression of GIP, GLP-2, and CCK in the SI of the adult guinea fowls (Fig.2) (Table.1).

Co-localization of gut hormones with ChA

ChA and double-immunostaining processes were used to identify the expression of the GIP, GLP-2, and CCKusing primary antibodies raised in different animal species for better labeling using two secondary antibodies, anti-goat IgG and anti-rabbit IgG labeled with one fluorochrome each. They were stained singly as red and green spots. When merging, the co-expression was noticed in these tissues as orange/yellow areas. SI sections from camel incubated with antibodies against GIP, CCK, GLP-2, and ChA were read. EECs containing theGIP, CCK, and GLP-2 showed co-expression of GIP, CCK, and GLP-2 along with ChA in the EECs of SI belong to camels (Fig.3).

DISCUSSION

The results showed the relative frequency and distribution of the EECs in the guinea fowl ISs using 3 antisera. The IRCs were displayed mostly in the villi of the SIs. Moreover, flask or triangular-shaped hormonal cells were noticed in the gut of these birds. GIP-IRCs have been detectedin the SIs of the adult guinea fowls, and this finding agrees with the result of (22) in turkey and conformity finding with (23) in chicks at hatching and agrees with identification of GIP genes in the chicken (13). The result disagrees with the findings that were concluded in which GIPhad not been demonstrated in the gastrointestinal tract of chicken (24), domestic pigeons (25), and ostriches (26).

In adult guinea fowl glucagon like pipted-2 antisera detect of endocrine cells in SIs. We detected endocrine cells in small intestine a specific glucagon antiserum same as in (27) in chicks at hatching.Antisera directed towards the CCK revealed numerous EECs in the low numbers in the duodenum of the adult guinea fowl as in (23).Using an immunohistochemistry method, COOH-terminal-based antisera of the CCK in chickenswas recorded to react to secretory granules within cells of the duodenum (28; 29; 30), duck (31), quail, pigeon, gull, and kite (32).

In conclusion, the current work identifies the presence of the GIP-, GLP-2-, and CCK-IRCs in the small intestine of adult guinea fowls. In particular, the present study describes for the first time the GIP-positive IRCs in the small intestines of these species. Moreover, we present a postulationfor the GIP role in the glucose-based metabolism augmenting insulin- and glucagon-based pancreatic activity.

REFERENCES

1- Konarzewski, M., C. Lilja, J. Kozlowski, and B. Lewonczuk. ″On the optimal growth of the alimentary tract in avian postembryonic development″. 1990. J. Zool. 222, 89–101.
2- Sundler, F., R. HIkanson, and S. Leander, ″Peptidergic nervous systems in the gut″. Clin. Gastroenterol. 1980. 9, 517–543.
3- Meier, J. J., M. A. Nauck, W. E. Schmidt, and B. Gallwitz,″Gastric inhibitory polypeptide: the neglected incretin revisited″. Regul. Pept. 2002. 107, 1–13.
4- Meier, J. J., and M. A. Nauck, ″Glucose-dependent insulinotropic polypeptide/gastric inhibitory polypeptide″. Best Pract. Clin. Endocrinol. Metab. 2004.18, 587–606.
5- Theodorakis, M.J., Carlson,O., Michopoulos,S., Doyle,M.E., Juhaszova,M., Petraki, K. &Egan,J.M. ″Human duodenal enter endocrine cells: source of both incretin peptides, GLP-1 and GIP″. Am. J Physiol. Endocrinol. Metab. 2006. 290(3):E550 E559.
6- El-Salhy, M., Wilander, E., Lundquist, M. ″Comparative studies of serotonin-like immunoreactive cell in the digestive tract of vertebrates″. Biomed. Res., 1985. 6:371-375.
7- Egerod, K.L.,Engelstoft, M.S., Grunddal, K.V., Nohr, M.K., Secher, A., and Sakata, I. ″A major lineage of enteroendocrine cells coexpress CCK, secretin, GIP, GLP-1, PYY and neurotensin but not somatostatin″. endocrinology. 2012.153(12):5782–5795.
8- Bunnett, N. W., and F. A. Harrison, ″Immunocytochemical localization of gastric inhibitory peptide and glucagon in the alimentary tract of ruminants″. Q. J. Exp. Physiol. 1986. 71, 433–441.
9- Damholt, A. B., H. Kofod, and A. M. J. Buchan, ″Immunocytochemical evidence for a paracrine interaction between GIP and GLP-+-producing cells in canine small intestine″. Cell Tissue Res. 1999. 298, 287–293.
10- Saito, T., J. Yamada, N. Kitamura, and T. Yamashita, ″An immunohistochemical study on the distribution of endocrine cells in the gastrointestinal tract of domestic pigeon, (Columba liviavar domestica)″. Z. Mikrosk. Anat. Forsch. 1989. 103, 237–246.
11- Yamanaka, Y., J. Yamada, N. Kitamura, and T. Yamashita, ″An immunohistochemical study on the distribution of endocrine cells in the chicken gastrointestinal tract. Z. Mikrosk″. 1989. Anat. Forsch. 103, 437–446.
12- Bezuidenhout, A. J., and G. Van Aswegen, ″A light microscopic and immunocytochemical study of the gastrointestinal tract of the ostrich (Struthiocamelus L.)″. Onderstepoort J. Vet. Res. 1990. 57, 37–48.
13- Irwin, D. M., and T. Zhang, ″Evolution of the vertebrate glucose-dependent insulinotropic polypeptide (GIP) gene″. Comp. Biochem. Physiol. Part D, 2006. 1, 385–395.
14- Hoyle, C. H. V., ″Neuropeptide families: evolutionary perspectives″. Regul. Pept. 1998.73, 1–33.
15- Sherwood, N. M., S. L. Krueckl, and J. E. McRory, ″The origin and function of the pituitary adenylate cyclase-activating polypeptide (PACAP)/glucagon superfamily″. Endocr. Rev. 2000. 21, 619–670.
16- Mayo, K.E., L.J. Miller, D. Bataille, S. Dalle, B. Goke, B. Thorens, and D.J. Drucker, ″International Union of Pharmacology. The glucagon receptor family. The glucagon receptor family″. Pharmacol. Rev. 2003. 55, 167–194.
17- Harmar, A.J., ″Family-B G-protein-coupled receptors″. Genome Biol. 2001. 2, 3013.1–3113.10.
18- Sivarajah, P., M. B. Wheeler, and D. M. Irwin, ″Evolution of receptors for proglucagon-derived peptides: isolation of frog glucagon receptors″. Comp. Biochem. Physiol. 2001. 128, 517–527.
19- Joost, P., and A. Methner, ″Phylogenetic analysis of 277 human G-proteincoupled receptors as a tool for the prediction of orphan receptor ligands″. Genome Biol. 2002. 3, 0063.1–0063.16.
20- Unger, R. H., and A. M. Eisentraut, ″Entero-insular axis″.Arch. Intern. Med. 1969. 123, 261–266.

21- AL-Bdyry S. R. and Alrammahi M. A.″ Frequency and distribution of the enteroendocrine cells in small and large intestine ofone humped camel (*Camelusdromedarius*)″AL-Qadisiya Journal of Vet. Med. Sci. 2016. Vol. 15 No. 1

22- Kadhim A. B. ″An Immunohistochemical Localization of Endocrinal Cells In The Epithelium of the Duodenum Mucosa Of Turkey (*Meleagarisgallpava*)″ Bas.J.Vet.Res. 2017. Vol.16, No.1.

23- Rawdon BB and Andrew A. ″An immunocytochemical survey of endocrine cells in the gastrointestinal tract of chicks at hatching″. Cell and Tissue Research, 1981.220: 279-292.

24- Polak, G.M., Pearse, A.E.G., Adams, C., Garaud, J.C. ″Immunohistochemical and ultrastructural studies on the endocrine polypeptide (APUD) cells of the avian gastrointestinal tract. Experimentia, 1974; 30: 564-.567.proventriculus of seven species of birds. Arch″. Histol. Jpn., 1985.48: 305-314.

25- Saito, T., J. Yamada, N. Kitamura, and T. Yamashita, ″An immunohistochemical study on the distribution of endocrine cells in the gastrointestinal tract of domestic pigeon,(Columba liviavar domestica). Z. Mikrosk″. 1989.Anat. Forsch.103, 237–246.

26- Bezuidenhout A. J .and Van Aswegen G. A Light Microscopic and Immunocytochemical Study Of The Gastrointestinal Tract Of The Ostrich *(STRUTHIO CAMELUSL. Onderstepoort I .vet. Res.,* 1990.57, 37-48.

27- Rawdon, B. B., ″Gastrointestinal hormones in birds: morphological, chemical, and developmental aspects″. J. Exp. 1984.Zool. 232, 659–670.

28- SUNDLER, F .. HAKANSON, R., HAMMER, R. A., ALUMETS, J. ,CARRAWAY, R., LEEMAN, S. E. & ZIMMERMAN, E. P., 1977.

29- ANDREW, A., DE MEY, ″The application of immuno-gold staining of thin sections to identification of gut endocrine cell types. - Proc. Electron Microsc″. Soc. South. Afr. 1981. 11,25-26.

30- RAWDON, B. B., LAYZELL, I, ANDREW, A.: Gastrin- and neurotensin-immunoreactive cells in the chick pylorus. - Proc. Electron Microsc. Soc. South. Afr. 1982.12, 87-88.

31- YAMADA,}., IWANAGA, T., OKAMOTO, T., YAMASHITA, T., MISU, M., YANAIHARA, N.: Ultrastructure of avian gastrin cell granules. - Arch. histol. jap. 1980. 43, 57-63.

32- YAMADA,}., IWANAGA, T., OKAMOTO, T., YAMASHITA, T., MISU, M., YANAIHARA, N.: Ultrastructure of avian gastrin cell granules. - Arch. histol. jap. 1980. 43, 57-63.

Table 1: Distribution of Enteroendocrine cells in which immunoreactive for regulatory peptides detected in the small intestine of adult guinea fowl.

Hormone	Duodenum	Jejunum	Ileum
GIP	**+++**	**±**	-
CCK	**+++**	**±**	-
GLP-2	-	**++**	+++

Relative frequencies: high+++, moderate: ++, few: +, rare: ±, and not detected: -.

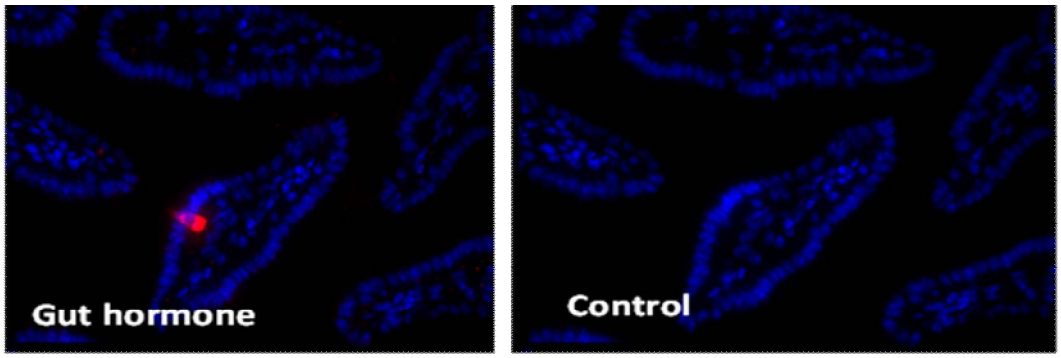

Figure 1: Wax embedded intestinal tissue sections from mice were probed with the antibodies to gut hormone (GIP, GLP-2 and CCK). Typical image showing that gut hormone (red cells) is subset-epithelial-based expressed. In the control section, when the primary antibodies were omitted, no staining was recorded for the gut hormones. Nuclei are blue-colored stained with 4؛6- diamidino -2- phenylindole (DAPI). 200X.

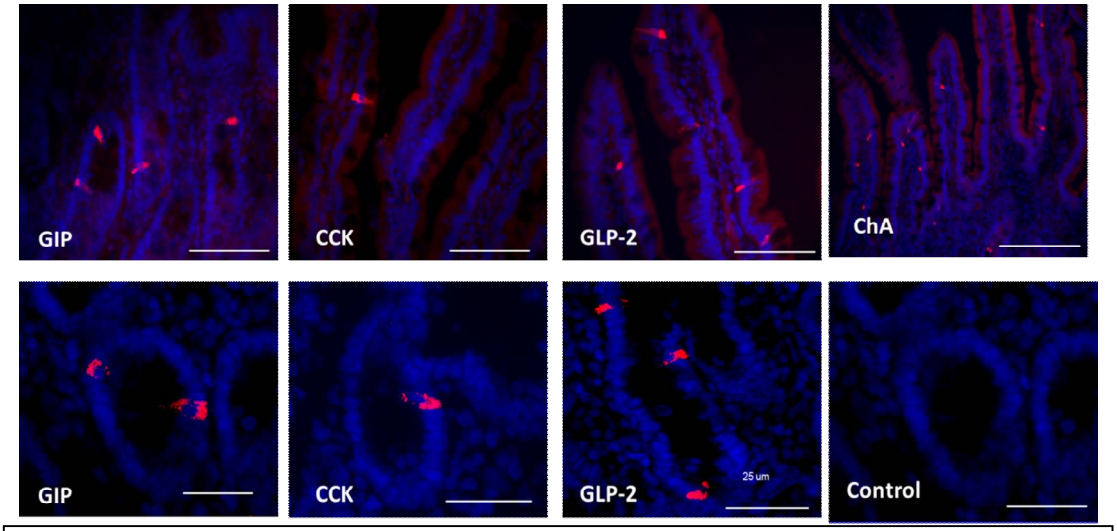

Figure 2: Typical images showing gut hormones(GIP and CCK in duodenum, GLP-2 in jejunum, and GLP-2 in ileum) as shown by the red spots in a subset of camel intestinal cells. In the control section, when the primary antibodies were omitted, no staining was recorded for the gut hormones. Nuclei are blue-colored stained with 4؛6- diamidino -2- phenylindole (DAPI). 200X.

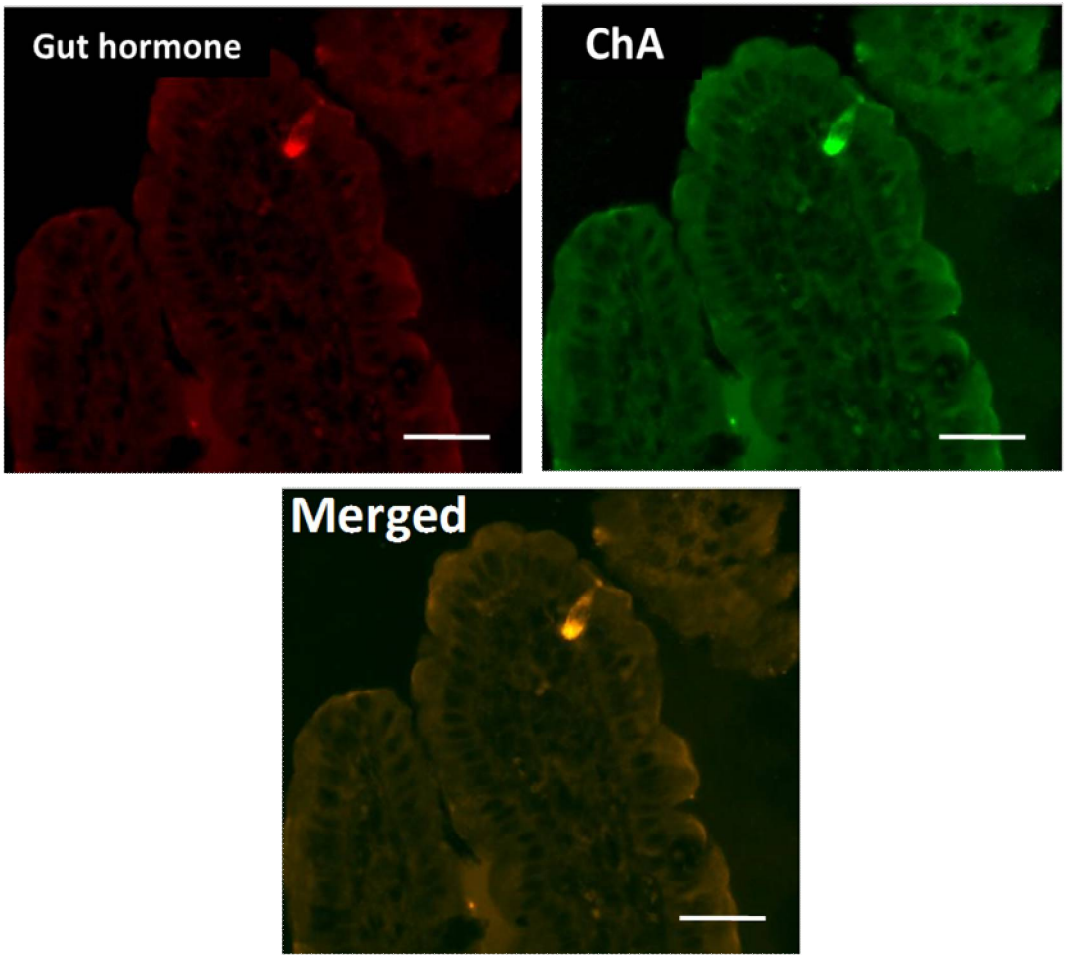

Figure (3): The sections of small intestine were labelled with the primary antibody to (red) and ChA(green). A representative immunofluorescence images showing co-localisation of ChA (green) with gut hormone (red). When the sections were overlaid, gut hormones and ChA were shown to be co-expressed in a same cell (yellow). Images are 400 X magnified.

Indian Journal of Natural Sciences www.tnsroindia.org.in ©IJONS

Vol.9 /Issue 51 / December / 2018 *International Bimonthly* *ISSN: 0976 – 0997*

RESEARCH ARTICLE

Documentation Distribution of Endocrine Cells and Expression of GIP, GLP-1 and GLP-2 Hormones in the Small Intestine of the Adult Male Bovine

Maha Abdul-Hadi Abdul-Rida Al-Abdula[1*], Hassaneen Ali Al-sharoot[2] and Hussein Bashar Mahmood[3]

[1,2]Department of Anatomy and Histology, College of Veterinary Medicine, University of Al-Qadisiyah.Iraq.
[3]Department of Anatomy and Histology, College of Veterinary Medicine, University of kerbala, Iraq.

Received: 20 Sep 2018 Revised: 24 Oct 2018 Accepted: 28 Nov 2018

***Address for Correspondence**
Maha Abdul-Hadi Abdul-Rida Al-Abdula
Department of Anatomy and Histology,
College of Veterinary Medicine,
University of AL-Qadisiyah, Iraq.
Email: Maha.alabdula@qu.edu.iq

ABSTRACT

Enteroendocrine cells are locatedalong the mucosa of the small intestine in mammals. These cells are related to express a variety of incretins hormones that controlled on metabolism of digested food and absorption. Furthermore, these hormones are in charged of secretions other hormones of other accessory glands that related into food digestion and level of carbohydrates in the blood, as well as protect, and induce proliferations of injured endothelial cells of small intestine. The function of these hormones has controlled on growth of human and animals and stimulate the obesity or deficiency of basic elements of the body. Current study had conducted on five adult male bovines, bulls were slaughtered, and small intestine identified and check from any lesions of diseases. Routine histological preparation was used for tissue of small intestine. Sections of small intestine was stained with H and E stains and identify the four tunicae that constitute duodenum, jejunum and ileum. These tunicae are involved with from internal to external "mucosa, submucosa, muscularis, serosa". Immunofluorescence method was applied to detect expressions of three specific hormones used anti-human GIP, GLP-1 and GLP-2 antibodies at different locations of small intestine. Our findings of immunofluorescence significantly revealedthat enteroendocrine cells are spread in lamina propria close to glands and also around the villi. These endocrines were huge expressed the GIP in duodenum, and jejunum but it absents in the ileum. However, GLP-1 and GLP-2 were significantly expressed in the jejunum and ileum, but not detected in the duodenum.Inconclusions, these results strongly confirmed that antihuman GIP, GLP-1 and GLP-2antibodies have large homology with epitope of antigens of bulls. Also, different level expressions of

hormones in different locations of small intestine play vast role in regulate digestion, absorption, and intake food of bovines.

Keywords: Enteroendocrine cells, Bovine, bulls, Small intestine, Duodenum, Jejunum, Ileum, Endocrine cells, GIP, GLP-1 and GLP-2.

INTRODUCTION

The gastrointestinal tract of mammals is filled the abdominal cavity of animal and hasanimportant functionin the body such as absorption, metabolism of food and act mechanical barrier toagainst microorganism invasions and their toxins. The small intestine of bulls is measured about 20 times longer than the length of the body and it is consist of three segments "duodenum, jejunum, and ileum". Additionally, the excretions of the pancreas, liver and gall bladder are drained into lumen of the small intestine, which are responsible for digestion of lipids, proteins and carbohydrates(Sherlock and Dooley 2008, Singh 2008). "Most of digestive process is completed in the small intestine and many nutrients" are absorbed via the small finger-like projections that are called villi into the blood and lymphatic systems(Ham 2002).

The villi are distributes in the epithelium of small intestine which play a huge role to increase surface area of absorption and facilitate" rapid absorption of water and nutritive materials", moreover in the sheep and cow the length of intestinal villi increase at the proximal part of small intestine are longer than in the distal part of small intestine(LUCINI, DE GIROLAMO et al. 1999, Ham 2002, Parveen, Pawan et al. 2013). The epithelium and intestinal glands of small intestine contain several types of cells involved with Paneth cells, columnar cells, absorptive cells, goblet cells, and enteroendocrine cells, subsequently" the distribution of these cell are different between the species" for example the Paneth cells the epithelium of (sheep ,water buffalo ,and camel) comprisehuge number of cells and located at the crypts(LUCINI, DE GIROLAMO et al. 1999, Ali, Nyberg et al. 2007, Daly, Al-Rammahi et al. 2012, Althnaian, Alkhodair et al. 2013, Parveen, Pawan et al. 2013).

As the small intestine is considered endocrine organ because it has many different types of endocrine cellswhich product varietyof"numerous peptide hormones such as, gastrin, serotonin, GIP (glucose-dependent insulinotropic"is produced by K cells(Meier and Nauck 2004, McIntosh, Widenmaier et al. 2009), and GLP1(glucagon-like peptide 1) ,GLP-2 " (glucagon-like peptide2and"PYY"(peptide YY), produced by L cells, CCK"(cholecystokinin) is made by I cells (Morozov 2002, Wang, Chi et al. 2003, Martin, Beck et al. 2006, Mellitzer and Gradwohl 2011).The epithelium of small intestine is released gastric inhibitory polypeptide (GIP)which consists of 153-amino acid proproteinalso known asgastroinhibitory peptide and the glucose-dependent insulinotropic peptide. This hormone considers inhibiting hormone in stomach and induce hormones secretions(Moens, Heimberg et al. 1996) it stimulate the pancreas to secret the insulin hormone which would lead to increase absorption of glucose via epithelium of small intestine and reduce bone resorption by inhibited the osteoclast activity in bone tissue because it might be mediating nutrient-related effects on bone function (Meier and Nauck 2005, Zhong, Itokawa et al. 2007).

Also, the intestinal epithelium is secreted a 42 amino acid hormone(glucagon-like peptide1) which are suppressed glucagon secretion, inhibits gastric emptying, and decreases appetite and food intake(Turton, O'shea et al. 1996, Flint, Raben et al. 1998). This hormone is mediated the insulin secretion may effect on the hyperinsulinaemia and reactive hypoglycaemia of this disorder(Kreymann, Ghatei et al. 1987).The glucagon-like peptide 2 (GLP-2) is secreted in stomach, small intestine and colon and the sequence protein of it isconsisted of 33 amino acid peptideencoded carboxyterminal to the sequence of GLP-1 in the proglucagon gene(Drucker 2001). This hormone is responsible on repair, growth and proliferations of epithelium and villi of small intestine after injury or complicated infections(Drucker, Erlich et al. 1996) also it is improved the nutrition absorption of digested food but impaired the GPL 2 secretions after postprandial in ileum and colon and has no effect on insulin secretion (Schmidt, Siegel et al.

1985, Jeppesen, Hartmann et al. 2001).The enteroendocrine cells are highly specialized mucosal cell spread inthe gut epithelium and scattered along the stomach into the colon that are different pattern of the distributions depending on the species. There are two kinds of these cells, firsttype is called openand present at the top of the epithelium and is called microvilli that project and lining the lumen of small intestine, and the second type called close" which is presentedat the cellular apex (Ham 2002, Junqueira, Carneiro et al. 2005).

Many researches are investigated on the"relative frequency and spreading"ofenteroendocrine cells in the intestinal tract of sheep,waterbuffalo,camel,equine,human,rat,mice, opossum(Krause, Yamada et al. 1985, Muta, Itsuno et al. 1994, LUCINI, DE GIROLAMO et al. 1999, xxHam 2002, Hosoyamada and Sakai 2005, Ali, Nyberg et al. 2007, Daly, Al-Rammahi et al. 2012, Althnaian, Alkhodair et al. 2013, Parveen, Pawan et al. 2013).These three hormones (GIP, GLP-1 and GLP-2) are very important hormones because they are played role in metabolism, digestion and absorption of nutrient and intake food, and the understand and control on function of these hormones could be helped to deal with obesity in human or exploit it to increase the weight and fatty of calves. Therefore, the aims of our study were to identify and document three important hormones (GIP, GLP-1 and GLP-2) in Iraqi bovine species which might be expressed in the mucosa or submucosa of small intestine and detect the level of their expression according to the location of the intestine. In addition, the anti-human (GIP, GLP-1 and GLP-2)bodies arelabelled and probed withthese hormones of different species bovine intestinal hormones which might be confirmed that there isa homology of sequence of proteins between different species,this would be interesting for researchers to develop other assays.

MATERIAL AND METHODS

Five small intestines of adult bulls were collected from Al-Qadisiyah's abattoir. The age of bulls were 2-3 years old and the weight was 150-175kg). Tissue were collected from different parts of small intestine after inspecting them from any pathological lesions to avoid abnormal tissue and diseases. Tissue were directly stored in the ice until use them in the Laboratory. Briefly, tissue was prepared for histological section by following the routine of histology, firstly tissue had fixed with 10% formaldehyde, then, dehydrated through series solutions of an ethanol-xylene, after thatembedded in paraffin to make blocks and sections of tissue to stain them with antibodies and routine stain. for histological examinations, the protocol of (Luna 1968, Ramos-Vara 2005) had been followed. The samples was passaged double in "100% ethanol for 2 x 10 minutes", then leave them air dry for 10 minutes. After that sections of tissue" were circled with ImmEdge Hydrophobic Pen" and leave them to dry for 10 minutes. Subsequently, sections of slides were immersed 2 x 5 minutes in 70% ethanol. Next, slides were rehydrated 2x in dH2O for 5 minutes. Slides were incubated "with 10% (v/v) normal donkey serum in a humidified chamber at room temperature. In the next step, sections were incubated overnight at 4○C with" primary antibodies" (Table 1).Then slides werewashedin the PBS for 5 x 5 minutes. FITC-conjugated IgG/IgY (Table 1) (Stratech, Scientific Limited, Suffolk, UK) wereapplied at a dilution of 1:500 for 1-hour", then washed with PBS for 5 x 5 minutes. Finally, slides were "visualized using an epifluorescence microscope" (MEIJI TECHNO, Model MT4300, Japan) and images were captured with a digital camera and images were analysed.

RESULTS

The histological segments of the small intestine were stained with routine stains "H&E" to distinguish and detect normal histological structures and the integrity of these parts, in particular, it clarified the epithelial cells of epitheliumand their attached microvilli.The results showed that villi and microvilli are attached clearly into epithelium of small intestine (Fig. 1.A.B.C).

The general histology of the small intestine wall ofbulls (duodenum, jejunum and ileum) were comprised with fourlayers, from internal to external "mucosa, submucosa, muscularis, serosa".In details, there are large similarity

between parts of intestine. Small intestine was lined by simple columnar epithelium based on basement membrane, many transvers folds are projected from epithelium which are continued a long small intestine and conformed the plicae circularis, however, most these folds are more common in the jejunum (Figure .1). furthermore, many villi were revealed in epithelium, that are responsible for absorption the digested food, ions and water. These villi are very developed in duodenum. As, lamina propria displayed duodenal or Brunner glands in duodenum, and intestinal gland which are opened at the base of villi. Similarly, Lamina propria was consisted of loose connective tissue, blood supply, lymph networks and adipose tissue. This layer was also extended into folds of intestine.The muscularis mucosa was made up smooth muscle which are arranged longitudinally and transversely. Nevertheless, this layer in the ileum was thicker than the duodenum and jejunum. Externally small intestine was surrounded by serosa which is comprised from connective tissue and mesothelium cells (Fig. 1 A,B&C).

The results of immunofluorescence were conducted and optimised by using three anti-human (GIP, GLP-1, GLP-2) antibodies of three hormones which are expressed from mucosa of small intestineand secondary antibody fluorescein isothiocyanate (FITC) to visualise them. The histological sections slides were incubated with specific different antibodies of hormones to against " GIP, GLP-1 and GLP-2" hormones and analysed them.The assay was developed and applied on another different species to test the homology between human and bovine proteins. Result were very neat and reproducible in the different parts of small intestine. The gastric inhibitory polypeptide (GIP)was highly expressed in enteroendocrine cells of mucosa of duodenum. The expression of GIP was shiny and high signal intensity; however, it was less expression in jejunum and absent in the ileum table (2) and Figure (2).This hormone is helped to decrease the stomach acidity secretions in duodenum.

Nevertheless, the glucagon-like peptide 1 (GLP-1) was not expressed in the duodenum, but it has clear level and expression in the jejunum, and highly expressed in the ileum table (2) and Figure (3). Furthermore, the glucagon-like peptide 2 (GLP-2) was huge intensity and significant level expression in the ileum. This evidence that this hormone has no effect on food intake in small intestinetable (2) and Figure (3).

In ourresults were solely displayed the expression of hormonesas the subpopulation of cells along with the villi of small intestine. Three hormones (GIP, GLP-1 & GLP-2) were clearly expressed in the duodenum of small intestine which are confirmed that hormones related into villi functions as well as it is related into metabolism and digestions of rest food. Furthermore, the location of three hormones (GIP, GLP-1, and GLP-2) were different in the mucosa and distributed in the lamina propria extended into the lower part of portion of duodenal glands less than villi in the columnar epithelium.Moreover, the enteroendocrine cells were scattered in the duodenum around the villi, crypts &Brunner's glands, but then again, theenteroendocrinecells were high commonly in villi of duodenum, less commonly on the " intestinal crypts and rarely in the Brunner's glands". While, the jejunumGIP immunoreactive cellswere rarely dispersed on villi. Similarity, GIP IR-cells were not identified in histological structure of the ileum. The enteroendocrinecells was contained expression of the GLP-1 and GLP-2 that are caudally increased along of the ileum compare with duodenum and jejunum (Table 2). Additionally, GLP-2 immunoreactive cellswere not observed in the histology of the duodenum and jejunum (Fig.4 C and D).

Inclusive, the expressions of "GIP, GLP-1 and GLP-2"hormones were detected using the immunostaining technique at three parts of small intestine (duodenum,jejunum,and ileum), consequently the enteroendocrine cells showed that high reaction signal for GIP hormone sited in the duodenum, even though endocrine cells are revealed high reaction for GLP-1 and GLP-2 in jejunum and ileum. Table (2).

DISCUSSION

The present researchiscovered threespecific hormones in the small intestine of the adult male bovine. The small intestineishistologically containfour tunicae "mucosa, submucosa, muscularis and serosa", mucosa is lined by simple columnar epithelium, which is based on basement membrane. lamina propria was beneath the epithelium and both

extended in branched folds. Also, the tubuloalveolar duodenal gland was "scattered in the submucosa at the upper part of the duodenum" and reduced in numbers toward the end and disappeared(Hampson 1986, Cesta 2006).The mucosa of small intestine iscontained massive endocrine glands in the body which are might be produced the hormones and abundant number of enteroendocrinecells. These have many functions of the small intestinesuch the "absorption and digestion of the food" combine with enzymes that are secreted from the endocrine gland(Krause, Yamada et al. 1985, Muta, Itsuno et al. 1994, Ham 2002, Hosoyamada and Sakai 2005, Samuelson 2007, Bacha Jr and Bacha 2012).

Our result showed that distribution arrangement of GIP hormone of male adult bovine wasidentified in the duodenum, less in the jejunum, but it is not observed in the ileum, but not GLP-1expression was detected in duodenum, however, the incretin hormones GIP and GLP-1 were detected in all parts of endocrine cells of small intestine of the porcine, rat, and human(Mortensen, Christensen et al. 2003). This suggested that expression GIP hormones in duodenum would be helped to reduce the acidity products of stomach and protect the small intestine.
Results was not detected the expression of glucagon-like peptide 2 (GLP-2) in the duodenum, and detected high level expression in the jejunum and ileum, but this hormone was identified in the gastrointestinal tract of human and rodents(Munroe, Gupta et al. 1999, Yusta, Huang et al. 2000). Our result strongly distinguished that glucagon-like peptide 2 (GLP-2) has humble effect in the duodenum due to high concentrations of GIP hormones.Enteroendocrine cells are highly specialized mucosal cells and are differ in location and interposed in mucosa and submucosa of small intestine between species of animal in the regional distribution, relative frequency and cell type(Wang, Chi et al. 2003, Martin, Beck et al. 2006). These cells are secreted hormoneswhich are effect on food intake, maintain blood glucose levels, reduce cholesterol levels, and various other physiological functions(Ahlman and Nilsson 2001). However, these cells have different activity in the small intestine according to their locations and distributions.

The cells which are responsible for secreting the (GLP-1 and GIP-2) are called L-enteroendocrinecells, these cells are produced and secreted hormones as response to absorb the nutritive carbohydrates, amino acids and lipids (Longuet, Sinclair et al. 2008)and located in the crypts and the villi and had different shapes,also the shape of subunits of endocrine cellswere commonly round or axle shape and open formand consider as second type of cell that is secreted" GIP called K-enteroendocrine"(Hosoyamada and Sakai 2005).Generally, in mammals, the co-expression of the GIP withchromogranin is considered a typical evidence of enteroendocrinethat approves the site an expression to be in enteroendocrine cells(Jang, Kokrashvili et al. 2007).In same way, our study exhibited that "GIP was expressed exclusively along the villus in the duodenum of small intestine" and the cells expressing GIP are looked triangular or flask in shape at middle and distal portion of small intestine. But, the scattering of K cells isdecreased along the length of the small intestine, this pattern of the GIP showedin the middle and distal portion of small intestine, same these results had been documented in other mammals(Theodorakis, Carlson et al. 2006, Moran, Al-Rammahi et al. 2010).
The tunica mucosa of duodenum plays an significant role in digestion, pancreatic secretionsand gall bladder functions in mammals under affecting the gastrointestinal hormones that are released from the" proximal part of small intestine". The first part of the duodenum is protected the epithelium of duodenum from acid-pepsin which released from the stomach on adult opossum. (Krause, Yamada et al. 1985).In conclusion, there are different expression of GIP, GLP-1, GLP-2 hormones in thesmall intestine of bulls, which are secretedby enteroendocrine cells.Our findings supportthat the expression of the incretin hormones play a role in regulate the intake of foods and induce other hormones which helped in accomplished process of metabolism of the bull.

REFERENCES

1. Ahlman, H. and O. Nilsson (2001). "The gut as the largest endocrine organ in the body." Annals of Oncology12(suppl_2): S63-S68.
2. Ali, M. A. H., et al. (2007). "Distribution of neuroendocrine cells in the small and large intestines of the one-humped camel (Camelus dromedarius)." Neuropeptides41(5): 293-299.

3. Althnaian, T., et al. (2013). "Histological and Histochemical Investigation on Duodenum of Dromedary Camel (Camelus dromedarius)." Science Internationa J1(6): 217-221.
4. Bacha Jr, W. J. and L. M. Bacha (2012). Color atlas of veterinary histology, John Wiley & Sons.
5. Cesta, M. F. (2006). "Normal structure, function, and histology of mucosa-associated lymphoid tissue." Toxicologic pathology34(5): 599-608.
6. Daly, K., et al. (2012). "Expression of sweet receptor components in equine small intestine: relevance to intestinal glucose transport." American Journal of Physiology-Regulatory, Integrative and Comparative Physiology303(2): R199-R208.
7. Drucker, D. J. (2001). "Glucagon-like peptide 2." The Journal of Clinical Endocrinology & Metabolism86(4): 1759-1764.
8. Drucker, D. J., et al. (1996). "Induction of intestinal epithelial proliferation by glucagon-like peptide 2." Proceedings of the National Academy of Sciences93(15): 7911-7916.
9. Flint, A., et al. (1998). "Glucagon-like peptide 1 promotes satiety and suppresses energy intake in humans." The Journal of clinical investigation101(3): 515-520.
10. Ham, T. S. (2002). "Regional distribution and relative frequency of gastrointestinal endocrine cells in large intestines of C57BL/6 mice." Journal of veterinary science3(3): 233-238.
11. Hampson, D. (1986). "Alterations in piglet small intestinal structure at weaning." Research in veterinary science40(1): 32-40.
12. Hosoyamada, Y. and T. Sakai (2005). "Structural and mechanical architecture of the intestinal villi and crypts in the rat intestine: integrative reevaluation from ultrastructural analysis." Anatomy and embryology210(1): 1-12.
13. Jang, H.-J., et al. (2007). "Gut-expressed gustducin and taste receptors regulate secretion of glucagon-like peptide-1." Proceedings of the National Academy of Sciences104(38): 15069-15074.
14. Jeppesen, P. B., et al. (2001). "Glucagon-like peptide 2 improves nutrient absorption and nutritional status in short-bowel patients with no colon." Gastroenterology120(4): 806-815.
15. Junqueira, L., et al. (2005). "Connective tissue." Basic histology text & atlas11: 91-122.
16. Krause, W., et al. (1985). "Quantitative distribution of enteroendocrine cells in the gastrointestinal tract of the adult opossum, Didelphis virginiana." Journal of anatomy140(Pt 4): 591.
17. Kreymann, B., et al. (1987). "Glucagon-like peptide-1 7-36: a physiological incretin in man." The Lancet330(8571): 1300-1304.
18. Longuet, C., et al. (2008). "The glucagon receptor is required for the adaptive metabolic response to fasting." Cell metabolism8(5): 359-371
19. LUCINI, C., et al. (1999). "Postnatal development of intestinal endocrine cell populations in the water buffalo." The Journal of Anatomy195(3): 439-446.
20. Luna, L. G. (1968). "Manual of histologic staining methods of the Armed Forces Institute of Pathology."
21. Martin, G., et al. (2006). "Gut hormones, and short bowel syndrome: the enigmatic role of glucagon-like peptide-2 in the regulation of intestinal adaptation." World journal of gastroenterology: WJG12(26): 4117.
22. McIntosh, C. H., et al. (2009). "Glucose-dependent insulinotropic polypeptide (gastric inhibitory polypeptide; GIP)." Vitamins & Hormones80: 409-471.
23. Meier, J. J. and M. A. Nauck (2004). "Glucose-dependent insulinotropic polypeptide/gastric inhibitory polypeptide." Best Practice & Research Clinical Endocrinology & Metabolism18(4): 587-606.
24. Meier, J. J. and M. A. Nauck (2005). "Glucagon-like peptide 1 (GLP-1) in biology and pathology." Diabetes/metabolism research and reviews21(2): 91-117.
25. Mellitzer, G. and G. Gradwohl (2011). "Enteroendocrine cells and lipid absorption." Current opinion in lipidology22(3): 171-175.
26. Moens, K., et al. (1996). "Expression and functional activity of glucagon, glucagon-like peptide I, and glucose-dependent insulinotropic peptide receptors in rat pancreatic islet cells." Diabetes45(2): 257-261.
27. Moran, A. W., et al. (2010). "Expression of Na+/glucose co-transporter 1 (SGLT1) is enhanced by supplementation of the diet of weaning piglets with artificial sweeteners." British Journal of Nutrition104(5): 637-646.

28. Morozov, I. (2002). "Structure and function of the small intestinal mucosa." Eksperimental'naia i klinicheskaia gastroenterologiia= Experimental & clinical gastroenterology(6): 88-92, 114.
29. Mortensen, K., et al. (2003). "GLP-1 and GIP are colocalized in a subset of endocrine cells in the small intestine." Regulatory peptides114(2-3): 189-196.
30. Munroe, D. G., et al. (1999). "Prototypic G protein-coupled receptor for the intestinotrophic factor glucagon-like peptide 2." Proceedings of the National Academy of Sciences96(4): 1569-1573.
31. Muta, K., et al. (1994). "Distribution and Localization of Endocrine Cells in the Human Gastro-intestinal Tract-In Relation to Histogenesis of Rectal Carcinoid." Acta medica Nagasakiensia39(4): 30-39.
32. Parveen, K., et al. (2013). "Histological architecture and histochemistry of duodenum of the sheep (Ovis aries)." Indian Journal of Veterinary Anatomy25(1): 30-32.
33. Ramos-Vara, J. (2005). "Technical aspects of immunohistochemistry." Veterinary pathology42(4): 405-426.
34. Samuelson, D. A. (2007). Textbook of veterinary histology.
35. Schmidt, W., et al. (1985). "Glucagon-like peptide-1 but not glucagon-like peptide-2 stimulates insulin release from isolated rat pancreatic islets." Diabetologia28(9): 704-707.
36. Sherlock, S. and J. Dooley (2008). Diseases of the liver and biliary system, John Wiley & Sons.
Singh, R. (2008). Digestive system.
37. Theodorakis, M. J., et al. (2006). "Human duodenal enteroendocrine cells: source of both incretin peptides, GLP-1 and GIP." American Journal of Physiology-Endocrinology and Metabolism290(3): E550-E559.
38. Turton, M., et al. (1996). "A role for glucagon-like peptide-1 in the central regulation of feeding." Nature379(6560): 69.
39. Wang, S. Y., et al. (2003). "Studies with GIP/Ins cells indicate secretion by gut K cells is KATP channel independent." American Journal of Physiology-Endocrinology and Metabolism284(5): E988-E1000.
40. Yusta, B., et al. (2000). "Enteroendocrine localization of GLP-2 receptor expression in humans and rodents." Gastroenterology119(3): 744-755.
41. Zhong, Q., et al. (2007). "Effects of glucose-dependent insulinotropic peptide on osteoclast function." American Journal of Physiology-Endocrinology and Metabolism292(2): E543-E548.

Table (1).This is a table showed primary and secondary antibodies that have applied to identify GIP, GLP-1 and GLP-2.

Primary antibody	**Host**	**Dilutions**
"Anti-human GIP'	Goat	1:100
"Anti-human GLP-1"	Goat	1:100
"Anti-human GLP-2"	Goat	1:100
Secondary antibody	**Label**	**Dilution**
Donkey anti-goat IgG	FITC	1:500

Table 2 : This table revealed the expression and absent expression of GIP, GLP-1 and GLP-2 hormones in the small intestine of adult male bovine.

Hormones	**(Duodenum)**	**(Jejunum)**	**(Ileum)**
"GIP"	**+++**	**±**	-
"GLP-1"	**-**	**++**	+++
"GLP-2"	**-**	**+++**	+++
(+++: high, ++: moderate, +: low, ±: low , -: not signal)			

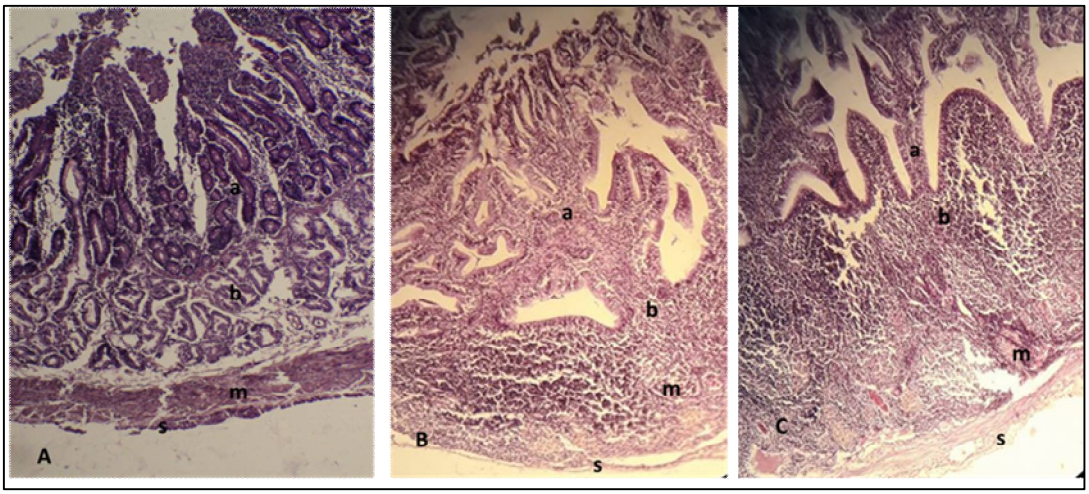

Figure .1:These images displayed the histological structure of small intestine of adult male bovine was stained with routine H&E stains. (A) This image showed the layers structures of duodenum. (B) This image showed the layers structures of jejunum. (C)This image showed the layers structures of ileum. 100 X (a, b and c) magnified.

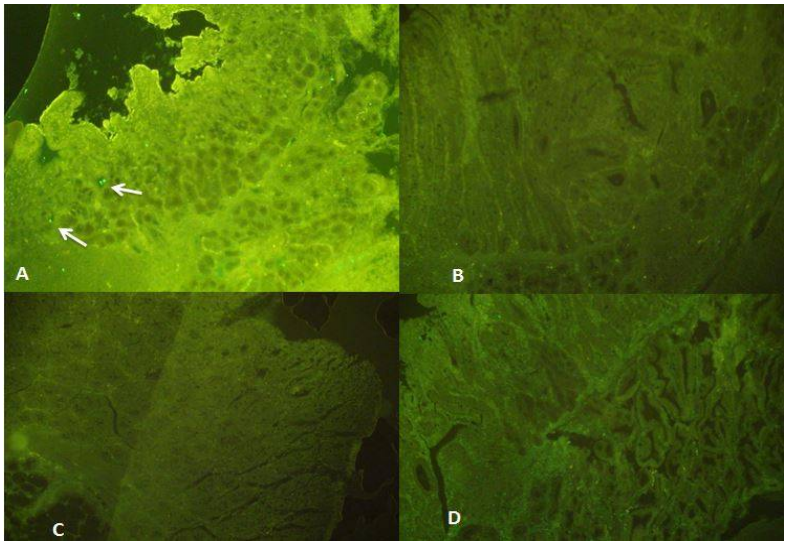

Figure 2 :**These images displayed the duodenal part of small intestine of adult male bovine was incubated with anti-human "GIP, GLP-1, GLP-2antibodies". (A) typical image showed the expression of (GIP) in the duodenal section and detected close the villi,upper and lower half of the glands of duodenum. (B) and (C) these images showed the duodenal sectionswere incubated with anti-human (GLP-1, GLP-2) antibodies and were not detected in duodenum. (D) This image showed the duodenal sections were only incubated with secondary antibody. 200X magnified.Arrow(s). Indicate positive staining.**

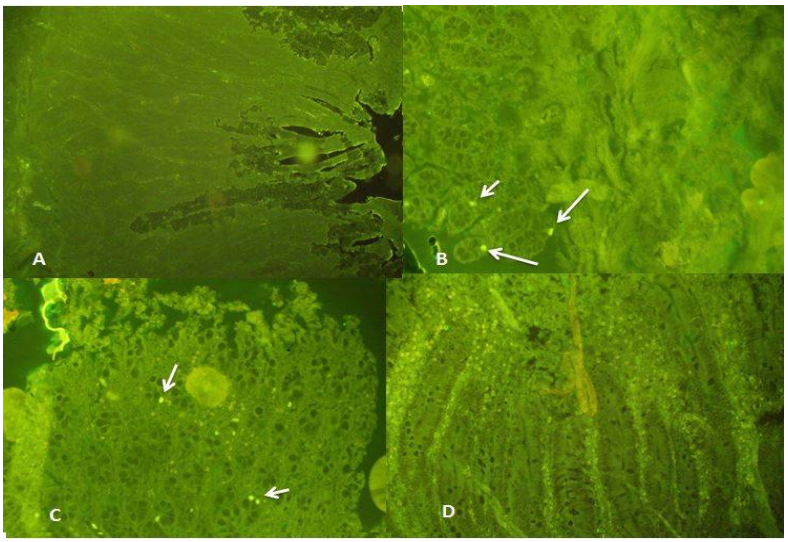

Figure (3):These images displayed the jejunalpart of small intestine of adult male bovine was incubated with anti-human "GIP, GLP-1, GLP-2 antibodies". (A) GIP hormone was not detected in the jejunal sections. (B) and (C) these images showed the jejunal sectionswere incubated with anti-human (GLP-1, GLP-2) antibodies and were detected in jejunal part in" villi,upper and lower half of the glands of jejunum". (D) This image showed the jejunal sections were only incubated with secondary antibody. 200X magnified.Arrow(s). Indicate positive staining.

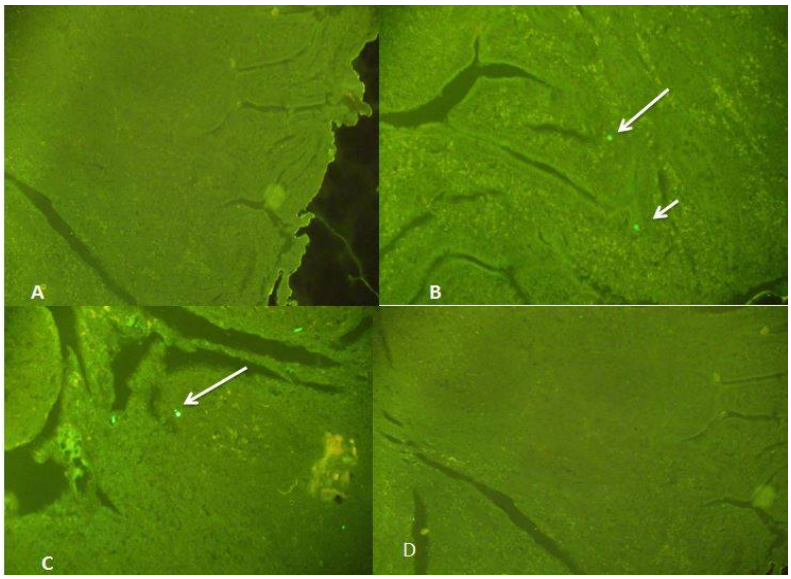

Figure 4:These images displayed the jIleum part of small intestine of adult male bovine was incubated with anti-human "GIP, GLP-1, GLP-2" antibodies. (A) GIP hormone was not detected in the Ileum sections. (B) and (C) these images showed the Ileum sectionswere incubated with anti-human (GLP-1, GLP-2) antibodies and were detected in Ileum part in" villi,upper and lower half of the glands of Ileum". (D) This image showed the jejunal sections were only incubated with secondary antibody. 200X magnified.Arrow(s). Indicate positive staining

Indian Journal of Natural Sciences www.tnsroindia.org.in ©IJONS

Vol.9 /Issue 51 / December / 2018 *International Bimonthly* *ISSN: 0976 – 0997*

RESEARCH ARTICLE

Preliminary Neo-Deterministic Seismic Hazard Assessment in Pakistan and Adjoining Regions

Farhana Sarwar[1]*, Saleem Iqbal[1],Franco Vaccari[2] ,Andrea Magrin[3]and Lala Rukh[1]

[1]Department of Mathematics, University of Balochistan, Quetta, Pakistan.
[2] Department of Mathematics and Geosciences,University of Trieste, Trieste, Italy
[3] Istituto Nazionale di Oceanografia e GeofisicaSperimentale, Udine, Italy

Received: 22 Sep 2018 Revised: 25 Oct 2018 Accepted: 27 Nov 2018

***Address for Correspondence**
Farhana Sarwar
Department of Mathematics,
University of Balochistan,
Quetta, Pakistan.
Email: f_saleem10@yahoo.com

ABSTRACT

The regional seismic hazard in Pakistan and adjoining regions is assessed using the Neo-deterministic seismic hazard assessment approach (NDSHA). Synthetic seismograms are generated by the modal summation technique at the nodes of a grid that covers the studied area. The main input for the computations consists of a set of earthquake sources and of the structural model where the seismic waves propagate. The earthquake sources are parameterised within the active seismogenic areas by defining the focal mechanism, the depth and the magnitude, obtained through the analysis and re-elaboration of the past seismicity. The peak displacement (D_{max}), peak velocity (V_{max}) and design ground acceleration (DGA) are then extracted from the synthetic signals and plotted on the 0.2° x 0.2° grid to construct the seismic hazard map of the studied area. There are few probabilistic hazard maps available for Pakistan, however, this is the first study aimed at producing a neo-deterministic seismic hazard map for Pakistan and adjoining regions.The most severe hazard is found in the epicentral zone of the great Muzaffarabad earthquakes of 2005 and its surroundings, where the DGA estimate falls in the highest range 0.60 *g* – 1.2 *g*. The peak velocity and displacement in the same region are estimated as 60–120 *cm* s^{-1} and 30–60 *cm*, respectively.

Keywords: Seismic hazard, Neo-deterministic, Earthquake catalogues, Seismogenic zones

INTRODUCTION

Pakistan is situated in a highly seismically active region which has experienced many disastrous earthquakes during historical as well as in recent times. The geographical map of Pakistan with adjoining regions considered in our studies is shown in Fig.1 .The strongest earthquakes that hit Pakistan in the recent history are the 1935 Quetta earthquake, M 7.4; the 1945 Makran coast earthquake, M above 8.0; the August 1931 Mach earthquake, M 7.3; the 1974 Pattan earthquake, M 6.0; the October 2005 Muzaffarabad earthquake, M 7.6[1], the 28 October 2008 Ziarat earthquake, M 6.4; the 24 September 2013 Awaran district (Balochistan) earthquake, M 7.8 and its September 28, 2013 M 6.8 aftershock. Given the high seismicity of the region, it has become necessary to better quantify the seismic hazard, to evaluate the rate of vulnerability and to develop tools to prevent or mitigate as much as possible the potential damaging effects of earthquakes. A reasonable approach is to apply the Neo-deterministic seismic hazard assessment (NDSHA) technique [2],[3]that can be effectively combined with intermediate term middle-range predictions [4], [5], [6], [7] at least to identify priorities of interventions for retrofitting and new urban planning. In recent times awareness has grown that people are usually not killed by earthquakes themselves but by their collapsing houses and other manmade structures or induced secondary effects. In many developed and industrialized countries,like Japan, protection from earthquakes, in conjunction with improved seismic hazard assessment, is entrusted chiefly to the broad application of advanced engineering know-how. But unfortunately,in developing countries like Pakistan the situation is different. Pakistan cannot yet afford excessive costof engineered earthquake-resistant buildings and still foresee potential applications of results of earthquakeprediction research for reducing human losses. However, earthquake losses could be significantly minimizedwith elementary design know how only, and by constructing rural housing at minimum cost by applying low-costtraditional measure of retrofitting, i.e., building materials and local skills. More emphasis should be givento pre-disaster planning and development and efforts must be put to cost effective prior actions focused atdeveloping knowledge-based hazard resilient public property, rather spending our time and resources on postdisaster relief and rescue operations that are not only expensive but difficult as well. Good understandingand know-how of the maximum credible earthquake that might occur, the threat to infra structures at thegiven site or zone, the geographical site effects and the dangers we confront, is essential for this sort ofscenario modelling and to achieve our purpose NDSHA is a more practical approach.

Seismic Hazard

Among the possible definitions of seismic hazard analysis, [9] describes it as the estimation of some measure of the strong earthquake ground motion expected to occur at a selected site. Approaches to seismic hazard assessment can be grouped into two broad categories: Deterministic (DSHA) and Probabilistic (PSHA)[10]. In both the approaches, available historical seismic records and geological data are used to identify and characterize the main seismic sources relevant to the site of interest, and to define the earthquake potential. The difference between these two methodologies lies in the way the seismic scenarios are defined. The PSHA defines the hazard as the likelihood for a specified ground motion parameter (e.g. peak ground acceleration, PGA) value to be exceeded within a certain time interval. The DSHA is defined by a controlling earthquake, an earthquake with a given magnitude that may occur in a given time interval (disastrous [say 500 years]; strong [say 140 years]; frequent [say 70 years]; etc.), without given an indication on how likely that given scenario is to occur [4].

The Neo-Deterministic Seismic Hazard Assessment (NDSHA)

In DSHA all distances from the sites to the potential earthquake sources, as well as the magnitudes of the earthquakes within the potential sources, are fixed [10]. The result is an estimate of the ground motion that the site would experience given the occurrence of an earthquake at some fixed distance and magnitude. Deterministic seismic hazard analyses are useful for site-specific studies, particularly those involving critical facilities in which the design criteria are based upon the occurrence of the largest possible seismic event [4],[10]. The deterministic

approach is also preferable in view of the limited seismological data availability and of the intrinsic difficulty of the probabilistic evaluation of the occurrence of earthquakes. As explained by the multiscale seismicity model [11], the actual problem is the selection of large enough dimensions of the areafor analysis without violating the Gutenberg-Richter as well as other related laws.

NDSHA, being based on the computation of a large set of synthetic seismograms, addresses some aspects largely overlooked in the probabilistic approach: (a) the effect of crustal properties on attenuation are not ignored; (b) the ground motion parameters are not derived from overly basic attenuation functions, but from synthetic time histories,and (c) the resulting maps address the issue of the deterministic definition of ground motion in a way which permits the generalisation of design parameters to locations where there is little seismic history [12], [13]. Various studies have been performed in the past to evaluate PSHA in Pakistan [e.g. [1], [14], [15]. The deterministic approach for seismic hazard analysis is not well documented in literature, and it is practiced differently in different parts of the world and even in different application areas [9].

MATERIALS AND METHODS

In this study, we compute the seismic hazard in the country using the NDSHA approach described in [2],[3], that allows for a first-order seismic zoning at regional scale, based on the knowledge of the average properties of seismic sources and structural models [16]. With NDSHA, the available information on the Earth structure parameters, the seismic sources and the level of seismicity of the area are used for the computation of synthetic seismograms, according to the flow chart shown in Fig. 2. Once estimated for the available data the synthetic seismograms permit us to calibrate in a quitepractical manner the engineering standards essential to appropriately design or retrofit the buildings, even in those areas that are seismically quiet, or where no proper data is available. In addition, the technique also permits to estimate the impact of several input factors on the concluding results. The immediate results of the technique are the maps exhibiting the distribution of the D_{max}, $V_{max}$and *DGA* for the studied area. The full description of the methodology is discussed in [17].

RESULTS AND DISCUSSIONS

Input Data

The input data needed to compute the synthetic seismograms are structural models, historical earthquakes catalogue, seismogenic zones and focal mechanisms.

Structural model

Structural models are defined by regional polygons (Fig. 3) that separate areas characterized by different average lithospheric properties; they are represented by a number of flat layers, each one described by its thickness, density, P- and S-wave velocities and corresponding Q values. The structural models and Q-Structure beneath the studied area has not been very well studied so far. In order to propose a suitable structural model, all available geophysical and geological information for the investigated territory have been considered after an extensive bibliographic research [18], [19], [20] [21], [22], [23], [24], [25], [26], [27], [28]. An average model is prepared giving more weight to the results obtained by [18]. For depths larger than 120 km the data has been taken exclusively from [18]. For each polygon an average structural model is prepared for our computation which is shown in Fig.4

Earthquake catalogue

An earthquake catalogue has been prepared after merging the Pakistan Metrological Department (PMD) catalogue and the National Earthquake Information Centre (NEIC) catalogue for a period of 102–years from 1905 to 2007 [29]

and from Indian catalogue for a period of 01-01-500 to 30-12-2016 [30], [31]. In NDSHA completeness of catalogue is not as essential as in PSHA and is in principle required only for events of M=5 and above. Furthermore, only the spatial distribution of those events is considered, disregarding their time distribution, which is often unreliable for ancient events. We may be misjudging the seismicity just in those Seismogenic Zones wheredamaging events are not reported in the catalogue, and only in those areas where the magnitude smoothing, described in Section 3, is not enough to account for the missing information. This insufficient information would also influence significantlythe results obtained with PSHA[18], where catalogue completeness at lower magnitudes is also required for a good characterization of the seismicity rate.As given by [32], attainable partial solution to find maximum expected magnitude can be achieved through aimed field studies of active faults for the identification of the seismogenic potential.A formal approach to the identification of seismogenic nodes has been developed by [33]. About Pakistan, in 1972 [34] used planar morphostructural nodes of the Pamirs and Tien Shan as candidates for earthquake-prone places.

Seismogenic zones

Seismogenic zones identify the areas with the active faults of the region. Pakistan geologically overlaps both with the Indian and the Eurasian tectonic plates where its Sindh and Punjab provinces lie on the north-western corner of the Indian plate while Balochistan and most of the Khyber-Pakhtunkhwa lie within the Eurasian plate which mainly comprises the Iranian plateau, some parts of the Middle East and Central Asia. The Northern Areas and Kashmir lie mainly in Central Asia along the edge of the Indian plate and hence are prone to violent earthquakes where the two tectonic plates collide [35]. Seventeen seismogenic zones have been defined for the entirearea of research comprising of Pakistan and adjoining regions of Iran, Afghanistan, Tajikistan, China, India as shown in Fig. 5. They represent areas characterized by a significant level of seismicity. The stress regime and the tectonic behaviour are assumed to be reasonably homogeneous within each zone. Most of the seismogenic zones are located along the collision plate boundary, i.e., along the Kirthar Suleiman Hindukush, Himalaya[18]. Seismic activity has generally been concentrated in the northern part of the country, the northern and southwestern parts of Balochistan Province, and the coastal areas of Sindh Province. Khattri[36] identified twenty-four source zones in India and neighbouring region on the basis ofseismotectonics and historical seismicity but the region around the Killari earthquake of 1993 (Mw 6.3) was not recognized in his study. Bhatia[37] identified eighty-six source zones for India and adjoining regions, based on the analysis of past data, and the Killari source zone was among them. The identified areal sources were smaller in size compared to those of Khattri [36]. In our study we have followed the same pattern of zoning as given in [18] and owing to the same justification by [18] the zoning suggested by [36] and [37] is not adopted as the proper definition criteria for zoning is not been followed for the complete studied area. For instance [36] has formed twenty-five zones for the complete region but due to varying size of the zones as some are considerably big and so cannot be considered homogeneous in their properties. Similarly, there is not a single event assigned to seismogenic zone 1 of [37] whereas for zone 81 an earthquake of M 7 is lying just outside it. As could be seen that few source zones 70-75 are formed on the basis of low magnitude local events, whereas in other parts of the studied area similar size earthquakes are not considered in the definition of Seismogenic zones. As in [38] the India and its neighbouring regions are divided into “32” Seismogenic zones, that were established on historical seismicity, geology and tectonic features but there is no zone with zero seismic activity and Seismogenic zones without gaps but in our research, we are focused on events with $M \geq 5$ and focal depths <50 km.

Fault plane solutions

In this research we have taken published Fault Plane Solutions (FPS) for the large events occurring before 1976 from[39], [40], [41], [42], [43], [44], [45], [46], however from 1976 and onwards the FPS are taken from Harvard CMTCatalogue. Each seismogenic zone is assigned a representative fault plane solution based on the mechanism associated with the strongest event, or with the best studied event, or the most frequent event. The thrust-type and strike-slip fault plane solutions are dominating the region of investigation (Fig. 5). The Karakoram ranges mostly

shows thrust fault mechanism due to the collision between Indian and Eurasian plate (zones 1and 2), Hunza and Gilgit valleys are situated in this zone.Generally, thrust faulting mechanism can be observed in the region of Hindu Kush (zones 3,4,14 and 15) occasionally normal faulting (zones 3 which comprise Main Karakoram Thrust MKT),also in Kashmir (zone 4) the earthquakes mainly shows thrust fault mechanism, zone 14 lies in the central Afghanistan which is seismically inactive. The zone- 5 comprises Kangra Valley fault (KVF) India, the mechanism is generally normal faulting while zone 6 and 7 shows thrust fault mechanism and consists of the Main Boundary Thrust **(**MBT) and represents the extensive zone of modern deformation and the devastating earthquakes. In Pakistan active faults are rather densely distributed on and in the vicinity of the MBT [35]. For zone 8 the CMT database do not have any focal mechanism solution, the solution has been taken from [18] which is vertical dip slip, the area lies in the region Rajasthan in India. In the zone 9,10 there are strike slip faults including Chaman fault, indicating that the boundary between Indian and Eurasian plate is of transform type. For zone 11, thrust as well as strike slip faults are dominating although no large earthquake is observed in this zone except 2011 earthquake [35], this zone has main cities namely Panjgur, Dalbandin, Nokundi and areas of Iran.The zone -12 and 17 has Kirthar fault with a relatively diffused seismicity. In the southern part of Pakistan, including Makran subduction zone(zone 13), faults are thrust and normal type due to the subduction of Arabian Sea plate under Eurasian plate and due to Murray ridge, we also observe that Nai-Rud fault is an active fault in this zone and has a NE-SW trending, almost parallel to the Nai-Rud valley and bears the characteristics of a thrust with left-lateral strike-slip component, the main cities in this region are Gawadar, Pasni, Karachi.Zone 16 shows reverse thrust mechanism and include Parts of Iran and boarder of Afghanistan.

Computations

For the definition of the seismic sources used to generate the synthetic seismograms, the seismicity described in the historical earthquake catalogue is discretised into cells of 0.2° × 0.2° (latitude and longitude) and each cell is assigned the magnitude value of the largest event that occurred within it (Fig. 6). This map of seismicity is then rearranged through a smoothing procedure to account for the spatial uncertainty in epicentres location that may be particularly severe for historical events [e.g. [33]] and for the source extension. A centredsmoothing window with a radius of three cells is considered, and the maximum value found in the window is assigned to the central cell. After smoothing, only the cells located within the seismogenic zones are retained, obtaining the conservative distribution of the maximum magnitude shown in Fig. 7.

A double-couple point source is then placed in the centre of each cell, with a focal mechanism consistent with the properties of the corresponding seismogenic zone. The observation points are placed at a grid with dimension of 0.2° × 0.2° over the whole studied area. They do not overlap with the sources, because the sources are placed in the center of each cell falling within the seismogenic zones, whereas, the observation points are placed at the corners of the grid, and inside the structural polygons of Fig. 3.

The synthetic signals are computed for frequencies up to 1 Hz. Depending upon the magnitude the hypo-central depth is not considered as constant parameter , it is taken as 10 km for sources with M <7:0, for sources with $7 \leq M$ <8 it is fixed to 15 km whereas it is fixed to 20 km for catastrophic earthquakes of $M \geq 8{:}0$ as in previous studies [47],[48],[49],[50],[51],[52],[53], [54]. This procedure is adopted to justify the relationship of magnitude-depth which is shown in the statistical parameters of the earthquake occurrences [e.g. [11]].To limit the number of synthetic seismograms to be computed, the maximum epicentral distance considered in the generation of the time series depends on the source magnitude: 150 km for $M < 6$, 200 km for $6 \leq M < 7$, 400 km for $7 \leq M < 8$ and 800 km for $M \geq 8$.After the seismicity, the source mechanisms, the structural models and the observation points are all defined, synthetic signals are computed. In the far field, i.e. roughly speaking for epicentral distances larger than the source depth, the modal summation technique [55, 56, 2,3] is used, as it is very efficient from the computational point of view. For paths, shorter than the hypocentral depth the discrete wavenumber technique is adopted [57], which gives the full wave field, including all body waves and near field, at the penalty of a longer computational time. At each site, the horizontal components (P - SV) radial and SH transverse syntheticseismograms are first computed for a

seismic moment of $10^{-7}Nm$. The magnitude and the finiteness of thesource are accounted using the size and time scaled point source model [58] which is based on an extendedsource model provided by the PULSYN06 algorithm [59]. As shown by [2] site structural model is utilizedalong the complete path if source-site path goes across one or more boundaries amongst structural models,as the station records are generally more sensitive to the local structural environment. A vector sum isestimated after rotating the horizontal components into a reference system at each site that are mutual tothe entire region (N-S and E-W directions). Resulting from any adjacent source, signal of highest amplitudeis selected and associated to the specific site. We concentrate on D_{max}, V_{max} and *DGA* amongst the strong ground motion representativeparameters. 1 Hz upper limit of frequency is adequate as observed by the Fourier spectra of displacementand velocity to consider controlling role of seismic waves but the same is not true for acceleration [e.g. [48]].Then again, choice of higher frequency limit cannot be applied in computations as the necessary informationof seismic sources and as well as of lateral heterogeneity are normally not accessible for the size of theareas usually required in zoning. The present average design response spectra can be used for extendingthe deterministic modeling for frequencies >1*Hz* for the case of acceleration [48]. The DGA values are obtained by scaling the chosen normalized design response spectrum (normalized elastic acceleration spectraof the ground motion for 5 per cent critical damping) with the response spectrum computed at frequencies<1*Hz*. After the October 8, 2005 earthquake, the government of Pakistan realized that implementation of building code according to the international standards was an imperative to avoid such losses of human lives. To address this issue, a Pakistan specific standard building code was developed but not properly implemented. Therefore, the EC8 European code for soil A is used in this study. The choice of the soil A, i.e. stiff soil, is justified by the fact that in all the regional structural models of Fig. 4 the topmost S-wave velocity is greater than 0.8 km/sec.

Seismic Hazard Maps

The spatial distribution of *DGA*, $V_{max}$and D_{max}obtained from the entire synthetic seismograms arecomputed as discussed in Section 3 has been mapped and presented in Figs 10-11, respectively.In terms of DGA, the most severe hazard is found in the epicentral zone of the great Muzaffarabad earthquake of M 7.6 , 2005 (Fig. 8) and its adjacent areas, where the DGA estimate is as high as 0.6 *g* – 1.20 g, and same value is observed in the epicentral zone of the September 24, 2013 Awaran district (Balochistan) earthquake, M 7.8, followed by its September 28, 2013, M 6.8 aftershock and the 1945 Makran coast earthquake, M above 8.0, occurred. It must be noted that the Gawadar, and Pasni ports are both included in the above-mentioned hazardous area.Islamabad, which is the capital city of Pakistan, has DGA estimate as high as 0.3 *g* – 0.6 *g*. Similarly, in the regions of Chaman fault, the epicentral zone of the Quetta earthquake of 1935, Suleiman ranges and upper Punjab have DGA values between 0.3 *g* –0.6 *g*. The northern areas of Pakistan have DGA values 0.15- 0.30 g, the DGA for Peshawar is 0.08-0.15 *g*.The areas of Sind, namely Hyderabad and Thatta, have DGA values 0.3 *g* –0.6 *g*. Lahore, the capital city of Punjab has DGA 0.15-0.30g, the same is observed in Balochistan plateau and in Karachi, the mega city of Pakistan. The Indus plain and the region of lower Punjab are characterized by DGA values in the range 0.04-0.08 *g*. Lower DGA is estimated for the region of Balochistan near Nokundi, in the range 0.02-0.04 *g*.

For displacement and velocities, the highest values are obtained in Muzaffarabad, Kashmir, Awaran, Makhran coast, Quetta and its surroundings with velocity and displacement in the range of 60–120 *cm* $s^{-1}$and 30–60 *cm*, respectively. In the other parts of the region, such as the capital of Pakistan Islamabad and its twin city Pindi, areas of Balochistan namely Khost, Surab, Pasni, and NWFP, Chitral, the maximum velocity is up to 30–60 *cm* s^{-1} and the maximum displacement is 15–30 *cm*. In the area of lower Punjab, the maximum velocity and displacement are in the range 2–4 *cm* $s^{-1}$and 7–15 *cm*, respectively. The areas of Sind like Karachi, Khairpur, Sukkur, Thar desert have velocity in the range of 15-30 *cms*$^{-1}$and displacement in the range of 15- 30 *cm*.

CONCLUSION

By computing realistic synthetic seismograms, the deterministic seismic hazard map has been prepared for Pakistan and adjoining areas in terms of D_{max}, $V_{max}$and DGA values.The seismic hazard is found to be highest in

Muzaffarabad, as the seismic hazard is controlled by the largest event in the area. The DGA value for this region is found to be 0.6 *g* – 1.20*g*. In the other regions of high seismicity, such as Islamabad, capital of Pakistan and Quetta, estimates of DGA values are as high as 0.30– .60*g*. The peak velocity and displacement are also high in these earthquake-prone zones. The ground shaking values are definitely high for the existing infrastructure and could result in great damage and huge socio-economic losses due to the high economic importance of the areas.

The neo-deterministic modelling of seismic hazard for the Pakistan and adjoining regions yields meaningful results and gives us a reasonable and economically logical scientific means for seismic zonation and hazard assessment. The main benefit of the approach lies in its capacity to directly evaluate the outcomes of source mechanics and wave propagation, while local site effects are roughly considered when using the design spectra to obtain the DGA from the synthetic response spectra. The expected PGA and computed DGA for a few strong earthquakes in Pakistan is shown in Table 1. We believe that the research and data we submit here will enrich the understanding of the seismic hazard in Pakistan and adjoining regions. Moreover, our research may help those civil and earthquake engineers who desire to launch thorough and detailed studies of earthquake hazard.

REFERENCES

1. Zaré, M., &Karmimi-Paridari, S. (2008). Balakot, Muzaffarabad Earthquake of 8 October 2005, Mw 7.6; Field Observations on Geological Aspects. In The 14th World Conference on Earthquake Engineering, Beijing, China. Retrieved from http://www. iitk. ac. in/nicee/wcee/article/14_01-1044.
2. Panza, G. F., Romanelli, F., & Vaccari, F. (2001). Seismic wave propagation in laterally heterogeneous anelastic media: theory and applications to seismic zonation. In Advances in geophysics (Vol. 43, pp. 1-95). Elsevier.
3. Panza, G. F., La Mura, C., Peresan, A., Romanelli, F., & Vaccari, F. (2012). Seismic hazard scenarios as preventive tools for a disaster resilient society. In Advances in geophysics(Vol. 53, pp. 93-165). Elsevier.
4. Sarwar, F.(2015). Seismic activities and its time prediction modelling: Ph.D. thesis of Farhana Sarwar(unpublished). Submitted to University of Balochistan, Quetta Pakistan.
5. Keilis-Borok, V., & Soloviev, A. A. (Eds.). (2013). Nonlinear dynamics of the lithosphere and earthquake prediction. Springer Science & Business Media.
6. Peresan, A., Kossobokov, V., Romashkova, L., &Panza, G. F. (2005). Intermediate-term middle-range earthquake predictions in Italy: a review. Earth-Science Reviews, 69(1-2), 97-132.
7. Peresan, A., Zuccolo, E., Vaccari, F., Gorshkov, A., &Panza, G. F. (2011). Neo-deterministic seismic hazard and pattern recognition techniques: time-dependent scenarios for North-Eastern Italy. Pure and Applied Geophysics, 168(3-4), 583-607.
8. http:// www.ezilon.com/maps/asia/pakistan-physical-maps.html. [Online].
9. Gupta, I. D. (2002). The state of the art in seismic hazard analysis. ISET Journal of Earthquake Technology, 39(4), 311-346.
10. Reiter, L. (1991). Earthquake hazard analysis: issues and insights. Columbia University Press.
11. Molchan, G., Kronrod, T., &Panza, G. F. (1997). Multi-scale seismicity model for seismic risk. Bulletin of the Seismological Society of America, 87(5), 1220-1229.
12. Vaccari, F., Tadili, B., El Qadi, A., Ramdani, M., Brahim, L. A., &Limouri, M. (2001). Deterministic seismic hazard assessment for North Morocco. Journal of Seismology and Earthquake Engineering, 3(1), 1-12
13. Peresan, A., Zuccolo, E., Vaccari, F., Gorshkov, A., &Panza, G. F. (2011). Neo-deterministic seismic hazard and pattern recognition techniques: time-dependent scenarios for North-Eastern Italy. Pure and Applied Geophysics, 168(3-4), 583-607.
14. Monalisa, Khwaja, A. A., & Jan, M. Q. (2007). Seismic hazard assessment of the NW Himalayan fold-and-thrust belt, Pakistan, using probabilistic approach. Journal of Earthquake Engineering, 11(2), 257-301.
15. Nespak National Engineering Services of Pakistan. (2007). Building Code of Pakistan Seismic Hazard Evaluation Studies", Ministry of Housing and Works, Government of Pakistan.

16. Panza, G. F., Romanelli, F., Vaccari, F., Decanini, L., &Mollaioli, F. (1999). Contribution of the deterministic approach to the characterization of seismic input (No. IC--99/149). Abdus Salam International Centre for Theoretical Physics.
17. Costa, G., Panza, G. F., Suhadolc, P., & Vaccari, F. (1993). Zoning of the Italian territory in terms of expected peak ground acceleration derived from complete synthetic seismograms. Journal of applied geophysics, 30(1-2), 149-160.
18. Parvez, I. A., Vaccari, F., &Panza, G. F. (2003). A deterministic seismic hazard map of India and adjacent areas. Geophysical Journal International, 155(2), 489-508.
19. Meltzer, A., Sarker, G., Beaudoin, B., Seeber, L., & Armbruster, J. (2001). Seismic characterization of an active metamorphic massif, Nanga Parbat, Pakistan Himalaya. Geology, 29(7), 651-654.
20. Roecker, S. W. (1982). Velocity structure of the Pamir-Hindu Kush Region: Possible evidence of subducted crust. Journal of Geophysical Research: Solid Earth, 87(B2), 945-959.
21. Johnson, M., & Vincent, C. (2002). Development and testing of a 3D velocity model for improved event location: A case study for the India-Pakistan region. Bulletin of the Seismological Society of America, 92(8), 2893-2910.
22. Roecker, S. W., Sabitova, T. M., Vinnik, L. P., Burmakov, Y. A., Golvanov, M. I., Mamatkanova, R., &Munirova, L. (1993). Three-dimensional elastic wave velocity structure of the western and central Tien Shan. Journal of Geophysical Research: Solid Earth, 98(B9), 15779-15795.
23. Pegler, G., & Das, S. (1998). An enhanced image of the Pamir–Hindu Kush seismic zone from relocated earthquake hypocentres. Geophysical Journal International, 134(2), 573-595.
24. Chatelain, J. L., Roecker, S. W., Hatzfeld, D., & Molnar, P. (1980). Microearthquake seismicity and fault plane solutions in the Hindu Kush region and their tectonic implications. Journal of Geophysical Research: Solid Earth, 85(B3), 1365-1387.
25. Zeitler, P. K., Koons, P. O., Bishop, M. P., Chamberlain, C. P., Craw, D., Edwards, M. A., ... & Kidd, W. S. (2001). Crustal reworking at Nanga Parbat, Pakistan: Metamorphic consequences of thermal-mechanical coupling facilitated by erosion. Tectonics, 20(5), 712-728.
26. Reiter, D., Rodi, W., & Johnson, M. (2005). Development of a tomographic upper-mantle velocity model beneath Pakistan and northern India for improved regional seismic-event location. Bulletin of the Seismological Society of America, 95(3), 926-940.
27. Vinnik, L., Singh, A., Kiselev, S., & Kumar, M. R. (2007). Upper mantle beneath foothills of the western Himalaya: subducted lithospheric slab or a keel of the Indian shield?. Geophysical Journal International, 171(3), 1162-1171.
28. Billington, S., Isacks, B. L., &Barazangi, M. (1977). Spatial distribution and focal mechanisms of mantle earthquakes in the Hindu Kush–Pamir region: a contorted Benioff zone. Geology, 5(11), 699-704.
29. Sarwar, F., Iqbal, S., & Kamal, S. (2011). An analysis of Pakistan's local network catalog of earthquake for the period of 1905–2007. Sci Int, 23(1), 13-18.
30. http://asc-india.org/menu/gquakes.htm.. [Online].
31. Bilham, R. (2004). Historical studies of earthquakes in India. Ann. Geophys, 47(2), 839-858.
32. Aoudia, A., Vaccari, F., Suhadolc, P., &Meghraoui, M. (2000). Seismogenic potential and earthquake hazard assessment in the Tell Atlas of Algeria. Journal of Seismology, 4(1), 79-98.
33. Panza, G.F., Irikura, K., Kouteva, M., Peresan, A., Wang, Z., &Saragoni, R. (2011). Advanced seismic hazard assessment, Pageoph Topical Volume. ISBN 978-3-0348-0039-6 and ISBN: 978-3-0348-0091-4.
34. Gelfand, I. M., Guberman, S. I., Izvekova, M. L., Keilis-Borok, V. I., &Ranzman, E. J. (1972). Criteria of high seismicity, determined by pattern recognition. In Developments in Geotectonics (Vol. 4, pp. 415-422). Elsevier.
35. Sarwar, F., Iqbal, S., Qaisar, M., Rehman, A., Akhtar, F., & Raza, S. M. (2016). Earthquake Statistics and Earthquake Research Studies in Pakistan. Open Journal of Earthquake Research, 5(02), 97.
36. Khattri, K. N., Rogers, A. M., Perkins, D. M., &Algermissen, S. T. (1984). A seismic hazard map of India and adjacent areas. Tectonophysics, 108(1-2), 93-134.
37. Bhatia, S. C., Kumar, M. R., & Gupta, H. K. (1999). A probabilistic seismic hazard map of India and adjoining regions. Annals of Geophysics, 42(6).

38. Seeber, L., Armbruster, J. G., & Jacob, K. H. (1999). Probabilistic assessment of earthquake hazard for the state of Maharashtra. Report to Government of Maharashtra Earthquake Rehabilitation Cell, Mumbai.
39. Molnar, P., Fitch, T. J., & Wu, F. T. (1973). Fault plane solutions of shallow earthquakes and contemporary tectonics in Asia. Earth and Planetary Science Letters, 19(2), 101-112.
40. Lisa, M., Khan, S. A., &Khwaja, A. A. (2004). Focal mechanism study of north Potwar deformed zone, Pakistan. Acta SeismologicaSinica, 17(3), 255-261
41. Verma, R. K., & Sekhar, C. C. (1986). Focal mechanism solutions and nature of plate movements in Pakistan. Journal of geodynamics, 5(3-4), 331-351.
42. Verma, R. K., Mukhopadhyay, M., &Bhanja, A. K. (1980). Seismotectonics of the Hindukush and Baluchistan arc. Tectonophysics, 66(4), 301-322.
43. Armbruster, J., Seeber, L., Quittmeyer, R., & Farah, A. (1980). Seismic network data from Quetta, Pakistan: The Chaman Fault and the fault related to the 30 May 1935 earthquake
44. Fitch, T. J. (1970). Earthquake mechanisms in the Himalayan, Burmese, and Andaman regions and continental tectonics in central Asia. Journal of Geophysical Research, 75(14), 2699-2709.
45. Chandra, U. (1978). Seismicity, earthquake mechanisms and tectonics along the Himalayan mountain range and vicinity. Physics of the Earth and Planetary Interiors, 16(2), 109-131.
46. Panza, G. F., Vaccari, F., &Cazzaro, R. (1999). Deterministic seismic hazard assessment. In Vrancea earthquakes: tectonics, hazard and risk mitigation (pp. 269-286). Springer, Dordrecht.
47. Orozova-Stanishkova, I. M., Costa, G., Vaccari, F., &Suhadolc, P. (1996). Estimates of 1 Hz maximum acceleration in Bulgaria for seismic risk reduction purposes. Tectonophysics, 258(1-4), 263-274.
48. Panza, G. F., Vaccari, F., Costa, G., Suhadolc, P., & Fah, D. (1996). Seismic input modelling for zoning and microzoning. Earthquake Spectra, 12(3), 529-566.
49. Alvarez, L., Vaccari, F., &Panza, G. F. (1999). Deterministic seismic zoning of eastern Cuba. pure and applied geophysics, 156(3), 469-486.
50. Bus, Z., Szeidovitz, G., & Vaccari, F. (2000). Synthetic seismogram based deterministic seismic zoning for the Hungarian part of the Pannonian basin. In Seismic Hazard of the Circum-Pannonian Region (pp. 205-220). Birkhäuser, Basel.
51. Markušić, S., Suhadolc, P., Herak, M., & Vaccari, F. (2000). A contribution to seismic hazard assessment in Croatia from deterministic modeling. In Seismic Hazard of the Circum-Pannonian Region (pp. 185-204). Birkhäuser Basel.
52. Radulian, M., Vaccari, F., Mandrescu, N., Panza, G. F., &Moldoveanu, C. L. (2000). Seismic hazard of Romania: deterministic approach. In Seismic Hazard of the Circum-Pannonian Region (pp. 221-247). Birkhäuser, Basel.
53. Živčić, M., Suhadolc, P., & Vaccari, F. (2000). Seismic zoning of Slovenia based on deterministic hazard computations. In Seismic Hazard of the Circum-Pannonian Region (pp. 171-184). Birkhäuser, Basel.
54. El-Sayed, A., Vaccari, F., &Panza, G. F. (2001). Deterministic seismic hazard in Egypt. Geophysical Journal International, 144(3), 555-567.
55. Panza, G. F., &Suhadolc, P. (1987). Complete strong motion synthetics. Seismic strong motion synthetics, 4, 153-204.
56. Florsch, N., Fäh, D., Suhadolc, P., &Panza, G. F. (1991). Complete synthetic seismograms for high-frequency multimodeSH-waves. Pure and Applied Geophysics, 136(4), 529-560.
57. Pavlov, V. M. (2009). Matrix impedance in the problem of the calculation of synthetic seismograms for a layered-homogeneous isotropic elastic medium. Izvestiya, Physics of the Solid Earth, 45(10), 850-860.
58. Parvez, I. A., Romanelli, F., &Panza, G. F. (2011). Long period ground motion at bedrock level in Delhi city from Himalayan earthquake scenarios. Pure and applied geophysics, 168(3-4), 409-477.
59. A. Gusev, Broadband kinematic stochastic simulation of an earthquake source: a refined procedure for application in seismic hazard studies," Pure Appl. Geophys , pp. 168, 155–200. doi: 10.1007/s00024-010-0156-3, 2011.

Fig.1 Geographical Map of Pakistan with Adjoining regions [8].

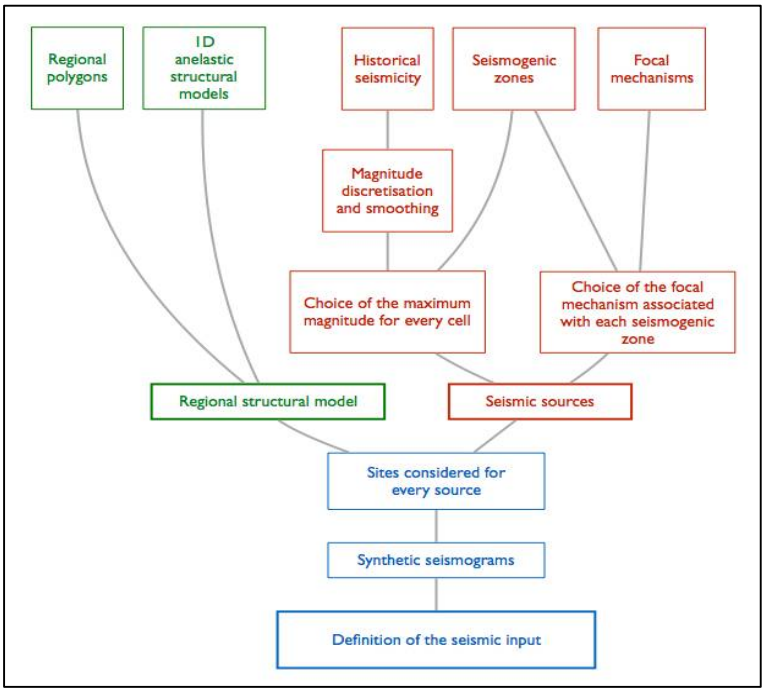

Fig. 2. The flow chart of the computation process.

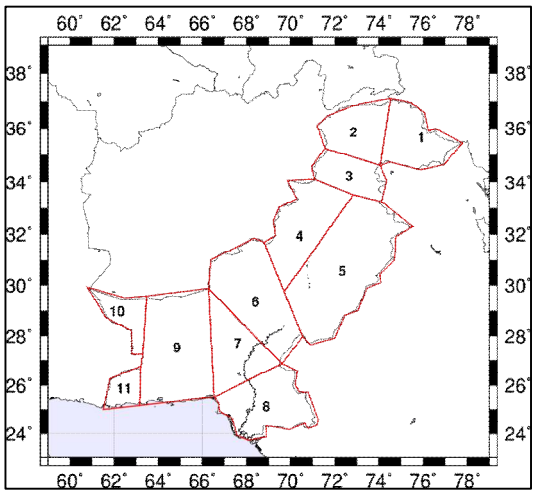

Fig. 3. Boundaries of regional structural polygons.

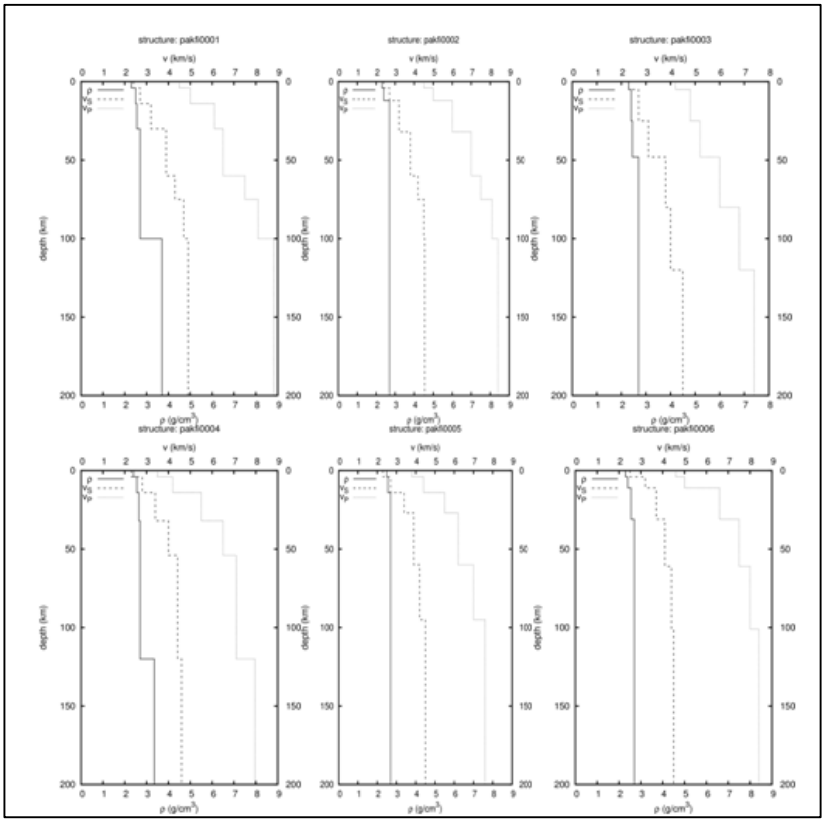

Fig. 4a. Layering of the regional structural models for polygons 1 to 6 of Fig. 2. The models continue to a depth of about 1000 km, but only the uppermost 200 km are shown here to better appreciate the details of crust and upper mantle properties.

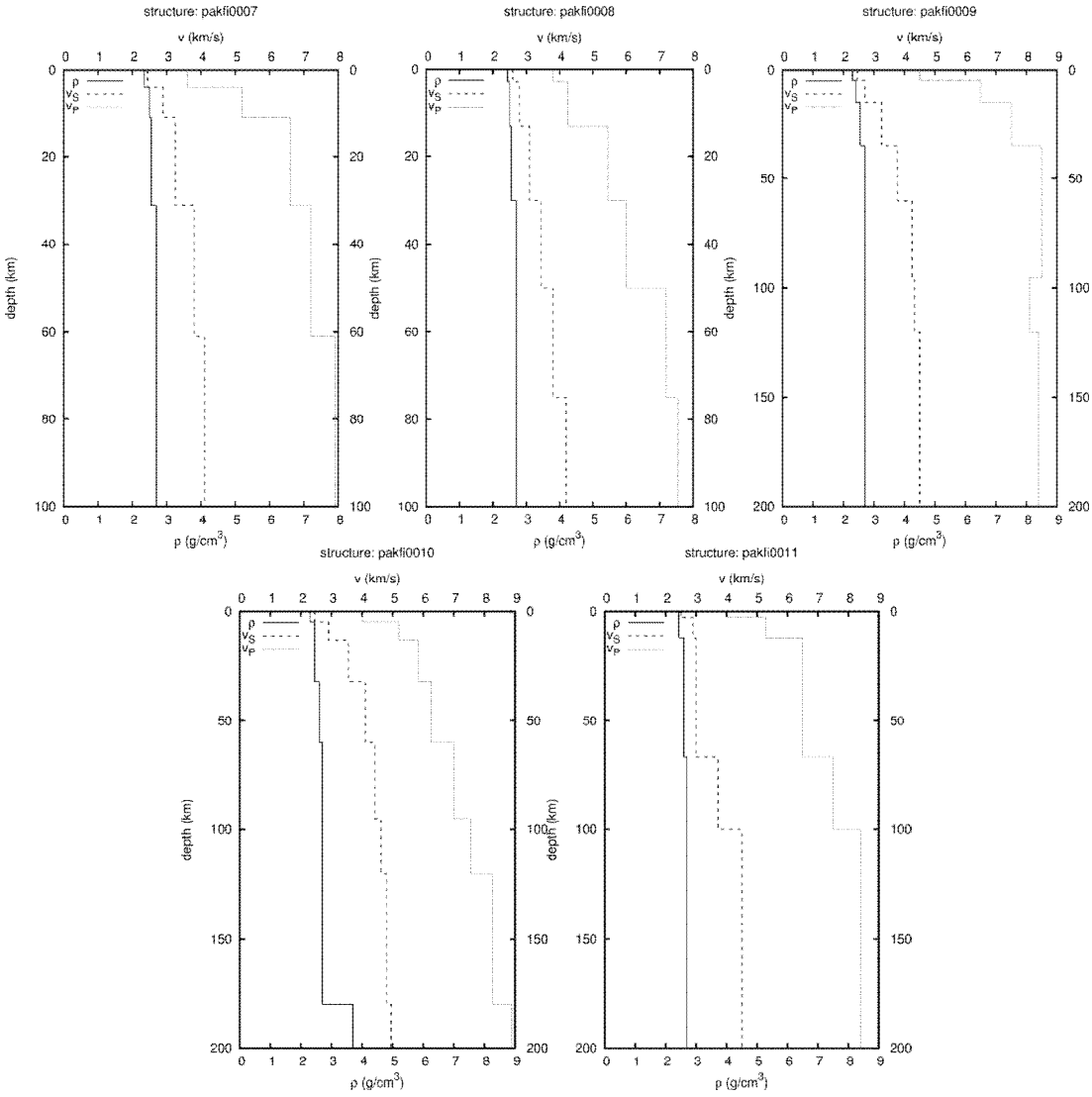

Fig. 4b. Same as Fig.3a for polygons 7 to 11 of Fig. 3.

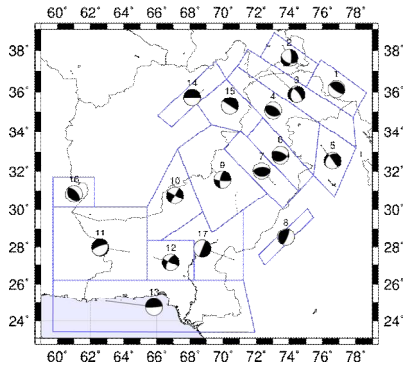

.

Fig. 5. Boundaries of the seismogenic zones, and the focal mechanism associated with the sources belonging to each seismogenic zone.

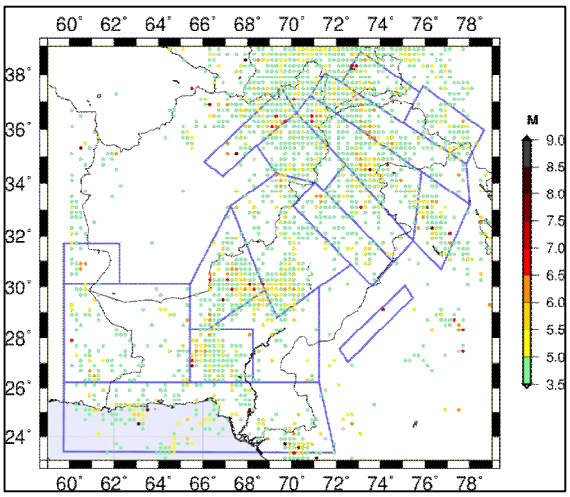

Fig. 6. Map of the observed seismicity, gridded into 0.2° x 0.2° cells.

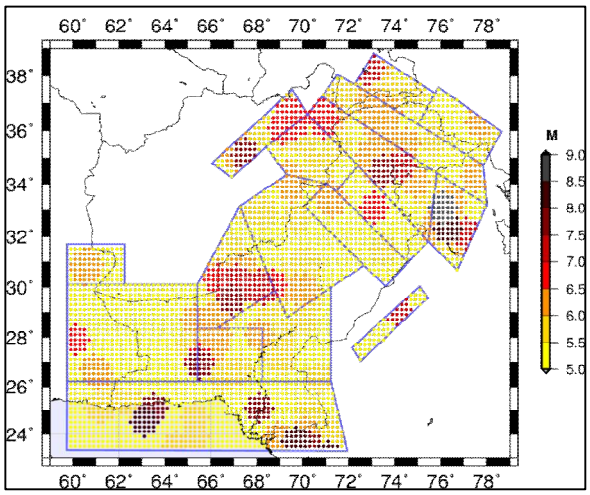

Fig. 7. Representation of the seismicity smoothed within the seismogenic zones.

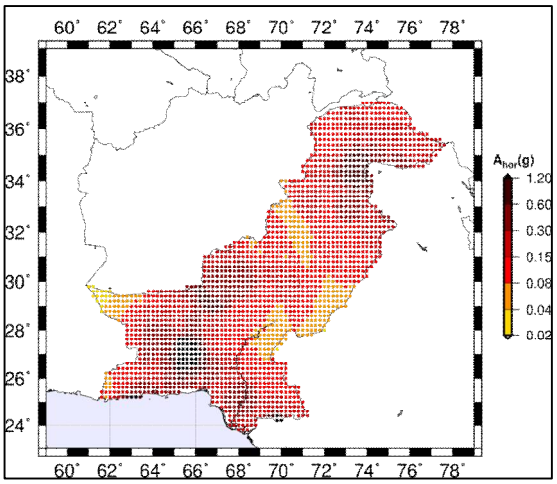

Fig. 8. Map showing the horizontal DGA values for the studied area.

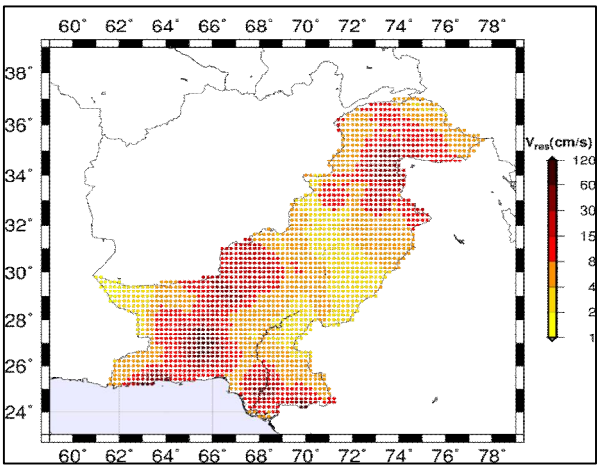

Fig. 9. Map of the maximum horizontal velocity for Pakistan.

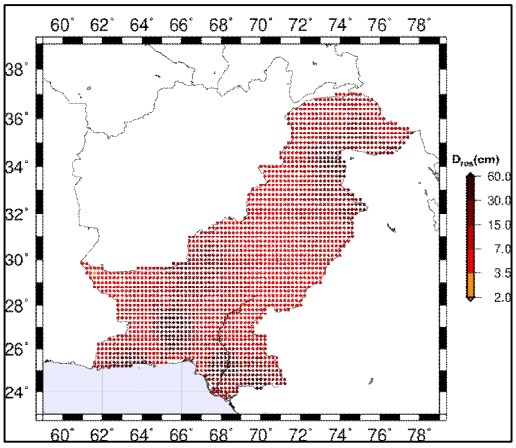

Fig. 10. Map of the maximum horizontal displacement for Pakistan.

Table 1. The expected PGA and computed DGA for a few strong earthquakes in Pakistan[4].

Longitude	Latitude	Region	PGA	DGA(g)	M	Date
73°30′E	33°40′N	Muzaffarabad	0.38	0.6 *g* – 1.20	8.0	8/10/2005
62°18′E	25°10′N	Gawadar	0.24	0.6 *g* – 1.20	7.6	1947
63°27′E	25°15′N	Pasni	0.32	0.6 *g* – 1.20	7.8	28/05/1945
72°90′E	35°10′N	Balakot Patan	0.26	0.3-0.6	6.2	28/12/1974
64°00′E	25°40′N	Makran	0.30	0.6 *g* – 1.20	7.7	1945
73°45′E	33°59′N	Bagh	0.42	0.3-0.6	7.6	8/10/2005

Indian Journal of Natural Sciences www.tnsroindia.org.in ©IJONS

Vol.9 /Issue 51 / December / 2018 *International Bimonthly* *ISSN: 0976 – 0997*

RESEARCH ARTICLE

Molecular Detection and Histopathological Studies of Rabies Viral Infection in Dogs of North Kerala

Shyam S.[1]*, Prasanna K. S.[2], Ajith Jacob George[3], Anoopraj R.[4] and Rajasekhar R.[5]

Department of Veterinary Pathology, College of Veterinary and Animal Sciences, Pookode, Wayanad-673 576,Kerala,India.

Received: 21 Sep 2018 Revised: 25 Oct 2018 Accepted: 27 Nov 2018

***Address for Correspondence**
Shyam S
Department of Veterinary Pathology,
College of Veterinary and Animal Sciences,
Pookode, Wayanad-673 576,
Kerala,India

ABSTRACT

Companion animals like dogs have become an unavoidable part of human society. Since most of the owners maintain a close interaction with their pets, diseases like rabies also have a zoonotic concern. Tissue samples from 41 dogs which had shown nervous symptoms prior to death were collected during necropsy. All nervous tissue samples collected were subjected to total RNA extraction. For detecting Rabies lyssa virus, N gene specific RT-PCR was conducted. In the test, 14 samples produced amplicons of 533 bp giving percentage positivity of 34.14 per cent. These samples were also subjected for dFAT and gave apple green fluorescence of varying intensities. Representative cases of Rabies lyssa virus positive PCR products were sequenced. The sequences were confirmed as belonging to the respective viruses by BLAST analysis. All isolates were having similarity with other Indian isolates. Major histopathological lesions noticed in brain tissue were Negri body in pyramidal cells of cerebrum, gliosis of pyramidal cell layer, perivascular cuffing around cerebral vessels, congestion of meningeal vessels and Babes nodules in case of samples which were detected positive for rabies.

Keywords: Rabies, Zoonotic disease, Lyssa virus, PCR, RT-PCR, BLAST, Histopathology

INTRODUCTION

As per 19th livestock census 2012 India has a dog population of 11.673 million, and it has 11, 92,353 in Kerala. Of this 2, 68,994 are stray dogs. Companion animals, especially dogs are conquering an important space in human society. Thus diseases affecting them has both sentimental as well as zoonotic importance. Many such diseases causes nervous symptoms, which leads to presumptive diagnosis as rabies.

MATERIALS AND METHODS

Collection of samples

Tissue samples were collected from 41 dogs died after showing nervous symptoms belonging to northern districts of Kerala *viz*, Wayanad, Kozhikode, Kannur and Kasaragod. Samples collected included cerebellum, cerebrum, and hippocampus portions of brain from dogs and cats (Table 1). The tissue samples were collected in sterile screw capped polypropelene vials using sterile scissors and forceps, and stored at -80ºC after proper labelling to prevent RNA degradation till further processing. For histopathological examination brain samples from dogs and cats were collected and were preserved in 10 per cent formalin until further processing.

Direct Fluorescent Antibody Test (d FAT)

Direct Fluorescent Antibody test was conducted using Fluorescine iso thiocyanate (FITC) conjugatated nucleocapsid monoclonal antibody (Merck, Germany) on impression smears from cerebrum, cerebellum, hippocampus and brain stem as per the standard protocol for FAT (Dean *et al.,* 1996) and observed under fluorescent microscope (Zeiss, Progres C5).

Histopathological Examination

Collection, fixation, processing and sectioning of brain samples

Brain samples were collected and stored in 10 per cent formalin and embedded in paraffin for histopathological examination. Sections were cut at four micron thickness. These thin sections were stained by routine Haematoxylin and Eosin (H&E) stain (Bancroft and Gamble, 2008).

RESULTS AND DISCUSSION

Rabies viral nucleocapsid antigen detection by direct fat

Brain impression smear from 41 samples were subjected to dFAT. Of these 41 samples, 12 were detected as positive giving a percentage positivity of 29.27 per cent (Table 2).

Gross Lesions

The important gross lesions observed in the brain were meningeal congestion, thickening of the meninges, oedema of the brain, engorgement of the cerebral and cerebellar vessels and sub meningeal and cerebral haemorrhages. Significant gross alterations were not seen in some of the cases.

Histopathological Lesions in Nervous System

Severe histopathological changes were observed in most of the cases under study. The major histopathological alterations in examined cases are listed in Table 3 and illustrations are given in Plates.

Confirmation of the Rabies Lyssa Virus by Molecular Sequencing

Representative positive samples obtained for Rabies lyssa virus sent for sequencing to AgriGenome Labs Private Limited, Cochin. When the chromatograms obtained after sequencing were analysed, it was observed that there were no errors. On BLAST analysis, the RV isolate showed 99 per cent similarity to Indian isolates.

ACKNOWLEDGEMENTS

The authors acknowledge the facilities and funding provided by the Head of the veterinary pathology department, Dean, CVAS, Pookode and the DAR, KVASU.

REFERENCES

1. Bancroft, J.D. and Gamble, M. 2008. Theory and practice of histological techniques. Churchill Livingstone Elsevier, Philadelphia, pp.121.
2. 19th Livestock Census - 2012 Annual Report. Available:http://dahd.nic.in/sites/default/files/Livestock%20%205.pdf
3. Dean, D. J., Abelseth, M. K., Atnasiu, P. 1996. The flourascent antibody test. In: Meslin, F. X., Kaplan, M. M., Koprowski, H eds.*Laboratory Techniques in Rabies*, fourth ed. Geneva: World Health Organisation. 800p

Table 1. Details of samples collected for testing rabies virus

Sl. No.	Case no.	Area/Location	Samples Collected	Species
1.	67/18	Meppadi	Hippocampus, cerebellum, cerebrum	Canine
2.	72/18	Adivaram	Hippocampus, cerebellum, cerebrum	Canine
3.	79/18	Meppadi	Hippocampus, cerebellum, cerebrum	Canine
4.	85/18	Kottiyoor	Hippocampus, cerebellum, cerebrum	Canine
5.	86/18	Korom	Hippocampus, cerebellum, cerebrum	Canine
6.	87/18	Peruvannamuzhi	Hippocampus, cerebellum, cerebrum	Canine
7.	96/18	Pozuthana	Hippocampus, cerebellum, cerebrum	Canine
8.	97/18	Mahe	Hippocampus, cerebellum, cerebrum	Canine
9.	99/18	Mananthavady	Hippocampus, cerebellum, cerebrum	Canine
10.	106/18	Narikuni	Hippocampus, cerebellum, cerebrum	Canine
11.	111/18	Mananthavady	Hippocampus, cerebellum, cerebrum	Canine
12.	112/18	Chulliyode	Hippocampus, cerebellum, cerebrum	Canine
13.	114/18	Thamarassery	Hippocampus, cerebellum, cerebrum	Canine
14.	116/18	Moopainad	Hippocampus, cerebellum, cerebrum	Canine
15.	117/18	Kenichira	Hippocampus, cerebellum, cerebrum	Canine
16.	119/18	Ezhamchira, Meppadi	Hippocampus, cerebellum, cerebrum	Canine
17.	120/18	Naduvannur	Hippocampus, cerebellum, cerebrum	Canine
18.	122/18	Vengapalli	Hippocampus, cerebellum, cerebrum	Canine
19.	123/18	Meenangadi	Hippocampus, cerebellum, cerebrum	Canine

20.	124/18	Meenangadi	Hippocampus, cerebellum, cerebrum	Canine
21.	127/18	Vythiri	Hippocampus, cerebellum, cerebrum	Canine
22.	128/18	Pulpally	Hippocampus, cerebellum, cerebrum	Canine
23.	133/18	Mananthavady	Hippocampus, cerebellum, cerebrum	Canine
24.	134/18	Kozhikode	Hippocampus, cerebellum, cerebrum	Canine
25.	143/18	Chingapuram	Hippocampus, cerebellum, cerebrum	Canine
26.	154/18	Madakkunnu	Hippocampus, cerebellum, cerebrum	Canine
27.	156/18	Kambalakkad	Hippocampus, cerebellum, cerebrum	Canine
28.	170/18	Kottiyoor	Hippocampus, cerebellum, cerebrum	Canine
29.	173/18	Kakkodi	Hippocampus, cerebellum, cerebrum	Canine
30.	174/18	Manathavady	Hippocampus, cerebellum, cerebrum	Canine
31.	180/18	Manathavady	Hippocampus, cerebellum, cerebrum	Canine
32.	181/18	Panamaram	Hippocampus, cerebellum, cerebrum	Canine
33.	182/18	Muttil	Hippocampus, cerebellum, cerebrum	Canine
34.	185/18	Neeleswaram	Hippocampus, cerebellum, cerebrum	Canine
35.	193/18	Padinjarathara	Hippocampus, cerebellum, cerebrum	Canine
36.	196/18	Nadavayal	Hippocampus, cerebellum, cerebrum	Canine
37.	201/18	Kozhikode	Hippocampus, cerebellum, cerebrum	Canine
38.	209/18	Venniyode	Hippocampus, cerebellum, cerebrum	Canine
39.	213/18	Manassery	Hippocampus, cerebellum, cerebrum	Canine
40.	215/18	Koyleri	Hippocampus, cerebellum, cerebrum	Canine
41.	229/18	Mananthavady	Hippocampus, cerebellum, cerebrum	Canine

Table 2. Results of brain samples tested for Rabies

Number of samples tested	Number of samples found positive	Per cent of positive samples
41	12	29.27

Table 3. Details of the gross and histopathological lesions in the examined cases

Sl. No.	Case No.	Species	Samples collected	Gross lesions	Histopathological lesions
1.	67/18	Canine	Hippocampus, cerebellum, cerebrum	Meningeal congestion, congestion of cerebral vessels	Gliosis of pyramidal cell layer, perivascular cuffing in cerebral vessels, congestion of meningeal vessels, babes nodules
2.	72/18	Canine	Hippocampus, Cerebellum, cerebrum	Meningeal congestion	(HP not done as the samples were found negative for RV in PCR)
3.	79/18	Canine	Hippocampus, Cerebellum, cerebrum	Thickened meninges	(HP not done as the samples were found negative for RV in PCR)
4.	85/18	Canine	Hippocampus, Cerebellum, cerebrum	Thickened meninges, engorged cerebral vessels	(HP not done as the samples were found negative for RV in PCR)
5.	86/18	Canine	Hippocampus, Cerebellum, cerebrum	Meningeal congestion	(HP not done as the samples were found negative for RV in PCR)
6.	87/18	Canine	Hippocampus, Cerebellum, cerebrum	Congestion of cerebral vessels	(HP not done as the samples were found negative for RV in PCR)
7	96/18	Canine	Hippocampus, Cerebellum, cerebrum	Meningeal congestion, congestion of cerebral vessels	Gliosis of pyramidal cell layer, perivascular cuffing in cerebral vessels, congestion of meningeal vessels, Babes nodules
8	97/18	Canine	Hippocampus, Cerebellum, cerebrum	Engorged cerebral vessels	(Histopathological (HP) examination not done as the samples were found negative for RV in PCR)

9.	99/18	Canine	Hippocampus, Cerebellum, cerebrum	Meningeal congestion, congestion of cerebral vessels	Negribody in pyramidal cells of cerebrum, gliosis of pyramidal cell layer, perivascular cuffing in cerebral vessels, congestion of meningeal vessels, Babes nodules
10.	106/18	Canine	Hippocampus, Cerebellum, cerebrum	Congested meningeal vessels	(Histopathological (HP) examination not done as the samples were found negative for RV in PCR)
11	111/18	Canine	Hippocampus, Cerebellum, cerebrum	Thickenig of the meninges	(Histopathological (HP) examination not done as the samples were found negative for RV in PCR)
12.	112/18	Canine	Hippocampus, Cerebellum, cerebrum	Meningeal congestion, congestion of cerebral vessels	(Histopathological (HP) examination not done as the samples were found negative for RV in PCR)
13.	114/18	Canine	Hippocampus, Cerebellum, cerebrum	Meningeal congestion, congestion of cerebral vessels	(Histopathological (HP) examination not done as the samples were found negative for RV in PCR)
14.	116/18	Canine	Hippocampus, Cerebellum, cerebrum	Thickened meninges	(Histopathological (HP) examination not done as the samples were found negative for RV in PCR)
15.	117/18	Canine	Hippocampus, Cerebellum, cerebrum	Meningeal congestion	(Histopathological (HP) examination not done as the samples were found negative for RV in PCR)
16.	119/18	Canine	Hippocampus, Cerebellum, cerebrum	Meningeal congestion, congestion of cerebral vessels	Gliosis of pyramidal cell layer, perivascular cuffing in cerebral vessels, congestion of meningeal vessels, babes nodules

17.	120/18	Canine	Hippocampus, Cerebellum, cerebrum	Engorged cerebral vessels	(Histopathological (HP) examination not done as the samples were found negative for RV in PCR)
18.	122/18	Canine	Hippocampus, Cerebellum, cerebrum	Meningeal congestion, congestion of cerebral vessels	Negribody in pyramidal cells of cerebrum, gliosis of pyramidal cell layer, perivascular cuffing in cerebral vessels, congestion of meningeal vessels, babes nodules
19.	123/18	Canine	Hippocampus, Cerebellum, cerebrum	Thickened meninges, oedema of the brain	(Histopathological (HP) examination not done as the samples were found negative for RV in PCR)
20.	124/18	Canine	Hippocampus, Cerebellum, cerebrum	Congested cerebral vessels	Degenerated neuron, vasculitis
21.	127/18	Canine	Hippocampus, Cerebellum, cerebrum	Engorged cerebral vessels	(Histopathological (HP) examination not done as the samples were found negative for RV in PCR)
22.	128/18	Canine	Hippocampus, Cerebellum, cerebrum	congested cerebral vessels	Degenerated neuron, vasculitis
23.	133/18	Canine	Hippocampus, Cerebellum, cerebrum	Meningeal congestion, congestion of cerebral vessels	Perivascular cuffing in cerebral vessels, congestion of meningeal vessels, Babes nodules.
24.	134/18	Canine	Hippocampus, Cerebellum, cerebrum	Thickened meninges	(Histopathological (HP) examination not done as the samples were found negative for RV in PCR)
25.	143/18	Canine	Hippocampus, Cerebellum, cerebrum	Oedema of the brain.	(Histopathological (HP) examination not done as the samples were found negative for RV in PCR)

26.	154/18	Canine	Hippocampus, Cerebellum, cerebrum	Meningeal congestion, congestion of cerebral vessels	Negribody in pyramidal cells of cerebrum, gliosis of pyramidal cell layer, perivascular cuffing in cerebral vessels, congestion of meningeal vessels.
27.	156/18	Canine	Hippocampus, Cerebellum, cerebrum	Meningeal congestion, congestion of cerebral vessels	Perivascular cuffing in cerebral vessels, congestion of meningeal vessels, Babes nodules
28.	170/18	Canine	Hippocampus, Cerebellum, cerebrum	Congestion of cerebral vessels	(Histopathological (HP) examination not done as the samples were found negative for RV in PCR)
29.	173/18	Canine	Hippocampus, Cerebellum, cerebrum	Thickened meninges, engorged cerebral vessels	(Histopathological (HP) examination not done as the samples were found negative for RV in PCR)
30.	174/18	Canine	Hippocampus, Cerebellum, cerebrum	Meningeal congestion, congestion of cerebral vessels	Gliosis of pyramidal cell layer, perivascular cuffing in cerebral vessels, congestion of meningeal vessels.
31.	180/18	Canine	Hippocampus, Cerebellum, cerebrum	Meningeal congestion, congestion of cerebral vessels	Gliosis of pyramidal cell layer, perivascular cuffing in cerebral vessels, congestion of meningeal vessels, babes nodules
32.	181/18	Canine	Hippocampus, Cerebellum, cerebrum	Congestion of cerebral vessels	(Histopathological (HP) examination not done as the samples were found negative for RV in PCR)
33.	182/18	Canine	Hippocampus, Cerebellum, cerebrum	Congestion of cerebral vessels	(Histopathological (HP) examination not done as the samples were found negative for RV in PCR)

34.	185/18	Canine	Hippocampus, Cerebellum, cerebrum	Meningeal congestion, congestion of cerebral vessels	Perivascular cuffing in cerebral vessels, congestion of meningeal vessels, Babes nodules
35.	193/18	Canine	Hippocampus, Cerebellum, cerebrum	Congestion of the cerebral vessels	(Histopathological (HP) examination not done as the samples were found negative for RV in PCR)
36.	196/18	Canine	Hippocampus, Cerebellum, cerebrum	Meningeal congestion, congestion of cerebral vessels	(Histopathological (HP) examination not done as the samples were found negative for RV in PCR)
37.	201/18	Canine	Hippocampus, Cerebellum, cerebrum	Meningeal congestion, congestion of cerebral vessels	Gliosis of pyramidal cell layer, perivascular cuffing in cerebral vessels, congestion of meningeal vessels, babes nodules
38.	209/18	Canine	Hippocampus, Cerebellum, cerebrum	Congestion of cerebral vessels	(Histopathological (HP) examination not done as the samples were found negative for RV in PCR)
39.	213/18	Canine	Hippocampus, Cerebellum, cerebrum	Meningeal congestion, congestion of cerebral vessels	(Histopathological (HP) examination not done as the samples were found negative for RV in PCR)
40.	215/18	Canine	Hippocampus, Cerebellum, cerebrum	Thickened meninges, engorged cerebral vessels	(Histopathological (HP) examination not done as the samples were found negative for RV in PCR)
41.	229/18	Canine	Hippocampus, Cerebellum, cerebrum	Congestion of cerebral vessels	Perivascular cuffing in cerebral vessels, congestion of meningeal vessels, babes nodules

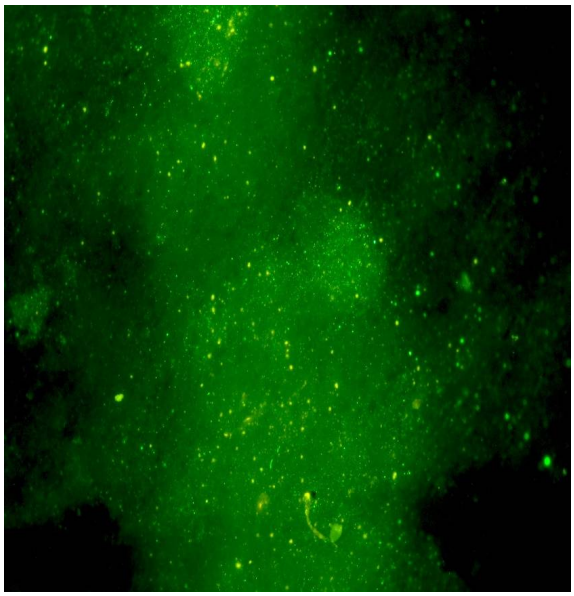

Fig.1.Dog hippocampus impression, 100x (dFAT)

Indian Journal of Natural Sciences www.tnsroindia.org.in ©IJONS

Vol.9 /Issue 51 / December / 2018 *International Bimonthly* *ISSN: 0976 – 0997*

RESEARCH ARTICLE

Study the Flood of 2015 in Wasit Province in Iraq

Gheidaa Sabeeh Al-Hassany*

Assistant Professor, Unit of Remote Sensing, College of Sciences, University of Baghdad,Iraq

Received: 20 Sep 2018 Revised: 24 Oct 2018 Accepted: 27 Nov 2018

***Address for Correspondence**
Gheidaa Sabeeh Al-Hassany
Assistant Professor,
Unit of Remote Sensing,
College of Sciences,
University of Baghdad,Iraq
Email: gheidaa_sab@yahoo.com

ABSTRACT

In most years, Iraq has kindly clam weather; it is generally not suffer of natural hazard like floods. In 2015 flood was occurred in most of Iraqi regions. This natural hazard is chose to be the remotely sensed studied subject by using the GIS tools to apply the remotely sensing techniques to give idea about this flood and its effects in a province in Iraq. The chosen province was Wasit. The used technique is change detection. It was applied on two multi-temporal image data of the satellite Landsat-8 for a scene in Wasit province to calculate the land areas that were affected by the flood of 2015.

Keywords: ArcGIS, flood, change detection.

INTRODUCTION

In remotely sensing applications, the changes are considered as surface component tolerations with different proportion. Land use and land cover change information is important information for a rezone of it's practically uses in diverse implementation, involving deforestation spoilage estimation, monitoring of disasters, urban growth, planning, and land administration. Singh (1989) was define change detection as ‘‘the process of identifying differences in the state of an object or phenomenon by observing it at different times’’. The change detection arrangements depend the multi-temporal datasets to qualitatively classification the temporally influences of phenomena and Identify changes. The remote sensing data has become an active source for change detection researches in the rezone of its high temporally resolution, digital form appropriate for computing, synoptic view, and vastest selection of accuracy of discriminations (spatial and spectral resolutions), [1].

Miscellaneous methods of processing data are active to reduce damage information, in addition to the raising obtain ability of high resolution data consequents to neoteric Prospects in the integration of domain survey with remote sensing. [2] Change detection analytics are famed as beneficial techniques in a vast range of implementation where

the temporally images are having the same coordinates were taken at two or in some times more different time dates were processed for the purpose of recognize changes, [3].

CD application with the Geographically Information System (GIS) is an operation that counts the changing attributes and gives an idea about the way that the attributes of a selected area had been changed between different duration. CD predominating includes contrasting aerial photographs or images of different types of satellites of the land areas captured at different periods of time, [4]. In multi-temporal scenes CD is the procedure of recognizing the locations of pixels that are significantly different for any two scenes in the range; these locations cover the alteration visor. Sundry factors might outcome in alteration visor like a movement of the object relatively to the surroundings, or changes in shape of the object, [1].

Generally, images are geo-registered before the CD process, for this reason each pixel in the first scene with the other of the same coordinates in the second temporally scene correspondence is established between these scenes. Moreover, after the map image of changes is produced, moreover analysis is important to minutely identify variations to individual structures in the scenes. CD processes are utilized in various fields, [5]. Subtraction of images (a multi-temporal) is subtracting the imagery of a date from other date. The resulted values of the subtract are positive and it could be negative in points of radiance change & zero in points of no change. When a 28gray levels an (i.e. 8_bit) analyses of pixel values are in the range from 0-255, but the difference values is in the potential range -255 to 255.

A transformation processes to the results are applied to transform them to positive values by applying a constant "c". This operation is expressed in mathematical as:

$$\Delta L_{ijk} = bv_{ijk}(1) - bv_{ijk}(2) + C \quad \ldots\ldots\ldots (1)$$

Where ΔL_{ijk} is the changing in a pixel value, $bv_{ijk}(1)$ is intensity value for date 1, $bv_{ijk}(2)$ is intensity value for date 2,

C : Constant (e.g.; 255), (i, j) Are the coordinates of the scene, and k represents the no. of bands.

It could be resulted differences in the values of brightness for the same surface materials that may occur by several rezones like: topographically conditions, shadows, season changes in sunlight angles and intensities, [6].

The flood Area and Data Forms

Wasit Governorate is a province in east of Iraqi country, in the south-east of Baghdad province and bordering Iran. At a Prior time to 1976 it was named as Kut Province.Major cities of Wasit are the capital Al Kut, Al-Hai and Al-Suwaira. Wasit has the Marshes of Shuwayja, Al-Attariyah, and Hor Aldelmj. The name was given from the Arabic word meaning "middle," as the previous city of Wasit location is along the Tigris River about midway distance between Baghdad & Basra. Wasit city was abandoned after the Tigris shifted course, [7]. The study area is located in Wasit province.

It was selected to be a study area because it is one of the Iraqi regions that are suffered from 2015 flood. In October 2015, a weather system brought torrential rains to many parts of the Middle East so Iraqi regions were from these parts. The using data is of Landsat 8 an image on November 14, 2015.The second image (figure.2) that shows flood waters north of the Tigris River near the town of Wasit (also called Kut); Landsat acquired an image having a same area on October 13, 2015, before the flooding as shown in figure.1 . Though, some farmland appears to be flooded. The scene coordinates: The lower left corner long.45.517825, Lat. 32.497428 and the upper right corner Long.46.207966, Lat. 32.865, 171. The two multi-temporally images were composed with false color, using a combination of IR and visible radiation (MODIS bands 7-2-1). Bare ground is brown. This band composition easiest the seeing of flood water.

METHODOLOGY

Before the start of the change detection technique, it was confirmed that an important qualifications must be available in the images to let the change detection be possible. These conditions are: The two images have the same resolution.

1. The two images are of a same resolution. The same number of points (the same size).
2. The same coordinates (latitude & longitude).
3. Captured by a same sensor.

CD technique of GIS has been applied on the remotely sensed data in the two images to detect the flood region in the scene. This method can be show as follows:-

1. Open the first scene and the second in the Arc-GIS program.
2. Activate the Arc tool box window.
3. Activate the 3D analyst tools.
4. Perform Raster math technique
5. A subtraction process was done for distinguishing different effects of flood in the studied regions. The subtraction mathematical process (Absolute differencing) to isolate the changed regions at the scene area; it is of pixel values that having absolute differences >0.
6. Perform normalization technique (i.e. Using Unique Values Criterion) on the resulted raster of subtraction process pixel values to produce different ranges of classes (white, three degrees of gray colures and black classes), to make the account of each class pixels be possible to calculate the area for each class .
7. The account of each class pixels was done by multiplying them by the spatial resolution value for this image to calculate each class area.

The areas of each changed class are represent the changed pixels in multi temporal image data for the same location where represent the affected regions in the scenes by the flooding.

RESULTS AND DISCUSSION

The utilized data (multi temporal images) were chosen to be the studied regions for this paper. These two images are a high resolution images (one meter for the pixel). When the process of CD was done, a raster of subtraction was resulted. It is contain five classes, the white class represents the regions of a large change the lower levels of changes regions were the three degrees of grey levels then all of these four classes are the affected regions in the multi-temporal scene by the flooding. And the black class represents the unchanged pixels (The unaffected regions in multi- temporal scene by the flooding). Figure (3) demonstrates the operational steps participated in method, while Table- (1) represents the number of points (pixels), Table2 represents the calculation of area of each class and the percentages of the calculation of areas of classes obtained by enforcement the change detection method.

CONCLUSION

The application of the techniques of CD in the past has been more complicated steps to let be applied because the pre-processing of multi-temporal satellite images are less developed than it is now where it requires the removal of differences in climatic effects such as: clouds, dust and storm effects and different brightness and human intervention. One of the techniques that were used to minimize the effects mentioned is the relative band technique and the principal component analyses.

REFERENCES

1. Hussain & Chen . Change detection from remotely sensed images: From pixel-based to object-based approaches ISPRS Journal of Photogrammetry and Remote Sensing 80 (2013) 91–106.
2. G. Bitelli, IMAGE CHANGE DETECTION ON URBAN AREA: THE EARTHQUAKE CASE
3. (Radke et al., 2005) Radke, R. J.; Andra, S.; Al Kofahi, O. and Roysam, B., 2005.Image Change Detection Algorithms: A Systematic Survey.IEEE Transactions on Image Processing, 14(3), pp. 294-307.
4. Priyanka Khandelwal, Krishna Kant Singh, B.K. Singh, "Unsupervised Change Detection of Multispectral Images using Wavelet Fusion and Kohonen Clustering Network." International Journal of Engineering and Technology (2013) A Mehrotra International Journal of Engineering and Technology 5 (2), 1401-1406
5. R. R. Vatsavai and J. Graesser, "Probabilistic change detection framework for analyzing settlement dynamics using very high-resolution satellite imagery." Procedia CS, vol. 9, pp. 907–916, 2012.
6. John, R. Jensoun, 1986. *Introductory Digital Image Processing*. Prentice-Hall, A. Division of Simon and Schiter, Inc P. 1, P. 235, 241, 244,.
7. *"Governor of Wasit province outgoing Mahdi al-Zubaidi hand over his post to Mahmoud Abdul Ridha Talal". DinarVets. 24 June 2013. Retrieved 30 January 2015*
8. NASA Earth Observatory, 2015 Flooding in Iraq : Natural Hazards http://earthobservatory.nasa.gov/ NaturalHazards/view.php?id=87011

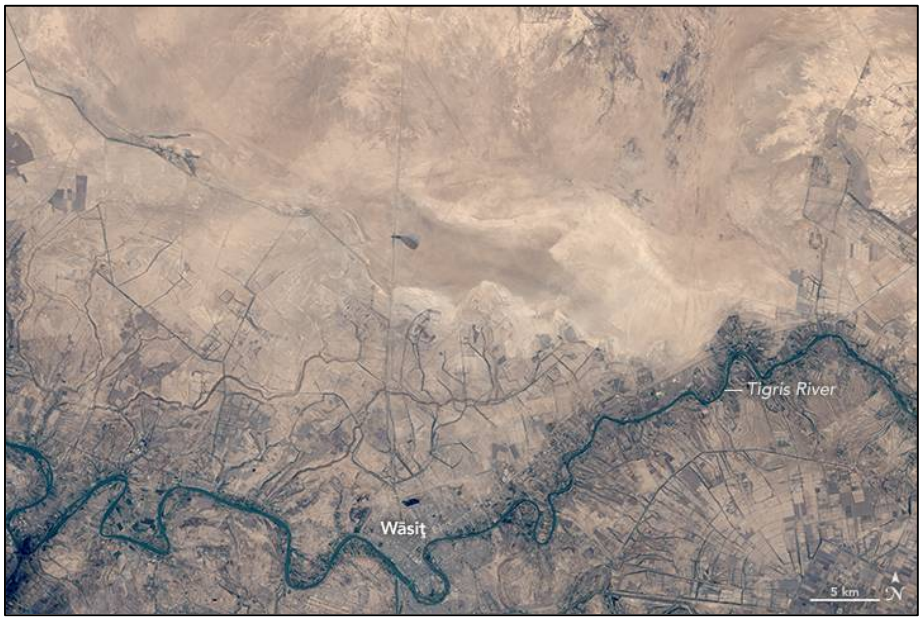

Figure1.Acquired October 13, 2015 large image (8 MB, JPEG, 4338x2892)

Figure 2, Acquired November 14, 2015 large image (8 MB, JPEG, 4338x2892), [8]

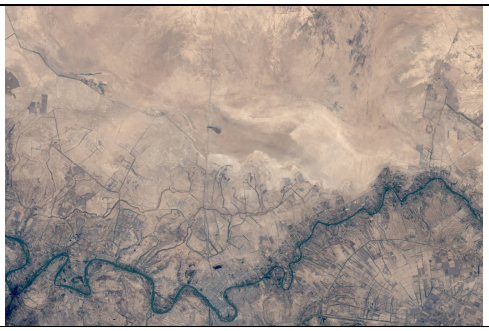

Figure3a, The first image (before the flood)

Figure 3b, The second image (after the flood)

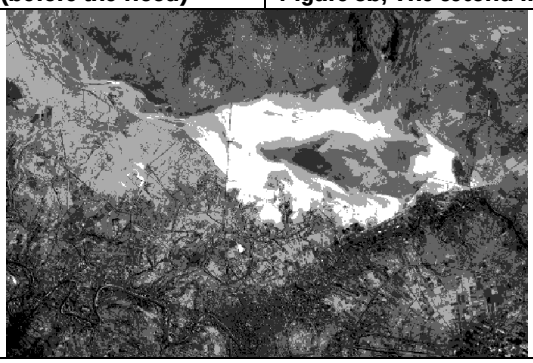

Figure 3c, The raster resulted by the process of subtraction for the first and second images (change detection raster)

Figure 3. Illustrated the operational steps involved in GIS change detection.

Table 1. The number of points of each class in the resulted raster of subtraction process of the two scenes (October 13, 2015 and November 14, 2015)		
Class color		**No. of class points (pixels)**
The affected	**White**	789609
	light gray	2668788
	Moderate gray	5126915
	Dark gray	3127341
Black The unaffected regions in the scene by the flooding		832843

Table 2. The area and the Percentage of each class in the resulted raster of subtraction process of the two scenes (October 13, 2015 and November 14, 2015)			
Class color		**Class area (m^2)**	**Percentages area of the class**
The affected regions in the scene by the flooding	White	789609	$\frac{789209}{12545496}*100=6.294\%$
	light gray	2668788	$\frac{2668788}{12545496}*100=21.273\%$
	Moderate gray	5126915	$\frac{5126915}{12545496}*100=40.867\%$
	Dark gray	3127341	$\frac{3127341}{12545496}*100=24.928\%$
Black The unaffected regions in the scene by the flooding		832843	$\frac{832843}{12545496}*100=6.639\%$

Indian Journal of Natural Sciences www.tnsroindia.org.in ©IJONS

Vol.9 /Issue 51 / December / 2018 *International Bimonthly* *ISSN: 0976 – 0997*

RESEARCH ARTICLE

The Centers of Atmospheric Activity as Potential Predictors for Long-term Forecast of Precipitation in Iraq

Mohanad Ismael Khalbas Albw Jbianah* and Osamah Basil Manji

Soil Sciences and Water Resources, College of Agriculture , University of Wasit , Iraq

Received: 03 Aug 2018 Revised: 06 Sep 2018 Accepted: 09 Oct 2018

***Address for Correspondence**
Mohanad Ismael Khalbas Albw Jbianah
Soil Sciences and Water Resources ,
College of Agriculture ,
University of Wasit , Iraq
Email:

ABSTRACT

Among the most important factors influencing the formation of the living conditions of the population, is the climate. The influence of meteorological conditions on people can be both favorable and unfavorable, so the information about the nature of these conditions gives the opportunity to plan the livelihoods of the population. The solution to this problem is very important for Iraq. The aim of this study is to increase the effectiveness of long-term precipitation forecast of the selected region.

To achieve this goal the following tasks were solved:

- Creation of information base of spatial - averaged characteristics of the precipitation regime of Iraq
- Analysis of precipitation regimes of Iraq
- The selection of potential predictors of long-term precipitation forecast of Iraq.
- Evaluation of potential prognostic predictors.

For Iraq the selected 11 stations. Used archive data for Historical Climatology Network monthly sums of precipitation at the meteorological stations around the globe. The observation period used in the study from 1896 to 2010

Keywords: Prophesying rain Iraq, activity centers atmospheric, analysis rain Iraq, chances of precipitation in Iraq

INTRODUCTION

Socio-economic relevance of prognostic meteorological data is increasing, particularly in connection with the ongoing climate change. However, to date there is a significant level of uncertainty long-term meteorological forecasts. Study of the conditions of formation, development, destruction and change macro synoptic processes, as is known, underlies long-term weather forecast. Therefore, research in the field of weather forecasting down to the identification of the peculiarities of atmospheric processes in the analysis of data features, to follow up the continuous development of these processes in time and space, to the study of their stability and conditions of the latter.There are a large number of works devoted to this problem[1,2,3,4,5]. Some researchers believe that noted in the General processes tend to preserve the appropriate weather[6,7].

Many studies focuses on the relationship between the anomalies of atmospheric circulation and weather conditions in some areas. A large number of scientists believes that the individual meteorological elements and their changes represent the cyclical nature[8,9,10,11]. A number of works devoted to the study of the fluctuating change in the atmospheric processes. It is assumed in this case that atmospheric processes are the result of superposition of various elementary waves of pressure, which, recover form a complex fluctuations of the pressure systems.Many researchers study different types of atmospheric circulation, and to correlate these types with the change of weather.Long-term weather forecasts are forecasts for a month, a season, several seasons. Forecasts for several years considered over the long-term, and forecasts for tens of years - the projections of modern climate change. Forecasts to 3-10 days in recent times usually referred to the medium-term weather forecasts[12,13,14,15,16].The methodological aspect and content, medium and short-term weather forecasts differ significantly from the long-term. The fact that the actual long-term forecasts are mainly projected deviations from climatic norms of air temperature and precipitation.

The prediction of the moisture regime is a priority in the field of long-term weather forecasts. The occurrence of atmospheric droughts and excessive moisture cause enormous economic damage. The relevance of improvement of methods of long-term precipitation forecast is not in doubt.The aim of this work is the diagnosis of the peculiarities of development of large-scale atmospheric processes associated with the formation of zones of significant precipitation to minimize the effects of possible severe weather. As the study area was the territory of Iraq. The main objective of the research work is to identify predictors which may contribute to the improvement of methods of long-term prediction of precipitation on the territory of Iraq. The selection of potential predictors of the moisture regime was based on modern ideas about the features micrometeorological processes of Iraq.

As potential predictors investigated were the centers of action of atmosphere (CDA): the anticyclone of the Azores, Hawaii and South Indian to improve long-term projections for precipitation in Iraq.

The centers of atmospheric action as a characteristic of the general circulation of the atmosphere

Areas of low or high pressure weather maps are called centers of atmospheric action. CDA are permanent (year-round) and seasonal, that is, expressed only in winter and summer. In the southern hemisphere to the CDA are constant pressure centers over the oceans: South Atlantic (anticyclone of St. Helena), the South Pacific anticyclone, the South Indian [17].

The centers of atmospheric action (CDA) are fixed at the average monthly climatic maps or mean monthly atmospheric pressure fields (Figure 1). Climate action center has a statistical result of the predominance in the area of pressure systems (mainly synoptic centers of action) of the same sign. As CDA characteristics, a maximum or minimum pressure and its location (latitude, longitude).

By the CDA include:

1. Northern Hemisphere
a) Permanent centers of action:
1) Icelandic cyclone (minimum)
2) Azores anticyclone (maximum)
3) North Pacific anticyclone
4) Aleutian depression.
b) Seasonal centers of activity:
5) Mediterranean winter cyclone
6) Asian (Siberian) winter anticyclone
7) North American (Canadian) winter anticyclone
8) South Asian summer cyclone
9) North American summer cyclone.

2. Southern Hemisphere

a) Permanent centers of action:
1) South Atlantic anticyclone
2) South Indian anticyclone
3) The South Pacific anticyclone
4) before the Antarctic zone of low pressure..

b) Seasonal centers of activity:
5) The South American summer (January) cyclone
6) South African summer cyclone
7) Australian summer cyclone
8) New Zealand summer cyclone
9) The South African winter (July)
10) Australian winter anticyclone.

MATERIALS AND METHODS

Effect of CDA on the Iraqi regime of precipitation

Seasonal rainfall forecast typically include evaluation of the global climate system and its implications for the upcoming season. Among the main factors that are taken into account in the development of seasonal forecasts of precipitation, are the sea surface temperature in the tropical part of the Indian, Atlantic and Pacific oceans.Other potential predictors, which are considered in the forecast include:

Centers of atmospheric action;
- Southern Oscillation and El Niño (ENSO);
- The quasi-biennial cycle and the stratospheric circulation
- The index of the Indian Ocean Dipole.

Precipitation atmospheric circulation depends on the moisture content and air supplied from the water surface. In the center of the action of the atmosphere are considered as characteristic of the atmospheric circulation.
An attempt was made to find predictors for long-term forecast of precipitation Iraq. As potential predictors were considered in accordance with the climatic conditions of Iraq are one of the main centers of action of the atmosphere:

• CDA Azores
• Hawaiian CDA
• South Indian CDA

To review data Historical Climatology Network archive Iraq humidification mode used [19] on the monthly precipitation totals at meteorological stations around the globe and according to the Hydrometeorological Service of Iraq.11 stations selected for the territory of Iraq. The list of stations with coordinates given in Table 1.

Observation period used in the study from 1896 to 2010 Location Iraq stations is shown in Figure 2.For the analysis of rainfall regime in Iraq carried out the spatial averaging of rainfall and created base on the Iraqi regime of rainfall data, contained in Annex A.We calculated the main statistical moments monthly totals spatial-averaged precipitation of Iraq:average values, standard deviations and coefficients of variation.:

$$\overline{Q}(m) = \frac{\sum_{y} Q^{C}(y,m)}{N(y)} \qquad (2.1)$$

$$\sigma(m) = \sqrt{\frac{\sum_{y} \left[Q^{C}(y,m) - \overline{Q}(m)\right]^{2}}{N(y)}} \qquad (2.2)$$

$$V(m) = \frac{\sigma(m)}{\overline{Q}(m)} 100 \qquad (2.3)$$

$\overline{Q}$ – the average size, mm;

σ – standard deviation, mm;

m month;

V Coefficient of variation.

RESULTS

According to the calculated climatic characteristics of the precipitation were constructed histograms of mean values, standard deviations and Coefficients of variation for the monthly precipitation totals of Iraq , given in figures 2 - 4.

Figure 2 is the histogram of the average values of the monthly precipitation totals Iraq.From figure 2 it is seen that for Iraq the dry season occurs from June to September. Low (0 mm) was observed in August. The wet season is fixed from October to May with a maximum in January (38 mm).

Figure 3 presents the average spread, which reaches a maximum (18.8mm) in November and minimum (0mm) in August. He, like the average value, also depends on the passage of air masses. In the summer, when over Iraq is a Western migration, standard deviation, minimum, and in winter,during the passage of the Passat – it is the most.

The coefficient of variation of a random variable is a measure of the relative scatter of a random variable; it shows what proportion of the average value of this quantity is its average spread. In contrast to the mean square, or standard deviation, measures not absolute, but a relative measure of the spread of the characteristic values in the statistical population. From the analysis of figure 2.4, it must be concluded that the highest values of the coefficient of variation reaches in August (165%) and the lowest (66%) in December. The highest values of the coefficient of variation reaches in the summer, when the average value and the standard deviation, the minimum, and in winter, at

high average and RMS, it is minimal.Further analysis was conducted annual precipitation Iraq. All the years, participated in the analysis, were assigned to the gradations. Annual precipitation totals were ranked in ascending order and divided into five equally gradations. As a result, following the graduation of Iraq precipitation were obtained for analysis of the impact of the characteristics of the CDA in the northern hemisphere on Iraq rainfall in the wet season (October - May):

B (ZNN) - considerably below the norm
b (LV) - Below normal
N (H) - About standards
(BH) - above the norm
A (ZVN) - significantly higher than the norm

The rest of the gradation monthly sums of precipitation Iraq to the wet season in the Appendix.Intervals gradations monthly sums of precipitation in Iraq for the wet season are summarized in Table 3.

For the 10 driest (from gradation B) and 10 of the wettest years (graduation from a)Calculate the average characteristics of CDA for all months of the wet season.Tables 4-6 we calculate the average CDA property values for all months of the wet season when opposing modes of Iraq precipitation.

If there are significant differences in the values of the characteristics of the CDA in different gradations of precipitation Iraq, this CDA characteristic can be recommended as a predictor of long-term forecast of precipitation Iraq. As a criterion for significant differences CDA values the criterion of similarity on G.YA Vangengeim [17].
Two characteristics CDA (B) and CDA (A) are similar to, if

| CDA (B) - CDA (A) | <ΣTsDA 0.67 (4)
Two characteristics CDA (B) and CDA (A) are different, if
| CDA (B) - CDA (A) | > ΣTsDA 0.67 (5)
σTsDA - the standard deviation of the characteristics of CDA

If the inequality (5), the characteristic of the CDA can be recommended as a predictor of long-term forecast of precipitation Iraq. Differences in characteristics of CDA in different gradations of Iraq rainfall in the wet season are shown in Table 7. In Table 7 are highlighted those features CDA and months, for which the difference between the CDA in different gradations of Iraq precipitation above the standard deviation of CDA and that can be recommended as potential predictors for the long-term forecast of precipitation Iraq.

As follows from the figure 5, the greatest number of predictors is celebrated in November. For long-term forecast of precipitation in November, you can use the characteristics of the Azores CDA, CDA Hawaii and South Indian CDA. As a predictor, you can use the characteristics of the Azores CDA in January and February.

CONCLUSION

The main objective of the study was the identification of predictors of the use of which can contribute to the improvement of methods of long-term forecast of precipitation in Iraq. Research the tasks solved with the following results:
- Database spatially-averaged precipitation characteristics based on theGlobal Historical Climatology Network archive was set up to assess Iraq's moisture regime.

- Are identified and assessed the possibility of use as potential predictors:Azores CDA, CDA Hawaiian and South Indian CDA for the long-term forecast of precipitation in Iraq. For long-term forecast of precipitation in November, can be used as a predictor of the Azores CDA, CDA Hawaiian and South Indian CDA. And also as a predictor, you can use the characteristics of the Azores CDA in January and February.

REFERENCES

1. Budyko, M. I. Climate and life. Leningrad: Gidrometeoizdat, 1971.- 470
2. Vorob'ev V. I. SYNOPTIC meteorology, Leningrad: Gidrometeoizdat, S.1991,616
3. Volcanoes, stratospheric aerosol and earth's climate. / Under the editorship of S. S. Khmelevtsov.- L.: Gidrometeoizdat, 1986.- 256 p.
4. Drozdov, O. A. and others Climatology, Leningrad: Gidrometeoizdat,1989,- p. 568
5. Matveev L. T. Rate of the General meteorology. Physics of atmosphere,Leningrad: Gidrometeoizdat, 1984.- 751 S.
6. Vinnikov, K. Y. climate Sensitivity - L.: Gidrometeoizdat, 1986.-220s.
7. John. Gribbin climate Change / TRANS. from English. under the editorship of E. K. Buettner and B. A. Zubakov, Leningrad:Gidrometeoizdat, 1980.- 359 p.
8. Budyko, M. I. Climate in the past and the future.- Leningrad:Gidrometeoizdat, 1980.-350C.
9. Girs, A. A., macro-circulation method of long-term meteorological forecasts.- Leningrad: Gidrometeoizdat, 1974.- 486 p.
10. Matveev L. T., the Theory of General atmosphere circulation and Earth's climate, Leningrad: Gidrometeoizdat, 1991, 296 p
11. Monitoring of General circulation of the atmosphere // Proceedings of hydrometcentre of the USSR-1989.-Vol. 322
12. Bagrov N. A., K. V. Kondratovich, PED, D. A., Ugryumov A. I. Longrange weather forecasts, Leningrad: Gidrometeoizdat, 1985,- 248 p.13.
13. Girs, A. A. Fundamentals of long-term weather forecasts, Leningrad:Gidrometeoizdat, 1960.-560 p.
14. Girs A. A. Kondratovich, K. V., Methods for long-term weather forecasts, Leningrad: Gidrometeoizdat, 1977,- p. 35328
15. The Zadok V. P., Vilfand R. M., New results in the development of statistical methods long-term weather forecasts and technology issue , 70 years to the Hydrometcenter of Russia,-1999,- p. 134 140
16. Chichasov, G. N. Technology long-term weather forecasts.- S-Pb.:Gidrometeoizdat, 1991,- 304 p.
17. S. P. Khromov , the basics of SYNOPTIC meteorology , Leningrad,Gidrometeoizdat, 1948, p. 695
18. The location of the centers of action of atmosphere [Electronic resource] http:// dic.academic.ru/ dic.nsf/bse/ 148750/Центры
19. Global Historical Climatology Network (abbr.: GHCN). Internet address: http://www.scd.ucar.edu/ dss/catalogs/ free.html.

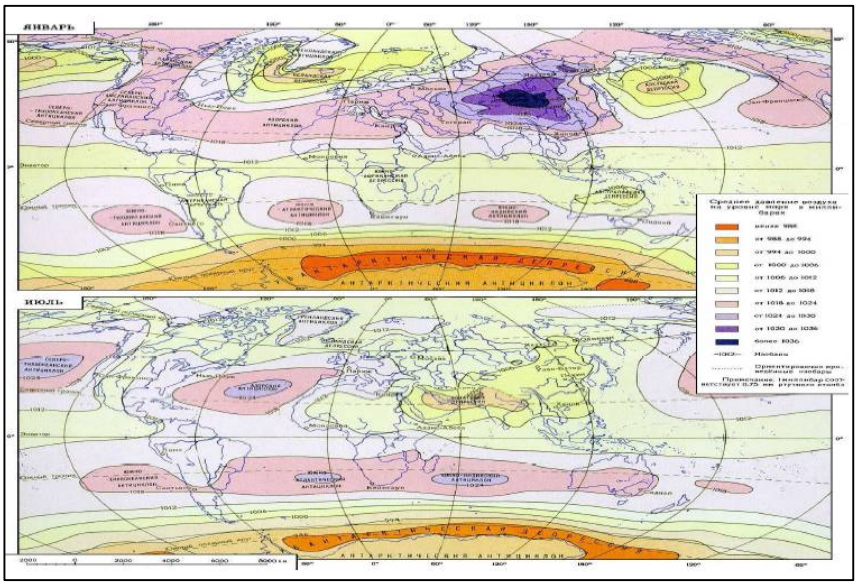

Figure.1 centers of atmospheric action

Table 1 - The meteorological station in Iraq

№	code station	station name	ϕ	λ
1	20940608000	MOSUL	36.30	43.20
2	20940621000	KIRKUK	35.50	44.40
3	20940637000	KHANAQIN IRAQ	34.30	45.40
4	20940642000	RUTBAH	33.00	40.30
5	20940650000	BAGHDAD	33.30	44.40
6	20940650002	HABBANIYA IRAQ	33.40	43.60
7	20940665000	KUT-EL-HAI	32.20	46.10
8	20940670000	NAJAF	32.00	44.30
9	20940672000	DIWANIYA	32.00	45.00
10	20940676000	NASIRIYA	31.00	46.20
11	20940689000	BASRAH	30.40	47.70

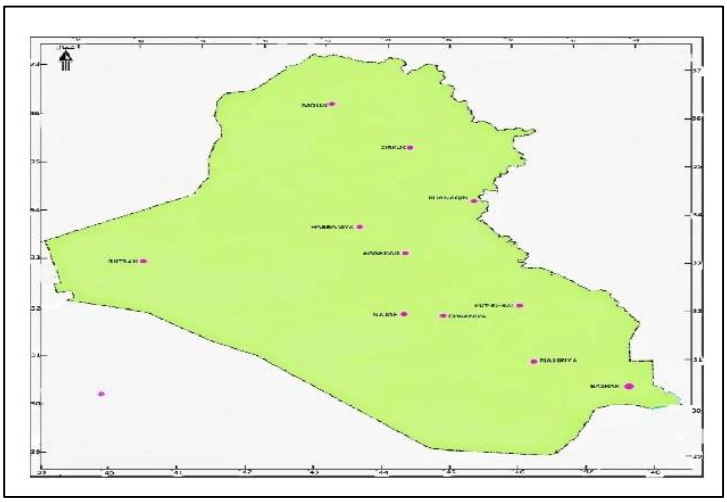

Figure 2. - The coordinates of the Iraq

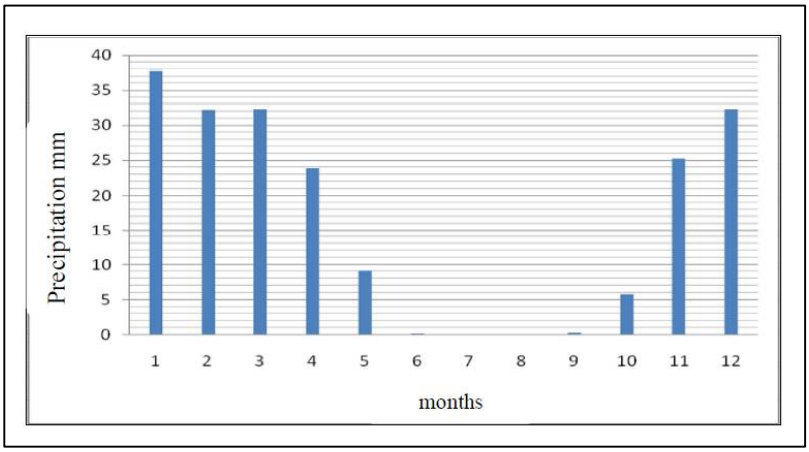

Figure 3. The histogram of the average values of the monthly precipitation totals Iraq

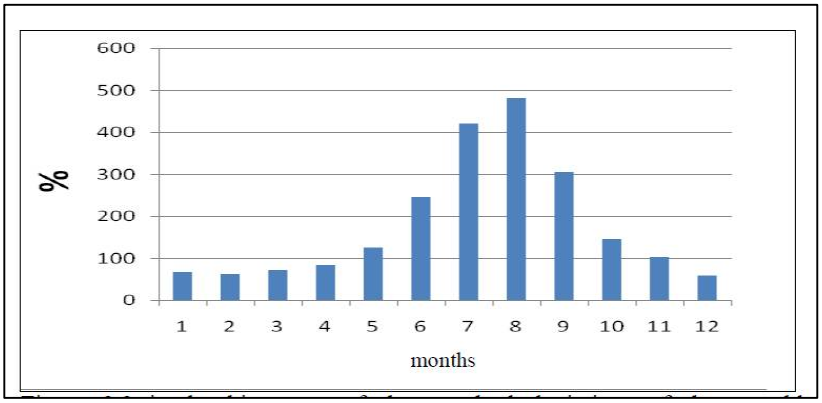

Figure 4. The histogram of the standard deviations of the monthly precipitation totals in Iraq

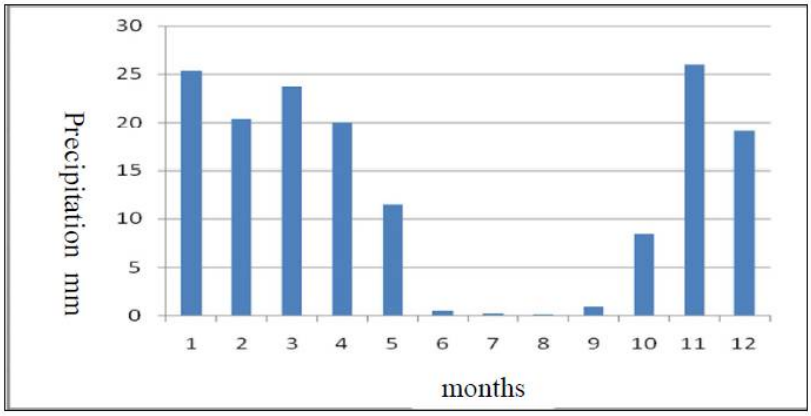

Figure 5. Histogram of coefficients of variation of the monthly precipitation totals in Iraq

Table 2. For January given gradation in Iraq precipitation

Years	B	Years	b	Years	N	Years	a	Years	A
1909	2	1925	14	1907	29	1947	41	1975	57
1920	2	1952	14	2007	29	1977	41	1926	58
2009	4	1963	14	1951	30	2003	41	2000	58
1902	5	1929	15	1990	30	1944	42	1994	59
1899	7	1942	17	1949	31	1991	43	1992	60
1987	7	1954	17	1957	31	1997	43	1970	61
1927	8	1903	18	2001	31	1999	44	1911	62
1964	8	1931	18	2008	31	1972	45	1945	62
1971	8	1897	19	1898	32	1913	47	1969	65
1978	8	1943	20	1950	32	1979	47	1965	73
1935	10	1936	21	1955	33	1985	48	1988	73
1900	11	1984	21	1960	33	2005	48	1933	75
1922	11	1956	22	1910	34	1934	50	1998	75
1941	11	1967	22	1983	34	1939	50	1919	83
1905	12	1906	23	1908	35	1981	51	1982	83
1948	12	1918	23	1914	35	2006	51	1940	87
1959	12	1995	24	1976	35	1974	55	2004	88
1968	12	1904	25	1921	37	1958	56	1923	89
1980	13	1966	25	1932	37	1993	56	1924	93
1989	13	1912	26	1928	38	2002	56	1996	98
2010	13	1953	26	1937	38	1930	57	1938	111
1901	14	1986	27			1946	57	1896	121

Table 3 -Intervals gradations monthly totals of Iraqi rainfall (in mm) for the wet season

Month	Graduation				
	B	в	N	a	A
October	1-2	2-4	4-7	8-13	13-43
November	1-6	6-13	13-21	26-48	49-141
December	3-14	16-25	26-34	34-49	49-83
January	2-14	14-27	29-38	41-57	57-121
February	3-13	13-25	25-38	38-49	51-109
March	1-14	14-21	21-30	30-51	52-108
April	1-7	7-15	16-25	25-42	43-90
May	1-2	3-4	4-8	8-16	18-63

Table.4 - Average values of the characteristics of the Azores CDA at different levels of precipitation Iraq.

1.January

Dry years		p	ϕ	λ	Wet years		p	ϕ	Λ
gradation(B) precipitation of Iraq					gradation(A) precipitation of Iraq				
Years	The amount of precipitation				Years	The amount of precipitation			
1909	2	1025.9	40	-20	1998	75	1022.7	30	-50
1920	2	1030.1	35	-25	1919	83	1025	30	-25
2009	4	1028	30	-35	1982	83	1022.5	30	-20
1902	5	1026.4	45	0	1940	87	1020.8	25	-35
1899	7	1026.3	30	-50	2004	88	1024.6	35	-20
1987	7	1022.6	50	0	1923	89	1031.5	40	-20
1927	8	1030.4	35	-30	1924	93	1025.7	30	-50
1964	8	1031.1	50	5	1996	98	1021.4	30	-55
1971	8	1025.1	25	-30	1938	111	1028.5	35	-25
1978	8	1030.2	40	-30	1896	121	1028.4	50	0
		1027.61	38	-21.5			1025.11	33.5	-30

2.February

Dry years gradation(B) precipitation of Iraq		p	ϕ	λ	Dry years gradation(A) precipitation of Iraq		p	ϕ	Λ
Years	The amount of precipitation				Years	The amount of precipitation			
1921	3	1025.4	50	0	1897	59	1027.5	40	-10
1944	3	1024.3	45	-20	1974	62	1025	35	-25
1899	4	1026.1	25	-45	1923	70	1025.7	30	-20
1904	4	1027.1	30	-30	1995	70	1027.7	30	-25
1958	4	1021.5	35	0	2006	71	1022.8	30	-35
1905	7	1030.5	40	-20	1986	72	1021.9	30	-30
2009	7	1024.8	30	-40	1992	73	1027.4	45	0
1896	8	1027.6	50	0	1980	74	1024.2	35	-25
1906	8	1028.5	40	-30	1926	93	1023.8	30	-30
1965	8	1030.6	50	-10	2003	109	1026.4	30	-35
		1026.64	39.5	-19.5			1025.24	33.5	-23.5

3.March

Dry years gradation(B) precipitation of Iraq		p	ϕ	λ	Wet years gradation(A) precipitation of Iraq		p	ϕ	Λ
Years	The amount of precipitation				Years	The amount of precipitation			
1975	1	1022.8	30	-25	1954	73	1025.2	30	-35
1921	2	1027.9	35	-35	1957	73	1018.8	25	-30
1930	2	1021.1	25	-40	1972	76	1023.2	30	-30
1919	3	1024.9	35	-25	1996	78	1021.9	30	-50
1935	4	1022.8	30	-30	1949	80	1024.6	45	-25
1937	4	1024.1	30	-30	1946	85	1027	25	-40
2004	4	1025.8	35	-35	1943	90	1025.4	30	-40
1927	5	1026.8	30	-30	1896	93	1025.8	35	-30
2006	6	1021.2	25	-35	1907	106	1029.4	40	-20
1901	7	1022.3	25	-45	1974	108	1025.2	30	-35
		1023.97	30	-33			1024.65	32	-33.5

4.**April**

Dry years		p	ϕ	λ	Wet years		p	ϕ	Λ
gradation(B) precipitation of Iraq					gradation(A) precipitation of Iraq				
Years	The amount of precipitation				Years	The amount of precipitation			
1922	1	1025.3	30	-30	1931	56	1023	40	-30
1947	1	1026.8	35	-25	2002	57	1026.1	35	-35
1912	2	1025.6	35	-25	1939	60	1025	30	-50
1920	2	1021.4	25	-50	1907	61	1026.1	30	-30
1958	2	1024.5	35	-30	1918	69	1022.4	30	-35
1979	2	1023.1	45	-20	1957	69	1024.9	35	-30
1913	3	1027.4	35	-35	1971	75	1022.5	30	-35
1905	4	1023.1	25	-40	1968	76	1021.4	30	-30
1928	4	1023.9	30	-40	1919	81	1024.1	35	-30
1967	4	1026.3	50	-20	1993	90	1024.7	35	-30
		1024.74	34.5	-31.5			1024.02	33	-33.5

5.May

Dry years		p	ϕ	λ	Wet years		p	ϕ	Λ
gradation(B) precipitation of Iraq					gradation(A) precipitation of Iraq				
Years	The amount of precipitation				Years	The amount of precipitation			
1896	1	1027	50	-20	1982	27	1024.7	35	-30
1899	1	1023.7	25	-35	1934	28	1024.9	35	-40
1905	1	1025.6	35	-30	1936	30	1025.3	40	-35
1906	1	1022.8	30	-40	1919	31	1024	25	-45
1930	1	1025.9	35	-30	1950	34	1023	30	-40
1940	1	1023.4	30	-45	1921	35	1028.3	35	-35
1954	1	1020.7	35	-20	1959	36	1023.6	30	-35
1991	1	1030.8	50	-20	1993	45	1022	30	-45
1999	1	1021.7	40	-50	1957	50	1024.3	35	-30
2008	1	1021.8	30	-35	1963	63	1029.9	40	-30
		1024.34	36	-32.5			1025	33.5	-36.5

6.October

Dry years		p	ϕ	λ	Wet years		p	ϕ	Λ
gradation(B) precipitation of Iraq					gradation(A) precipitation of Iraq				
Years	The amount of precipitation				Years	The amount of precipitation			
1900	1	1022.5	30	-30	1925	21	1020.4	30	-30
1918	1	1025	35	-30	1966	21	1017.9	30	-45
1926	1	1019.3	30	-40	1994	24	1020.4	30	-30
1927	1	1018.7	50	5	1993	25	1020	35	-50
1934	1	1021.7	35	-30	1997	25	1018.1	50	5
1941	1	1023.5	45	-5	2008	26	1026	35	-30
1946	1	1020.2	25	-35	1991	27	1021.9	45	-50
1947	1	1021.7	50	5	1982	31	1022.6	35	-20
1950	1	1022.2	40	-30	1937	35	1022.9	40	-40
1962	1	1021.9	35	-40	1987	43	1025.9	40	-45
		1021.67	37.5	-23			1021.61	37	-33.5

7.November

Dry years		p	ϕ	λ	Wet years		p	ϕ	Λ
gradation(B) precipitation of Iraq					gradation(A) precipitation of Iraq				
Years	The amount of precipitation				Years	The amount of precipitation			
1901	1	1023.2	50	0	1989	65	1022.1	35	-40
1904	1	1023	45	-15	1997	66	1020.6	30	-30
1905	1	1027.1	30	-35	1935	70	1025.3	35	-35
1912	1	1026	40	-20	1992	71	1027.1	35	-20
1922	1	1025	45	-10	1928	77	1025.4	35	-25
1943	1	1027.4	40	-25	1967	77	1026.4	45	-25
1966	1	1028.2	45	-30	1921	80	1024.3	30	-50
1978	1	1027.9	45	0	1994	94	1022.3	35	0
2010	1	1018.7	40	-25	1984	96	1022.8	30	-35
1917	2	1026.7	40	-20	1926	141	1027.3	35	-30
		1025.32	42	-18			1024.36	34.5	-29

8. December

Dry years		p	ϕ	λ	Wet years		p	ϕ	Λ
gradation(B) precipitation of Iraq					gradation(A) precipitation of Iraq				
Years	The amount of precipitation				Years	The amount of precipitation			
1937	3	1022.2	35	-25	1997	66	1022.1	30	-25
1907	4	1026.8	30	-35	1954	67	1025.8	35	-30
1998	4	1025.4	30	-40	1988	68	1029.7	45	-5
1896	5	1026.4	30	-30	1992	70	1024.4	35	-30
1901	5	1023.3	35	-25	2003	72	1021.7	35	-15
1903	5	1028.3	30	-35	1938	75	1025.7	30	-30
1928	5	1025.4	40	-25	2000	77	1022.5	30	-45
1976	5	1023.5	30	-35	1991	78	1029.5	50	5
1905	6	1026.9	50	5	1987	80	1021.8	25	-30
1965	6	1025.7	35	-25	1949	83	1024.5	35	-40
		1025.39	34.5	-27			1024.77	35	-24.5

Table 5 - Average values of the South Indian CDA performance at different levels of precipitation Iraq - 1.January

Dry years		p	ϕ	λ	Wet years		p	ϕ	Λ
gradation(B) precipitation of Iraq					gradation(A) precipitation of Iraq				
Years	The amount of precipitation				Years	The amount of precipitation			
1909	2	1024	38	60	1933	75	1020.27	36	84
1920	2	1021.25	42	64	1998	75	1029.9	44	86
1902	5	1024.4	32	84	1919	83	1014	24	48
1987	7	1027.5	38	82	1982	83	1028.6	38	74
1927	8	1028.9	40	90	1940	87	1012.3	26	48
1964	8	1025.7	36	58	2004	88	1026.57	32	92
1971	8	1026.5	42	60	1923	89	1023.3	28	88
1978	8	1032.15	38	82	1924	93	1021.5	42	48
1935	10	1020.95	28	82	1996	98	1025.9	32	94
1900	11	1028	38	82	1938	111	1027.1	36	84
		1025.935	37.2	74.4			1022.944	33.8	74.6

2.February

Dry years gradation(B) precipitation of Iraq		p	ϕ	λ	Dry years gradation(A) precipitation of Iraq		p	ϕ	Λ
Years	The amount of precipitation				Years	The amount of precipitation			
1921	3	1024.33	30	66	1990	56	1038.6	40	52
1944	3	1013	28	50	1940	57	1016.9	26	50
1904	4	1018.9	44	70	1974	62	1036.7	42	92
1958	4	1034.3	42	70	1923	70	1030.2	42	64
1905	7	1027.5	46	92	1995	70	1026.6	38	66
1906	8	1024.97	42	52	1986	72	1031	32	86
1965	8	1025.55	34	68	1992	73	1029	42	70
1902	10	1032.5	36	86	1980	74	1033.4	42	62
1968	10	1030.2	38	88	1926	93	1027.1	30	84
1984	10	1038.3	44	62	2003	109	1027.87	38	80
		1026.955	38.4	70.4			1029.737	37.2	70.6

3.March

Dry years gradation(B) precipitation of Iraq		p	ϕ	λ	Wet years gradation(A) precipitation of Iraq		p	ϕ	Λ
Years	The amount of precipitation				Years	The amount of precipitation			
1975	1	1034.6	44	94	1981	69	1035.4	34	80
1921	2	1029.5	36	60	1954	73	1034.6	42	72
1930	2	1023.7	26	64	1957	73	1027.55	38	92
1919	3	1022.1	28	48	1972	76	1033	40	68
1935	4	1031.5	38	76	1996	78	1030	40	46
1937	4	1027.9	40	80	1949	80	1032.5	34	78
2004	4	1030.3	44	78	1946	85	1020.1	24	96
1927	5	1027.95	44	44	1943	90	1025.45	36	54
1901	7	1032.2	46	82	1907	106	1028.35	36	92
1909	7	1027.3	38	78	1974	108	1033	36	78
		1028.705	38.4	70.4			1029.995	36	75.6

4.April

Dry years		p	ϕ	λ	Wet years		p	ϕ	Λ
gradation(B) precipitation of Iraq					gradation(A) precipitation of Iraq				
Years	The amount of precipitation				Years	The amount of precipitation			
1922	1	1030.45	40	94	1931	56	1029.8	42	58
1947	1	1027.6	32	64	2002	57	1032.6	40	48
1912	2	1015	44	44	1939	60	1027.05	30	68
1920	2	1019.6	24	50	1907	61	1025	26	94
1958	2	1032.4	36	90	1918	69	1018.5	26	50
1979	2	1029.5	36	70	1957	69	1033.4	34	76
1913	3	1027.7	42	58	1971	75	1033.6	44	80
1905	4	1025	40	44	1968	76	1029.62	38	94
1928	4	1029.4	32	56	1919	81	1021.35	26	54
1967	4	1029.4	38	52	1993	90	1034	44	62
		1026.605	36.4	62.2			1028.492	35	68.4

6.May

Dry years		p	ϕ	λ	Wet years		p	ϕ	Λ
gradation(B) precipitation of Iraq					gradation(A) precipitation of Iraq				
Years	The amount of precipitation				Years	The amount of precipitation			
1905	1	1027.9	44	66	1982	27	1034	36	94
1906	1	1029.5	44	46	1934	28	1029.4	38	54
1930	1	1034.25	40	92	1936	30	1034.8	46	70
1940	1	1032.65	34	74	1919	31	1031.85	32	44
1954	1	1037.3	42	58	1950	34	1030.53	38	52
1991	1	1030	38	76	1921	35	1030	30	84
1999	1	1032.1	36	70	1959	36	1025.1	30	92
1913	2	1024.4	38	96	1993	45	1030.5	40	58
1920	2	1020.27	26	48	1957	50	1029	42	48
1922	2	1036.2	46	60	1963	63	1029.05	32	56
		1030.457	38.8	68.6			1030.423	36.4	65.2

7.October

Dry years		p	ϕ	λ	Wet years		p	ϕ	Λ
gradation(B) precipitation of Iraq					gradation(A) precipitation of Iraq				
Years	The amount of precipitation				Years	The amount of precipitation			
1900	1	1029	38	58	1992	15	1036.4	38	96
1918	1	1026	26	54	1925	21	1028.3	44	78
1926	1	1025.6	46	44	1966	21	1029.7	36	62
1927	1	1034.3	38	84	1994	24	1034.8	34	46
1934	1	1030.55	38	50	1993	25	1032.5	36	58
1941	1	1026.15	30	60	1997	25	1037	32	62
1946	1	1030.8	34	54	1991	27	1033.8	46	60
1947	1	1035.8	38	60	1982	31	1033.25	44	58
1950	1	1031.6	40	62	1937	35	1035.2	36	66
1962	1	1045.4	42	80	1987	43	1030.6	34	68
		1031.52	37	60.6			1033.155	38	65.4

9.November

Dry years		p	ϕ	λ	Wet years		p	ϕ	Λ
gradation(B) precipitation of Iraq					gradation(A) precipitation of Iraq				
Years	The amount of precipitation				Years	The amount of precipitation			
1901	1	1023.3	38	56	1989	65	1031	26	94
1904	1	1027.9	42	60	1997	66	1035.53	46	54
1905	1	1022.25	44	56	1935	70	1030.8	40	58
1912	1	1022	24	50	1992	71	1038.1	34	94
1922	1	1030.95	46	68	1928	77	1026.1	28	96
1943	1	1021	30	44	1967	77	1025.4	30	72
1966	1	1027.3	42	60	1921	80	1030.85	38	90
1978	1	1030	40	88	1994	94	1029.3	34	56
1917	2	1023	26	50	1984	96	1030.34	34	56
1933	2	1035.47	40	94	1926	141	1034.3	38	96
		1026.317	37.2	62.6			1031.172	34.8	76.6

10.December

Dry years		p	ϕ	λ	Wet years		p	ϕ	Λ
gradation(B) precipitation of Iraq					gradation(A) precipitation of Iraq				
Years	The amount of precipitation				Years	The amount of precipitation			
1937	3	1025.6	32	84	1997	66	1025.9	40	52
1907	4	1033.5	44	54	1954	67	1029.3	34	82
1998	4	1029.6	40	88	1988	68	1030	34	84
1901	5	1027.28	44	78	1992	70	1027.47	32	84
1903	5	1031.8	44	46	2003	72	1030.7	42	62
1928	5	1027.55	32	76	1938	75	1026.1	38	68
1976	5	1023.65	34	90	2000	77	1031.9	36	78
1905	6	1029.6	42	82	1991	78	1024.6	36	96
1965	6	1024.8	40	92	1987	80	1027	34	78
1932	9	1026.3	36	78	1949	83	1026.7	34	94
		1027.968	38.8	76.8			1027.967	36	77.8

Table 6 - Average values of the characteristics of the Hawaiian CDA at different levels of precipitation Iraq- 1.January

Dry years		p	ϕ	λ	Wet years		p	ϕ	Λ
gradation(B) precipitation of Iraq					gradation(A) precipitation of Iraq				
Years	The amount of precipitation				Years	The amount of precipitation			
1909	2	1019.2	25	230	1933	75	1028.9	35	215
1920	2	1026.3	45	245	1998	75	1018.6	25	230
2009	4	1026.9	45	245	1919	83	1027.2	40	250
1902	5	1025.7	30	225	1982	83	1023.4	35	225
1899	7	1026.8	30	225	1940	87	1026.1	45	255
1987	7	1023.8	45	245	2004	88	1024.2	40	245
1927	8	1024	45	255	1923	89	1025.2	35	215
1964	8	1026	30	220	1924	93	1026.4	45	245
1971	8	1025.2	35	225	1996	98	1021.4	30	230
1978	8	1025.1	45	255	1938	111	1023.1	45	245
		1024.9	37.5	237			1024.45	37.5	235.5

2.February

Dry years gradation(B) precipitation of Iraq		p	ϕ	λ	Dry years gradation(A) precipitation of Iraq		p	ϕ	Λ
Years	The amount of precipitation				Years	The amount of precipitation			
1921	3	1023.5	30	225	1940	57	1018.6	45	255
1944	3	1026.2	35	220	1974	62	1025	35	225
1899	4	1029.2	35	225	1923	70	1027.9	45	250
1904	4	1023.2	45	195	1995	70	1022.1	45	250
1958	4	1019.4	25	235	2006	71	1024.8	45	245
1905	7	1025.2	45	255	1986	72	1018.7	30	235
2009	7	1028.1	40	200	1992	73	1019.2	40	250
1906	8	1021.9	45	250	1980	74	1019.3	45	255
1965	8	1023.3	40	225	1926	93	1021.8	30	230
1902	10	1021.4	25	235	2003	109	1021.2	40	225
		1024.14	36.5	226.5			1021.86	40	242

3.March

Dry years gradation(B) precipitation of Iraq		p	ϕ	λ	Wet years gradation(A) precipitation of Iraq		p	ϕ	Λ
Years	The amount of precipitation				Years	The amount of precipitation			
1975	1	1025.1	35	210	1981	69	1022.7	30	210
1921	2	1023.6	25	230	1954	73	1025	45	215
1930	2	1024	35	215	1957	73	1021.7	30	225
1919	3	1023.3	30	225	1972	76	1022.2	35	230
1935	4	1023.2	35	220	1996	78	1020	45	255
1937	4	1023.3	35	195	1949	80	1023.1	30	200
2004	4	1024.6	30	190	1946	85	1029.5	35	210
1927	5	1028.3	30	220	1943	90	1021.5	40	205
2006	6	1024.8	40	200	1907	106	1028.1	40	205
1901	7	1027.1	30	220	1974	108	1020.5	25	230
		1024.73	32.5	212.5			1023.43	35.5	218.5

4.April

Dry years		p	ϕ	λ	Wet years		p	ϕ	Λ
gradation(B) precipitation of Iraq					gradation(A) precipitation of Iraq				
Years	The amount of precipitation				Years	The amount of precipitation			
1922	1	1030.6	35	220	1931	56	1023.2	35	185
1947	1	1025.7	35	225	2002	57	1024.3	35	220
1912	2	1026.9	30	215	1939	60	1025.3	35	190
1920	2	1025.2	35	220	1907	61	1023.6	30	210
1958	2	1024.2	30	220	1918	69	1023.8	35	185
1979	2	1024.4	40	210	1957	69	1026.1	35	195
1913	3	1026.3	30	210	1971	75	1026	35	200
1905	4	1022.2	30	215	1968	76	1029.2	35	220
1928	4	1023.8	30	220	1919	81	1023	30	220
1967	4	1031.6	40	210	1993	90	1024.4	30	220
		1026.09	33.5	216.5			1024.89	33.5	204.5

5.May

Dry years		p	ϕ	λ	Wet years		p	ϕ	Λ
gradation(B) precipitation of Iraq					gradation(A) precipitation of Iraq				
Years	The amount of precipitation				Years	The amount of precipitation			
1899	1	1028.7	35	215	1982	27	1027.6	40	220
1905	1	1026.7	35	215	1934	28	1021.8	30	210
1906	1	1024.6	30	220	1936	30	1024.3	35	205
1930	1	1026.5	35	215	1919	31	1022.8	35	220
1940	1	1023.4	35	190	1950	34	1028.2	35	220
1954	1	1024.3	35	185	1921	35	1023.8	35	225
1991	1	1026.6	35	220	1959	36	1025.7	35	220
1999	1	1027.2	35	220	1993	45	1022.1	30	195
2008	1	1024.3	35	220	1957	50	1020.7	30	220
2009	1	1021.2	35	225	1963	63	1026	35	195
		1025.35	34.5	212.5			1024.3	34	213

6.October

Dry years		p	ϕ	λ	Wet years		p	ϕ	Λ
gradation(B) precipitation of Iraq					gradation(A) precipitation of Iraq				
Years	The amount of precipitation				Years	The amount of precipitation			
1900	1	1023	30	220	1925	21	1021.6	35	220
1918	1	1023.2	30	220	1966	21	1022.7	35	225
1926	1	1019.6	30	175	1994	24	1021.9	35	220
1927	1	1022.5	30	215	1993	25	1021.7	35	175
1934	1	1022.8	35	185	1997	25	1022.9	35	225
1941	1	1023	35	215	2008	26	1023.8	35	185
1946	1	1026.2	40	215	1991	27	1023	40	220
1947	1	1022	35	190	1982	31	1021.7	40	195
1950	1	1021.3	30	195	1937	35	1019.6	25	170
1962	1	1020.9	30	175	1987	43	1021.8	35	210
		1022.45	32.5	200.5			1022.07	35	204.5

7.November

Dry years		p	ϕ	λ	Wet years		p	ϕ	Λ
gradation(B) precipitation of Iraq					gradation(A) precipitation of Iraq				
Years	The amount of precipitation				Years	The amount of precipitation			
1901	1	1023.9	40	250	1989	65	1024.2	35	175
1904	1	1023.5	40	250	1997	66	1024	35	185
1905	1	1024.5	30	220	1935	70	1023.8	45	245
1912	1	1023.6	30	220	1992	71	1023.3	45	245
1922	1	1023.6	45	245	1928	77	1022.4	45	250
1943	1	1024.7	45	245	1967	77	1025.1	35	205
1966	1	1022.3	45	195	1921	80	1021.8	30	230
1978	1	1024.8	35	220	1994	94	1028.3	35	215
2010	1	1025.5	35	220	1984	96	1022.5	30	210
1917	2	1024.8	45	245	1926	141	1019.7	25	195
		1024.12	39	231			1023.51	36	215.5

8.December

Dry years		p	ϕ	λ	Wet years		p	Φ	Λ
gradation(B) precipitation of Iraq					gradation(A) precipitation of Iraq				
Years	The amount of precipitation				Years	The amount of precipitation			
1937	3	1021	40	255	1997	66	1024.5	40	245
1907	4	1023	25	230	1954	67	1026.2	40	250
1998	4	1028.5	35	225	1988	68	1025.7	35	225
1901	5	1025.8	40	245	1992	70	1025.7	35	220
1903	5	1028	45	245	2003	72	1021.8	40	250
1928	5	1025.4	40	250	1938	75	1024.9	35	220
1976	5	1024.4	40	245	2000	77	1025.3	45	245
1905	6	1026.1	45	245	1991	78	1023.8	40	250
1965	6	1024.4	35	205	1987	80	1023.1	30	220
2008	6	1025.2	35	220	1949	83	1025.5	35	220
		1025.18	38	236.5			1024.65	37.5	234.5

Table 7. Differences in characteristics of CDA in different gradations of Iraq rainfall in the wet season

Month	The Azores			Hawaiian			South Indian		
	p	ϕ	λ	p	ϕ	λ	p	Φ	Λ
October	0.06	0.5	10.5	0.38	-2.5	-4	-1.63	-1	-4.5
November	0.96	7.5	11	0.61	3	15.5	-4.85	2.4	-14
December	0.62	-0.5	-2.5	0.53	0.5	2	0	2.8	-1
January	2.5	4.5	8.5	0.45	0	1.5	2.99	3.4	-0.2
February	1.4	6	4	2.28	-3.5	-15.5	-2.78	1.2	-0.2
March	-8.68	-2	0.5	1.3	-3	-6	-1.29	2.4	-5.2
April	0.72	1.5	2	1.2	0	12	1.88	1.4	-6.2
May	-0.66	2.5	4	1.05	0.5	-0.5	0.03	2.4	3.4

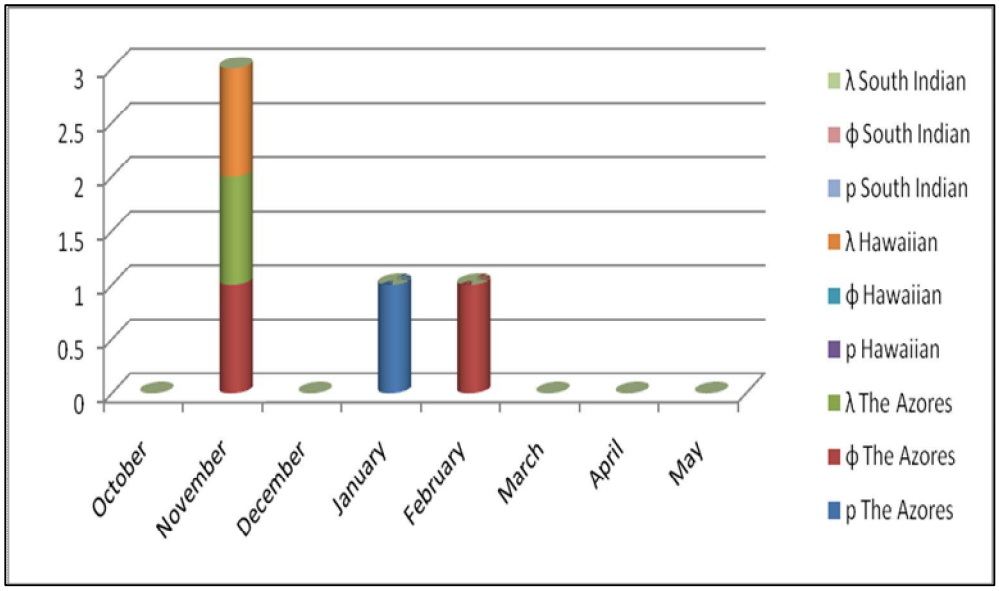

Figure .5 - The number of predictors characteristic CDA for long term precipitation forecast Iraq .

Appendix A Spatially averaged amount of precipitation Iraq

Table A.1 - Spatially averaged amount of precipitation Iraq

Years	January	February	March	April	May	June	July	August	September	October	November	December
1896	121	8	93	12	1	0	0	0	0	0	3	5
1897	19	59	17	11	7	0	0	0	0	0	19	37
1898	32	31	30	8	13	0	0	0	0	0	18	29
1899	7	4	14	9	1	0	0	0	0	3	27	30
1900	11	30	26	0	0	1	0	0	0	1	43	36
1901	14	0	7	6	4	0	0	0	1	0	1	5
1902	5	10	45	48	0	0	0	0	0	12	52	12
1903	18	26	12	11	0	0	0	0	0	0	5	5
1904	25	4	21	20	25	0	0	0	0	13	1	30
1905	12	7	51	4	1	0	0	0	1	0	1	6
1906	23	8	10	14	1	0	0	0	0	0	44	19
1907	29	24	106	61	20	0	0	0	0	7	4	4

1908	35	16	17	6	3	0	0	0	0	0	0	12
1909	2	18	7	8	4	0	0	0	0	6	6	20
1910	34	13	37	6	5	0	0	0	0	0	20	25
1911	62	15	60	24	5	0	0	0	0	0	18	37
1912	26	13	19	2	0	0	0	0	0	4	1	31
1913	47	24	14	3	2	0	0	0	0	0	17	27
1914	35	48	19	53	4	0	0	0	0	0	0	0
1915	0	0	0	0	0	0	0	0	0	0	0	0
1916	0	0	0	0	0	0	0	0	0	0	0	0
1917	0	0	0	0	0	0	0	0	0	0	2	46
1918	23	37	22	69	5	0	0	0	0	1	62	34
1919	83	29	3	81	31	0	0	0	0	0	0	30
1920	2	38	66	2	2	0	0	0	4	9	10	52
1921	37	3	2	6	35	0	0	0	0	0	80	28
1922	11	26	26	1	2	0	0	0	0	0	1	36
1923	89	70	19	19	3	0	0	0	0	5	3	25

Table A.1

1924	93	40	25	6	7	1	0	0	0	12	10	46
1925	14	22	29	15	4	0	0	0	0	21	17	25
1926	58	93	49	18	5	0	0	0	0	1	141	49
1927	8	40	5	32	23	0	0	0	0	1	33	22
1928	38	52	11	4	0	0	0	0	0	0	77	5
1929	15	38	7	16	4	0	0	0	0	2	44	34
1930	57	38	2	31	1	1	0	0	1	0	9	36
1931	18	42	9	56	24	0	0	0	0	2	13	13
1932	37	24	16	6	4	0	0	0	0	0	6	9
1933	75	43	33	22	0	0	0	0	0	0	2	14
1934	50	33	17	19	28	0	0	0	0	1	2	44
1935	10	20	4	20	8	0	0	0	0	6	70	53
1936	21	35	14	27	30	0	0	0	0	0	28	53
1937	38	13	4	29	8	0	0	0	0	35	64	3
1938	111	42	33	13	9	0	2	0	0	0	51	75
1939	50	55	54	60	2	0	0	0	0	4	34	58
1940	87	57	22	26	1	0	0	0	0	11	33	25
1941	11	51	35	34	0	0	0	0	0	1	4	49
1942	17	25	26	10	0	0	0	0	0	8	28	26
1943	20	44	90	23	2	0	0	0	0	6	1	21

1944	42	3	29	15	10	0	0	0	0	0	54	27
1945	62	13	13	5	14	0	1	0	0	2	48	42
1946	57	39	85	48	15	0	0	0	0	1	18	34
1947	41	23	36	1	16	0	0	0	0	1	32	19
1948	12	25	18	35	4	0	0	0	0	0	2	52
1949	31	40	80	21	7	0	0	0	0	0	0	83
1950	32	32	28	13	34	0	0	0	0	1	19	21
1951	30	51	38	7	5	0	0	0	1	4	15	40
1952	14	39	20	19	3	0	0	0	0	0	12	44
1953	26	52	49	38	3	0	0	0	0	6	31	27
1954	17	49	73	43	1	0	0	0	0	4	50	67
1955	33	12	27	28	13	0	0	0	0	0	16	50
1956	22	19	21	46	0	0	0	0	0	0	3	42
1957	31	37	73	69	50	2	0	0	2	3	53	22
1958	56	4	12	2	2	0	0	0	0	0	26	40
1959	12	23	37	25	36	1	0	0	0	5	16	12
1960	33	12	29	15	2	0	1	0	0	0	48	12

Table A.1

1961	0	0	0	0	0	0	0	0	0	0	0	0
1962	0	0	0	0	0	0	0	0	0	1	19	28
1963	14	39	17	52	63	0	0	0	0	10	9	38
1964	8	39	17	9	0	0	0	0	0	0	6	25
1965	73	8	17	27	2	0	0	0	1	13	9	6
1966	25	41	29	9	4	0	0	0	1	21	1	13
1967	22	46	16	4	18	0	0	0	0	13	77	17
1968	12	10	11	76	0	0	0	0	0	6	0	51
1969	65	14	36	42	15	0	0	0	0	7	17	22
1970	61	11	23	7	3	0	0	0	0	1	8	16
1971	8	0	26	75	9	0	0	0	0	1	15	0
1972	45	20	76	0	11	0	0	0	0	0	0	0
1973	0	0	0	9	0	0	0	0	0	1	0	38
1974	55	62	108	21	0	0	0	0	0	0	8	35
1975	57	0	1	37	15	0	0	0	0	0	0	0
1976	35	27	23	29	4	0	0	0	0	2	0	5
1977	41	12	10	28	5	0	0	0	0	3	9	34
1978	8	22	20	0	0	0	0	0	0	0	1	35

1979	47	12	19	2	5	1	0	0	0	8	13	32
1980	13	74	42	20	6	0	0	0	0	0	21	9
1981	51	49	69	18	8	0	0	0	0	11	30	30
1982	83	36	30	55	27	0	0	0	2	31	45	22
1983	34	25	27	19	22	0	0	0	0	0	13	23
1984	21	10	51	20	12	0	0	0	0	12	96	34
1985	48	46	32	27	6	0	0	0	0	3	31	44
1986	27	72	34	39	18	0	0	1	0	8	64	25
1987	7	19	54	6	7	0	0	0	0	43	12	80
1988	73	55	53	44	0	1	0	0	0	9	10	68
1989	13	32	62	0	3	0	0	0	0	3	65	27
1990	30	56	23	18	3	0	0	0	0	5	11	20
1991	43	55	66	6	1	0	0	0	7	27	32	78
1992	60	73	39	16	22	1	0	0	0	15	71	70
1993	56	40	24	90	45	0	0	0	0	25	42	26
1994	59	24	46	32	4	0	0	0	1	24	94	57
1995	24	70	52	51	8	3	0	0	2	0	9	18
1996	98	40	78	31	9	0	0	0	1	3	10	47
1997	43	29	54	25	8	1	0	0	0	25	66	66

Table A.1

1998	75	28	64	20	9	1	1	0	0	0	5	4
1999	44	46	27	5	1	0	0	0	0	5	9	36
2000	58	14	20	11	3	0	0	0	0	9	28	77
2001	31	30	42	15	4	0	0	0	1	3	13	50
2002	56	18	54	57	4	0	0	0	0	13	18	54
2003	41	109	32	14	4	0	0	0	0	2	56	72
2004	88	29	4	34	12	0	0	0	0	2	49	25
2005	48	24	34	11	3	0	0	0	1	0	10	12
2006	51	71	6	36	6	0	0	0	0	18	14	32
2007	29	27	21	25	5	0	0	0	0	0	0	12
2008	31	12	8	4	1	0	0	0	1	26	18	6
2009	4	7	16	14	1	0	0	0	1	14	19	32
2010	13	23	20	23	20	0	0	0	0	2	1	22

Indian Journal of Natural Sciences www.tnsroindia.org.in ©IJONS

Vol.9 /Issue 51 / December / 2018 *International Bimonthly* *ISSN: 0976 – 0997*

RESEARCH ARTICLE

Effect of Sodium Alginate Edible Coating with Clove (*Syzigium aromaticum*) Bud Oleoresin on Quality of Broiler Chicken Breast Fillets

Lijin James[1]*, Renuka Nayar[1], Christina Paulose[1], Kavitha Rajagopal[1], Sunanda C[2] and Shelcy S Akkara[1]

[1]Department of Livestock Products Technology, College of Veterinary and Animal Sciences, Kerala Veterinary and Animal Sciences University,Pookode, Wayanad. Kerala – 673 576,India
[2]Deptartment of Statistics,College of Veterinary & Animal Sciences, Kerala Veterinary and Animal Sciences University,Pookode, Wayanad, Kerala– 673 576,India

Received: 23 Aug 2018 Revised: 25 Oct 2018 Accepted: 27 Nov 2018

***Address for Correspondence**
Lijin James
MVSc scholar
Department of Livestock Products Technology
College of Veterinary and Animal Sciences
Kerala Veterinary and Animal Sciences University
Pookode, Wayanad. Kerala – 673 576,India.
Email: himlijinjames@gmail.com

ABSTRACT

The present study was carried out to evaluate the effect of edible coating of broiler chicken breast using sodium alginate incorporated with varying concentrations of clove (*Syzigiumaromaticum*) bud oleoresin and to assess the shelf life of coated as well as uncoated breast fillets under aerobic packaging in chiller storage (4±1°C). Coated breast fillets were made by coating with solution containing sodium alginate (two per cent) and glycerine (one per cent) incorporated with different concentrations of clove, T 1- sodium alginate coating alone, T2- three per cent clove incorporated, T3- four per cent clove incorporated and T4- five per cent clove incorporated and compared with control (C). Physico-chemical properties such as drip loss and cooking loss showed significantly ($p<0.01$) lower values for control when compared to treatments on all days of storage. There was a significant ($p<0.01$) increase in drip loss in all the samples throughout the storage period. pH values of both control and treatments increased significantly ($p<0.01$) on storage.Water holding capacity did not differ significantly in control and treatment groups on all days of storage except on day 0. TBARS number was significantly ($p<0.01$) lower for C than treatments on day 0. From day 3 onwards T 1 showed significantly ($p<0.01$) higher values than C and other treatments till day 12.Tyrosine values for treatment fillets significantly ($p<0.01$) increased across storage except in control where there was no significant difference. There was a significant ($p<0.01$) decrease in hardness for all the samples across storage. Phenolic content of 3, 4, and 5 percent solutions were assessed as 0.552± 0.13, 0.879 ± 0.19 and 1.38 ± 0.21 µg TAE /ml of coating solutions, respectively. DPPH (2, 2'-diphenyl-1-picryl hydrazyl) assay revealed radical scavenging activity of 3, 4, and 5 per cent

clove oleoresin containing coating solution (1 in 100 dilution) to be 21.82± 0.18 per cent, 27.27± 0.32per cent and 35.45 ± 0.21 per cent, respectively. Radical scavenging activity of sodium alginate coating solution (1 in 100 dilution) containing 0.5µg of phenolics as tannic acid equivalents was found to be 4.55 ± 0.15 per cent. The same for clove oleoresin (1 in 200 dilution) containing 25µg of phenolics as tannic acid equivalents was found to be 56.19 ± 0.23 per cent. Aerobic plate counts of all treatments from day 6 onwards, were significantly ($p<0.01$) lower than that of control, with the lowest counts for T 4. Psychrotrophic count was significantly ($p<0.05$) lower for T 2, T 3 and T 4 when compared to C and T 1. Shelf life of control (C) and sodium alginate alone treated (T1) samples was found to be 15 days. Clove incorporated sodium alginate coated samples, T 2, T 3 and T 4 had a better shelf life and lasted till 18th day of chiller storage. Clove oleoresin can be used for extending the shelf life of alginate coated breast fillets with good sensory attributes and can be considered as a preservation method with natural antimicrobial or antioxidant agents.

Keywords: Chicken breast fillets, Sodium alginate, Edible coating, Clove bud oleoresin, Chiller storage

INTRODUCTION

Biodegradable or edible coating is a suspension of edible materials which forms coating over a food product by becoming a part of it. It improves the mechanical properties, sensory attributes and enhances the shelf life of various food products. Materials for edible coating can be polysaccharides, proteins or lipids. Sodium alginate can form films besides several other properties like water-solubility, strength, glossiness, tastelessness, odourlessness, flexibility, reduction in oxygen and oil permeability (Xiao *et al*., 2014).Incorporation of antimicrobials or antioxidant compounds in the edible coating may cause a delay in meat rancidity, prevents discolouration, arrests the proliferation of spoilage and pathogenic microorganisms and also improves the nutritional quality (Baldwin *et al*., 2011).Clove bud oleoresin is prepared by solvent extraction from clove bud and is considered as a strong antioxidant among herb and other spice extracts. The effective component, eugenol is the main reason for its antioxidant activity. Clove being a spice, adds flavour to the product. Considering the Indian scenario where masala and spices are very commonly added to almost every meat product, use of clove gives an appealing flavour to the product.Taking all these into consideration, the proposed study was carried out to evaluate the effect of sodium alginate edible coating incorporated with varying concentrations of clove (*Syzigiumaromaticum*) bud oleoresin on broiler chicken breast, packed aerobically and stored under chiller condition(4±1°C).

MATERIALS AND METHODS

Birds procured from local market were slaughtered hygienically, dressed and breast fillets were harvested. The fillets were chilled overnight at 4±1°C for further processing on the next day. An edible coating containing two per cent sodium alginate and one per cent glycerol was given to all fillets except for control breast fillets.

Preparation of coating solution

A coating solution was prepared with sodium alginate and glycerol as plasticizer, the levels of which were standardised after preliminary trials as,

a) Sodium alginate (two per cent)
b) Glycerol (one per cent)

Sodium alginate (Nice chemicals, Pvt. Ltd. Kochi, Kerala) was mixed with filtered water and was heated to 90^0 C with constant stirring till it was completely dissolved. After cooling to 70^0 C, glycerol was added, mixed and then cooled to ambient temperature. The coating solution was divided into four, one without oleoresin and the remaining three incorporated with clove (*Syzigiumaromaticum*) bud oleoresin (M/S Plant lipids (Pvt.) Ltd., Cochin) at 3, 4 and 5 per cent levels, the concentrations were standardised after preliminary sensory evaluation.

Fillets were divided in to five groups and subjected to various treatments such as; C- control fillets without edible coating, T 1- fillets with edible coating without oleoresin, T 2- fillets with edible coatings incorporated with three percent clove oleoresin, T 3- fillets with edible coatings incorporated with four percent clove oleoresin and T 4- fillets with edible coatings incorporated with five percent clove oleoresin. Coating was given by dipping fillets in sodium alginate coating solution for 30 seconds, draining for 30 seconds, and then dipping in two per cent calcium chloride solution for 30 seconds and draining for 30 seconds. After draining coated fillets were kept in hot air oven at 40^0C for 30 min. Further all the fillets were packed aerobically in high density polyethylene (HDPE) pouches (above 65µm) and sealed by continuous sealing machine and kept in chiller (4 ± 1^0C) for storage. All the fillets were analysed for physico-chemical attributes.

Physico-chemical attributes

Drip loss of breast fillets was calculated using the following formula.

$$\text{Drip loss (per cent)} = \frac{\text{Initial weight (g)} - \text{Final weight (g)}}{\text{Initial weight (g)}} \times 100$$

Cooking loss was calculated as per Boccard*et al.* (1981). pH of the samples was measured using a digital pH meter as described by AOAC (2012). Water holding capacity was estimated as per Wardlaw*et al*. (1973).Thiobarbituric acid reactive substances (TBARS) number were determined as per Witte *et al*. (1970) with modifications.Tyrosine values of control and treatment samples were estimated as per the method described by Pearson (1968). The concentration of total phenolics of coating solution was determined by the Folin-Ciocalteu (F-C) assay (Escarpa and Gonzalez, 2001) with slight modification. 2,2-diphenyl-1-picryl hydrazyl (DPPH) assay was done to evaluate the antioxidant activity of the coating solution. This was done by the modified method of Singh *et al*. (2002). The DPPH radical scavenging activity was expressed as percentage maximum of coating solution. The DPPH activity of oleoresin was also calculated by the above method. The aliquot containing 50µg of phenolics was obtained from 1 in 100 ml dilution of clove oleoresin.

Colour values of the samples were determined objectively as per Page *et al*. (2001) using Hunter Lab Mini Scan XE Plus Spectrophotometer (Hunter Lab, Virginia, USA) with diffuse illumination.Warner-Bratzler Shear Force (WBSF) of each sample was determined by the method outlined by Wheeler *et al.* (1997) using Universal Testing Machine– Shimadzu Texture Analyzer Model EZ-SX (Shimadzu Corporation, Kyoto, Japan).

Microbiological parameters

All the microbiological parameters were determined by following standard methods of American Public Health Association. Readymade media (Hi-Media and Sisco Research Laboratories, India) were used for all the microbiological examinations after serial dilution of the samples.

Aerobic plate count (APC) was evaluated as per the procedure of Morton (2001). Psychrotrophic count was expressed as per the procedure of Beuchat and Cousin (2001).

Proximate principles

Samples were analysed for proximate principles like moisture on days 0, 3, 6, 9 and 12 and fat, protein and ash on day 0as per AOAC (2012). The proximate principles were expressed as percentage of sample on wet matter basis. Carbohydrate and energy values of the samples were also calculated.

Sensory evaluation

The sensory evaluation of poultry meat was conducted by a semi trained panel consisting of faculty and post graduate students from the Department of Livestock Products Technology, College of Veterinary and Animal Sciences, Pookode using a three point Hedonic scale score card for raw fillets and a nine point Hedonic scale score card for cooked fillets.

Statistical analysis

The data obtained were statistically analyzed by one-way ANOVA, repeated measures ANOVA, Kruskal- Wallis test, Wilcoxon signed rank test, Friedman test, Mann Whitney test using SPSS software (VERSION 21) as per Snedecor and Cochran (1994).

RESULTS AND DISCUSSION

Physico-chemical attributes

Control had significantly ($p<0.01$) lower drip loss values than all the treatments on all days of storage. There was a significant ($p<0.01$) increase in drip loss in all the samples throughout the storage period. Similar results were obtained by Rodriguez *et al*. (2011) who observed higher drip loss values in refrigerator stored salmon fish fillets with edible coating of whey protein concentrate incorporated with sorbitol and glycerol when compared to uncoated fillets.

Control had significantly ($p<0.01$) lower cooking loss values than treatments on all days of storage. Throughout the storage period, pH values of both control and treatments increased significantly at one per cent level.Kristam*et al*. (2016) found similar trend of increase in the pH values in sodium alginate coated and uncoated chicken nuggets when stored under refrigerator conditions. Matiacevich*et al*. (2015) and Khare*et al*. (2016) also noticed an increase in pH of chicken breast fillets coated with alginate–thyme oil–propionic acid combination and carrageenan-cinnamon oil-citric acid combination, respectively and stored under refrigerator (4±1°C) conditions.

Water holding capacity did not differ significantly in control and treatment groups on all days of storage except on day 0.TBARS number was significantly ($p<0.01$) lower for C than treatments on day 0. From day 3 onwards T 1 showed significantly ($p<0.01$) higher values than C and other treatments till day 12. Control and treatment breast fillets showed significant ($p<0.01$) increase in TBARSvalues on storage and the values were highest on day 12.A progressive increase in TBARSvalues on storage was reported by Khare*et al*. (2016) in breast fillets coated with carrageenan, citric acid and cinnamon oil and stored in chiller.

Tyrosine values of all samples significantly ($p<0.01$) increased across storage except in control where there was no significant difference. Tyrosine values in refrigerator stored (4±1°C) chicken meat increased irrespective of the different ecofriendly packaging materials used for packing (Thamizhannal*et al*., 2017).

Colour of fillets was measured using Hunter Lab Mini Scan XE Plus Spectrophotometer and except on day 3, C had significantly ($p<0.01$) lower 'L' values when compared to treatments. A significant increase in lightness values was observed by Antoniewski*et al*. (2007) in gelatin coated chicken fillets, packed in modified atmospheric package and stored at 4±1°C for two weeks.C and T 1 showed a significantly ($p<0.01$) higher 'a' values when compared to other samples on all days of storage. On storage, redness values significantly ($p<0.01$) reduced for C. Shan *et al*. (2009) found a reduction in 'a' values for pork incorporated with natural spice and herb extracts and observed that clove could avert the discolouration of pork during storage at ambient temperature. There was significant ($p<0.01$) difference in 'b' values between samples on days 0, 9 and 12, with C showing the lowest value and T 4, the highest. On storage, there was no significant difference between the values in any of the sample.Lu *et al*. (2010) reported increase in 'b' values for sodium alginate coated fish fillets incorporated with cinnamon, nisin and EDTA and the values were higher than control uncoated fish fillets.

Except for day 0, on all other days, shear force values were the highest for control and significantly ($p<0.01$) lower for treatments. There was a significant ($p<0.01$) decrease in hardness of all the samples across storage. Total phenolics was expressed as µg tannic acid equivalent (TAE) /ml of coating solution. Phenolic values of 3, 4, and 5 percent solutions were assessed as 0.552± 0.13, 0.879 ± 0.19 and 1.38 ± 0.21 µg TAE /ml of coating solution, respectively. Babuskin*et al*. (2014) while assessing the effect of spice extracts on shelf life extension of poultry meat, observed a phenolic content of 24.65 ± 0.83 mg gallic acid per g of clove (*Syzigiumaromaticum*) extract.

DPPH (2, 2'-diphenyl-1-picryl hydrazyl) assay was done and the radical scavenging activities of 3, 4, and 5 per cent clove oleoresin containing coating solutions (1 in 100 dilution) were assessed to be 21.82± 0.18 per cent, 27.27± 0.32per cent and 35.45 ± 0.21 per cent, respectively. Radical scavenging activity of sodium alginate coating solution (1 in 100 dilution) containing 0.5µg of phenolics as tannic acid equivalents was found to be 4.55 ± 0.15 per cent. The same for clove oleoresin (1 in 200 dilution) containing 25µg of phenolics as tannic acid equivalents was found to be 56.19 ± 0.23 per cent.

Microbiological characteristics

From day 6 onwards, aerobic plate counts of all treatments were significantly ($p<0.01$) lower than that of control, with the lowest counts for T 4.Keshriand Sanyal (2009) also observed reduced total viable count in beef patties coated with sodium alginate incorporated with ascorbates when compared to uncoated samples and stored for 21 days under refrigerator(4±1°C) conditions.Psychrotrophic count was significantly ($p<0.05$) lower for T 2, T 3 and T 4 when compared to C and T 1.

Proximate analysis

Proximate analysis revealed no significant difference between the samples with respect to fat, protein, ash, carbohydrate and energy levels.When compared to day 0, a significant ($p<0.05$) decrease was noted for moisture content in control and treatment samples on day 12.Mallika*et al*. (2017) also reported lower moisture values for control chicken balls than the balls wrapped with sodium alginate film and sodium alginate films incorporated with clove.

Sensory attributes

Organoleptic evaluation was done for attributes like colour, tenderness, odour in raw fillets and appearance, flavour, juiciness, tenderness, after taste and overall acceptability in cooked fillets. For raw fillets, appearance and texture values showed no significant difference between control and treatments and also across storage. Odour scores for control and T1 reduced on day 9 and 12 whereas the scores were higher for T2, T3, and T4. For cooked fillets, appearance, texture and juiciness scores did not vary significantly between samples. Flavour, after-taste and overall

acceptability also did not vary significantly between samples on all days except on day 6, where there was a significant difference ($p<0.05$) between samples.

Shelf life of control (C) and sodium alginate alone treated (T1) samples was found to be 15 days. C and T1 showed signs of spoilage like off odour after day 15. Clove incorporated sodium alginate coated samples, T 2, T 3 and T 4 had a better shelf life and lasted till 18th day of chiller storage.Poultry meat is highly susceptible to lipid oxidation due to its high content of polyunsaturated fatty acids and hence extra care is needed to increase its keeping quality. If given an edible coating with incorporation of natural antioxidants or antimicrobials, its shelf life can be very well extended. Thus it can be concluded that clove oleoresin at 3-5 per cent level can effectively be used for extending the shelf life of alginate coated breast fillets. However based on the cost of production T 2 may be recommended for adoption in poultry meat industry.

ACKNOWLEDGMENTS

The authors would like to thank Dean, CVAS, Pookode and faculty and staff of Dept of LPT for the facilities offered. The first author also acknowledges Kerala Veterinary and Animal Sciences University for providing funds for conducting the research work.

REFERENCES

1. Xiao, Q., Gu, X. and Tan, S. Drying process of sodium alginate films studied by two-dimensional correlation ATR-FTIR spectroscopy. Food Chem. 2014; **164**: 179-184.
2. Baldwin, E.A., Hagenmaier, R. and Bai, J. eds. Edible coatings and films to improve food quality. CRC Press. 2011;
3. Boccard, R., Butcher, L., Casteels, S., Cosentino, E., Dransfield, E., Hood, D.E., Joseph, R.L., Mac Dougall, D. B., Rhodes, D.M., Schon, J., Tinbergen, B.J. and Touraille, C. Procedures for measuring meat quality characteristics in beef production experiments. Livestock Prod. Sci. 1981; **8**: 385.
4. AOAC. Meat and meat products. In: Official Methods of Analysis of Analytical Chemists. (19th Ed.)Association of Official Analytical Chemists. Inc., Arlington, Virginia. pp. 2012; 931-948.
5. Wardlaw, F.B., Maccaskill, L.H. and Acton, J.C. Effect of post mortem muscle changes in poultry meat loaf properties. J. Food Sci. 1973; **38**: 421-424.
6. Witte, V.C., Krause, G.F. and Bailey, M.E. A new extraction method for determining 2-thiobarbituric acid values of pork and beef during storage. J. Food Sci. 1970; **35**: 582-585.
7. Pearson, D. Application of chemical method for assessment of beef quality. In Methods related to protein breakdown. J. Sci. Food Agric. 1968; **19**: 364-366.
8. Escarpa, A. and Gonzalez, M. C. Approach to the content of total extractable phenolic compounds from different food samples by comparison of chromatographic and spectrophotometric methods. Anal. Chim. Acta. 2001; **427**: 119-127.
9. Singh, R.P., Murthy, K.N.C. and Jayaprakasha, G.K. Studies on the antioxidant activity of pomegranate (*Punicagranatum*) peel and seed extracts using in-vitro models. J. Agric. Food Chem. 2002; **50**: 81-86.
10. Page, J.K., Wulf, D. M. and Schwotzer, T.R. A survey of beef muscle colour and pH. J. Anim. Sci. 2001; **79**: 678-687.
11. Wheeler, T.L., Shakelford, S.D., Johonson L.P., Miller, R.K. and Koohmaraie, M. A comparison of warner-bratzler shear force assessment within and among institution. J. Animal Sci. 1997; **75**: 2423-2432.
12. Morton, R.D. Aerobic plate count. In: Downes, F.P., and Ito, K (ed.), Compendium of Methods for the Microbiological Examination of Foods. (4thEd.). APHA, Washington, D.C. 2001; pp. 63-67.
13. Cousin, M.A., Jay, J.M. and Vasavada, P.C. Psychrotrophic microorganisms. In: Downes, F.P., and Ito, K (ed.), Compendium of Methods for the Microbiological Examination of Foods. (4th Ed.). APHA, Washington, D.C. 2001; pp. 159-166.
14. Snedecor, G.W. and Cochran, W.G. Statistical Methods. (8th Ed.) The Iowa State Univ., Ames, Iowa, 1994; 313p.

15. Rodriguez-Turienzo, L., Cobos, A., Moreno, V., Caride, A., Vieites, J.M. and Diaz, O. Whey protein-based coatings on frozen Atlantic salmon (Salmosalar): Influence of the plasticiser and the moment of coating on quality preservation. Food Chem. 2011; **128**(1): 187-194.
16. Kristam, P., Eswarapragada, N.M., Bandi, E.R. and Tumati, S.R. Evaluation of edible polymer coatings enriched with green tea extract on quality of chicken nuggets, Vet. Wld. 2016; **9**(7): 685-692.
17. Matiacevich, S., Acevedo, N. and López, D. Characterization of Edible Active Coating Based on Alginate–Thyme Oil–Propionic Acid for the Preservation of Fresh Chicken Breast Fillets. J. Food Process. Preserv. 2015; **39**(6): 2792-2801.
18. Khare, A.K, Abraham, R.J.J, Rao, V.A. and Babu, R.N. Utilization of carrageenan, citric acid, and cinnamon oil as an edible coating of chicken fillets to prolong its shelf life under refrigeration conditions, Vet. Wld. 2016; **9**(2): 166-175.
19. Thamizhannal, M., Rao, V.A., Raja, S.S., Arul, S., Thanigaivel, P. and Ruban, W. Proteolytic Changes in Chicken Meat Packed in Ecofriendly Packaging Materials. Int. J. Pure App. Biosci. 2017; **5**(1): 277-281.
20. Antoniewski, M.N., Barringer, S.A., Knipe, C.L. and Zerby, H.N. Effect of a gelatin coating on the shelf life of fresh meat. J. Food Sci. 2007; **72**(6): E382-E387.
21. Shan, B., Cai, Y.Z., Brooks, J.D. and Corke, H. Antibacterial and antioxidant effects of five spice and herb extracts as natural preservatives of raw pork. J. Sci. Food Agri. 2009; **89**(11) 1879-1885.
22. Lu, F., Ding, Y., Ye, X. and Liu, D. Cinnamon and nisin in alginate–calcium coating maintain quality of fresh northern snakehead fish fillets. LWT-Food Sci. Technol. 2010; **43**(9): 1331-1335.
23. Babuskin, S., Babu, P.A.S., Sasikala, M., Sabina, K., Archana, G., Sivarajan, M. and Sukumar, M. Antimicrobial and antioxidant effects of spice extracts on the shelf life extension of raw chicken meat. Int. J. Food Microbiol. 2014; **171**: 32-40.
24. Keshri, R.C. and Sanyal, M.K. Effect of sodium alginate coating with preservatives on the quality of meat patties during refrigerated (4±1^{0}C) storage. J. Muscle Foods. 2009; **20**(3): 275-292.
25. Mallika, E., Veena, D. and Reddy, G. Quality of chicken balls on application of edible Film Wraps Enriched with Natural Spice Oils. Int. J. Livestock Res. 2017; **7**(6): 202-210.

Table 1. TBARS numbers of control and treatment fillets on different storage days

Storage days ---------- Treatments	**Day 0**	**Day 3**	**Day 6**	**Day 9**	**Day 12**	**F-value (p-value)**
C	0.008^{cD} ± 0.002	0.008^{cD} ± 0.001	0.016^{C} ± 0.003	0.029^{abB} ± 0.005	0.040^{A} ± 0.008	20.617** (<0.001)
TI	0.018^{bB}± 0.002	0.02^{aB} ± 0.0004	0.017^{B} ± 0.001	0.036^{aA}± 0.003	0.036^{A} ± 0.001	31.951** (<0.001)
T2	0.016^{bC} ± 0.001	0.005^{dD} ± 0.0002	0.013^{C} ± 0.01	0.028^{abB} ± 0.004	0.035^{A} ± 0.001	44.288** (<0.001)
T3	0.017^{bB} ± 0.002	0.009^{cC} ± 0.0002	0.016^{C} ± 0.001	0.023^{cB} ± 0.001	0.042^{A} ± 0.002	98.577** (<0.001)
T4	0.036^{aA} ± 0.003	0.014^{bC} ± 0.001	0.015^{C} ± 0.001	0.020^{cB} ± 0.001	0.030^{A} ± 0.001	98.439** (<0.001)
F-value (p-value)	24.575** (<0.001)	46.523** (<0.001)	1.034^{ns} (0.409)	3.811* (0.015)	1.437^{ns} (0.251)	

C- Control, T 1- Edible coated fillets without oleoresin, T 2- Edible coated fillets with 3% oleoresin, T 3- Edible coated fillets with 4% oleoresin, T 4- Edible coated fillets with 5% oleoresin. ** Significant at 0.01 level; * significant at 0.05 level; ns-non-significant; *Means having different small letter as super script are significantly different (p<0.05) within a column*; *Means having different capital letter as super script are significantly different (p<0.05) within a row.*

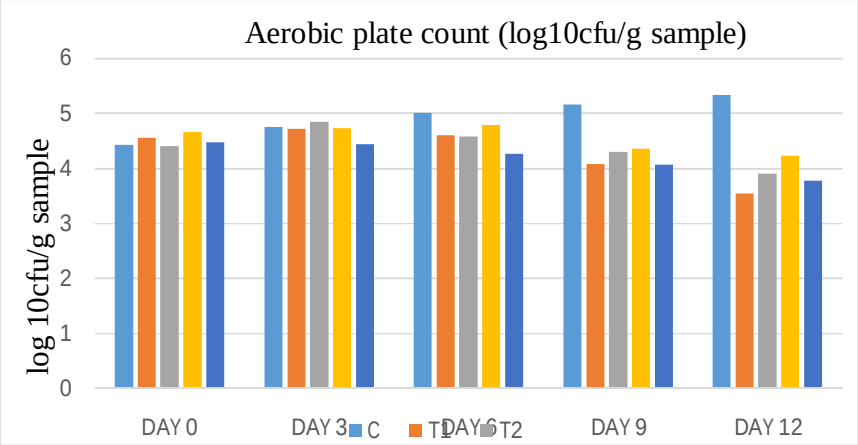

Fig 1: Aerobic Plate Counts (log $_{10}$ cfu/g sample) of control and treatment fillets on different storage days

Indian Journal of Natural Sciences www.tnsroindia.org.in ©IJONS

Vol.9 /Issue 51 / December / 2018 *International Bimonthly* *ISSN: 0976 – 0997*

RESEARCH ARTICLE

Quantum Repeater Based on Multiplexed Single Photon Source MUX-SPS

Wijdan M. Khudhair*, Jawad A. K Hasan, Adnan N. Kadhim

Institute of Laser for Post graduate Studies, University of Baghdad, Baghdad, Iraq.

Received: 05 Sep 2018 Revised: 08 Oct 2018 Accepted: 12 Nov 2018

***Address for Correspondence**
Wijdan M. Khudhair
Institute of Laser for Post graduate Studies,
University of Baghdad,
Baghdad, Iraq
E-mail: wijdanmahmood@gmail.com

ABSTRACT

In this work, a new scheme for quantum repeater based on multiplexed single photon source is suggested. Long distance quantum communication requires establishment of a distant pair of entangled quantum bits, e.g. photons presented in laser sources, that is the first step towards the more secure message transmission. There are many proposed schemes to achieve such task using many different ideas and one of them was proposed by [16], who suggested a quantum repeater QR protocol based on pair photon sources PPS. But, pair photon source suffers from a mechanism error due to probability of losing one photon of pairs during its transmission through the fiber or by detector failure; it will not have the desired entangled state consequently these error's effect on entanglement distribution rates. However, single photon sources [18] suggested implementing the new quantum repeater scheme, which makes it possible to eliminate errors inherent in quantum repeater protocols using photon-pair sources. Here, an efficient architecture for quantum repeaters based on multiplexing single-photon sources MUX-SPS in combination with multiplexing multimode quantum memories MM-QM is suggested to make improvement in entanglement distribution over long distance quantum communications, using only a single photon to entangle an arbitrary photon number of remote quantum memories.

Keywords: Quantum communication, quantum memory, entangled photon sources, entanglement distribution rate, multiplexing technology.

INTRODUCTION

Quantum entanglement is at the core of quantum physics [1] and at the same time, the basis of most quantum communication protocols such as quantum cryptography [2], quantum dense coding [3], quantum teleportation [4], [6]. Quantum teleportation, is based on quantum entanglement [5]. Each of those schemes allows efficient

communication beyond the abilities of their classical counterparts, which result in a new developing quantum information technology. Quantum communication, networking, and computation schemes exploit entanglement as their crucial resource However, while the realization of such schemes is routine work in the laboratory; important problems appear in long-distance applications. At present, the only appropriate system for long-distance quantum communication is photons. Entangled state distribution over long distances is an important challenging task. The direct distribution of entangled states is limited by transmission losses of photons.

To overcome this problem, quantum repeaters are essential [7]. Implementations of quantum repeaters have been proposed in different schemes [8-11]. A basic idea of all protocols is the creation of entanglement between neighboring nodes (A and B) (see Fig. 1). The fundamental step of quantum repeaters is dividing the full distance into shorter elementary links. Each elementary link consists of two quantum memories that must be entangled independently for each link. This entanglement can then be extended to the neighboring links using entanglement swapping [19] to (A and B) become entangled. However, as photons generally arrive in a probabilistic fashion due to loss during transmission, such measurements are inherently inefficient. For instance, this leads to exponential scaling of the time required to establish entanglement. Quantum memories [26-30] at quantum repeater can be used to overcome this problem, which are generally realized through the reverse mapping of quantum states between light and matter [13, 14].

QR Scheme Based on Photon Pair Sources PPS

An approach for implementation of quantum repeaters of the long-distance quantum communication was proposed in 2001 [8]. It permits to generate and swap the entanglement and use it in quantum teleportation. The excitation probability for generation of single photon from the atomic ensemble in QM which is used to entangle the photon emitted from an entangled photon source is small. In order to avoid multi-photon emission error occurred with excitation of a single photon in an atomic ensemble of QM for each entanglement generation attempt, long entanglement generation time is required. To eliminate this problem, multiplexing quantum memory is suggested by [15] which offer higher entanglement distribution rates by multiplexing multimode quantum memory (MM-QM). (See Fig. 2).The proposed scheme [16], which used a combination of photon pair sources (PPS) and MM-QM such as controlled reversible inhomogeneous broadening CRIB-based memory protocol [20] and multimode quantum memory based on atomic frequency combs AFC [21], should allow the realization of a quantum repeater protocol that is much faster and more robust than the protocol proposed by [8]. The performance of PPS and MM-QM (see Fig.3) is limited by the PPS error mechanism, since even if the PPSs are ideal, the probability that two pairs will be emitted is limited by ***I*** 4 in total. Also, if one photon of pairs is lost during its transmission through the fiber or by detector failure, it will not have the desired entangled state.

The entanglement distribution rate between the endpoints (A and B) of the entire quantum channel has to be calculated to evaluate the performance of the multiplexed quantum repeater. Neighboring elementary links must perform entanglement swapping, including a BSM ' at the node of neighboring elementary links {where the prime serves to distinguish this BSM from the one performed at the center station} (see Fig. 3).To ensure that the elementary entanglements of neighboring links in are the same modes, a frequency conversion may be necessary before the entanglement swapping BSM' in order to have telecom wavelength. Then, if the nodes of all elementary links successfully perform a BSM' (probabilistic), entanglement is created between the end points of the quantum channel. The calculation of the success probability of entanglement creation and entanglement distribution rate across the quantum channel is calculated as [22]:

The probability of success of entanglement creation:

$$P_{(success)} = \frac{(N_{mem}N_{ch})^{2^n}}{2^{n-1}}\left(1-\left(1-\frac{1}{2}\eta_{det}^{2}\alpha^{2}10^{\frac{-\alpha L}{10}}\right)^{m}\right)^{n} \quad (1)$$

The entanglement distributionrate R (success), which is equal to P (success) divided by the time between successive attempts.The time between successive attempts is given by (w m) / B. Therefore [22]:

$$R_{success} = \frac{B}{wm} \frac{(\eta_{mem}\eta_{d2})^{2n}}{2^{n-1}} (1-(1-\frac{1}{2}\eta_{d1}^{2}\rho^{2}10^{\frac{-\alpha L}{n}})^{m})^{n} \quad (2)$$

Where:B is quantum memories total bandwidth, w is the bandwidth inefficiency, m is QM modes number,η_{d1} is the efficiency of the center station's detectors, α is the loss coefficient of the channel and lossy quantum channel length L, detection efficiency of BSM 'is η_{d2}.Splitting the channel into (n)elementary links, η_{mem}quantum memory efficiency, ρ is the probability of source to emit one pair of maximally entangled photons.

QR Scheme Based on Single Photon Sources SPS

As it had been mentioned above, some of PPS errors may be overcome using single-photon sources SPS suggested by [18] since it is free of these fundamental errors. Here, quantum repeater scheme based on SPS is suggested to improve the entanglement distribution rate. The architecture of this scheme is shown in Fig. 4. Each elementary link contains two SPSs and MM-QMs. When the MM-QMs are excited, each one of the two MM-QMs create one photon and each one of the SPSs emit single photon which is split on the beam splitter BS into two modes, one is transmitted toward MM-QM to entangle the excited photon, the other is transmitted to single photon detector SPD to perform BSM at the central station. So the SPS scheme is compatible with the multi-mode quantum memories [16], spatial and frequency multiplexing [15], and improved entanglement swapping [17].

To evaluate the performance of the suggested scheme the total time required for entanglement distribution rate is calculated [25] :

$$p(n) = (1-P_0)^{n-1}P_0 \quad (3)$$

Where, P_0 is the probability of success entanglement probability,$P_0 = 2p_1\beta^{2}\eta_t\eta_d$ [33],$\eta_d$is the detection efficiency, $\eta_t = \exp(-\frac{L_0}{2L_{att}})$is the fiber transmission efficiency,$L_0 = \frac{L}{2^n}$ is the length of an elementary link,$n$is the elementary links number, L is the entire quantum channel length,L_{att} is attenuation length = 22 km.So it can calculate the actual rate of entanglement creation R(success) of SPS, as the reciprocal of the time between successive attempts. The time between successive attempts is given by (w × m) /B. Therefore:

$$R_{(success\ SPS)} = \frac{B}{wm} p(n) \quad (4)$$

Using SPS with MM-QM, the entanglement distribution rate can be improved better than thatwith PPS. (See Fig.5).

QR Scheme Based on Multiplexed Single Photon Sources MUX-SPS

A reconfiguration of multiplexed quantum nodes, which improves communication rates using MM-QM (see Fig.2) with multiplexed single-photon sources MUX-SPS (see Fig.6) [12], is suggested to make furthermore entanglement distribution rate improvement. Since a single-photon source (see Fig.4)is a key essential for scaling many optical quantum technologies. The quantum repeater QR scheme using MM-QM in combination with MUX-SPS is suggested and illustrated in Fig. 7.

Heralded Single-Photon Source Parameters:

The type of detector presented in HSPS scheme illustrated in Fig. 6 (a) is considered. The two important types are: this hold detector TD [24] and number-resolving detector NRD [23], [31].

For TD type, the probability for the detector on the idler arm to trigger having at least one photon is given by[12]:

$$P_{trigTD} = \frac{|\xi|^2\eta_i}{1-|\xi|^2(1-\eta_i)} \quad (5)$$

While the probability that the heralded state is a single-photon is[12] :

$$P_{singleTD} = (1-|\xi|^2)\eta_s \frac{[1-(|\xi|^2(1-\eta_s))^2(1-\eta_i)]}{[1-|\xi|^2(1-\eta_s)]^2[1-|\xi|^2(1-\eta_s)(1-\eta_i)]^2} \quad (6)$$

Where: $\eta_i$the idler arm efficiency, η_s is the overall transmission on the signal arm efficiency see Fig. 6 (a). The source is characterized by a squeezing parameter ξ, determined by the laser pump intensity and strength of the non linearity.

Now consider the NRD type, calculating the probability on the idler arm to trigger to get only one photon gives[12]:

$$P_{trigNRD} = \frac{(1-|\xi|^2)|\xi|^2\eta_i}{(1-(1-\eta_i)|\xi|^2)^2} \quad (7)$$

The probability of heralded state a single-photon is[12]:

$$P_{singleNRD} = (1-(1-\eta_i)|\xi|^2)^2\eta_s\left(\frac{(1+(1-\eta_i)(1-\eta_s)|\xi|^2)}{(1-(1-\eta_i)(1-\eta_s)|\xi|^2)^2}\right) \quad (8)$$

Furthermore, HSPSs architectures are considered as high efficiency single-photon sources with low multi-photon contamination if their components are close to ideal and with number-resolving detector efficiency is near 99% [23].A single-photon source capable of producing a 100 Hz rate of 20-40 photon states with less than 10% multi-photon contamination is possible. With lower-loss switches and the high efficiency detectors, a MUX source approaching the threshold requirements for a fully fault-tolerant universal quantum computer should be possible. A general MUX source can be characterized in a similar way to the HSPS. The probability per clock-cycle that at least one photon in an array of N HSPSs triggers is given by[12]:

$$P_{trig}^{MUX} = 1-(1-P_{trig})^N \quad (9)$$

And the probability per clock-cycle that at least one source emits a triggered single photon is [12]:

$$P_1 = P_{single}(1-(1-P_{trig})^N) \quad (10)$$

Depending on type of detector of HSPSs of Fig. 6 (a) the probability to produce a single photon of the MUX-SPS illustrated in Fig. 6 (b) will increase[32]. By calculating (10), then used it to calculate (3) and (4), entanglement distribution rate (4) of MUX-SPS will be increased higher than that by using SPS. Higher improvement of entanglement distribution rate of MUX-SPS is achieved using NRD which has a higher photon detecting efficiency than TD, as illustrated in Fig. 8.

CONCLUSIONS

As shown in Fig. 5 the entanglement distribution rate of SPS outperforms on the entanglement distribution rate of PPS and these results are likely expected since SPS free of errors which PPS suffered from. Consequently, long distances quantum channel is achieved by SPS scheme. Furthermore, the higher entanglement distribution rate using the MUX-SPS is satisfied as shown in Fig. 8 taking into consideration the NRD which has a high efficiency detection. The advantage of using such a method is reducing the needed to higher waiting time for creating an entangled pair, Then it will reduce the detrimental effects of the de coherence effect on the quantum memories in use.

ACKNOWLEDGMENTS

We would like to express our deep gratitude and appreciation to the Institute of Laser for Postgraduate Studies, to the members of the photonic department for their helpful suggestions.

REFERENCES

1. E. Schrödinger,"Diegegenwärtige Situation in der QuantenmechanikNaturwissenschaften", vol. 23, pp. 807–812, (1935).
2. D. S. Naik, C. G. Peterson, A. G. White, A. J. Berglund, and P. G. KwiatEntangled state quantum cryptography: eavesdropping on the ekert protocol Phys. Rev. Lett , vol. 84, p. 4733, (2000).
3. Dylan J. Saunders, Adam J. Bennet, Cyril Branciard and Geoff J. Pryde, Science Advances. Vol. 3, no. 4, e1602743.DOI: 10.1126/sciadv.1602743, 28 Apr (2017).
4. Liu-Yong Cheng, Guo-Hui Yang, Qi Guo, Hong-Fu Wang &Shou Zhang, Scientific Reports volume 6, Article number: 19482 (2016).
5. C. H. Bennett and G. Brassard, in Proceedings of the International Conference on Computers, Systems and Signal Processing 175 (IEEE, New York, 1984); C. H. Bennett et .al., Phys. Rev. Lett. 70, 1895 (1993); A. K. Ekert, Phys Rev. Lett. 67, 661 D. Bouwmeester et al., Nature; (1991).London 390, 575 (1997); E. Knill, R. Laflamme, and G J. Milburn, Nature (London) 409, 46 (2001).
6. H.-J. Briegel et al., Phys. Rev. Lett. 81, 5932 (1998) .
7. L. M. Duan et al,Nature (London) 414, 413 (2001).
8. J. I. Cirac et al., Phys. Rev. Lett. 78, 3221 (1997)
9. L. Childress et al., Phys. Rev. Lett. 96, 070504 (2006).
10. P. van Loock et al., Phys. Rev. Lett. 96, 240501 (2006)
11. Damien Bonneau , Gabriel J. Mendoza[12] Jeremy L. O, Brien and Mark G, Thompsony , arXiv:1409.5341v2 [quant-ph] 29 Apr (2015).
12. A. I. Lvovsky, B. C. Sanders, and W. Tittel, Nat. Photon, 706 ,3. (2009).
13. F. Bussieres, N. Sangouard, M. Afzelius, H. de Riedmatten C. Simon, and W. Tittel, J. of Mod. Opt. 60 1519, (2013).
14. O. A. Collins, S. D. Jenkins, A. Kuzmich, and T. A. B Kennedy, Phys. Rev. Lett. 98, 060502 (2007).
15. C. Simon, H. de Riedmatten, M. Afzelius, N. Sangouard, H. Zbinden, and N. Gisin, Phys. Rev. Lett. 98, 190503. (2007).
16. L. Jiang, J.M. Taylor, and M.D. Lukin, quantph 0609236, (2006).
17. N. Sangouard, C. Simon, J. c. v. Min´a˘r, H. Zbinden, H. de Riedmatten, and N. Gisin. Phys. Rev. A 76, 050301 (2007).
18. Qi-Chao Sun et al, Entanglement swapping over 100 km optical fiber with independent entangled photon-pair sources, Optica DOI: 10.1364/OPTICA.4.001214, (2017).
19. Afzelius, M., C. Simon, H. de Riedmatten, and N. Gisin, Phys. Rev. A 79, 052329, (2009).
20. Neil Sinclair, ErhanSaglamyurek, Hassan Mallahzadeh, Joshua A. Slater, Mathew George RaimundRicken,Morgan P. Hedges, Daniel Oblak, Christoph Simon, Wolfgang Sohler, and Wolfgang Titte , arXiv:1309.3202v3 [quant-ph] 18 Jul (2014).
21. D. Sahin, A. Gaggero, Z. Zhou, S. Jahanmirinejad, F. Mattioli, R. Leoni, J. Beetz, M. Lermer, M. Kamp, S. Höfling, and A. Fiore. Waveguide photon-number-resolving detectors for quantum photonic integrated circuits. Applied Physics Letters, 103(11) (2013).
22. MarsiliF., VermaV. B., SternJ. A., HarringtonS., LitaA. E., GerritsT., VayshenkerI., BaekB., ShawM. D., MirinR. P., and NamS. W. Detecting single infrared photons with 93% system efficiency. Nat Photon, 7(3):210–214, 03 (2013).
23. Nicol o Lo Piparo, William J. Munro, and KaeNemoto, phoarXiv:1807.02940v1 [quant-ph] 9 Jul (2018).

24. KhabatHeshami, Duncan G. England, Peter C. Humphreys, Philip J. Bustard,Victor M. Acosta, Joshua Nunn & Benjamin J. Sussman,) Quantum memories:emerging applications and recent advances, Journal of Modern Optics, 63:20, 2005-2028, DOI:10.1080/09500340.2016.1148212(2016).
25. Chaneliere, T.et al. Storage and retrieval of single photons transmitted between remote quantum memories. Nature, 438, 833–836 (2005).
26. Daniel Viscor, Weibin Li and Igor Lesanovsky, "Electromagnetically induced transparency of a single-photon indipole-coupled one-dimensional atomic clouds" New J. Phys17033007., doi:10.1088/1367-2630/17/3/033007,(2015).
27. Cyril Laplane, Pierre Jobez, Jean Etesse, Nicolas Gisin, and Mikael Afzelius, arXiv:1705.03679v1 [quant-ph] 10 May (2017).
28. MichałParniak, MichałDąbrowski, Mateusz Mazelanik, Adam Leszczyński, MichałLipka&WojciechWasilewski, Nature Communicationsvolume 8, 2140 (2017).
29. TakaYukikiyOhara , Ryo Okamoto, and Shigeki Takeuchi "Realization of multiplexing of heralded single photon sources using photon number resolving detectors" . Optical Society of America. (2016).
30. A. L. Migdall, D. Branning, S. Castelletto, and M. Ware, arXiv:quant-ph/0205140v2 22 May (2002).
31. N. Sangouard, C. Simon, H. de Riedmatten, and N. Gisin, Rev. Mod. Phys. 83, 33 (2011).

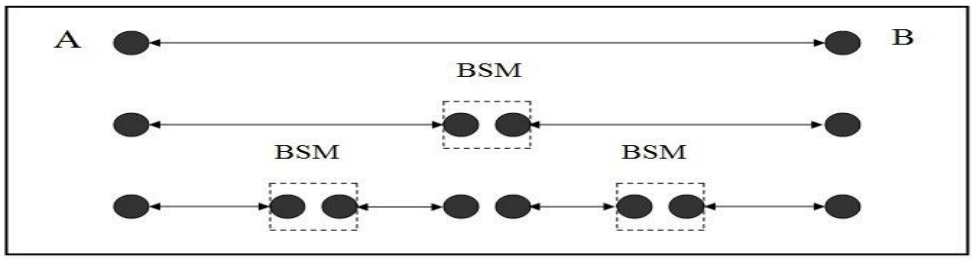

Figure1: Quantum repeater scheme, shows the entanglement between two distant locations (A and B) .The circles represents quantum memories connected by elementary links, (BSM) is Bell State Measurement.

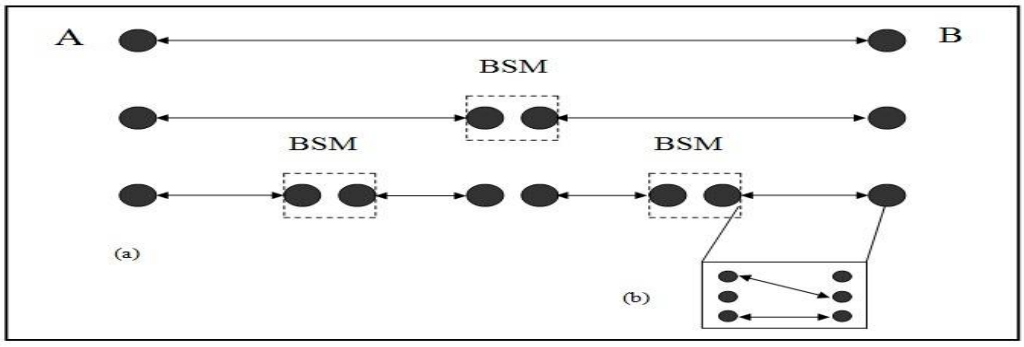

Figure 2: (a) Quantum repeater scheme. (b) Multiplexing multimode quantum memory

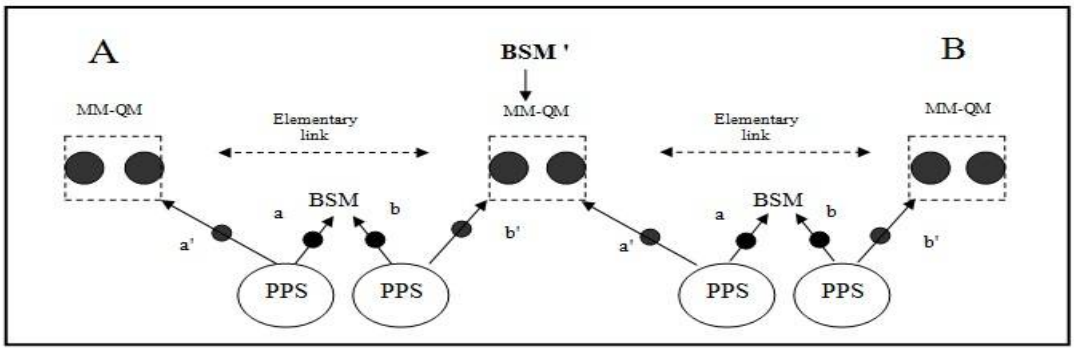

Figure 3:The scheme of a quantum repeater based on multiplexing multimode quantum memory MM-QM and pair photon source PPS. As shown BSM' performs inside nodes located between two elementary links, while BSM performs at the central station at elementary links between two nodes.

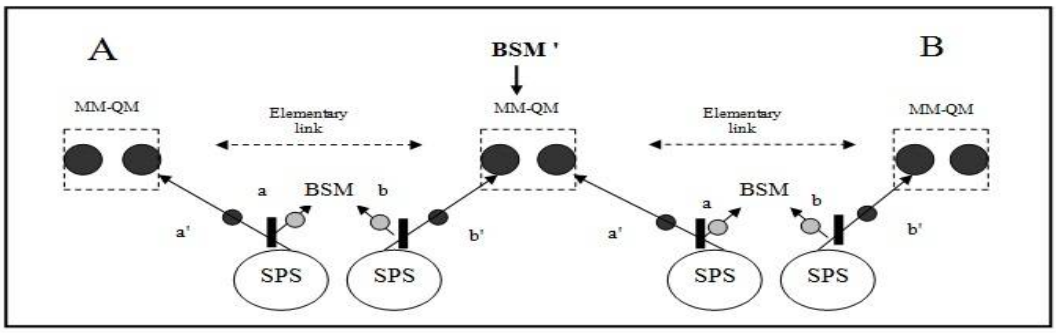

Figure 4.Quantum repeater scheme using single photon source protocol SPS. Sources and memories are represented by circles. Vertical bars denote beam-splitters BS.

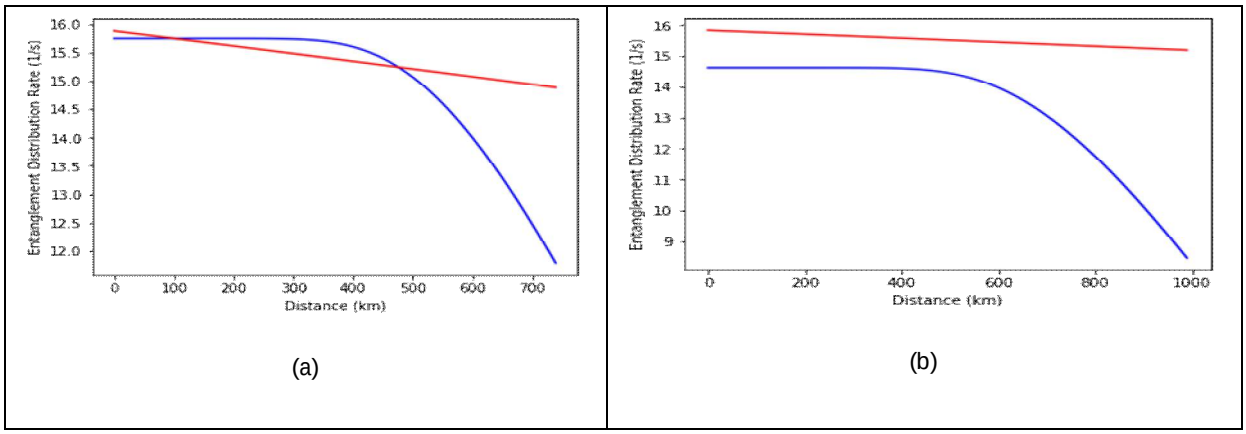

Figure5. Entanglement distribution rate with long distance, (red line) denoted the MQM with SPS, (blue line) denoted the MM-QM with PPS, $\eta_{mem} = \eta_d = \rho = 90\%, p_1 = 0.1, \beta = 0.16, \alpha = 0.2$ **dB/km,** $B = 100\ MHz$ **m = 100 modes, w = 10. (a) n = 4, (b) n = 5.**

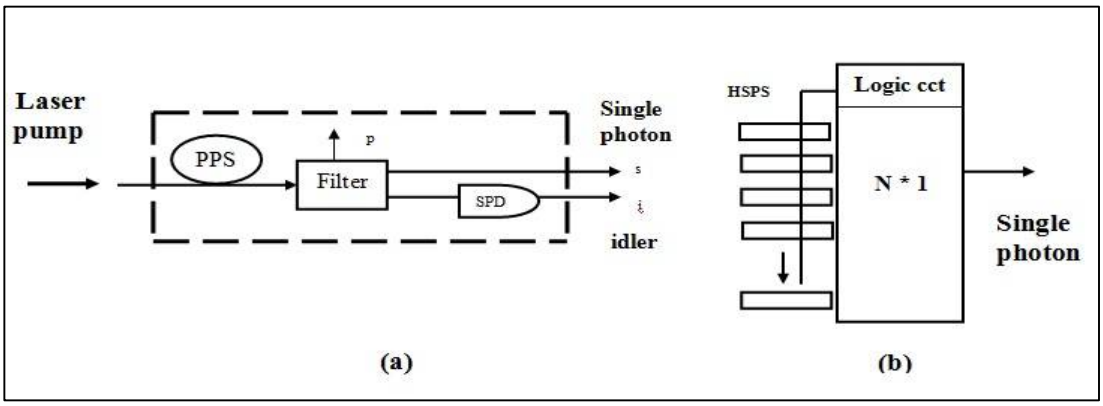

Figure 6.(a) Heralded single-photon source (HSPS). A laser pumps a parametric pair source, which spontaneously emits a signal and an idler photon. A filter splits the pump, signal, and idler. The idler photon is detected by a single-photon detector (SPD), heralding the presence of the signal photon. (b) A general multiplexed (MUX) single-photon source. N HSPSs are pumped all together, the idler photons are detected while the signal photons are stored in a long delay line. A classical logic unit determines the configuration for the N ×1 switching network based on the detection signals, routing a successfully produced single photon to the output [12].

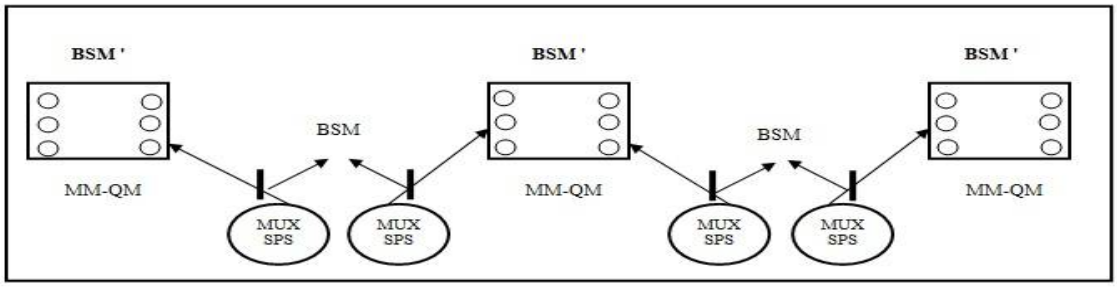

Figure7. The suggested QR scheme using MM-QM in combination with MUX-SPS.

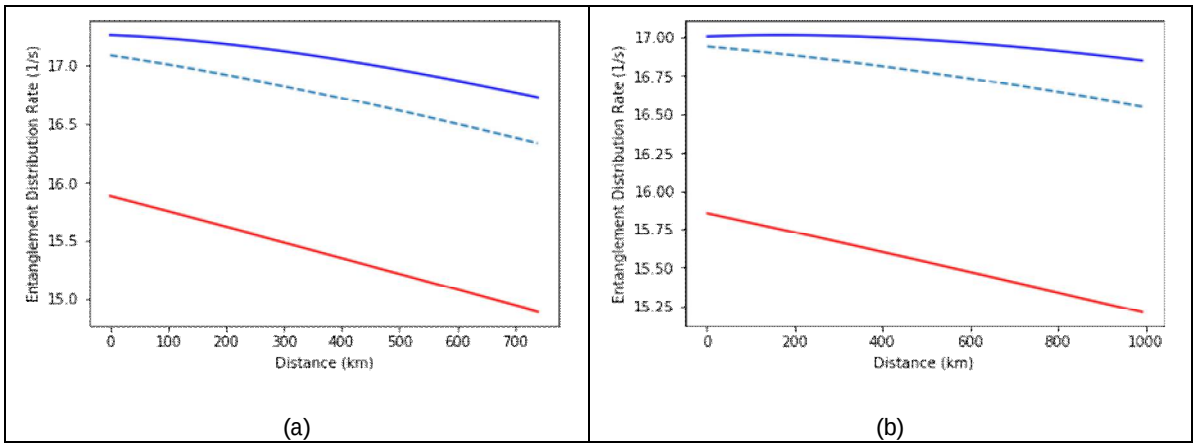

Figure 8. Entanglement distribution rate of QR based on MUX-SPS .(Blue line) of NRD-type of MUX-SPS with MM-QM.(Dashed line) of TD-type of MUX-SPS with MM-QM.(Red line) of SPS with MM-QM. N = 10, $|\xi|^2 = 0.5$; $\eta_i = \eta_s = 0.9$.(a) n = 4, (b) n = 5.

Indian Journal of Natural Sciences www.tnsroindia.org.in ©IJONS

Vol.9 /Issue 51 / December / 2018 *International Bimonthly* *ISSN: 0976 – 0997*

RESEARCH ARTICLE

Detection of IL11, IL8 and Some Blood Parameters in Recurrent Spontaneous Abortion in Sample of Iraqi Women

Aseel S. Mahmood* and Sabeeha A. Al- Sarray

Biotechnology Department, College of Science, University of Baghdad, Baghdad, Iraq

Received: 05 Sep 2018 Revised: 06 Oct 2018 Accepted: 10 Nov 2018

***Address for Correspondence**
Aseel S. Mahmood
Biotechnology Department,
College of Science,
University of Baghdad,
Baghdad, Iraq
E-mail: aseel78nm@yahoo.com

ABSTRACT

Recurrent miscarriage is defined as three or more consecutive miscarriages before 20 weeks of gestation, considers is common occurrence and often changes among different communities, this paper is aimed to determine the role ofInterleukin-11 andInterleukin-8 in recurrent miscarriage. This study included 45 abortive Iraqi women with (three, four and six abortion) and15 apparently healthy pregnant women who represented a control group. All participants were subjected to several tests as measurements IL-11 and IL-8 as well as some blood parameters. The results of this study demonstrated that aborted women with 6 abortion have the highest level of IL11 and IL8 , The Mean ± SE of IL-11 ,IL-8 (136.86 ± 2.84 , 152.22 ± 1.66) compared with control(75.50 ± 1.01 d,85.63 ± 0.86 d) respectively ,(P-value≤0.0001). as well as hematological parameters show highly significant differences in all groups. It can be concluded that serum interleukin-11 and interleukin-8 was increased in patients as compared to the control group. Study deduces that IL-11 and IL-8 involved in the induction of occurring of repeated abortion.

Key words: recurrent spontaneous abortion, Interleukin-11, Interleukin-8

INTRODUCTION

Recurrent miscarriage refers to the consecutive loss of pregnancy before the 20th gestational week for three or more times (Szekeres-Bartho *et al*.,2008).A number of etiological factors have been described for recurrent miscarriages, including immunologic factor, genetics, endocrine disorder, placental abnormality, environmental factors, nutritional, and infection with microorganisms like rubella, *Toxoplasma gondii*, , herpes ,Cytomegalovirus, syphilisand maternal disease such as thyroid disease and diabetes mellitus (Abdul–HadiCHabuk et al.,2016). Immune cells like T cells may play an important role in implantation process and in the phenomenon of fetal allograft tolerance as in pre-implantation and embryo development (Piccinni *et al*., 2015).Pregnancy requires physiological adaptations in all

maternal systems, including the immune system. Cytokines were a critical immune regulatory molecules, responsible for determining the nature of an immune response, have been shown to influence on all steps of reproduction and playing a fundamental role in pregnancy outcome (Sharief et al.,2014)

There are two distinctive cytokine profiles, leading to their classification as Th1 and Th2. The differences in cytokines produced by these cells lead to differences in immune function. Th1-type cytokines, especially IFN-y and TNF-α have been demonstrated to impair embryo development and trophoblast growth in vitro, and to mediate abortion in mice. The cytokines IFN-y and TNF- αre involved in apoptosis of trophoblast cells and can also inhibit outgrowth. On the other hand, the Th2-type cytokines, IL-4 and IL-10, are found in the decidua during normal murine pregnancy. It has been suggested that a predominantly Th1 response at the maternal-fetal interface is associated with fetal loss, while a predominantly Th2 response is associated with fetal survival(Chao et al., 1995;Chenet al.,1995;Ho HN et al;1996) Interleukin-11 is one of the IL-6 family of cytokines. Quondam studies were suggested that IL-11 perhaps play a role of endometrial function in human.Studied in mice have Proposed the paramount of IL-11 in succeeded pregnancy outcome infemale mice .IL-11 perhaps play different roles in function of endometrium and implantation.(Laird et al.,2006).Interleukin (IL)-8 is a chemokine produced by macrophages and other cell types such as pithelial cells. Indeed, IL-8 induces chemotaxis of neutrophils, hence other granulocytes to migrate toward the site of infection(Sensini,2006),their action is directed towards either myeloid or non myeloid cellular targets (Mohammedet al.,2012). IL-8 also produces from endometrium that is abortogenic. The myometrium, endometrium, and outer decidua contain mast cells that are increased by more than ten-fold in decidua in abortions. Mast cells are essential for inflammation by liberating several multifunctional cytokines including IL-8(Al-Dahmosh et al.,2013).

The haemostatic system plays an important role in the successful completion of implantation and placentation. The implantation of the fertilized egg into the uterine deciduas is linked to compatible contact between the fetus, placenta and mater-nal circulation. The contact between the placenta and maternal circulation is of vital importance to the success of the pregnancy. Prothrombotic changes and thrombosis prevent this process and may cause miscarriage(Van Dreden et al.,2012).

MATERIALS AND METHODS

Patients and control

The present study was conducted in the city of Baghdad, Iraq, throughout the period between march 2018 and June 2018. The study was carried out with the participation of 45 Iraqi women who have had recurrent abortions, and a further 15 healthy pregnant Iraqi women who collectively represented the control group. The subjects were divided into three groups: a) subjects suffering from three abortion, b) subjects suffering from four abortion c) subjects suffering from six abortion.

Blood collection

Five ml of venous blood sample was obtained from each patient and control subject by sterile disposable syringe under sterile condition, put into sterile gel tube, was let to stand for half to one hour at room temperature, after clotting the centrifugation was carried out at 3000 rpm for 5 minutes, then the serum was divided into two equal parts, the first part was used for haematological test and the second part put into a sterile plan tube was kept at -20° C until being used for immunological tests. laboratory findings: WBC(White blood cell) , HGB(Hemoglobin), PLT(Platelet Count) and PCT(Procalcitonin).

Immunological tests

For determination the levels of IL8 and IL11, the enzyme-linked immunosorbent assay (ELISA) technique and the kit (Homo sapiens (Human) was used

Statistical Analysis

The Statistical Analysis System- SAS (2012) program was used to effect of difference factors in study parameters. Least significant difference –LSD test (ANOVA) was used to significant compare between means variables in this study.

RESULTS AND DISCUSSION

The results showed in Table (1) highly significant increase in IL-11 concentration in group three for six abortion (136.86 ± 2.84 a) followed by group of four abortion(107.60 ± 1.76).followed by group of three abortion(92.36 ± 1.62 c) Regarding the distribution groups of Recurrent miscarriage among to numbers abortions compared to control(75.50 ± 1.01) was significant difference at ($p<0.0001$) between different groups. There are few studies looking at endometrial IL-11 in women with implantation failure or recurrent miscarriage. However, one study has suggested that IL-1l production is compromised in stromal cells derived from the endometrium of women with infertility (Karpovich et al., 2005) and another study has shown decreased expression ofIL-11 in epithelial cell, but not IL-11Rαrecepter in the endometrium of recurrent miscarriage women compared with controls (Linjawi et al., 2004).Chen et al., 2002,and Chen et al.,2004 found thatIL-11 expression in both chorionic villi and decidua were higher in women with normal pregnancies compared with women with anembryonic pregnancies. IL-11 is expressed by both stromal and epithelial cells, although expression in stromal cells is negligible until the late secretory phase of the cycle, where concentrations increase during decidualization. In contrast, epithelial IL11 expression is greatest in the early secretory phase of the cycle (von Rango et al., 2004), and this differential expression in the two different compartments may suggest that epithelial and stromal IL-11 may play different roles in endometrial function. IL-11 has been shown to play a role in stromal cell decidualization in vitro (Dimitriadis et al., 2002).

Elevated levels of IL-11 appear detrimental for placental vasculature development; evidenced in vivo in mice, whereby exogenous IL11 resulted in striking morphological differences in the placental labyrinth (Winship et al., 2015), In settings of inflammation in other tissues, IL11 can act directly on macrophages and T cells to elicit an anti-inflammatory response (Ellis et al., 2006). Studies in mice have suggested the importanceIL-11in successful pregnancy outcome ,Female mice with eitheran inactive or null mutation for the IL-11 receptor IL-11R is fertile and their blastocysts implant ,IL-11 was expressed in endometrium, andexpression is menstrual dependent cycle,IL-11 is expressed by both(epithelial, stromal cells),epithelial IL-11 expression is greatest in the early secretory phase of the Cycle, differential expression in the two different compartments may suggest that epithelial and stromal IL-11 may play different roles in endometrial function and implantation.(Laird et al.,2006).The result in table (2) showed highly significant increase in IL-8 concentration in women with six abortion(152.22 ± 1.66) followed by women with four abortion(116.28 ± 1.92) followed by women with three abortion (100.52 ± 1.88) compared to control(85.63 ± 0.86).P-value ≤0.0001for all group.

The highest level of IL-8 in aborted women may be due to the release of IL-8 from the endometrium as well as from an increased number of resident mast cells that are degranulated in abortions. Uterine mast cells degranulate after stress exposure of pregnant mice, possibly leading to release of IL-8 and TNF-α that could be involved in abortions. Furthermore, during pregnancy, IL-8 is produced by a variety of cells, mainly monocytes and macrophages .IL-8 induced activation of neutrophils and elastase activity in the intrauterine environment that has been implicated in the mechanisms of rupture of fetal membrane and cervical ripening,IL-8perhaps play a vital role in the mechanism

inflammation leading to abortions by enrolling neutrophils and lymphocytes in the endometrium, increase of IL-8 in aborted women perhaps due to the release the endometrium to IL-8 addendum from an increased number of resident mast cells that are degranulated inabortions (Al-Dahmoshi*et al*.,2013) Elevation of IL-8 levels in the current study revealed increasing of infammatory process in aborted women and attraction of lymphocyte and neutrophil to endometrium. This result agrees with Zicari et al.(2002) who reported that infammatory cytokines such as IL-8 might plays a vital role in the mechanism of protease-induced neurogenic infammation leading to labor or abortions by enrolling neutrophils and lymphocytes in the endometrium. Furthermore, Madhappan, et al.(2003) proposed that IL-8 levels in fetal tissue samples from cases of miscarriage were elevated compared to those from an elective abortion group. On the other hand, Koumantaki et al. mentioned that women with spontaneous abortions had pointedly decreased plasma level of IL-8 compared to those with normal pregnancies.(Koumantaki et al.,2001)

The results in table 3 and table 4 showed highly significant differences in blood parameters between aborted women related toIL-11and aborted women related to IL-8 The assessment of WBC counts from blood samples is one of the most common approaches in evaluating the systemic inflammatory response and its intensity in non-pregnant women. During pregnancy, the maternal WBC count assessment has limited value owing to a broader range of reference values present across the trimesters than during non-pregnancy periods (Edelstam et al.,2001). Neutrophils are the major type of leucocytes on differential counts .This is likely due to impaired neutrophilic apoptosis in pregnancy (Gatti et al., 1994; Konijnenberget al.,1997) The result showed decreasing in haemogloben level in all groups compared to control and this may be due to hemodilution and partly due to increased platelet activation and accelerated clearance (Shehlata et al.,1999). Vitamin B12 deficiency can affect the pregnancy outcome for both mother and the offspring. For women who want to get pregnant, a vitamin B12 deficiency is considered an increased risk factor of developing pre-eclampsia, intra-uterine growth retardation, preterm labor(Sande et al.,2013).

Vitamin B12 is involved in the methionine metabolism and its deficiency is associated with hyperhomocysteinemia and vice versa. Vitamin B12 has been identified to play a pivotal role in RPL. The implicated mechanisms of vitamin B12 deficiency leads to faulty and sporadic ovulation producing a faulty oocyte. Also, vitamin B12 deficiency leads to incomplete trophoblastic invasion of spiral arteries thereby leading to defective placentation (Sawant , 2015). Vitamin B12 deficiency can also cause megaloblastoid uterine epithelium leading to early spontaneous abortion (Bennett ,2001).It is well known that pregnancy is a hypercoagulable state attributing to alterations of coagulation proteins Gersh et al.,2009; Patel et al.,2011).It is associated with changes in platelets functions and during pregnancy loss, and thrombocytic functions return to normal after 12 weeks (Bates et al.,2012). In the study of Van Dreden *et al*.,(2012), they observed an increasing level of platelet activating factors in serum samples from women who have suffered two or more RPL and they attributed its implications to placental function and fetal growth.

CONCLUSIONS

Immune system play a major role in successful pregnancy ,any alteration in immune cell during pregnancy period lead to complication and miscarriage , IL11 and IL8 show highly significant increasing in all group of abortion as well as blood parameters show slight increasing in all study group except for hemoglobin which shows slight decreasing in all group.

REFERENCES

1. Gersh KC, Nagaswami C, Weisel JW. Fibrin network structure and clot mechanical properties are altered by incorporation of erythrocytes. *ThrombHaemost* 2009; 102: 1169-1175.
2. Patel BG, Lessey BA. Clinical assessment and management of the endometrium in recurrent early pregnancyloss. *SeminReprod Med* 2011; 29: 491-506.

3. Bates SM, Greer IA, Middeldorp S, Veenstra DL, Prabulos AM, Vandvik PO, et al. VTE, thrombophilia, antithrombotic therapy, and pregnancy: Antithrombotic therapy and prevention of thrombosis, 9th ed: American college of chest physiciansevidence-based clinical practice guidelines. *Chest* 2012; 141(2Suppl):e691S-736S.
4. Van Dreden P, Woodhams B, Rousseau A, Favier M, Favier R. Comparative evaluation of Tissue factor and Thrombomodulin activity changes during normal and idiopathic earlyand late foetal loss: the cause of hypercoagulability? Thromb Res 2012;129:787-92..
5. Gatti L, Tinconi PM, Guarneri D, Bertuijessi C, Ossola MW, Bosco P, Gianotti G. Hemostatic parameters and platelet activation by flow-cytometry in normal pregnancy: a longitudinal study. Internat J Clin Lab Res. 1994;24(4):217–219.
6. Sande H V, Jacquemyn Y, Karepouan N and AjajiM(2013): Vitamin B12 in pregnancy: Maternal and fetal/neonatal effects. Open Journal of Obstetrics and Gynecology, 3(2013): 599-602.
7. Edelstam G, Lowbeer C, Kral G, Gustafsson SA, Venge P. New reference values for routine blood samples and human neutrophiliclipocalin during third-trimester pregnancy. Scand J Clin Lab Invest. 2001;61(8):583–92..
8. Konijnenberg A, Stokkers E, Post J. Extensive platelet activation in preeclampsia compared with normal pregnancy: enhanced expression of cell adhesion molecules. Am J Obstet Gynecol. 1997;176(2):461–469.
9. Bennett M (2001): Vitamin B12 deficiency, infertility and recurrent fetal loss. The Journal of reproductive medicine, 46(3):209-212.
10. Sawant V (2015): The role of serum vitamin B12 and homocysteine in recurrent pregnancy loss. Indian Journal of Scientific Research, 6(2):91.
11. Shehlata N, Burrows RF, Kelton JG. Gestational thrombocytopenia. ClinObstet Gynecol. 1999;42:327–334.
12. Zicari A, Ticconi C, Realacci M, Cela O, Santangelo C, Pietropolli A, et al. Hormonal regulation of cytokine release by human fetal membranes at term gestation: Effects of oxytocin, hydrocortisone and progesterone on tumour necrosis factor-alpha and transforming growth factor-beta 1 output. J ReprodImmunol 2002;56:123-36.
13. Madhappan B, Kempuraj D, Christodoulou S, Tsapikidis S, Boucher W, Karagiannis V, et al. High levels of intrauterine corticotropin-releasing hormone, urocortin, tryptase, and interleukin-8 in spontaneous abortions. Endocrinology 2003;144:2285-90.
14. Koumantaki Y, Matalliotakis I, Sifakis S, Kyriakou D, NeonakiM,Goymenou A, et al. Detection of interleukin-6, interleukin-8, and interleukin-11 in plasma from women with spontaneous abortion. Eur J ObstetGynecolReprodBiol 2001;98:66-71.
15. Szekeres-Bartho J, Balasch J. Progestagen therapy for recurrent miscarriage. Hum Reprod Update 2008; 14: 27–35
16. Michimata T. , Sakai M., Miyazaki S., Ogasawara M.S., Suzumori K., Aoki K., Nagata K. and Saito S., Decrease of T-helper 2 and T-cytotoxic 2 calls at implantation sites occurs in unexplained recurrent spontaneous abortion with normal chromosomal content, Hum. Reprod., 18, 1523-1528 (2003)
17. Mohammed K.G., El-Shammary A.B., Al-Jobouri S.A. and Al-Sagheer H.A, The role T-helper-17 in toxoplasmosis among women with abortion, Kufa Med. J., 15(1), 239-244 (2012)
18. Ito M., Nakashima A., Ina S., Okabe M., Bac N.D., Yoneda S., Shiozaki A., Tsuneyama K., Nikaido T., Hidaka T. and Saito S., Interleukin-17 (IL-17) and tumor necrosis factor a synergistically increase IL-8 production by amniotoicmethenchymal cells in preterm delivery cases with chorioamnionitis, J. Reprod. Immunol., 84, 75–85 (2010)
19. Al-Dahmoshi, Hussein O.M.; Al-Mammori, Raheem T.O ; ShareefHasanain K.I. , Al-Khafagee Noor S.K.(2013). Study of IL-8 and IL-17 levels among certain group of Repeated Spontaneous Abortion Women with or without Toxoplasmosis, Iraq. International Research Journal of Biological Sciences. Vol. 2(8), 37-41.
20. Roua Jamal AbdulkhaliQ1 , Sabaataher Mohammed2 , Ahmed Abdul-Hassan Abbas. 2017. The Role of Some Cytokines inwomenwithRecurrent Abortion in Iraqi Women. P J M H S Vol. 11, NO. 2, APR – JUN 2017.
21. Abdul–HadiCHabuk F. R. H., Al-Saadi H. K. Z. and AlHamairy A. K. Effect of the Experimental Infection with Toxoplasma gondii on some Biochemical aspects and Histological Changes for the Liver and Spleen in Female Rats.International Journal of PharmTech Research. 2016, 5(11): 142-150

22. Madhappan B., Kempuraj D., Christodoulou S., Tsapikidis S.,Boucher W., Karagannis U., Athanassiou A. andTheoharidesT.C., High levels of Intrauterine Corticotropinreleasing,hormone, Urocortin, Tryptase, and Interleukin-8 inspontaneous abortions, *Endocrinology*, 144, 2285-2290(2003)
23. Sharief M., Mohammed R. and Shani W. S. The role of Th1 and Th2 cytokines among women with recurrent spontaneous miscarriage. Scientific J Med Sci. 2014, 3(7) 345-351.
24. Piccinni M. R., Lombardelli L., Logiodice F.,. T helper cell mediated-tolerance towards fetal allograft in successful pregnancy. *Clinical and Molecular Allergy*. 2015, 13(1): 9-12.
25. Karpovich N, Klemmt P, Hwang JH et al. 2005 The production of IL11 and decidualisation are compromised in endometrial stromal cells derived from patients with infertility. Journal of Clinical Endocrinology and Metabolism 90, 1607–1612.
26. Linjawi S, Tuckerman EM, Blakemore AIF et al. 2004 Expression of IL11 and IL11Rα in the endometrium of women with recurrent miscarriage. Journal of Reproductive Immunology 64, 145–155
27. Chen HF, Chao KH, Shew JY et al. 2004 Expression of LIF and its receptor is not altered in the decidua and chorionic villi of human anembryonic pregnancy. Human Reproduction 19, 1647–1654.
28. Chen HF, Lin CY, Chao KH et al. 2002 Defective production of IL-11 by decidua and chorionic villi of human anembryonic pregnancy. Journal of Clinical Endocrinology and Metabolism 87, 2320–2328.
29. Dimitriadis E, Robb L, Salamonsen LA 2002 IL11 advances progesterone-induced decidualisation of human endometrial stromal cells. Molecular Human Reproduction 8, 636–643.
30. Von Rango U, Alfer J, Kertschanska S et al. 2004 IL11 expression: its significance in eutopic and actopic human implantation. Molecular Human Reproduction 10, 783–792
31. LairdS.M., TuckermanE.M.,andLi TS. 2006 .Cytokine expression in the endometrium of women with implantation failure and recurrent miscarriage. Vol 13 No 1. 2006 13–23
32. SAS. 2012. Statistical Analysis System, User's Guide. Statistical. Version 9.1th ed. SAS. Inst. Inc. Cary. N.C. USA
33. Chao KH, Yang YS, Ho HN et al. Decidual natural killer cytotoxicity decreased in normal pregnancy but not in anembryonic pregnancy and recurrent spontaneous abortion. AM J ReprodImmunol 1995; 34:274-80.
34. Ho HN, Chao KH, Chen CK et al. Activation status of T and NK cells in the endometrium throughout menstrual cycle and normal and abnormal early pregnancy. Hum Immunol 1996; 49:130-36
35. Chen HF, Ho HN, Chen SU et al. Interleukin-1 beta (IL-1 beta) is increased in the follicular fluids of patients with premature luteinization. Am J ReprodImmunol 1995; 34:356-62.
36. Sensini A. Toxoplasma gondii infection in pregnancy: Opportunities and pitfalls of serological diagnosis. ClinMicrobiol Infect 2006;12:504-12.
37. Ellis et al., 2006M. Ellis, *et al.*Modulation of the systemic inflammatory response by recombinant human interleukin-11: a prospective randomized placebo controlled clinical study in patients with hematological malignancy Clin. Immunol., 120 (2006), pp. 129-137
38. Winship et al., 2015 A.L. Winship, *et al.*Interleukin-11 alters placentation and causes preeclampsia features in mice Proc. Natl. Acad. Sci. U. S. A., 112 (2015), pp. 15928-15933
39. SM Laird, EM Tuckerman, T-C Li.2006.Cytokine expression in the endometrium of women with implantation failure and recurrent miscarriage.*Vol 13 No 1. 13–23.*
40. Zicari A., Ticconi C., Realacci M., Cela O., Santangelo C.,Pietropolli A., Russo M.A. and Piccione E., (2002) Hormonalregulation of cytokine release by human fetal membranes atterm gestation:effects of oxytocin, hydrocortisone andprogesterone on tumor necrosis factor-alpha and transforminggrowth factor-1 output, *J.Reprod. Immunol.*, 56, 123-136
41. Al-Dahmoshi, Hussein O.M.; Al-Mammori, Raheem T.O.; ShareefHasanain K.I., Al-Khafagee Noor S.K.2013.Study of IL-8 and IL-17 levels among certain group of Repeated Spontaneous Abortion Women with or without Toxoplasmosis, Iraq. Vol. 2(8), 37-41, *Int. Res. J. Biological Sci.*

Table 1. IL-11 concentration in studies group

Abortion group	Mean ± SE of IL-11
Three times	92.36 ± 1.62a
Four times	107.60 ± 1.76 b
Six times	136.86 ± 2.84 c
Control	75.50 ± 1.01 d
LSD value	5.459 **
P-value	0.0001
** (P<0.01).Means having with the different letters in same column differed significantly	

Table 2. IL-8 concentration in studies group

Abortion group	Mean ± SE of IL-8
3	100.52 ± 1.88a
4	116.28 ± 1.92 b
6	152.22 ± 1.66 c
Control	85.63 ± 0.86 d
LSD value	4.652 **
P-value	0.0001
** (P<0.01).Means having with the different letters in same column differed significantly	

Table 3. Hematological parameters in abortion groups related to IL-11

Abortion group : IL-11	Mean ± SE			
	WBC	HGB	PLT	PCT
3	9.15 ± 0.50ab	9.50 ± 0.22 c	319.93 ± 24.26 a	0.258 ± 0.01 a
4	7.33 ± 0.13 c	8.98 ± 0.14 c	264.67 ± 12.67 b	0.241 ± 0.01 b
6	9.26 ± 0.13 a	10.59 ± 0.22 b	337.26 ± 14.93 a	0.276 ± 0.01c
Control	8.38 ± 0.15 b	12.84 ± 0.25 a	294.53 ± 14.96ab	0.170 ± 0.01d
LSD value	0.793 **	0.619 **	48.99 **	0.027 **
P-value	0.0001	0.0001	0.0056	0.0001
** (P<0.01). Means having with the different letters in same column differed significantly				

Table 4. Hematological parameters in abortion groups related to IL-8

Abortion group : IL-8	Mean ± SE			
	WBC	HGB	PLT	PCT
3	8.95 ± 0.15ab	9.86 ± 0.14 b	331.20 ± 18.80 a	0.270 ± 0.01 a
4	7.49 ± 0.17 c	9.41 ± 0.25 b	223.20 ± 4.80 c	0.220 ± 0.01 b
6	9.46 ± 0.46 a	9.87 ± 0.09 b	269.53 ± 9.86bc	0.232 ± 0.01c
Control	8.38 ± 0.15 b	12.84 ± 0.26 a	294.53 ± 14.96ab	0.170 ± 0.01d
LSD value	0.771 **	0.566 **	37.42 **	0.0222 **
P-value	0.0001	0.0001	0.0001	0.0001
** (P<0.01). Means having with the different letters in same column differed significantly				

Indian Journal of Natural Sciences www.tnsroindia.org.in ©IJONS

Vol.9 /Issue 51 / December / 2018 *International Bimonthly* *ISSN: 0976 – 0997*

RESEARCH ARTICLE

Improving Dephasing Parameter of Sequential Quantum Repeater Using Non Identical Quantum Memories

Adnan N. Kadhim*, Jawad A. Hasan and Wijdan M. Alkhalidy

Institute of Laser for Postgraduate Studies, University of Baghdad, Baghdad, Iraq

Received: 06 Sep 2018 Revised: 10 Oct 2018 Accepted: 13 Nov 2018

***Address for Correspondence**
Adnan N. Kadhim
Institute of Laser for Postgraduate Studies,
University of Baghdad,
Baghdad, Iraq
E-mail:

ABSTRACT

One of the remarkable issues of quantum key distribution (QKD) is the subject of how to distribute key over randomly long distances. The transitivity of an optical channel diminishes quickly as the length of the channel develops (exponentially, on account of fiber). To overcome this issue, quantum repeaters (QRs) are first proposed by Briegel et al. [1], where an entanglement connection method is utilized to expand the whole length of entanglement by using multi pairs quantum memories (QMs) components. Previous QRs use ***identical*** quantum memories (QMs) to include their nodes [2]. The execution of the quantum channel is influenced by the dephasing parameter $f_{dp[n]}$ alludes to the degradation of the state stored in a QM after some time. Thus, our scheme of QRs utilizing ***non - identical*** QMs of various decoherence (storage) times T_2 and efficiencies, of the QRs nodes is proposed here to increase the dephasing parameter $f_{dp[n]}$ and lessen the errors caused by dephasing. Practically, entangling two non-identical QMs is demonstrated [3,4]. The outcomes show that the proposed QRs scheme demonstrates better execution contrasted with the schemes utilizing ***identical*** QMs.

Key words: Quantum Communication, Quantum Key Distribution, Quantum Repeater, Quantum Memories, Entanglement

INTRODUCTION

The present advances in the field of quantum data have conveyed various fascinating and novel developments. While an expansive number of these developments are still in their most earliest stages, and not physically executed, some quantum progresses, in a general sense quantum key distribution (QKD), have recently been promoted [5].

Regardless of QKD being a more creative development appeared differently in relation to its quantum accomplices, in spite of all that it faces an underlining issue. Long distance communications have not been recognized, with current records on the demand of a few hundred kilometers [6]. This obstacle is a consequence of the loss experienced by photons as they travel through media.To overcome this issue intermediate stations (relays) prepared among Alice and Bob, who by then freely use QKD to develop secret keys with it [7]. The relay could at that point make alone secret key for Alice and Bob to use. Then again, messages could be coordinated through the relay, which encrypts and decrypts the messages using the two secret keys as appropriate. The idea can be immediately connected with various intermediate stations reaching out over a subjective distance.

These intermediate or relays stations are depicted as quantum repeaters [8]. First proposed in [1], quantum repeaters are associate quantum devices set along the channel among Alice and Bob, sufficiently isolating it into various low-loss channels. A full repeater plan may incorporate the use of various stations, each containing diverse qubits [9,10,11,12,13,14]. The basic thought of most quantum repeater plans is to segment the general channel into N smaller channel portions known as links. Generally, the capacity of the quantum channel scales straightly with transmitivity η, while isolating the channel to numerous connections will empower the key rate to scale as $\eta^{1/N}$. For the quantum repeater to fill in as arranged, there must be some additional helper devices between links alluded to as nodes, every one of which includes two quantum memories (QMs). The system will utilize an entanglement swapping plan at each node, adequately connecting the links together [2]. Quantum memories are an important part in various quantum repeater schemes, which can be characterized as any physical system that can create, store, and read-out a quantum state [15]. there are various assortments of QMs, each with their own specific subtleties.

The significant properties for QM execution are the preparation efficiency, the preparation time of generating a memory-photon entangled state, the de coherence time T_2 of the stored state, the efficiency of coupling the photon into the fiber, and the wavelength of emitted photons. If QMs are executed in a communication channel, de coherence times ought to be sufficiently longer than communication times so as to less error. also, the wavelength of emitted photons is important too, as the attenuation and dispersion of photons in fiber are dependent on wavelength. The most insignificant fiber attenuation occurs around 1550 nm [16], making it an ideal wavelength for communications. In the event that the photons emitted by the QMs are not at a sensible wavelength for low- loss in a fiber, a wavelength conversion must be performed There have been different proposed and shown physical executions for QMs, including yet not confined to nitrogen-vacancy centers [17, 18], trapped atoms [19, 20], and atoms in optical cavities [21]. Trapped ions have been shown to have de coherence times on the request of seconds [22, 23, 24], while the coupling efficiency is around 0.03%-0.05% [25, 26]. In any case, the coupling efficiencies can be expanded to more than 30% by utilizing optical cavity [27].

Most quantum repeater QRs contains two identical QMs in each node [2], each node capable of emit entangled memory-photon states on demand with some probability. The emitted photons, which acquired initially with a particular laser-matter interaction, are sent through a fiber to Alice and Bob, where they are detected in the computational or diagonal bases. A Bell state measurement BSM is performed on the two states stored in the QMs as Alice and Bob herald a successful detection. While an optical Bell state measurement OPSM performed on the emitted photons between the inner nodes. In the case of successful detection, then entanglement of identical [28,29] will be created between these nodes as appeared in Fig.1.

The activity of quantum repeater also requires a classical channel associating the two distant parties,, the majority of the nodes, and optical Bell state together to make the entanglement swapping conceivable [30].To start a quantum channel decoherence time T_2 of first quantum memory must adequate to effectively cover every one of the tasks times of the steps specified above, which imply that the first quantum memory has longer storage time than the others. So it might be helpful to utilize non identical kinds of QMs in every node to utilize the trade of T_2, efficiencies and waiting time.

Entanglement between non- identical atoms is exhibited by two groups of scientists from University of Oxford and the other from the National Institute of Standards and Technology and the University of Washington [3, 4]. The group from University of Oxford [3] utilize two unique isotopes of calcium, while the other group utilizes beryllium and magnesium atoms [4]. The calcium particles could keep their states for about a minutes and about a second and a half for beryllium atoms. The two groups expressed that their two atoms are entangled with a high probability arranged by 0.998 for the first and 0.979 for the second. Related to every quantum memory is a dephasing (decoherence) time T_2 . The dephasing alludes to the degradation of the state stored in a QM after some time. The dephasing parameter $f_{dp[n]}$ which is related with the error presented by dephasing in the QMs is given by:

$$f_{dp}[n] = \mathrm{E}\left[e^{-\sum_{i=1}^{i=2n} t_i / T_2} \right] \quad \text{.....(1)}$$

Where t_i is the waiting time or communication time in each quantum memory.

The dephasing parameter $f_{dp[n]}$ depends upon the sum of the general storage times of states in every quantum memory, for the sequential protocol considered in our study, we can decide an unequivocal condition for this expression. Using the quantum memory numbering convention in Fig. 1 and expecting the protocol works from Alice to Bob, the odd numbered QMs in each node store their states longer than the even numbered QMs. This is a result of the odd numbered QMs sitting tight for the dynamic interface with effectively herald a detection before a Bell state measurement can be performed on the two QMs in a node, while the even numbered QMs simply need to sit tight for the classical communication time from the heralding signals. This recommends the states stored in the even numbered QMs will have a touch of holding up time, and accordingly a lower dephasing error. For example, Table (2) explicitly shows the waiting time of the QMs in a three-nodes quantum repeater. The connection time constants τ_i represent the repetition rate of a trial per link [2]:

for inner links:

$$\tau_p = \frac{L_i}{c} + T_{prep} \quad \text{.....(2)}$$

While for the outer link:

$$\tau_b = \frac{2L_b}{c} + T_{prep} \quad \text{.....(3)}$$

Generally the equation of the daphasing parameter $f_{dp[n]}$ for n - node identical QMs sequential quantum repeater can be written as follows [2].

$$f_{dp}[n] = e^{\frac{-(3-2x)L}{cT_2}} \left(\frac{P_{OBSM}}{e^{\tau_p / T_2} + P_{OBSM} - 1} \right)^{n-1} \left(\frac{P_b}{e^{\tau_b / T_2} + P_b - 1} \right) \quad \text{.....(4)}$$

Where, n is number of nodes and P_{OBSM} represents the success probability of optical Bell state measurement OBSM, if there is no mode – mismatching ($\gamma = 1$) and in the absence of dark count this probability is:

$$P_{OBSM} = 0.5\eta_{inner}^{2} \quad \text{.....(5)}$$

$$\eta_{inner} = \eta_{tot} . e^{-\frac{Li}{2Latt}} \quad \text{.....(6)}$$

And $\eta_{tot} = \eta_p \eta_\lambda \eta_c \lambda_d$ which represents the total efficiency of the channel.

Where, η_p : preparation efficiency, η_c : coupling efficiency, η_λ : wavelength conversion efficiency, and η_d : detector efficiency. The explanation and values of the parameters appeared in the Eqs.(1 - 6), are shown in table 1 [29]. The waiting times formulae of the QMs in a three-node quantum repeater are shown in table 2.

Proposed Repeater Architecture Scheme

Alluding to QR scheme by [2], here we present an architecture scheme for QR utilizing non identical QMs in every node as opposed to utilizing identical QMs in all nodes, contingent upon the possibility of entangling different kinds of QMs species accomplished by [3, 4] to abuse the diversity of decoherence times for each QM to improve the execution of the QR particularly the dephasing parameters $f_{dp[n]}$ as it is vital to diminish the error caused by dephasing. From Eq.4, the dephasing parameter $f_{dp[n]}$ limits to unity as the decoherence time $T_2 \to \infty$, which will vanish the impact of the error presented by dephasing [2]. As in [31, 32,2] there is a tradeoff between the QMs storage time (decoherence time) and their efficiencies, which constrains the execution of the QR. Moreover, the creation of long decoherence time memories with high fidelity isn't simple [33]. So our scheme (non identical QMs repeater) planned to improve the QR execution by utilizing a limited number of long decoherence time QMs in the QR nodes while it is better to use the high efficiency QMs of short decoherence time for the rest nodes of the QR.

Table 2 outlined the waiting times for each QM of the QR recommended by Christian [2]. Clearly, QM1 needs the longest waiting time in this manner we propose that QM1 must be chosen from long decoherence time memory species, while other odd QMs require less decoherence time, and even QMs require shorter decoherence time contrasted with the odd QMs. This design will diminish the errors caused by dephasing in QMs and improve Table the ability of QR in distributing the entanglement for long distances. The equation of dephasing parameter (Eq.1) must be re- formulated in the accompanying method to be compatible with our scheme of non identical QMs repeater, as in Eq.7

$$f_{dp}[n] = \mathrm{E}\left[e^{-\sum_{i=1}^{i=2n} t_i / T_i} \right] \quad \text{.....(7)}$$

Where T_i represent the decoherence time for the it QM and $1 \le i \le 2n$.

Substituting the values for t_i illustrated in table (2) for three node QR scheme result in:

$$f_{dp}(n) = \mathrm{E}[e^{-\frac{2L_a + L_i}{T_1 c}} . e^{-\frac{2L_i + 2L_b}{T_2 c}} . e^{-\frac{4L_i}{T_3 c}} . \prod_{i=1}^{i=n-1} e^{-\frac{\tau_p Q_i}{T_i}} . e^{-\frac{\tau_b Q_b}{T3}}] \quad \text{..... (8)}$$

Where Q_i, Q_b are all independent random variable.

For any geometric random variable Q with a probability of success p, the expectation value $\mathrm{E}[e^{-aQ}]$ can be written as:

$$E[e^{-aQ}] = \sum_{k=1}^{\infty} p(1-p)^{k-1} e^{-aQ} = \left(\frac{p}{e^{a} + p - 1} \right) \text{.....(9)}$$

Where a is a constant.

Hence, (Eq. 8) can be simplified and re written as follows:

$$f_{dp}(n) = e^{-\frac{2La + Li}{T_1 c}} . e^{-\frac{2Li + 2Lb}{T_2 c}} . e^{-\frac{4Li}{T_3 c}} . \left[\frac{P_{OBSM}}{e^{\tau_p / T_1} + P_{OBSM} - 1} \right] .$$

$$\left[\frac{P_{OBSM}}{e^{\tau_p / T_3} + P_{OBSM} - 1} \right] . \left[\frac{P_b}{e^{\tau_b / T_3} + P_b - 1} \right] \text{.....(10)}$$

Generalize (10) for n-node sequential QR leads to:

$$f_{dp}(n) = e^{-\frac{2La + Li}{T_1 c}} . e^{-\frac{(n-1)Li + 2Lb}{T_2 c}} . e^{-\frac{(2n-2)Li}{T_3 c}} . \left[\frac{P_{OBSM}}{e^{\tau_p / T_1} + P_{OBSM} - 1} \right] .$$

$$\left[\frac{P_{OBSM}}{e^{\tau_p / T_3} + P_{OBSM} - 1} \right]^{(n-2)} . \left[\frac{P_b}{e^{\tau_b / T_3} + P_b - 1} \right] \text{.....(11)}$$

Where, T_1 is the decoherence time for QM1, T_2 decoherence time for all even QMs, and T_3 decoherence time for odd QMs except QM1.

To compare the impact of various decoherence times on the dephasing parameter $f_{dp[n]}$ of n (let n = 3, 5, 7, 9, 25) node identical OMs repeater scheme of QMs decoherence time (T_2 = 60s [3] with efficiency of 0.009) and for n (let n = 3, 5, 7, 9, 25) node non identical QRs of QMs decoherence times (T_1 = 60s with efficiency of 0.009, $T_2 = T_4 = T_6$ = 1.5s [4] with efficiency of 0.09, and $T_3 = T_5$ = 16 s [34] with efficiency of 0.03), Fig.2, demonstrates that of the non identical QMs repeater scheme is superior to that of the identical QMs repeater scheme and it is expanded with expanding the number of nodes, which totally enhances the rate at which quantum key will be appropriated from Alice to Bob

CONCLUSIONS

From the non identical QR scheme proposed in this paper it tends to be seen that the interaction between the decoherence time and efficiency prompts enhance $f_{dp[n]}$ when contrasted with that of the identical QR as appeared in Figs (2). Also, our scheme is desirable since the realization of all QMs with long decoherence time in the identical QR repeater scheme is not simply done.

This discussion is interpretable since at a certain location of QR nodes of the Q channel such as the first node the decoherence time is the powerful parameter to achieve the entanglement distribution to the whole nodes of the channel. So it is desirable to utilize QMs types of long decoherence time regardless of whether they have low efficiencies. Whereas other nodes in the channel require less memory life time, so the efficiency related with these types of memories can be exploited to improve the execution of QR by increasing $f_{dp[n]}$. This approach is by all accounts sensible and bolstered by the discoveries of the specialists about the opposite relationship of the memory life time with its efficiency.

ACKNOWLEDGMENT

We would like to express our deep gratitude and appreciation to the members of photonic department for their helpful suggestions.

REFERENCES

1. H. J. Briegel, W. Dur, J. I. Cirac, and P. Zoller, Phys. Rev. Lett. 81, 5932 (1998).
2. Christian Mastromattei. Assessing the Practicality of a Simple Multi-node Quantum Repeater. MSc Thesis, University of Waterloo, Ontario, Canada, (2017).
3. C. J. Ballance, V. M. Sch afer, J. P. Home, D. J. Szwer, S. C. Webster, D. T. C. Allcock, N. M. Linke, T. P. Harty, D. P. L. Aude Craik, D. N. Stacey, A. M. Steane and D. M. Lucas. Hybrid quantum logic and a test of Bell's inequality using two different atomic isotopes. Nature 528, 384–386 ,17 December (2015)
4. T. R. Tan, J. P. Gaebler, Y. Lin, Y. Wan, R. Bowler, D. Leibfried, and D. J. Wineland. Multi-Element Logic Gates for Trapped-Ion Qubits. Nature 528, 380–383 ,17 December (2015).
5. V. Scarani, H. Bechmann-Pasquinucci, N. J. Cerf, M. Dufisek, N. L utkenhaus, and M. Peev. The security of practical quantum key distribution. Rev. Mod. Phys., 81:1301{1350}, Sep (2009).
6. H.-L. Yin et al. Measurement-device-independent quantum key distribution over a 404 km optical fiber. Phys. Rev. Lett., 117:190501, Nov (2016).
7. C. Elliott, New Journal of Physics 4, 46 (2002).
8. S. Guha et al., Rate - loss analysis of an efficient quantum repeater architecture, arXiv: 1404.7183, (2014).
9. D. Luong, L. Jiang, J. Kim, and N. Lutkenhaus. Overcoming lossy channel bounds using a single quantum repeater node. Applied Physics B, 122(4):1-10, (2016).
10. H. Krovi, S. Guha, Z. Dutton, Joshua A. Slater, C. Simon, and W. Tittel, Applied Physics B, 122, 3, 1-8 (2016)
11. G.Z. Song , F. Zhou Wu, M. Zhang, and G.J. Yang, Scientific Reports, V (6), {28744} (2016).
12. F. Rozpdek et al. Parameter regimes for a single sequential quantum repeater. Quantum Sci. Technol. 3 034002, (2018).
13. Goodenough, K., Elkouss, D., and Wehner, S. Assessing the performance of quantum repeaters for all phase-insensitive gaussian bosonic channels. New Journal of Physics, 18(6):063005, (2016).
14. S. Muralidharan, J. Kim, N. Lutkenhaus, M. D. Lukin, and L. Jiang, Phys. Rev. Lett. 112, 250501 (2014).
15. C. Simon et al. Quantum memories. The European Physical Journal D, 58(1):1{22}, May (2010).
16. N. Massa. Fiber optic telecommunication. Fundamentals of Photonics. University of Conneticut, (2000).
17. L. Childress, J. M. Taylor, A. S. S_rensen, and M. D. Lukin. Fault-tolerant quantum communication based on solid-state photon emitters. Phys. Rev. Lett., 96:070504, Feb (2006).
18. S. E. Vinay and P. Kok. Practical repeaters for ultralong-distance quantum communication. Phys. Rev. A, 95:052336, May (2017).
19. B. B. Blinov, D. L. Moehring, L.-M. Duan, and C. Monroe. Observation of entanglement between a single trapped atom and a single photon. Nature, 428(6979):153{157}, Mar (2004).
20. J. Volz, M. Weber, D. Schlenk, W. Rosenfeld, J. Vrana, K. Saucke, C. Kurtsiefer, and H. Weinfurter. Observation of entanglement of a single photon with a trapped atom. Phys. Rev. Lett., 96:030404, Jan (2006).

21. H. P. Specht, C. Nolleke, A. Reiserer, M. Upho, E. Figueroa, S. Ritter, and G. Rempe. A single-atom quantum memory. Nature, 473(7346):190{193}, May (2011).
22. S. Olmschenk, K. C. Younge, D. L. Moehring, D. N. Matsukevich, P. Maunz, and C. Monroe. Manipulation and detection of a trapped Yb+ ion hyperfine qubit. Phys. Rev. A, 76:052314, Nov (2007).
23. R. D. Graham, S.-P. Chen, T. Sakrejda, J. Wright, Z. Zhou, and B. B. Blinov. A system for trapping barium ions in a microfabricated surface trap. AIP Advances, 4(5), (2014).
24. T. P. Harty, D. T. C. Allcock, C. J. Ballance, L. Guidoni, H. A. Janacek, N. M. Linke, D. N. Stacey, and D. M. Lucas. High-fidelity preparation, gates, memory, and readout of a trapped-ion quantum bit. Phys. Rev. Lett., 113:220501, Nov (2014).
25. S. Olmschenk, D. N. Matsukevich, P. Maunz, D. Hayes, L.-M. Duan, and C. Monroe. Quantum teleportation between distant matter qubits. Science, 323(5913):486{489}, (2009).
26. D. N. Matsukevich, P. Maunz, D. L. Moehring, S. Olmschenk, and C. Monroe. Bell inequality violation with two remote atomic qubits. Phys. Rev. Lett., 100:150404, Apr (2008).
27. T.Kim, P.Maunz, and J. Kim. Efficient collection of single photons emitted from a trapped ion into a single-mode fiber for scalable quantum-information processing. Phys. Rev. A, 84:063423, Dec (2011).
28. Horodecki, R., Horodecki, P., Horodecki, M. & Horodecki, K. Quantum entanglement. Rev. Mod. Phys. 81, 865–942 (2009).
29. Wen Wei Ho and Dmitry A. Abanin. Entanglement dynamics in quantum many-body systems. Phys. Rev. B 95, 094302, 1 March (2017).
30. L.-M. Duan, M. D. Lukin, J. I. Cirac, and P. Zoller, Nature 414, 413{418}, 22 November (2001).
31. P. Jobez, I. Usmani, N. Timoney, C. Laplane, N. Gisin and M. Afzelius. Cavity-enhanced storage in an optical spin-wave memory. New Journal of Physics 16, 083005, (2014).
32. Y.-W. Cho, G. T. Campbell, J. L. Everett, J. Bernu, D. B. Higginbottom, M. T. Cao, J. Geng, N. P. Robins, P. K. Lam, and B. C. Buchler, Highly efficient optical quantum memory with long coherence time in cold atoms. Optica, Vol. 3, Issue 1, pp. 100-107 (2016)
33. K. Khodjasteh, J. Sastrawan, D. Hayes, Todd J. Green, Michael J. Biercuk & L. Viola. Designing a practical high-fidelity long-time quantum memory. NATURE COMMUNICATIONS, 4:2045, Jun (2013).
34. Y. O. Dudin, L. Li, and A. Kuzmich. Light storage on the time scale of a minute. Physical Review A, 87:031801(R), (2013).

Table 1: Parameters description and values used for analysis of this quantum repeater system.

Parameters	Parameter Description	Experimental Value
T_{prep}	QM-Photon preparation time	2 μs
T2	QM dephasing time	(1 – 60) s
C	Speed of light in fiber	$2 * 10^8$ m/s
Latt	Fiber attenuation length	22 Km
eM	Misalignment parameter	0.01
P_{dark}	Dark count probability per detector	$1.8 * 10^{-11}$
η_d	Detector efficiency	0.7
PBSM	BSM success probability	1
λ_{BSM}	BSM ideality factor	0.98

Table 2: QM waiting times for a three-node quantum repeater. The parameter Qi denotes the number of trials the successive link requires [2].

Node	QM	Waiting Time
1	1	$\frac{2L_a}{c}+\frac{L_i}{c}+\tau_p Q_1$
1	2	L_i/c
2	3	$\frac{2L_i}{c}+\tau_p Q_2$
2	4	L_i/c
3	5	$\frac{2L_i}{c}+\tau_b Q_b$
3	6	$2L_b/c$

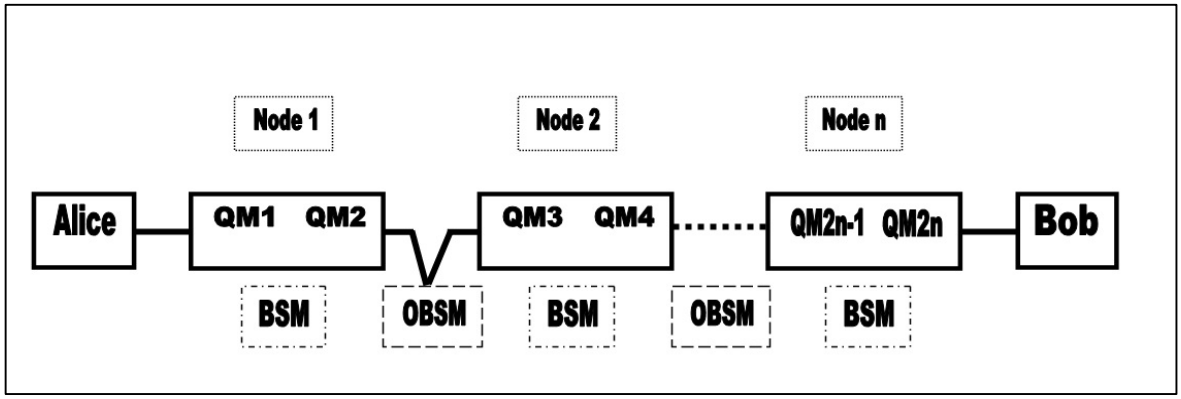

Figure 1: N - Node quantum repeater scheme, BSM performed inside each node, OBSM performed between each neighboring two nodes.

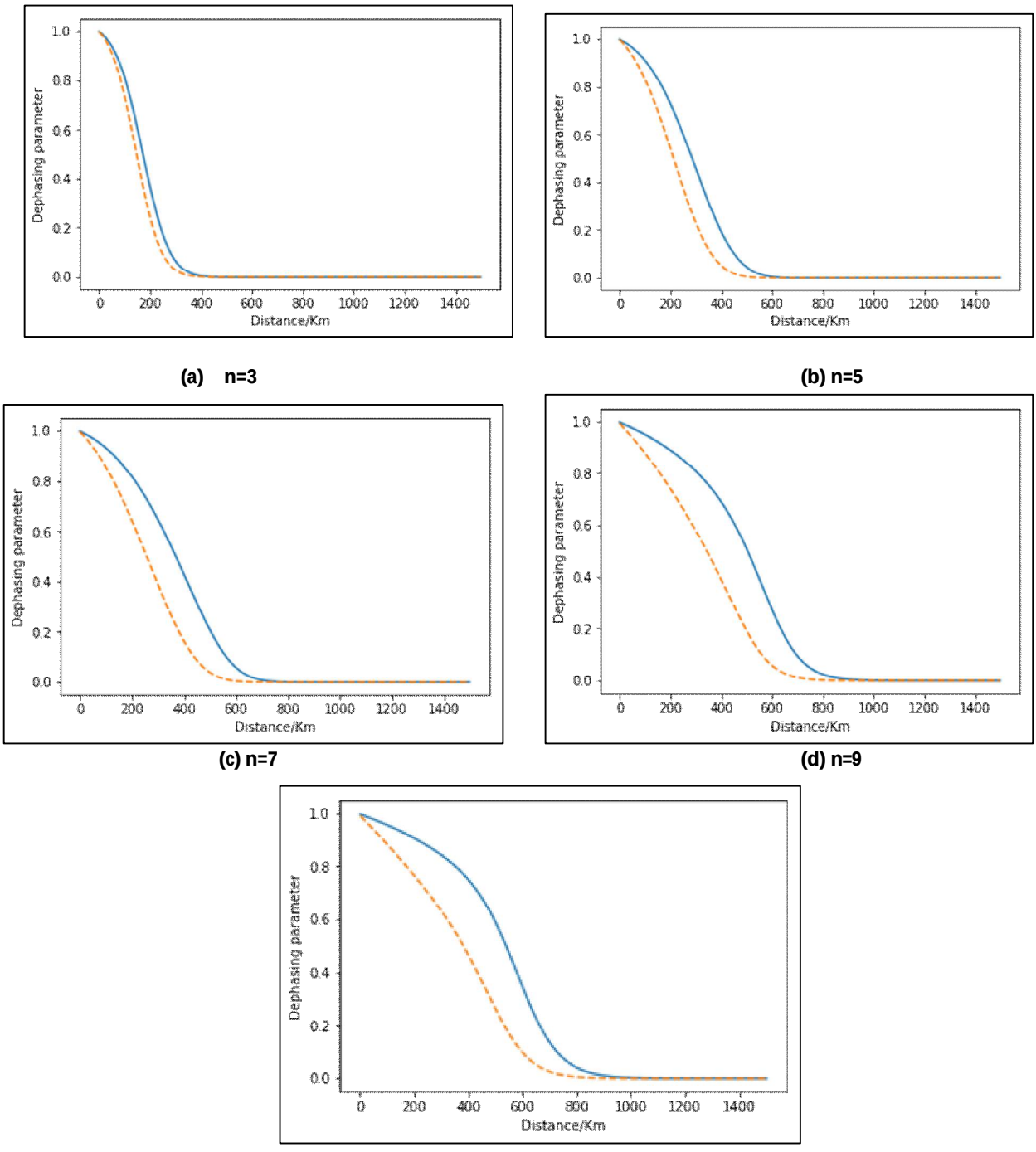

(a) n=3 **(b) n=5**

(c) n=7 **(d) n=9**

(e) n=25

Figure (2). Dephasing parameters $f_{dp[n]}$ of identical QMs (dashed line) and of non identical QMs (bold line) where, x = y = 0.25, and the number of nodes are (3,5,7,9,25) in (a,b,c,d,e)

Indian Journal of Natural Sciences www.tnsroindia.org.in ©IJONS

Vol.9 /Issue 51 / December / 2018 *International Bimonthly* *ISSN: 0976 – 0997*

RESEARCH ARTICLE

The Effect of Interaction between *E.Coli* and *Salmonella typhimurium* Sonicated Antigen on the Immune Response of Rabbits

Ikram Abbas Abood Al-Samrrae* and Alaa Taha Hanoun

Department of Microbiology, College of Veterinary Medicine, University of Baghdad, Baghdad, Iraq.

Received: 13 Sep 2018 Revised: 17 Oct 2018 Accepted: 19 Nov 2018

***Address for Correspondence**
Ikram Abbas Abood Al-Samrrae
Department of Microbiology,
College of Veterinary Medicine,
University of Baghdad,
Baghdad, Iraq

ABSTRACT

The sonicated *E.coli* (KWCSAg-EC) and *Salmonella typhimurium* (KWCSAg-ST) that prepared to immunize the rabbits evaluate their immune response by immunoglobulin-G (IgG) by using Enzyme Linked Immunosorbent Assay and Delayed Type Hypersensitivity-skin test ;for this perpose ,twenty four rabbits of both sexes,1.5-3Kg body weight were divided into four equal groups ;the first group immunized by KWCSAg-EC (1000mg/ml) subcutaneously (S/C) ,the second group immunized by KWCSAg-ST(1000mg/ml) (S/C);the third group immunized by KWCSAg-EC(500 mg/ml) and KWCSAg-ST(500 mg/ml) (compound antigen)(S/C) and fourth group injected by 1 ml PBS (PH7.2) as negative control group subcutaneously .The results of delayed type hypersensitivity-skin test showed an increase in the means of erythema and induration in the 1st group after 24hrsand 48hrs while 2nd group recorded the lowest means after 24hrs and 48hrs .These means showed significant differences (P<0.01) compared with injections by 1:2 and 1:4 diluted Ags .While result of IgG showed that the highest concentration was at 28th day in 3rd group ,while lowest concentration at 28th day in the recorded 2nd group with significant differences (P<0.01).

Key words: *E.coli, Salmonella typhimurium,* KWCSAg-ST, IgG

INTRODUCTION

Escherichia coli is widely are distributed in the intestine of animal and human and form part of the normal intestinal flora (constitute about 0.1% of gut flora)[1]; Most strains are non-pathogenic but the virulent strains can cause gastroenteritis, urinary tract infections and neonatal meningitis and opportunistic ones that normally affect immune-compromised patients exists[2].Virulent strains are also responsible for hemolytic syndrome,mastitis,septicaemia, pneumonia[3] and Diarrheal disease are major problem in third world countries which are responsible for death of millions people and animal each year, [4][5],it can either acute or chronic[6] causing of 46% of calve and lamps

mortality[7], The dendritic cells are potent antigen presenting cell that activate naive T cell[8].The cellular or humeral response in the defense of the organism that response undergo multi-step differentiation process lead to secrete of different cytokine; in the humeral response IL4-IL5-IL9-IL6-IL10-andIL3 are produced[9] ;while cellular cell produceIF-y,TNF-B,IL10 and IL2 which activate macrophages and responsible for cell mediated immunity and phagocyte dependent protective response[10].

Salmonella (spp) has long been recognized as a common cause of foodborne gastroenteritis in humans and responsible for significant economic losses in the food industry[11]. which can spread from animals to humans via contaminated food, are currently a severe health hazard worldwide and cause substantial financial losses in the food industry[12]. Poultry, meat products, and eggs are most commonly identified as food sources responsible for outbreaks of salmonellosis.The main host defense against *Salmonella* species occurs through the neutrophils mononuclear cells. These inflammatory cells produce cytokines as TNF-α, IFN- γ, IL-1, IL-2, IL-6, IL 8[13]. IL-2 is the major growth factor of T lymphocytes[14]; and interleukin 4 (IL4) is a cytokine that induces differentiation of naive helper T cells (Th cells) to Th2 cells[15].they have many roles, among the usage of antibiotics has lead to the multiple antibiotic-resistant bacteria such as *Salmonella* [16]&*E.coli*[17].Amajor inference in vaccine development is that there are often many different isolates of a given pathogen proficient in casing disease &vaccination against another on strain .This problem has indicated to the industry &government agencies an increasing requirement for effective vaccines to control this important zoonotic infections[18].

MATERIALS AND METHODS

Bacteria Isolation

E.coli and *Salmonella typhimurium* were isolated from fecal samples of sheep and identification by API20E in Central Public Health/Baghdad-Iraq.

Antigens Preparation

A-Killed whole cell sonicated *E.coli* antigen (KWCSAg-EC) and Salmonella typhimurium antigen (KWCSAg-ST) prepared according to [19].
B-The protein concentration of *E.coli* and *Salmonella typhimurium* was measured by Biuret method according to [20].

2-3-Laboratory Animal (Rabbits) Immunization

Twenty four rabbits of both sexes,1.5-3Kg body weight, which were randomly divided in to fourth equal groups (6 animals for each group).as follows:

The first group immunized with 1000 mg/ml of KWCSAg-EC subcutaneously. The second group immunized with 1000 mg/ml of KWCSAg-ST subcutaneously .The third group immunized with 500 mg/ml KWCSAg-EC and 500 mg/ml KWCSAg-ST antigens(compound antigen) subcutaneously ,and fourth group injected 1ml of PBS (PH7.2) as negative control group.

Blood Sample

Blood sample (5ml) were collection from the heart puncture of all animals at days 12-28-42-56 post immunization and serum stored in deep freeze (-20 c°) according to[21].

Immunological Tests

A-Delayed Type Hypersensitivity (DTH)- skin test this test was done according to [22].
B-The Tube agglutination test (TAT)was done according to[23].
C-Enzyme –Linked immunosorbent Assay (ELISA) commercial kit Cusabio(China kit).

RESULTS AND DISCUSSION

A-Delayed Type Hypersensitivity (DTH) Skin Test

The results of skin test was showed elevation in the mean diameter of erythema at 24 hrs in all treatments as shown Table,1;The highest mean (9.16±0.16) was found in the group of the rabbits immunized by KWCSAg-EC (1000 mg/ml) Table 1.Whilelowest (6.33±0.21) was found in the group of rabbits immunized by KWCSAg-ST (1000 mg/ml) Table 1 .In general all diameter's were decreased along period (24 and 72 hrs) and dilution (diluted 1:2 and 1:4) in all treatments .Concentration the means of induration ,it was shown increasing in the means at 48 hrs in all treatments as illustrated in Table 2.The trend of response in the means significant decrease (P<0.01) across the period and dilutions .The highest mean of duration (6.38±0.70) was detected in the rabbits immunized rabbits by KWCSAg-EC (1000 mg/ml) whereas the lowest (4.33±0.21) was noticed in the rabbits immunized by KWCSAg-ST (1000 mg/ml).

B-Tube Agglutination Test

The results of tube agglutination test at 12,28,42,56,days post immunization showed elevated antibody titers in all immunized rabbits compared with control groups, the means of all groups reached the peak at 28 days ,the means of group compound antigen was 1280and KWCSAg-EC 853.33 with significant differences(P<0.01),compared with control group.

C- Enzyme –Linked Immunosorbent Assay (ELISA) (Immunoglobulin G)

The results of tube agglutination test at 12,28,42,56,days post immunization showed elevated antibody titers in all immunized rabbits compared with control groups, the means of all groups reached the peak at 28 days ,the means of group compound antigen was 18 and KWCSAg-EC 815.16 with significant differences(P<0.01),compared with control group.

DTH-Skin test represented by the mean of skin erythema and induration reaction for each immunized group; that occurred due to the role of memory cell which modulate the Th-1 to secrete Interferon-γ (INF-γ), potent mediator that stimulates the migration of macrophage to the site of reacted area of skin[24]. while the macrophage secrete Interleukin-1 (IL-1) that enhance proliferation and differentiation of other T cells into T helper-1(Th-1) cells which secrete Interleukin-2 (IL-2) that consider a chemotactic factor, causing attraction of macrophages around area of activated T cells[25],the T-cell induce the helper activity secretion of lymphokine (CD4+) that recognize the antigen–MHC II complex, then developed into cytotoxic cells (CD8+) which recognize the class I MHC molecule[26]. Our result agree with the studies which obvious that *E.coli* O157 antigen are able to induce cellular immune response as detected by DTH-skin test immunization animal whose record a highly significant increasing of skin erythema in 24 hr and increase in induration after 72 hr, Kshash and Rosenthal and Tan and Yousif , who recorded that depend on ability and activity of Th-cells to recognize antigen and secrete IL-1, which enhanced proliferation and differentiation of other T-cell into Th-cells, which secrete IL-2 as a chemoat-ractive factor to attract macrophage around the area of activated T-cell that also secrete INF- that enhancing the cytolysis activity of accumulated macrophages leading into skin thickness[27][28].The antibodies titer was elevated after 28 days of booster dose administration, in all

immunized groups compared with control group, especially in the first group, which had the highest antibodies titer, our findings agree with Oladejo and Adebolu which showed the antibody titration against*E.coli* O157 antigen as first dose elevated then reach to the peak after booster dose from post immunization[29]. Also, agreement with Karmali which the recorded the shiga-like toxin neutralization antibody produced different titration agents *E.coli* antigen[30].IgG concentration represented the variation of humoral immune response between the groups as a result of stimulation of different numbers of B-cell activation and differentiation to the plasma cell that will produce the neutralizing antibody[31][32],as well as ,this variation may be resulted due to the injection of KWCSAg prepared from different groups; each one have different numbers of antigen determinants different number of T-cell[33].The titer of antibodiesin this study markedly elevated after 12 days post immunization compared with control group ,then reach to the peak after 28 days post immunization especially in 3rd group which immunized with KWCSA-EC and KWCSA-ST compound antigen . Many studies proved that the outer membrane protein of *E.coli* that contain H antigen which reacted with H antisera to produce agglutination reaction also in somatic antisera O;Most of plasma cells during secondary immune response secrete IgG, IgA and IgE antibodies .Yet few plasma cells also secrete IgM antibodies during secondary immune response. Killed vaccines do not multiply inside cells.These vaccines are taken up by APCs, complexes to MHC and II molecules and presented to CD4+T cells, which in turn help mainly the B cells. Hence these vaccines induce strong humoral immune response[34].

REFERENCES

1. Dethlefsen L.,Eckburg PB,Bik EM,Bernstein CN,Purdom E.(2005)."Diversity of the human intestinal microbial flora".Science 308:1635-1638.
2. Nataro,J.and Karper,J.(1998).Diarrheagenic Escherichia coli. Clin Microbial Rev 11,142-201.
3. George M.Garrity Ed .(2005).The Gammaproteobacteria.Bergeys Manual of Systematic Bacteriology .2B (2nd ed).New York: Springer.pp.1108.
4. Guerrant,R.L.;Van Gilder,T.;Steiner,T.S.;Theilman,M.N.;Slutsker,L. and Tauxe,R.V.(2001).Practice guidelines for the management of infectious diarrhea.Clin.Infect.Dis.,32:331-35.
5. Rodstits,O.M;Gay,O.M.;Hincheliff,K.W.and Coststable,K.W(2007).Veterinary Medicine.A text book of the cattle,horses,sheep,pigs and goat.8th editition.Slsevier.USA.PP:163.
6. Sandler,R.S.;Stewart,W.F.;Liberman,,J.N.;Ricci,J.A.and Zorich,N.L.(2001).Abdominal pain ,bloating and diarrhea in the Unted states:prevalence and impact.Dig.Dis.Sci.,45(6):1166-71.
7. Schoenian,S.(2007).Diarrhea(scours)in small ruminants.Maryland cooperative Exttension.Sheep and Goat specialist Western Maryland research and Eduction Center.
8. Moll,H.(2003).Dendritic cells and host resistance to infection cell.Microbiol.5:493-500.
9. Curtis,J.L.(2005).Cell-mediated adaptive immune defense of the lungs.Proc.Am Thorac.Soc2:412-16.
10. Romaqnani,S.(1999).Th1/Th2 cells.Inflamm.Bowel Dis.Nov;5(4):285-94.
11. Scapin, D.; Grando, W. F.; Rossi, E. M.; Perez, K. J.; Malheiros, P. S. and Tondo, E. C. (2013). Antagonistic activity of *Lactobacillus acidophilus* LA10 against *Salmonella enterica* serovar *Enteritidis* SE86 in mice. Brazilian J. Microbol. 44, 1, 57-ISSN 1678-4405.
12. Uppington,H.; Menager, N.;Boross, P.;Wood, J.; Sheppard, M.;Verbeek, S.and Mastroeni, P. (2006). Effect of immune serum and role of individual Fcγ receptors on the intracellular distribution and survival of *Salmonella enterica* serovar *typhimurium* in murine macrophages.
13. Kaur, J. and Jain, S.K. (2011). Role of antigens and virulence factors of *Salmonella enterica* serovar Typhi in its pathogenesis. Microbiol. 167: 199– 210.
14. Khan,M.M.(2008).Immunopharmacology,Role of Cytokines.P.33-53.Spr.Scien.Busin.Media.LLC.
15. Sokol, C. L.; Barton, G. M.; Farr, A. G. and Medzhitov, R. (2008). A mechanism for the initiation of allergen-induced T helper type 2 responses. Nat. Immunol. 9 (3): 310–318.
16. Weill,F.X.;R.;Praud,K.;Kerouanton,A.;Fabre,L.;Brisabois,A.;Grimont,P.A.and Cloeckaert,A.(2004).Emergence of extended-spectrum-beta-lactamase(CTX-M-9)-Producing multiresistant strains of Salmonella enterica serotype in poultry and human in France.J.Clin.Microbiol.,42,5767-5773.

17. Allison KR,Bynildsen MP,Collins JJ(2011) Metabolite-enabled eradication of bacteria persisters by aminoglycosides.Nature 473(7346):216-220.
18. Weill,F.X.;Timinouni,M.;Polomack,L.andGrimont,P.A.(2006).Multi-drug resistance to Salmonella typhimurium from human influence.J.Clin.Microbiol.;44(3):701-708.
19. Westerman RB, He Y, Keen JE, Littledike ET, Kwang J. Production and characterization of monoclonal antibodies specific for the lipopolysaccharide of Escherichia coli O157. Journal of Clinical Microbiology. 1997; 35(3):679-684.
20. Henry, R.J.; Cannon, D.C. and Winkelman, J.W. (1974). Clinical Chemistry, Principles and techniques. 2nd Eds. Harber and Row Company. England.
21. Weiss DJ, Wardrop KJ. Schalm's Veterinary Hematology. Wiley-Blackwell. 6th ed. USA, 2010.
22. Hudson,L. and Hay,F.C.(1980).''Practical immunology".3rd ed .Black-well scientific publication,Oxford London.
23. Harley,J.P. and Prescott,L.M.(2001). Laboratory Exercises in Microbiology.2nd ed. W.M.C.Brown pubisher.England 322-338.
24. Rosenthal KS, Tan JS. Rapid Review of Microbiology and Immunology, Amazon Company, USA, 2007.
25. Miller RA. The Cell Biology of Aging. Gerontology Journal. 1989; 44:B4-B8.
26. Tizard IR. Veterinary Immunology. W. B. Sauders Comp. Philadelphia, USA, 1992.
27. Rosenthal KS, Tan JS. Rapid Review of Microbiology and Immunology, Amazon Company, USA, 2007.
28. Yousif AA, Al-Taai NA, Mahmood NM. Humoral and Cellular Immune Response Induced By E. coli [O157:H7 and O157:H7:K99] Vaccines in Mice. International Journal of Immunology Research. 2013; 3(1):17-20.
29. Oladejo BO, Adebolu TT. Mechanisms of Immunity to *Escherichia Coli* O157:H7 In Albino Rats: Role of homologous antibodies. European Journal of Biology and Medical Science Research. 2013; 1(2):31-39.
30. Karmali MA, Petric M, Lim C, Fleming PC, Arbus GS, Lior H. The association between idiopathic hemolytic uremic syndrome and infection by verotoxin-producing *Escherichia coli*. Journal of Infectious Disease. 1985; 151(5):775-82.
31. Bergman, M.A.;Cummings, L.A.;Rassoulian, S.L,Smith,K.D.;Lara, J.C.;Aderem,A. and cookson,B.T.(2005).CD4+T cells and toll-like receptors recognize Salmonella antigens expressed in bacterial surface organelles.Inf. and Immun.;73(3):1350-1356.
32. Simonase,J.;Strid,M.A.;Molbak,K.;Krogfelt,K.;Linnerberg,A. and Teunis,P.(2008).Sero-epidemiology as a tool to study the incidence of Salmonella infection in humanes.J.Epidemiol.Infect.;136(7):895-902.
33. Lentsch ,R.H.;Batema,R.P.and Wanger, J.E.(1981).Detection of Salmonella infection by polyvalent Enzyme-Linked Immunosorbe Assay(ELISA).J.Clin.Microb;14(3):281-287.
34. Jayapal,V.(2007).In fundamentals of medical immunology,180-324. Jaype Brothers medical publisher (p)LTD,New Delhi.

Table 1: Mean of diameter erythema in rabbits immunized by KWCSA-EC and KWCSA-ST

Erythema Mean (mm)				
Hours	**Groups**	**G1**	**G2**	**G3**
24	**Crude Ag**	9.16 ± 0.16 A a	6.33 ± 0.21 A a	8.50 ± 0.22 A a
	1:2	8.33 ± 0.49 A a	6.16 ± 0.94 AB a	6.83 ± 0.40 B a
	1:4	6.33 ± 0.33 B a	4.50 ± 0.42 B a	4.67 ± 0.42 C a
	PBS	1.83 ± 0.16 C a	0.33 ± 0.21 C a	1.83 ± 0.16 D a
28	**Crude**	8.50 ± 0.50 A a	4.67 ± 0.71 A b	7.16 ± 0.31 A ab
	1:2	6.50 ± 0.50	5.66 ± 0.21	5.16 ± 0.31

		B b	A ab	B b
	1:4	5.50 ± 0.22 B b	4.16 ± 0.16 A ab	4.33 ± 0.56 B ab
	PBS	0.50 ± 0.22 C b	0.666 ± 0.21 B a	0.667 ± 0.21 C b
72	**Crude**	6.50 ± 0.50 A b	4.33 ± 0.21 A b	6.16 ± 0.94 A b
	1:2	5.66 ± 0.21 AB b	4.16 ± 0.16 A b	4.33 ± 0.55 B b
	1:4	4.66 ± 0.21 B c	3.33 ± 0.21 B b	3.16 ± 0.31 B b
	PBS	0.666 ± 0.21 C b	0.166±0.16 C a	0.166 ± 0.16 C b

1st group KWCSAg-EC 1000µG/ml ,2nd group KWCSAg-ST 1000 µG/ml ,3rd group KWCSAg-EC 500 µG/ml &KWCSAg-ST 500µG/ml *(P<0.01). Means having with the different small letters (between Groups) in same column and capital letters (between days) in same row differed significantly.

Table, 2: Mean of diameter induration in rabbits immunized by KWCSA-EC and KWCSA-ST

Induration Mean (mm)				
Hours	**Groups**	**G1**	**G2**	**G3**
24	**Crude Ag**	2.67 ± 0.42 A c	2.33 ± 0.21 A a	1.50 ± 0.22 A b
	1:2	1.83 ± 0.16 A c	2.33 ± 0.21 A a	0.667 ± 0.21 B b
	1:4	0.50 ± 0.22 B c	0.833 ± 0.16 B b	0.166 ± 0.16 B b
	PBS	0.67 ± 0.21 B a	0.50 ± 0.22 B a	0.166 ± 0.16 B a
28	**Crude**	6.83 ± 0.70 A a	4.33 ± 0.21 A a	6.17 ± 1.12 A a
	1:2	4.50 ± 0.22 B a	3.50 ± 0.76 AB a	4.83 ± 0.40 AB a
	1:4	4.33 ± 0.21 B a	3.33 ± 0.42 B a	3.50 ± 1.02 B a
	PBS	0.833 ± 0.16 C a	0.666 ± 0.21 C a	0.166±0.16 C a
72	**Crude**	4.67 ± 0.21 A b	4.00 ± 1.33 A a	4.17 ± 0.60 A a

	1:2	3.83 ± 0.16 B b	3.44 ± 0.70 A a	3.16 ± 0.60 A a
	1:4	3.67 ± 0.21 B b	2.83 ± 0.94 A a	3.15 ± 0.60 A a
	PBS	0.50 ± 0.22 C a	0.166±0.16 B a	0.50 ± 0.22 B a

1st group KWCSAg-EC 1000µG/ml ,2nd group KWCSAg-ST 1000 µG/ml ,3rd group KWCSAg-EC 500 µG/ml &KWCSAg-ST 500µG/ml

Table,3: Means of antibody titers of immunized rabbits by agglutination tube test.

Time Group	Antibody titers-			
	12days	28days	42days	56days
KWCSAg-EC	426.67 ± 53.96 A b	853.33 ± 107.94 B a	512.00 ± 0.00 A b	341.33 ± 53.97 A b
KWCSAg-ST	170.67 ± 26.98 B b	320.00 ± 64.00 C ab	597.33 ± 215.87 A a	128.00 ± 0.00 B b
KWCSCAg	512.00 ± 114.48 A b	1280.00 ± 256.00 A a	798.00 ± 114.48 A b	469.33 ± 42.67 A b
C	15.00 ± 3.41 B a	12.00 ± 0.00 C a	13.33 ± 4.21 B a	11.67 ± 4.01 C a

Table,4:Mean of IgG concentration of immunized rabbits with KWCSAg in ELISA test

Time / Concentration	IgG concentration			
	12days	28days	42days	56days
KWCSAg-EC	11.67 ± 1.85 A a	15.16 ± 1.49 B a	13.16 ± 0.87 B a	11.16 ± 2.04 A a
KWCSAg-ST	6.50 ± 0.56 B c	10.67 ± 0.61 C a	8.83 ± 0.47 C b	6.83 ± 0.94 B c
KWCSCAg	12.83 ± 0.98 A b	18.00 ± 0.57 A a	16.33 ± 1.20 A a	13.17 ± 0.91 A b
Control	5.33 ± 0.76 B a	5.16 ± 0.87 D a	5.50 ± 0.84 D a	5.00 ± 1.00 B a

Indian Journal of Natural Sciences www.tnsroindia.org.in ©IJONS

Vol.9 /Issue 51 / December / 2018 *International Bimonthly* *ISSN: 0976 – 0997*

RESEARCH ARTICLE

Verification the Pollution of Tigris River in South of Baghdad using Remote Sensing Techniques

Rafah Rasheed Ismail *, Noor Zubair Kouder and Zainab Fadel Hussein

Department of Astronomy and Space, College of Science, University of Baghdad, Baghdad, Iraq.

Received: 16 Sep 2018 Revised: 19 Oct 2018 Accepted: 21 Nov 2018

***Address for Correspondence**
Rafah Rasheed Ismail
Department of Astronomy and Space,
College of Science,
University of Baghdad,
Baghdad, Iraq
E-mail: Moh19721976@scbaghdad.edu.iq

ABSTRACT

This paper describes the use of remote sensing techniques in verification of the polluted area in Diyala River and Tigris River and the effected of AL-Rustamiyah wastewater treatment plant, which is located on Diyala River, one of the branches of Tigris River in south of Baghdad. SPOT-5 a French satellite image of Baghdad, Iraq was used with ground resolution of 2.5 m in May 2016. ENVI 5.1 software programming was utilized for Image processing to assess the water pollution of Diyala and Tigris River's water. Five regions were selected from a study area and then classified using the unsupervised ISODATA method. The results indicated that four classes of water quality which are successful in assessing and mapping water pollution which confirmed that the Tigris River water is subjected to pollution from Diyala River which agree with the ecological tested of water samples collected from five regions in the study area. Were The value of turbidity, Total Organic carbon, Salinization, conductivity and a measure of acidity or alkalinity (pH) in Tigris River is Ranging (60.8 - 242.6 FTU) , (19.234 - 25.95 mg/L), (0.6487 – 0.7315 g/L),(1047-1159 µm/m) and (8.06-8.16) respectively.

Keywords: Pollution, Organic material, turbidity, Diyala River, Tigris River.

INTRODUCTION

Water is necessary of the Organisms life. It must be saved and shielded from all kind of toxics .The human body and Organisms living require it, but in its pure form without any sort of tainting [Amit,2013]. Water contamination happens when unwanted effluents scatter in the water system which leads to water quality change. Water contamination is partitioned into two main sources, a natural Source which includes acid rain and thermal effluents from volcanic territories but they are not common on earth, domestic sources that are essentially sewage and clothing wastes, produced in houses and different dwellings. In built-up areas, nearby squanders are collocated in sewage

pipes and transmitted to control areas either for treatment or to throw away into a conduit without treatment. This considered as the major planned wellspring of water contamination [Sulaiman, 2016]. Sewage treatment is the elimination contaminants from wastewater, primarily from domestic sewage. Physical, chemical, and biological processes are used to take out contaminants and produce treated wastewater that is secure for the natural environment. The finished product of this treatment is usually a highly viscous waste or slurry, called sewage sludge. The sludge has to suffer more treatment before being suitable for use or application to land [Franklin, 2013]. Al-Rustamiyah wastewater treatment plant is the oldest and biggest sewage treatment plant in Iraq; it is located in the south of Baghdad capital of Iraq .The plant have serious problems associated with overflow and low capacity of Al-Rustamiyah Sewage [Raheek, 2017]. Satellite remote sensing has become a significant tool for monitoring and administration of natural wealth and the environment [Amit, 2013].

Water absorbs long visible rays and near-infrared more and radiated more short visible rays, so water usually looks blue or greenish- blue in color by the intensity of the reflection of short wave radiation. Contaminated water looks lighter in color than pure water, that is because the turbidity reflects the long-rays better, but it cannot distinguish water turbid water pure shallow due to the similarity of the cases. The presence of chlorophyll in algae leads to greater absorption of the blue rays and are shown in green water. Characterize surface water plays a major role in the complexity of the process of interpretation of the characteristics of the water by remote sensing [Thomas, 2004].

Classification is one of the information extracting strategies which are utilized to arrange the object into predefined gatherings. It is the most often utilized basic leadership errands of human action. A classification issue happens when an object needs to be assigned into a predefined group or class in light of various watched attributes identified with that object. The classification additionally assumes essential part in the remote sensing and satellite image characterization. Image classification is a complicated procedure that might be influenced by numerous components. A big number of classification strategies can be found in the writing; for the most they have been classified as either supervised or unsupervised classification [Anand, 2014]. The unsupervised classification, also called clustering, the classes produced from this classification are "spectral classes" and may not correlate with "information classes" as determined by supervised classification [Jian, 2009].

POLLUTION OF WATER

The pollution of water causes adversely affects in water quality, this pollution include: Organic pollutants، Heavy metal،Microbial contamination، Toxic organic compounds،Traces of chemicals and pharmaceutical،Suspended particles (Turbidity)، Nuclear waste، Salinization and Acidification [Andreas, 2001]: Organic Pollutants can be further divided into (a) Oxygen Demanding wastes which mainly produced from local and municipal wastewater, (b) Synthetic Organic Compounds, These incorporate pesticides, manufactured cleansers, food additives, pharmaceuticals, bug sprays, paints, synthetic fibers, plastics and solvents . The vast majority of these mixes are poisonous and bio refractory organics (c) Oil which enters in to water through oil spills, leak from oil pipes, and wastewater from production and refineries. Being lighter than water it spreads over the surface of water, separating the contact of water with air. This pollutant is also responsible for endangering water birds and coastal plants due to coating of oils and adversely affecting the normal activities [Andreas, 2001].

Suspended particles (Turbidity) is caused by particles poised or dissolved in water that distributed light making the water appear hazy. Particulate substance can include sediment - especially silt, suspended organic and inorganic matter, algae, and other tiny organisms. [Sulaiman, 2016].Salinization mainly happening in arid and semiarid regions although it can also occur naturally, unsustainable irrigation and inadequate drainage endorses secondary salinization. It can also be the result of irrigation with salt water, after freshwater has been replaced in coastal aquifers due to over-abstraction [Merchán, 2015].

Acidification The acidification process is related to leaching of atmospheric-derived sulphate and excess nitrate from soils to surface waters. in runoff to a extent be accompanied by acidifying hydrogen ions and inorganic aluminum that are toxic for many aquatic organisms[Cui,2014].

STUDY AREA

Al-Rustamiyah wastewater treatment plant is considered the wastewater collected through the sewerage network in Baghdad located (44°31'04.8"E 33°16'33.6"N) in Diyala river one of Tigris River tributaries, the study area including the Diyala river within the boundaries of Baghdad and the region of the confluence of the Diyala river and Tigris river south of Baghdad it is bounded by the longitudes 44° 42' to 44° 56' E and Latitude 33° 41' to 33° 19' N. In this work we determine five regions, three on Diyala River (before ,at and after) Al-Rustamiyah wastewater treatment plant and two on Tigris river southern Baghdad(before and after) The confluence of Diyala river and Tigris river. Figure (1) shows the original view of Baghdad city and the study area inside the square. While figure (2) shows the selected regions from Study area (A). Where (B and C) represent two regions on Diyala river before and at Al-Rustamiyah wastewater treatment plant respectively. And (D) represent three regions (on Diyala river before confluence with Tigris River, on Tigris River (before and after) the confluence of the Diyala River).

Software Used

SPOT-5 French satellite image (panchromatic image) with diminutions: 13014 x 12563, Data type: byte, size: 490,585,528 bytes, File type: TIFF, Projection: UTM, Zone 38 N and Pixel: 2.07 x 2.46 meter was used to verification water pollution by using Environment for Visualizing Images (ENVI 5.1) software programs. It's includes all the basic image processing functions.

MATERIALS AND METHODS

Pre-Processing

After download the satellite Image for Baghdad city in (19/5/2016), we performed a spatial subset for satellite image by Region of Interest (ROI) Tool to extract the study area. the radiance data in our images includes interference from the atmosphere we need to address to ensure our burn analysis is accurate. ENVI has many methods for correcting the effects of atmosphere on image data one of them (used in this work) is Quick Atmospheric Correction Tool that relies on the diversity of observed pixel spectra (materials) contained in an image scene to determine atmospheric correction parameters, Figure (3) show the image of study area before and after atmospheric correction.We subset three regions from study area for classification ;the first regions is on Diyala River before Al-Rustamiyah wastewater treatment plant, the second is on Diyala River at Al-Rustamiyah wastewater treatment plant ,and third regions of The confluence of the Tigris River and Diyala River.

Physical and Chemical Tests

Five samples were taken from each of the five regions and tested the water turbidity by using (Microprocessor turbidity meter) with scale (0-1000 FTU), Total Organic carbon, Salinization , conductivity using conductivity meter and Acidification (PH) using Microprocessor PH meter to identifying the Pollution water. Figure (9) illustrates the devises used in tested. For total Organic Carbon tested we use Oxalic acid $C_2H_2O_4$ (0.1 N), Potassium Permanganate $KMnO_4$ (0.1N), Sulfuric acid concentrate H_2SO_4. We take 100 ml of water sample and add 10 ml of H_2SO_4 then add 10 ml of $KMnO_4$. The solution is placed in a water bath at 90 ° C for half an hour, after cooling the solution add 10 ml of $C_2H_2O_4$. We observe the disappearance of the purple color of potassium permanganate, which means the

presence of organic matter, and must be corrected with potassium permanganate and calculate the volume of the bottom of the burette. Total Organic carbon (T.O.C.) can calculate by the equation (1)

T. O. C. = V*3.16……. (1) where V is the volume bottom of the burette

Table (1) presents the results of water pollution tested of the five regions water samples in the study area and figures (10-14) illustrate the bar chart presents the results of water pollution tested of the five regions in the study area.

CONCLUSIONS

1. The results indicated that the possibility of remote sensing techniques to identifying water pollution and water turbidity.
2. Four categories, of water quality, these are natural water, turbidity water, Shallow water or river sediments and Water covered with a layer of plants. These results were successful in assessing and mapping water pollution and confirmed that the Diyala river water is source of pollution in Tigris River.
3. This results agreement with physical and chemical tests of the water samples collected from five regions in study area, where high levels of pollution were detected in Diyala river.
4. The results obtained indicate the inefficiency of Al-Rustamiyah wastewater treatment plant.
5. It is clear that water pollution in Tigris river is increasing after it confluence with Diyala river, where turbidity increases from 60.8 to 242.6 , Total Organic Carbon increases from 19.234 to 25.95,conductivity increases from 1047 to 1159.

Recommendation

1. Maintenance and rehabilitation of treatment units in of Al-Rustamiyah wastewater treatment plant to ensure the discharge of water conforming to the specifications of the Diyala river.
2. Expansion of the station through the addition of new processing units and the adoption of the design of the city of Baghdad, which corresponds to the population growth in the city
3. Recent statistics from the Ministry of Planning have shown an increase in the population of the city of Baghdad to about 80 million people, which requires the establishment of new sewage treatment plants

REFERENCES

1. Amit ,K., " Water Pollution and Treatment" , International Journal of Environmental Engineering and Management, Vol. 4, No.3, PP.191-198, 2013 .
2. Anand, U.; Santosh, K. S. and Vipin, G.S.," Impact of features on classification accuracy of IRS LISS-III images using artificial neural network ", International Journal of Application or Innovation in Engineering and Management ,V. 3,PP. 311-317, October 2014.
3. Andreas, R., Keya, C., and Eleftheria, K., " Protect water Resources: Pollution Prevention ", International Conference on Freshwater, 2001.
4. Cui, X. & Choo, K.-H. "Natural organic matter removal and fouling control in low pressure membrane filtration for water treatment" Environmental Engineering Research, (2014).
5. Franklin L. Burton, George Tchobanoglous, Ryujiro Tsuchihashi, H. David Stensel, Metcalf & Eddy, Inc." Wastewater Engineering: Treatment and Resource Recovery",McGraw-Hill Education,2013.
6. Jian, G. Liu and Philippa, J. Mason," Essential Image Processing and GIS for Remote Sensing", First edition Wiley Blackwell, London, 2009.

7. Merchán D., Auqué L.F., Acero P., M.J.Gimeno M.J., Causapé J."Geochemical processes controlling water salinization in an irrigated basin in Spain: Identification of natural and anthropogenic influence"Science of The Total Environment,502: 330-343, 2015.
8. Raheek I. Ibrahim," Upgrading of Al-Rustamiyah Sewage Treatment Plant Through Experimental and Theoretical Analysis of Membrane Fouling",Iraqi Journal of Chemical and Petroleum Engineering ,Vol.18, No.2,PP 95 - 107 , 2017.
9. Sulaiman A. Alrumman, Attalla F. El-kott, Sherif M. A. S. Keshk" Pollution: Source and Treatment" American Journal of Environmental Engineering, 6(3): 88-98, 2016.
10. Thomas M. Lillesand, Ralph W. Kiefer, Jonathan W. Chipman," Remote Sensing and Image Interpretation", Fifth Edition, Wiley,America,2004.

Table (1): water pollution tested of the five regions water samples in the study area.

	Tested / No. of samples	Turbidity (FTU)	Total Organic carbon (mg/L)	Salinization (g/L)	conductivity (µm/m)	Acidification (PH)
Diyala River before Al-Rustamiyah wastewater treatment plant	1	256	15.01	0.7216	1169	7.8
	2	270	14.37	0.6327	1124	7.2
	3	277	15.03	0.7678	1034	7.5
	4	263	15.26	0.6998	1130	7.9
	5	259	14.28	0.6456	1143	7.6
	mean	**265**	**14.79**	**0.6935**	**1120**	**7.6**
Diyala River at Al-Rustamiyah wastewater treatment plant	1	453	54.67	1.7238	2767	7.4
	2	422	52.26	1.7386	2795	7.6
	3	436	54.07	1.7453	2803	7.3
	4	438	54.11	1.7659	2835	7.4
	5	436	54.29	1.7134	2750	7.5
	mean	**437**	**53.88**	**1.7374**	**2790**	**7.44**
Diyala River after Al-Rustamiyah wastewater treatment plant	1	376	38.86	0.8333	1329	7.2
	2	381	38.21	0.8727	1384	7.4
	3	336	38.82	0.8252	1311	7.4
	4	337	39.13	0.8289	1317	7.3
	5	365	37.98	0.8321	1319	7.3
	mean	**359**	**38.6**	**0.83844**	**1332**	**7.32**
Tigris River before the confluence of the Diyala River	1	56	18.75	0.6175	1027	8
	2	58	19.36	0.6491	1048	8
	3	61	18.12	0.6252	1009	8.2
	4	65	20.11	0.7015	1102	8

	5	64	19.83	0.6502	1049	8.1
	mean	**60.8**	**19.234**	**0.6487**	**1047**	**8.06**
Tigris River after the confluence of the Diyala River	1	244	24.85	0.7572	1198	8.2
	2	245	24.28	0.6853	1086	8
	3	239	28.45	0.7402	1172	8.2
	4	248	24.18	0.7157	1138	8.3
	5	237	27.99	0.7591	1201	8.1
	mean	**242.6**	**25.95**	**0.7315**	**1159**	**8.16**

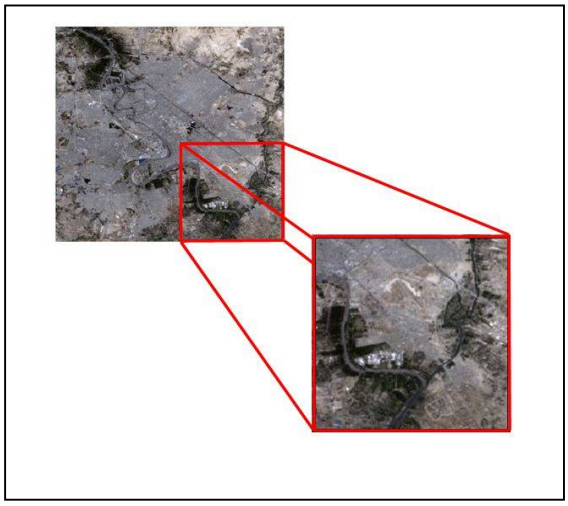

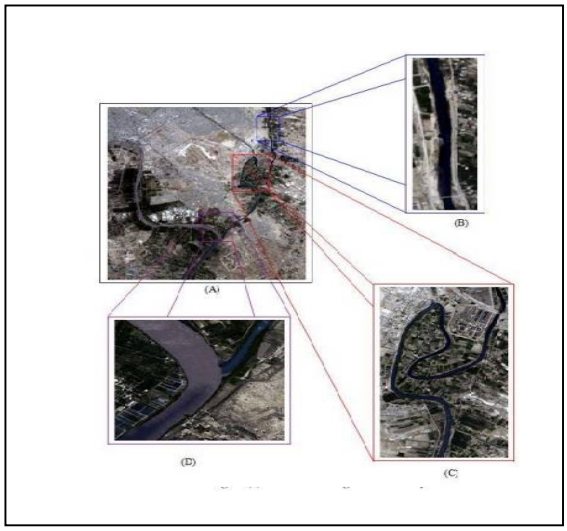

Figure (1): Baghdad satellite image and the study **Figure (2): The selected regions from study area in 2016**

(A) study area
(B) the region on Diyala River before Al-Rustamiyah wastewater treatment plant
(C) the region on Diyala River at Al-Rustamiyah wastewater treatment plant
(D) the region of The confluence of the Tigris River and Diyala River

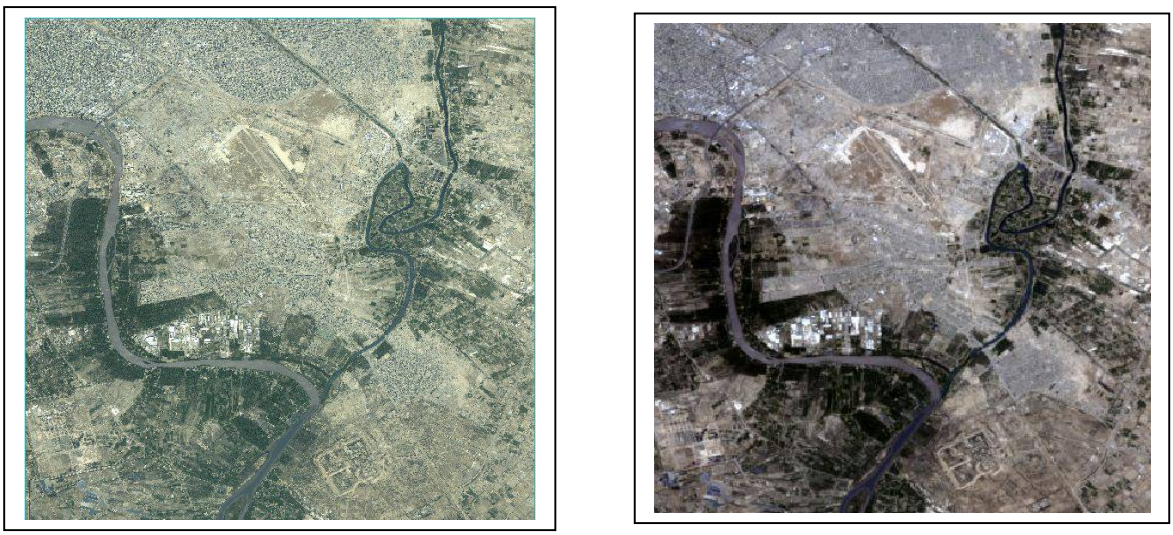

(A) ***(B)***

Figure (3): study area before and after atmospheric correction
(A) Before Atmospheric Correction (B) After Atmospheric Correction

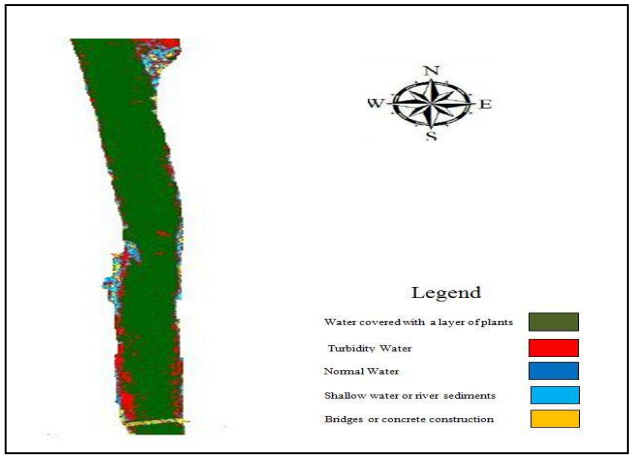

Figure (4): Results of unsupervised ISODATA classification for satellite image of Diyala River before Al-Rustamiyah wastewater treatment plant

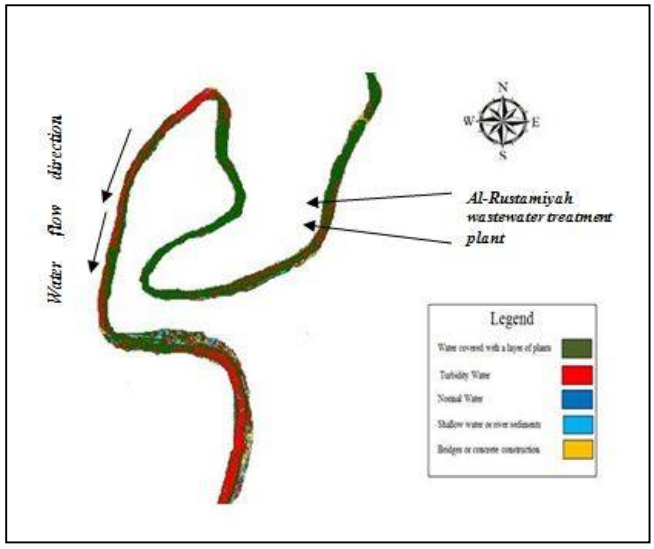

Figure (5): Results of unsupervised ISODATA classification for satellite image of Diyala River at Al-Rustamiyah wastewater treatment plant

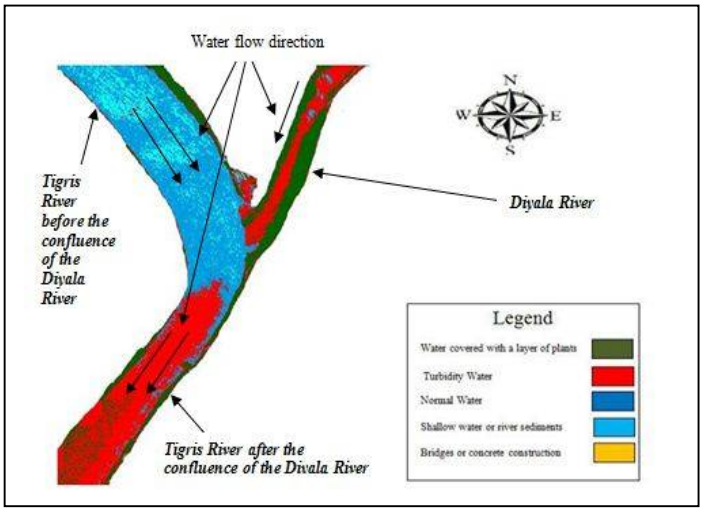

Figure (6): Results of classification for satellite image of Tigris River (before and after) the confluence of the Diyala River)

Figure (7): Tigris River in June 2016

Figure (8): Diyala River in June 2016

Figure (9): the devises used in water tested

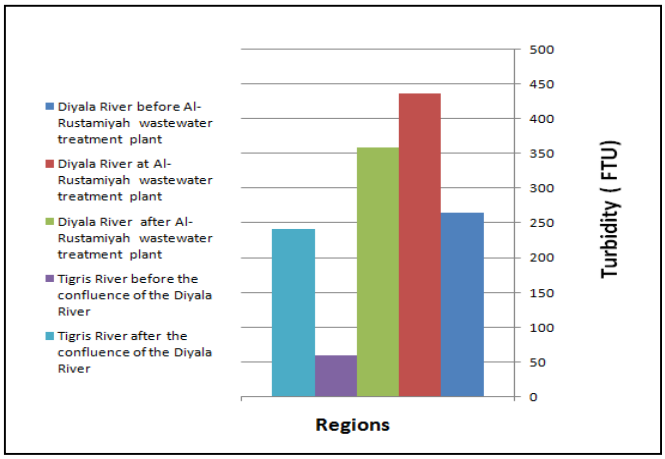

Figure (10): The Turbidity values of the samples from the water of five regions.

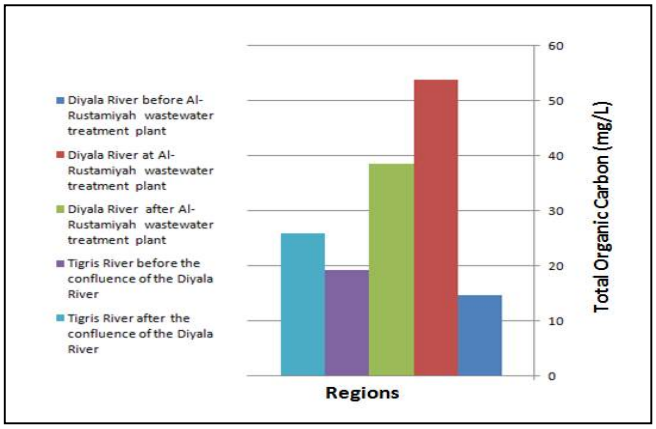

Figure (11): The Total Organic Carbon values of the samples from the water of five regions.

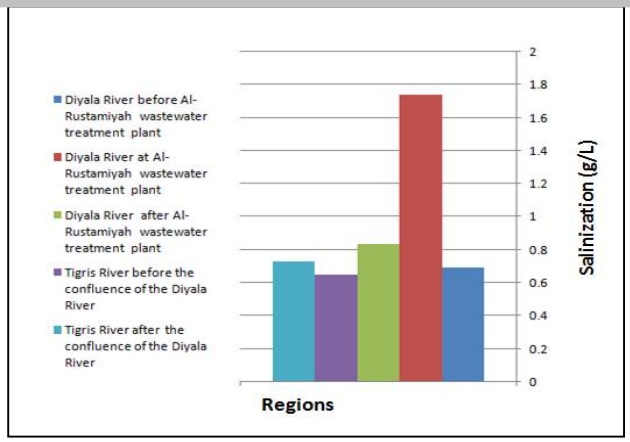

Figure (12): The Salinization values of the samples from the water of five regions.

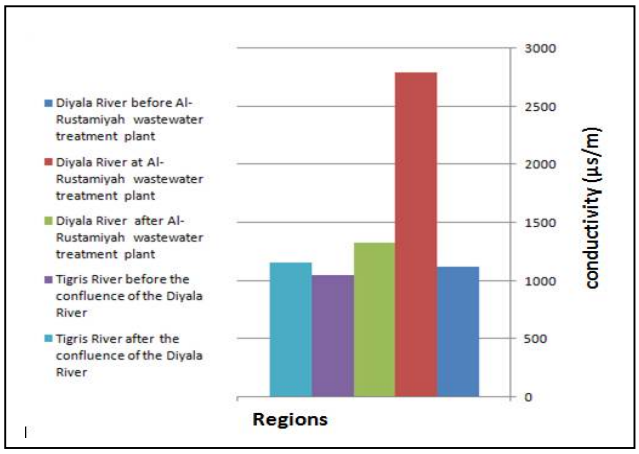

Figure (13): The conductivity values of the samples from the water of five regions.

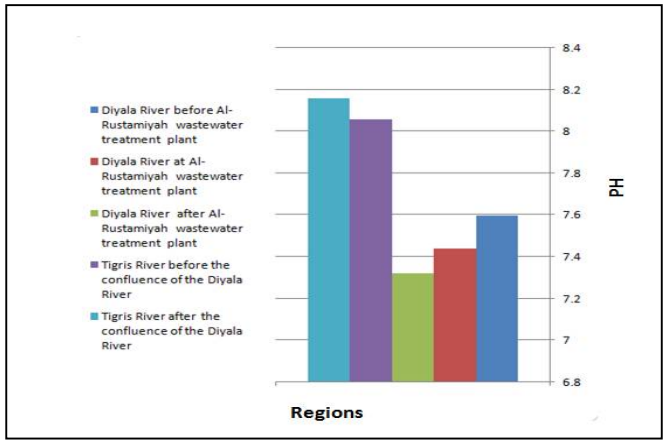

Figure (14): The PH values of the samples from the water of five regions.

Indian Journal of Natural Sciences www.tnsroindia.org.in ©IJONS

Vol.9 /Issue 51 / December / 2018 *International Bimonthly* *ISSN: 0976 – 0997*

RESEARCH ARTICLE

Morphostructure Model for Euphrates River Basin in West and Central Iraq

Zeyad Jameel Al- Saedi* and Mustafa Rashead Al-Obaidi

Geology Department, college of science, University of Baghdad, Baghdad, Iraq.

Received: 15 Sep 2018 Revised: 18 Oct 2018 Accepted: 21 Nov 2018

***Address for Correspondence**
Zeyad Jameel Al- Saedi
Geology Department,
College of science,
University of Baghdad,
Baghdad, Iraq
E-mail: zeyadjameel@gmail.com

ABSTRACT

The study area is located in Iraq, which represents part of Euphrates River Basin. The aims are to describe the structure and geomorphology of Euphrates Basin, and to interpret the relationship between Euphrates River Basin and the major fault systems in the area. Studying knickpoints, where each point was considered as a fault along the river. The study adopted strike-slip faults – extensional (listric) faults model. Most of these Faults are intersected with Euphrates River in (51) sites, 18 of them arestrike-slip faults cuts basement rocks and effects on the surface, other (33) normal faults belong to Tertiary and Quaternary periods. These faults represent compression and extension regimes. Najd system is of northwest – southeast direction and determines the general course of the Euphrates River. While the local recent faults control meanders directions. The values and trends of stress axes were different in Ramadi and Baghdad $\sigma1>\sigma2>\sigma3$while in Najaf the values became $\sigma1>\sigma2=\sigma3$ due to stress change in Arabian plate because of the convergence that occurred at the end of the Cretaceous period along the rim of the Arabian plate. Three seismic sections were studied to determine the subsurface structures.

Keywords: Euphrates River Basin, Flower structure, Graben, Knick point, Morphostructure Mode

INTRODUCTION

Iraq is one of the riparian countries within basins of Tigris-Euphrates Rivers in the Middle East region. Euphrates River, The longest river in southwest Asia, it is one of the two main constituents of the Tigris-Euphrates river system. The river rises in Turkey and flows southeast across Syria and through Iraq. Euphrates descends between major

ranges of the Taurus Mountains to the Syrian plateau. It then flows through western and central Iraq to unite with the Tigris River and continues, as Shatt Al-Arab, to the Arabian Gulf. [1].

Rivers and their drainage networks are better than those that reflect these changes because of their dynamism and the effect of its flow by simplifying changes and surface effects such as simple change in the gradient and sudden change in the topographic effect due to intersect of river course by sub-surface faults appear on the surface as a result of modern tectonic activation.[2]. [3]mentioned ; the recent tectonic activity of the structures of sub-surface domes in different areas of central Iraq was one of the main factors that led to important changes in the behavior of large and small rivers. The Tigris and Euphrates rivers in some areas of the Mesopotamia Valley change the direction of their flow in a sudden manner without the presence of visible superficial natural phenomena forcing them to such behavior. For example, the transformation of the Euphrates River in the areas of Hit- Ramadi. He believe that the modern motivating factor of the subsurface geological structures that these rivers intersect in the above mentioned regions, which represent most of the oil fields not visible on the surface of the earth, were one of the natural factors that led to such change in the direction of the river. The areas of the subsurface structures and the result of the modern activation of these structures have suffered a continuous rise, although it may not exceed a few (cm) per hundred years, but up to a few meters after thousands of years, which may lead to important changes in the topography of easy and low and smooth elevation such as in central and southern Iraq, where the rise (26) m to a few meters above sea level. As a result, this increase in the area of the intersection of the structures with the river over thousands of years leads to the rise of the river bed and an additional decrease in its slope.[4]

They studied Shithatha area, as included in the study analysis of Abu Jir fault zone. They used Bouguer anomaly map of the area in quality and quantity methods, which show two sets of faults, first sets trending N-S (Abu- jir fault zone),and second set is trending E-W (Immam Ahmad fault). [5]Studied the tectonic and structural evolution of Anah region west Iraq, by seismic, drill hole and Surface geological data, have been integrated to infer the tectonic and structure of the Anah region. [6] Makes detailed geological survey on Lissan area in Karbala-Najaf plateau and concluded that the area is effected of Abu-Jir fault zone and all the scarps (ridges) and depressions are due to the effect of the strike-slip Abu-Jir fault zone. [7] They studied water resources within Tigris-Euphrates Rivers in IRAQ and concluded average monthly water flow measurements for 15 stream flow gaging stations within basins of these rivers in Iraq with population growth rate data in some of its part were used to evaluate the reality of the current situation and future challenges of water availability and demand in Iraq. The region is currently facing water shortage problems due to the increase of the demand and climate changes. [8]Studied drainage indications on the growth of Anah Anticline, He conclude that Anah anticline is suffering from lateral and vertical growths by using different parameters. [9] Studied the effect of Abu-Jir fault zone on the distribution and quality of ground water in Iraq he conclude existence relation between the direction of groundwater flow and the direction of the fault zone which is considered as a natural discharge area and controls the movement of the groundwater flow direction. The aims of the study are to describe the structure and geomorphology of Euphrates basin, and to interpret the relationship between Euphrates River Basin and the major fault systems in the area.

STUDY AREA

Due to the large area of Euphrates River and the different tectonic parts that the river passes through, the study area was divided into three reaches namely (Ramadi, Baghdad, and Najaf) with an area of (7726.2 , 4998.8 , and 15022.4) km^2 respectively. As shown in figure (1).

MATERIALS AND METHODS

Morphostructural analysis is a tool of structural geomorphology, which aims at clarifying the direct and indirect linkage between shapes of the Earth's current surface and the structure of the Earth's crust, whose development and

character are currently dependent on the development of the mantle and core [10],[11].The various methods of morphostructural analysis are based either on field research or a set of morphometric techniques and methods of remote sensing, analyzing interdisciplinary reference charts, aerial or satellite images and digital elevation models (DEMs), most commonly in the environment of geographic information systems (GIS). The Euphrates River pass throw different tectonics divisions (stable shelf: Rutba-Jazera Zone, Salman Zone and Mesopotamian Zone). [12], most of that areas are tectonically unrest. Present study achieved by diagram (1).

To achieve present study, the following materials were used:

1. Digital Elevation Model with 30 m resolution was subset to three areas as in figure (1).And was used to determine the location of knick points, the high and low areas and delineated faults.
2. High resolution images (quick birds) with 0.6 m as well as Google Earth images to identified urban, vegetations and facilities near the River Basin.
3. Topographical Maps: a numbers of topographic maps of scale 1:100000 compiled by directory of military survey in order to know the road, villages and other features.
4. Seismic sections distributed along the study areas in order to recognize the subsurface structures.
5. And relevant articles, reports and thesis related with study.

Tectonic History of Iraq

The Arabian plate is surrounded by active tectonic margins [13]; the northern and eastern margins of the plate are composed of the compression regimes of the Taurus suture zone to the north and Zagros thrust zone in the east [14] and [13]. Three major fault systems were available in Iraq N-S Nabitah (Idsas) System, the NW-SE Najd System and the NE-SW or E- W Transversal System. [12].These faults systems formed during Late Precambrian Nabitah orogeny. They were re-activated repeatedly during the Phanerozoic. As shows in figure (2).
Euphrates river was affected by Najd faults system (from figure2) especially the Euphrates Boundary Fault Zone is one of the most prominent Najd fault reaches. It runs along the Euphrates River in S Iraq and continues towards the Rutba area in W Iraq. In the S the fault zone comprises a series of step faults sometimes associated with grabens, and forms the boundary between the Quaternary Mesopotamian Plain and the rocky desert of SW Iraq. The rose diagram for Euphrates River shows the dominated direction N75W and N65W which is same of Najd Faults system. As in figure (3).

RESULTS

From this study the following results can be achieved:

Model Building for Euphrates River

Digital Elevation Model with (30) m resolution was used and subset to three reaches (Ramadi, Baghdad, and Najaf) as we mention earlier. Using Arc GIS10 to get profiles to every reach According to geometric properties, morphological features such as (meanders, plateaus), as well as the directions of the river.
Knickpoint

During floods the floodplain receives a layer of fine sediment that settles out of suspension as the flood waters spread over the floodplain and decrease in velocity. The point of change in slope is called a knickpoint. Knickpoints migrate slowly upstream; thereby extending the new, lower longitudinal profile as the river eats its way upstream.

Knickpoints can be generated in a number of ways: for instance if a stream's base level drops a knickpoint is created, tectonic activity can produce uplift thereby generating a knickpoint, and knickpoints are developed where streams flow over erosionally resistant rocks.[15].As in figure (4).

In order to get net slip in Euphrates River we take high value of knickpoint and subtract from low value of knickpoint to every reaches of study area.Diagram (2) shows the variation of net slip of the areas. From diagram (2) we notice that Al-Ramadi zone represent high values in net-slip in Euphrates River. And the map after projected the knickpoint on the river showed in figure (5).

Fault Delineation

Faulting is fundamentally a brittle mechanism for achieving shear displacement. At deep crustal levels, where rocks tend to deform plastically under conditions of elevated temperature and confining pressure, shear displacement is achieved by the development of shear reaches. Faults range in length and displacement from small breaks with offsets wholly contained within individual hand specimens or small outcrops or larger cliff exposures, to regional crustal breaks extending hundreds to more than 1000 km and accommodating cumulative offsets of tens to hundreds of kilometers. [16], [17], [18] and [19]. After determined the location of knickpoints as first step delineation of faults is recognized the low and high areas along the river course, this done by making contours in different contour intervals for every segments.

Euphrates Structural Model

Generally, Strike-slip fault systems occur at transform boundaries, which are boundaries where two plates slide past one another without the creation or subduction of lithosphere; they can also occur within plates and as components of convergent orogens. Because of this geometry, such arrays are called **flower structures** In transpressive reaches, a **positive flower structure** develops, in which the slip on subsidiary faults has a thrust-sense component (Diagram 3 A); whereas in transtensile reaches, a **negative flower structure** develops, in which the slip on subsidiary faults has a normal-sense component (Diagram8B). The assumption that every knickpoint represent potential fault as we mention earlier, we delineate every fault considering many rules such as v-shape rule, curved of the river (meanders),shapes of water bodies e.g. Lakes as well as high and low areas. We get 51 faults along study area in Euphrates River Basin. As shown in figure (6). The research adapted structural model based on the relationships between fault geometry, displacement, Structure and geomorphology as well as previous data. The model in the Euphrates River basin a strike-slip - extensional model of normal faults. In which; the old stage represented by strike-slip faults represented by the directions of Najd faults. As shown in figure (7). While the extensional model represent by continue curved (listric) faultsdifference in the amount of expansion and the system of stress and strain along the river where the values and trends of stress axes were different in Ramadi and Baghdad $\sigma1>\sigma2>\sigma3$while in Najaf the values became $\sigma1>\sigma2=\sigma3$ due to of stress change in Arabian plate because of the convergence that occurred at the end of the Cretaceous period along the rim of the Arabian plate. As shown in figure (8).

Validity of Euphrates structural model.

Validate our structural model for Euphrates River done by used; Seismic data.

Interpretation of the Regional Seismic Sections

In the mapping of subsurface structures, seismic data are invaluable and since the 1960 have revolutionized our understanding of faults and folds geometry. Some seismic data are collected for purely academic purposes, but the vast majority of seismic data acquisition is motivated by exploration for petroleum and gas. Most seismic data are thus from rift basins and continental margins [19].Seismic reflections surveys, carried out by Iraqi Exploration

Company. Due to the vast area of study area three scattered seismic lines were selected to cover the research area most of it near the Euphrates River Basin. As shown in figure (9).

The interpretation of seismic sections that used in study as follow.

Seismic Time Section KB-38

The shot point between (1000-1992), the length of this section is 99.200 km and its direction SW-NE it lies in Ramadi area (near al Baghdadi city), Four sequences (H, H1, H2 and H3) appeared in this section, the upper part (H) represent recent deposits of Quaternary age, the reflector (H1) represent Formations of Tertiary age. The reflector (H2) represent Formations of Cretaceous age (upper cretaceous), the reflector (H3) represent Formation of Lower Cretaceous age. Structurally; normal fault with different dip directions reflect tectonic activity may be because of Abu-Jir fault. As shown in figure (10).
Seismic Time Section WRH-22

The shot point is between (950-1900), the length of the section 90 km and it is direction SW-NE it lies in Baghdad area (west of Habanyia lake). Four sequences (H, H1, H2 and H3) appeared in this section, the upper part (H) represent recent deposits of Quaternary age, the reflector (H1) represent Formations of Tertiary age. The reflector (H2) represent Formations of Cretaceous age (upper cretaceous), the reflector (H3) represent Formation of Lower Cretaceous age. Structurally; the seismic section consists many steeply dipping of normal faults that converge downward. It represents negative flowers structures (consist of a shallow structure bounded by upward spreading strands of a strike slip fault that have mostly normal separation), and block move obliquely apart (divergent) or parallel to each other (negative flower may be occur), (Foaud, 2000). As shown in figure (11).

Seismic Time Section MD-23

The shot point is between (157-510), the length of the section 35 km and it is direction SW-NE it lies in Najaf area. Four sequences (H, H1, H2 and H3) appeared in this section, the upper part (H) represent recent deposits of Quaternary age, the reflector (H1) represent Formations of Tertiary age. The reflector (H2) represent Formations of Cretaceous age (upper cretaceous), the reflector (H3) represent Formation of Lower Cretaceous age. Structurally; the seismic section appears strike-slip fault (flower structure negative) and normal faults with different directions. As in figure (12).

CONCLUSIONS

This study has the following conclusions

The using of Digital Elevation Model was very efficient to draw many profiles along Euphrates River to specified knickpoints on river course. River profiles is sensitive for any vertical movement as a result of uplift and subsidence in every periods as well as the change of river slop due to change in lithology all leads to form knickpoints along the Euphrates River course. The rose diagram for Euphrates River shows different direction of Euphrates River but dominated direction N75W and N65W which is compatible with the Abu-Jir and Euphrates Boundary Fault zone. Euphrates River cut most of Transverse faults and parallel to Najd faults because of reactivation processes to these faults. Euphrates River can be divided into six tectonic Reaches on the base of change in river directions, four of them located East of the river represent recent sediments and two located West of Euphrates River represent old sediments. The alternately in orientation of Euphrates River is reflect where they are move in relation to change in fault orientation which reflect also the pre-existing structures such as; Rutba block, Anah Graben, Salman Zone, Abu-Jir fault, Euphrates fault, Mesopotamian and there intersection between them, the Anah Graben, Abu-Jir Zone and Euphrates Graben it represent a transtension structure. The Euphrates River basin is a part of the long Western gentle

limb of Mesopotamian geosynclines, this situation a result of sliding along the Western limb. The Euphrates River is a combination of fault and joint systems. It represents a sequence of tectonic events that influenced the Arabian plate from the pre-Cambrian to the present time. It contains many articulate areas that connect these different systems of joints and faults. According to seismic time sections, there are two types of faults; Normal faults of listric faults within H and H1 only (Quaternary and Tertiary age) and strike-slip faults within H2 and H3 (Cretaceous and Lower Cretaceous age). The model in the Euphrates River basin a strike-slip - extensional model of normal faults. In which; the old stage represented by strike-slip faults represented by the directions of Najd faults. While the extensional model represent by continues curved (listric) faults.

REFERENCES

1. Al-Jabbari, M, and Al-Ansari, N., 2000. The Hydrology. Published by ministry of higher education and scientific research. 1063PP.
2. Al-Qayim, B. 2007.Geomorphic Criteria for Tectonic Activity in Al-Jezera area. *Art college magazine.* No.95.in Arabic.
3. Al-Sakini, J.A. 1987. Neotectonic activity in Basrah vicinity and the dryness of western cannels of Shatt Al-Arab. Marine science center, Basrah University. 415-416, (in Arabic).
4. Tariq, S. Al-Dine, and Hussein, H. K.. 1986: Gravity study of Shithatha area. Iraqi, *Jour. Sci.,* V. 27, 185pp.
5. Fouad, S.F.1997. Tectonic and structural evolution of Anah region, west Iraq. Unpub. Ph. D. thesis, Univ. of Baghdad.
6. Hassan, Karim and Galib, Azhar. 2004. Detailed Geological Survey on Lissan area in Karbala-Najaf plateau.GEOSERV, Report no.2870.
7. Al-Ansari,N, Sherwany, Govand and Issa.I. 2014. Expected Future of Water Resources within Tigris-Euphrates Rivers Basin, Iraq. *Journal of Water Resource and Protection*, 2014, 6, 421-432.
8. Sissakian,V. Abdul Ahad, Ayda, Al-Ansari, Nadhir and Knutsson,Sven.2016. Drainage Indications on the Growth of Anah Anticline, West of Iraq. *Journal of Earth Sciences and Geotechnical Engineering,* vol. 6, no.1, 29-46 pp.
9. Abed, Salwan Ali, 2017. Occurrence of Anatidae in Sawa Lake: A Ramsar Wetland Site in Southern Iraq, Journal of Advanced Zoology, J. Adv. Zool. 38 (1) 43-51.
10. Alsa'di,M. A., 2010. Effect of Abu-Jir Fault Zone on the Distribution and Quality of Ground Water in Iraq. Ph. D. thesis, College of Science, University of Baghdad. 184 p.
11. Fairbridge, R. W. 1968. Terraces, fluvial —Environmental controls in Geomorphology. 1124-1138pp. Springer Berlin Heidelberg.
12. Demek, J., 1987. Mountains and low lands: geographic lexicon of čsr, academia, praha, 584 pp., (inCzech).
13. Jassim, S. Z., and Goff, J. C. 2006. Geology of Iraq, Published by Dolin, Pragh and Moravian Mueseum, Brno, 302p p.
14. Stern,B and Johnson,P. 2010. Continental lithosphere of the Arabian Plate: A geologic, petrologic, and geophysical synthesis. https://www.researchgate.net/publication/222917446.
15. Fox, J., and Ahlbrandt, T. S., 2002. Petroleum geology and total petroleum systems of the Widyan Basin and Interior Platform of Saudi Arabia and Iraq. *USGS Bulletin 2202-E.*
16. Ibraheen, Lujain Hussein, and Salwan Ali Abed. 2017. "Accumulation Detection of Some Heavy Metals in Some Types of Fruits in the Local Market of Al-Diwaniyah City, Iraq." *Rasayan Journal of Chemistry* 10 (2) 339–43. doi:10.7324/RJC.2017.1021641.
17. Al-Grawi, E.D.C., and G.R.L. Al-Awsi. 2018. "Expression of CDKN2A (P16/Ink4a) among Colorectal Cancer Patients: A Cohort Study." *Journal of Pharmaceutical Sciences and Research* 10 (5).
18. Salim, Mudhafar A and Abed Salwan Ali, 2017. Avifauna Diversity of Bahr Al-Najaf Wetlands and the Surrounding Areas, Iraq. Jordan Journal of Biological Sciences. Vol. 10 (3), Pages 167 – 176.

19. https://wmblogs.wm.edu/cmbail/the-longhill-drainage-ditch-when-knickpoints-move.
20. Davis, George. Reynolds, Stephen. And Kluth.C. 2012. Structural Geology of Rock s and Regions. John Wiley printed in U.S.A. P.840.
21. Ramsay, J. G., and Huber, M. I. 1987. The Techniques of Modern Structural Geology: Folds and Fractures, v. 2, Academic Press, 700pp.
22. Van der Pluijm, B. A., and Marshak, S. 2004. Earth Structure: An Introduction to Structural Geology and Tectonics: USA, W.W. Norton, 656 pp.
23. Fossen, H., 2010. Structural Geology: United States of America, Cambridge University Press, 457p p.

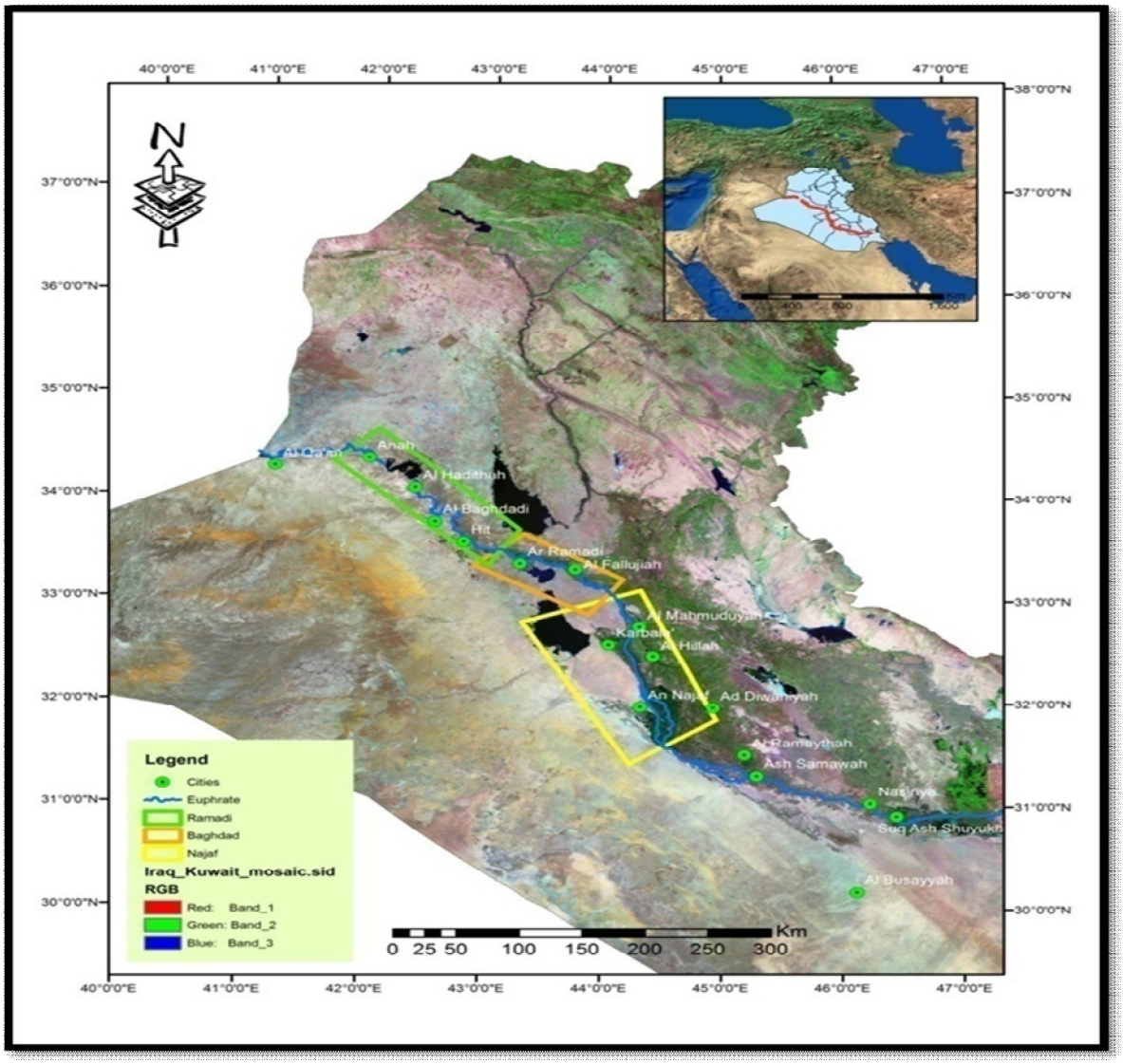

Figure (1) Location and divisions of study area

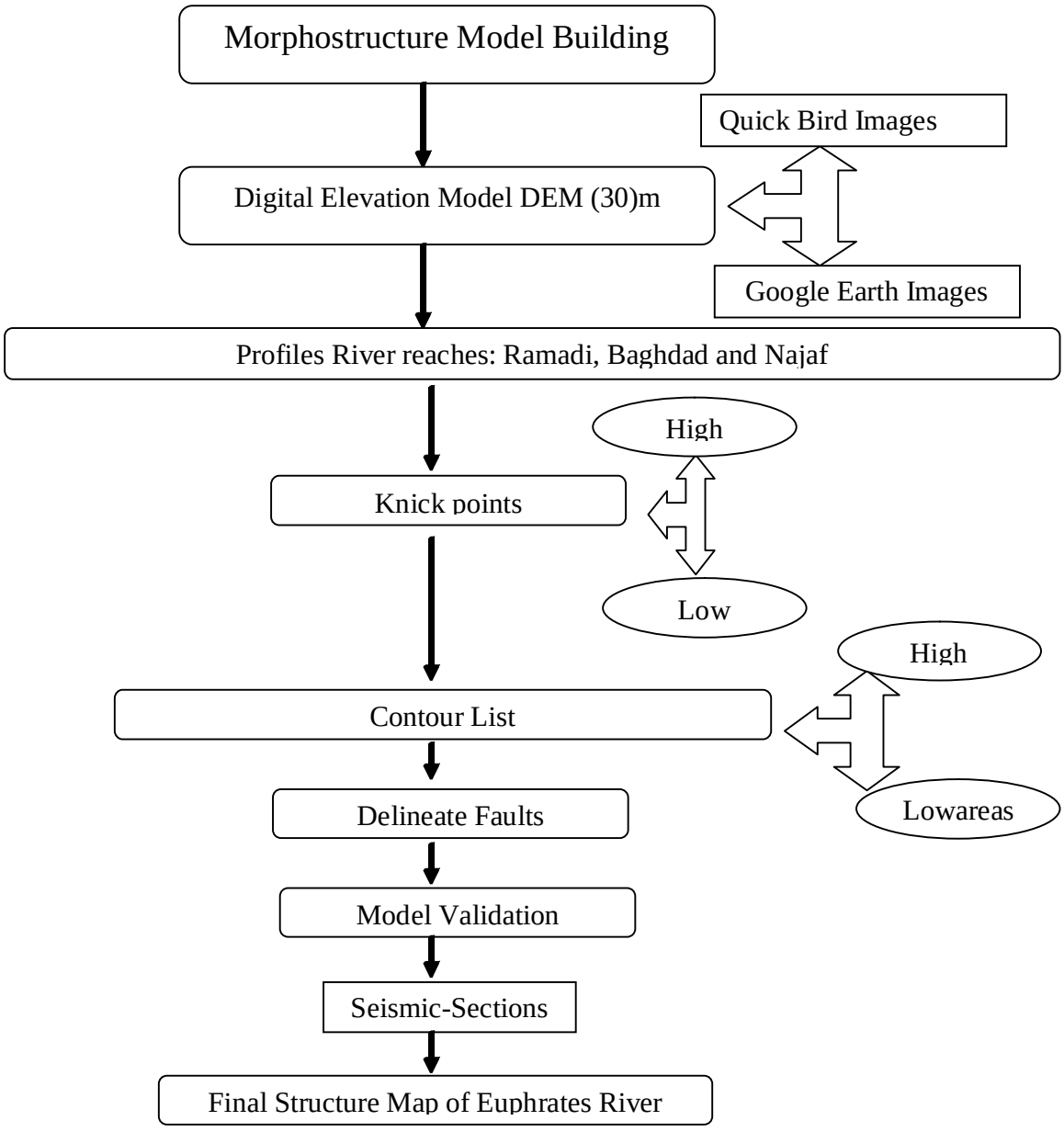

Diagram (1) Flowchart of morphostructure model forEuphrates River

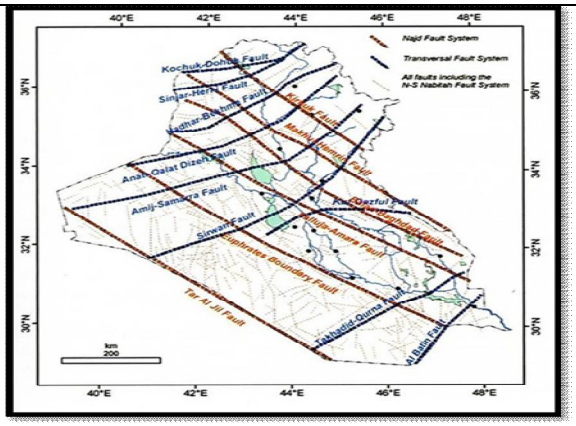

Figure (2)
Distributions of Faults in Iraq (after Jassim&Goff, 2006)

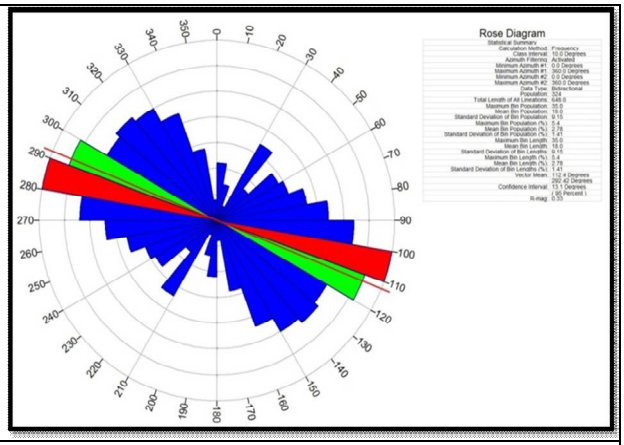

Figure (3) Rose diagram represent general direction for Euphrates River

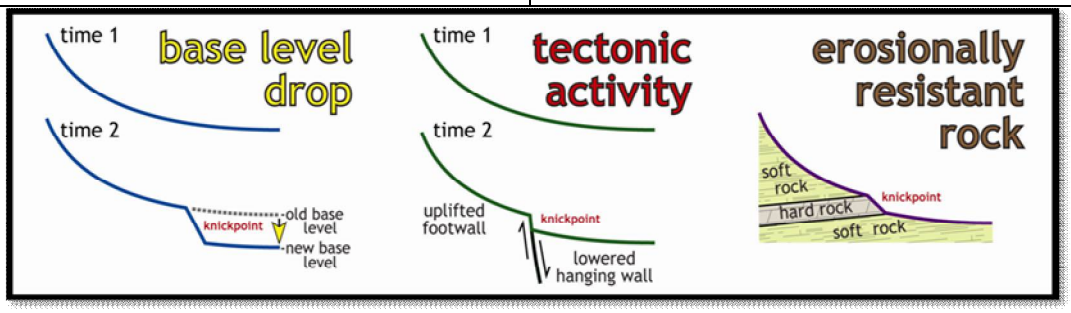

Figure (4) Types of generating knickpoints. [https://wmblogs.wm.edu/cmbail/the-longhill-drainage-ditch-when-knickpoints-move].

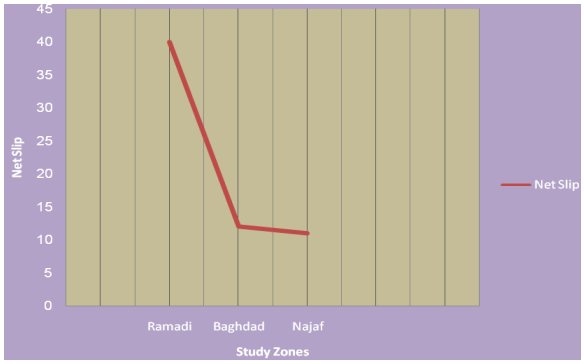

Diagram (2) the net slip of the studiedreaches

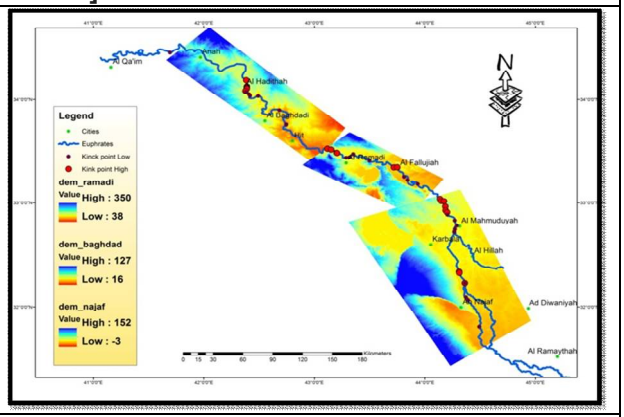

Figure (5) shows the high and low knickpoint along the Euphrates River

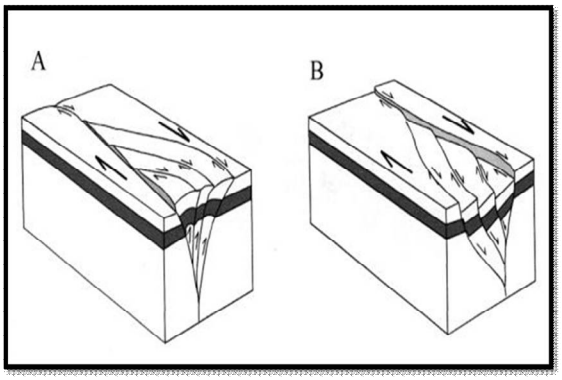

Diagram (3) diagram shows A- Flower structure Positive B- Flower structure Negative after [pluijm& Marshak, 2004

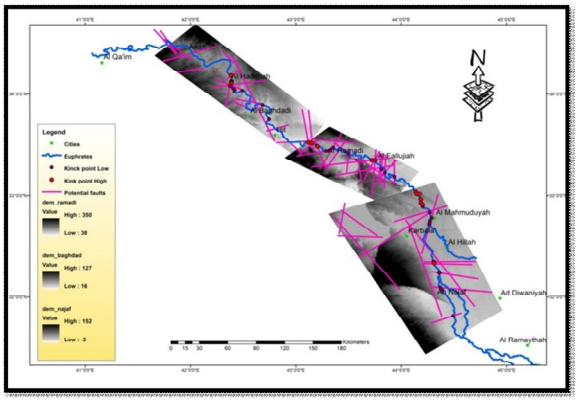

Figure (6) Faults along Euphrates River basin delineated by knickpoint method

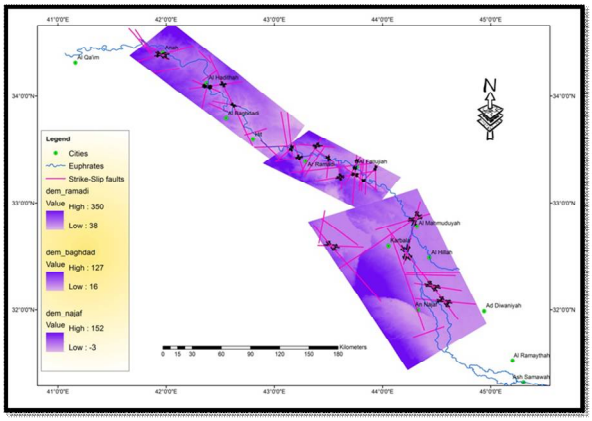

Figure (7) Strike-Slip Structural map for Euphrates River Basin

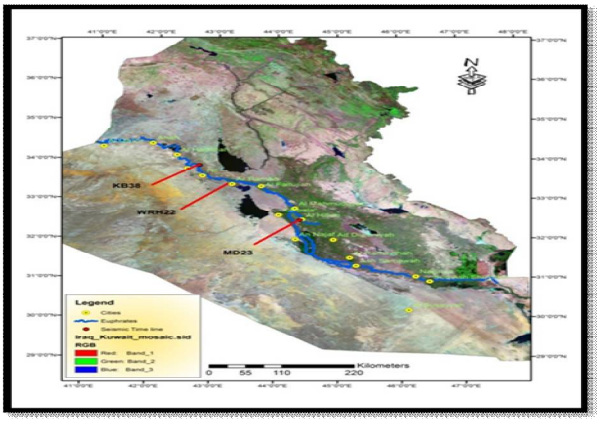

Figure (9) Seismic time sections in study area

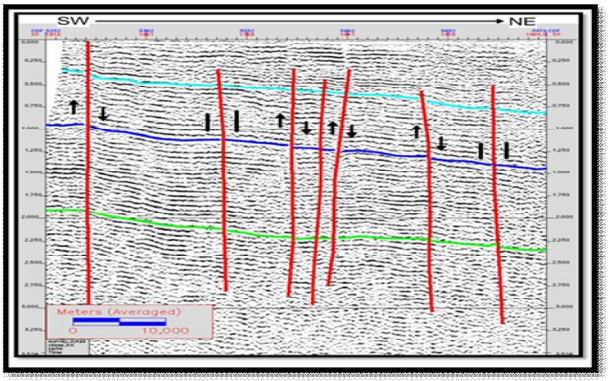

Figure (10) Example of Seismic Time Section KB-38 in Ramadi area

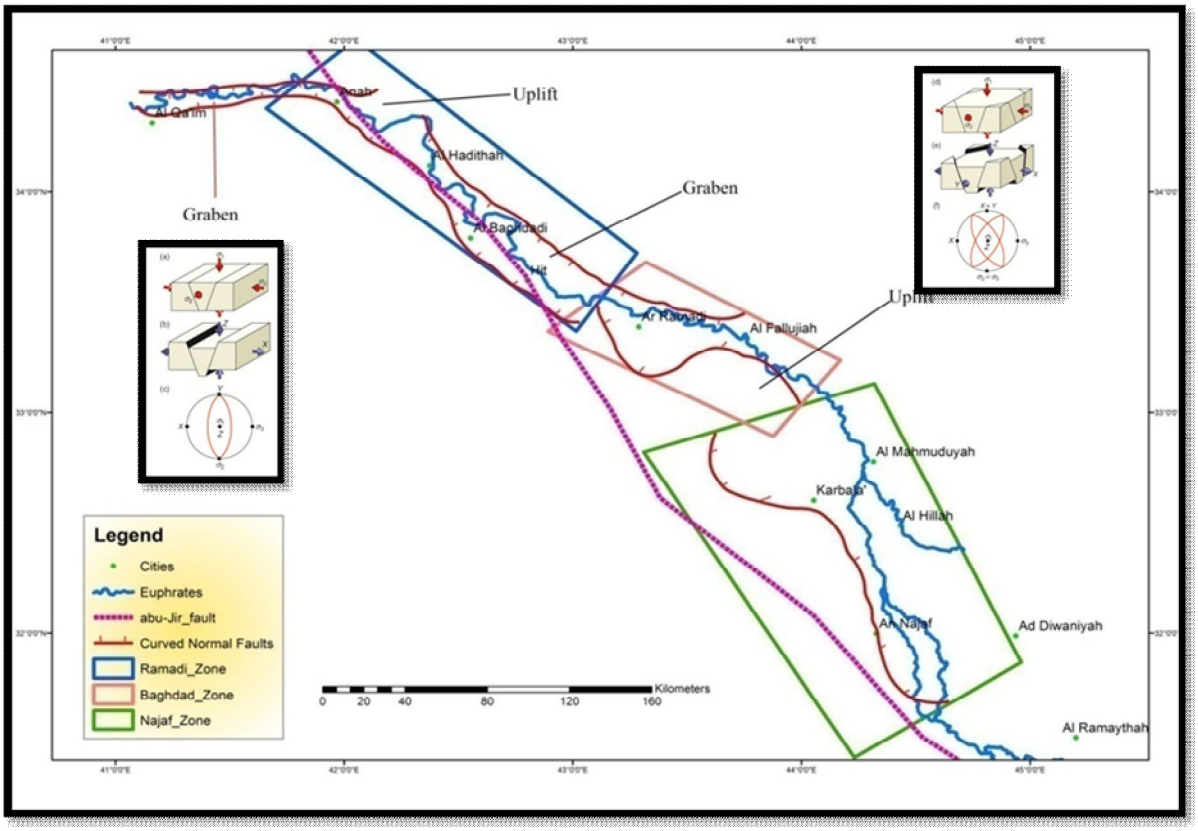

Figure (8) faults delineated by extensional model represented by continue curved Listric along Euphrates River basin

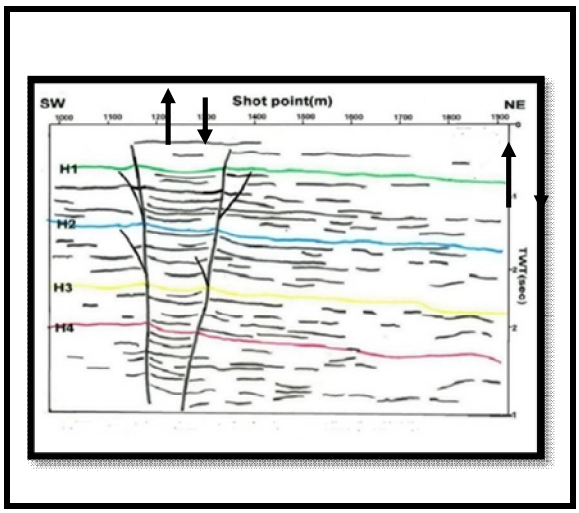

Figure (11) Example of Seismic Time Section WRH-22 in Baghdad area

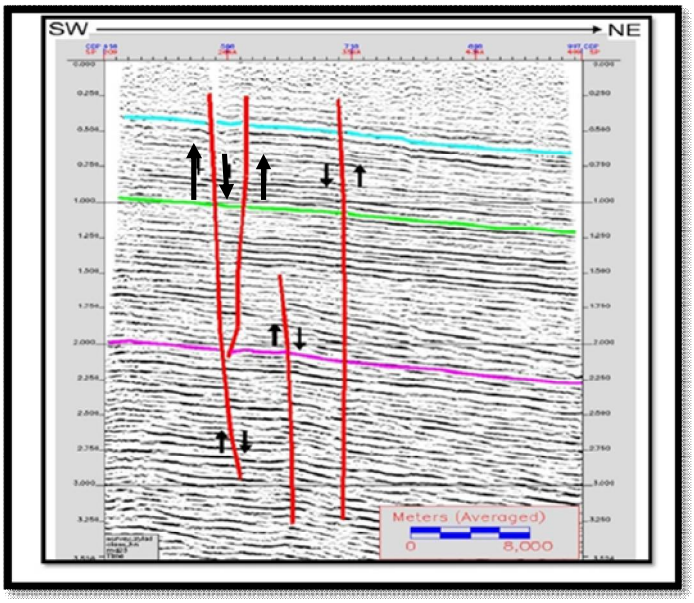

Figure (12) Example of Seismic Time Section MD-23 in Najaf area

Indian Journal of Natural Sciences www.tnsroindia.org.in ©IJONS

Vol.9 /Issue 51 / December / 2018 *International Bimonthly* *ISSN: 0976 – 0997*

RESEARCH ARTICLE

Synthesis and Biological of New Schif Bases Oxazole Compounds

Abbas A. Shalan Al-Saidi* and Moayd N. Mohammed

College of Agriculture, University of Al-Qadisiyah, Diwaniyah, Iraq

Received: 17 Sep 2018 Revised: 19 Oct 2018 Accepted: 22 Nov 2018

***Address for Correspondence**
Abbas A. Shalan Al-Saidi
College of Agriculture,
University of Al-Qadisiyah,
Diwaniyah, Iraq.
Email:moayad_alshbani@qu.edu.iq

ABSTRACT

The aim of the present work is the synthesis of schif bases were derived from 5-p amino phynyloxazole in the presence of 4-methyl benzaldehyde,4-bromo benzaldehyde, 4-dimethyl amino benzaldehyde and benzaldehyde. The structures of the synthesized compound were determined on the basis of their FIIR, and H-NMR. The antibacterial activity was evaluated in DMSO.

Keywords: Oxazole , 5-p-aminophenyle oxazole glycine , benzaldehyde.

INTRODUCTION

The synthesis and properties of oxazolewere reviewed in 1987 by [1,2,3]RonaldGriggsfrom azomthineyliden. [4,5]Moayad N. Mohammedsynthesis oxazolederivatives form symmetrical and unsymmetrical benzilswith α-amino acids the oxazolemoietehave broad spectrum of biological activity[6,7]and are found in alarge number of natural products[8]and function material[9]. Onthe other hand arylatedoxazolesare of great interest motonlydue to their bilologicalproperties but also due to their importance as organic materials such as scintillatecompound and florescentdyes. For their biological activity and exhibit antifungalantibacterial antiviraland antimicrobial properties. All the compounds characterized on the basis of the melting layer chromatography infraredspectra , elemental analysis date Another study includes the biological activity.

EXPERIMENTS

Physical Measurements

All chemicals used in the syntheses were of reagent grade and used without further purification . All meltiypoints were determined open capillary and using TLC, C.H. N, IR and HNMR.

synthesis of Oxazole(11-12)

4-amino benzoyl (0.01) molewas added to asolution made up of α-amino acid glycine (0.01 mole) and sodium ethanol (30 ml). The reaction mixture was refluxed in a water both the evaluation of Carbone dioxide had ceased the hot mixture wasfractional crystallization,the products was re dissolved in ethanolfor re- crystallization and then dried to give product.

Synthesis of new Schiff Bases

Be aldehydederivatives(0.01 mole) in 50 ml of absolute ethanol with drops glacial acetic acid were stirredfor 15min .them(0.01 mole) 5-p-amino phenyl oxazolewas added and stirred for (1-3 h) . The solidformed was filtered and re-crystallized from ethanol.

Astudy of biological activity

The introduction of the prepared in the vitality of the study is to investigate the extent of bio-effectiveness .it has included the study of the effect of the prepared compounds in the two types of bacteria isolated from medical conditions (human) and it has studied and diagnosed and proved their attributes . It has identified its resistance to different antibiotics that are also carried out the development operations and increased the numbersof these bacteria in temperature (37 C) .These types of bacteria are *staphylococcus aureus*and Salmonella .
The results of antibacterial were presents in Table (4) .

RESULTS AND DISCUSSION

The precursor required for our present study were preparedin 6-80% yield by the treatment of 4,5-di-p-aminophenyle oxazolewith different aromatic Benz aldehyde product the newly Schiff bases characterized by spectral IR .C.H. and HNMR. The physical characterization and spectral data are presented in tables 1-3 physical characterization and analytical data of new schiff bases. The result of antibacterial were presented in table 4 .The results of the study have showed that many of the affective ant microbiologicalpreparedcompoundstowards these types of bacteriawhere inhibition zones have ranged from (5-15)mm . The results have showed also a close relationship between the efficiency of the microbiological of the prepared compounds and the nature of redeeming groups in their structures.

CONCLUSION

In the paper , the main new five Schiff base , were synthetized all the synthesized compounds were evaluated for in vitro antibacterial.

REFERENCES

1- Atto.A.T. and Habib. A.T. J .Iraqi .chem .soc1987 , 33-2.
2- Mckee .M.L; Kerwn .S.M. Boorg- Med –chem.2008 , 16 , 1775.
3- RodriguesA.D ;Ramiresc ; org.lett .1999 , 1 , 527.
4- Don M.J ;shen.c. J. Nat prod. 2005 , 68 , 1066.
5- AL-NASHI, A.P.AliAbed Raheem; AL-AOSI, G. R. L. (2013). Isolate and diagnose the bacteria present in the hospital in the city of Diwaniyah and the statement of the mechanisms to control the use of antibiotics and antiseptics. Al-Qadisiyah Journal of Pure Science, V. 18 (3): 11-20.
6- Majmadar .K.C ;situ. G. Tetranedo letters 2012. 53. 1553- 1557.

7- Leaver , I.H ; Milligan . B. Dyes pigm. 1984, 5, 109.
8- Richard . J.P; John .R.K .Bioorgank and medicinal chemistry. 2010 . 18-4821-4829.
9- Guuthromp.M.J ;Benchom .C.D. Trends pharmacol.sci, 2002 , 23 , 183.
10- Lateef, G., Al-Thahab, A., &Chalap Al- Grawi, E. (2018). Linkage between H. pylori Infection and TNF-α polymorphism in The Pregnant Women. *International Journal Of Research In Pharmaceutical Sciences, 9* (SPL1). doi:10.26452/ijrps.v9iSPL1.1298
11- Mouayad .N.M . J. chm – chem . Eng. 2012. 6- 682-685.
12- Mouayad.N.M . J. chm – chem. Eng. 2012. 6- 885-888.
13- Shamran, A. R, Shaker, Z. H, Al-Awsi, G. R. L, Khamis, A .S , Tolaifeh, Z. A. and Jameel, Z. I, 2018. RAPD-PCR IS A GOOD DNA FINGERPRINTING TECHNIQUE TO DETECT PHYLOGENETIC RELATIONSHIPS AMONG STAPHYLOCOCCUS AUREUS ISOLATED FROM DIFFERENT SOURCES IN HILLA CITY, IRAQ. Biochemical and Cellular Achieves. Vol. 18, Supplement 1, pp. 1157-1161.
14- Mouayad .N.M . J. chm – Qadisiyaof pure science 2013, 1 ,18.
15- Al-Grawi, E.D.C., and G.R.L. Al-Awsi. 2018. "Expression of CDKN2A (P16/Ink4a) among Colorectal Cancer Patients: A Cohort Study." *Journal of Pharmaceutical Sciences and Research* 10 (5).
16- Mouayad .N.M . J. chm – Qadisiya of pure science 2017, 5 ,22.

Table 1 Analytical data

Comp	Molecular formula	Colour	Yeld	(calc)-found%		
				C	H	N
1	$C_{12}H_{16}N_2O$	White	67	78.260	4-968	8-695
				78-257	4-869	8-584
2	$C_{21}H_{15}N_2OCl$	Yellow	60	72-727	4-298	8-08
				72-619	4-298	8-079
3	$C_{21}H_{15}N_{20}OBr$	White	65	64-445	3-836	7-161
				64-384	3-765	7-157
4	$C_{22}H_{18}N_2O$	Orange	75	80-981	5-521	8-588
				80-795	5-487	8-497
5	$C_{23}H_{21}N_3O$	white	70	77-746	5-915	11-830
				77-678	5-876	11-792

Table 2 FTIK date for new Schiff base

com	VC=C	C=N	otherγ cm^{-1}
1	1600	1650	
2	1590	1640	
3	1640	1690	C-Cl (830)
4	1630	1680	C-Br (570)
5	1610	1710	C-N (820)

Table-3 H^1NMR data for new Schiff base

Comp	Structure	H^1NMR DMSo-d6
	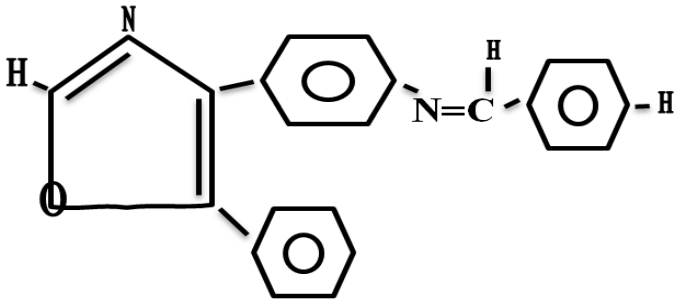	(c-H) 7-90-781 ppm of oxazole (s) (c-H) schiffbase (S) 804 ppm Ph (m) 6.4-7.5 ppm Ph-N (m) 6-6-8-6
	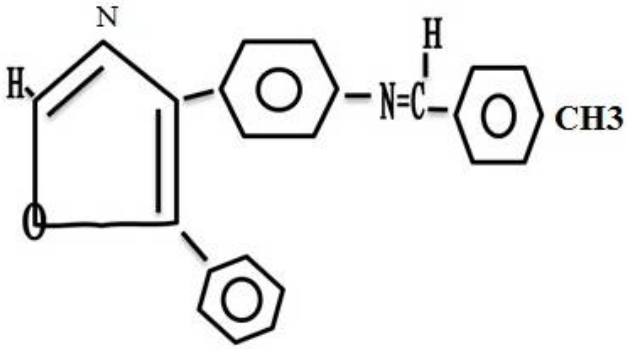	c-H 7-89-7-84 (s) ppm c-H 8-4 (s) ph 8-4 (S) ppm ph (m) 7-3- 8.72 ppm ph- (cH3) 7.5 ph N- 6.8 (m)
	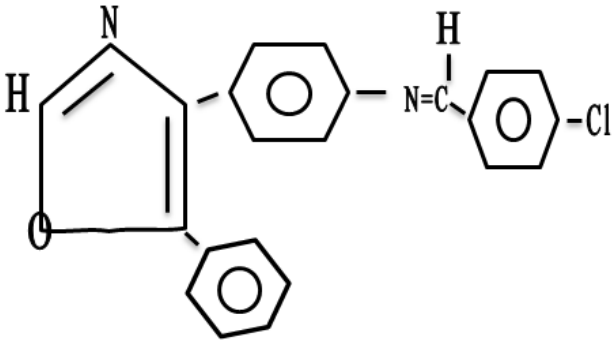	c-H 7-81 – 7.74 (S) c-H 8.3 (S) ph (M) 6-3- 6-5 ph-cl 7.3 – 8.7 (M) ph N6-7-8-7 (M)

Table 4 Biological activity of new Schiff bases

Com / bacteria	Positive *St. aurous*	G-negative *E.coli*
1	5mm	8 mm
2	9mm	8 mm
3	6mm	7 mm
4	15 mm	10mm
5	11 mm	10 mm
1-5= +	Slightly active	
0-10= ++	Active	
11-15 = +++	Highly active	

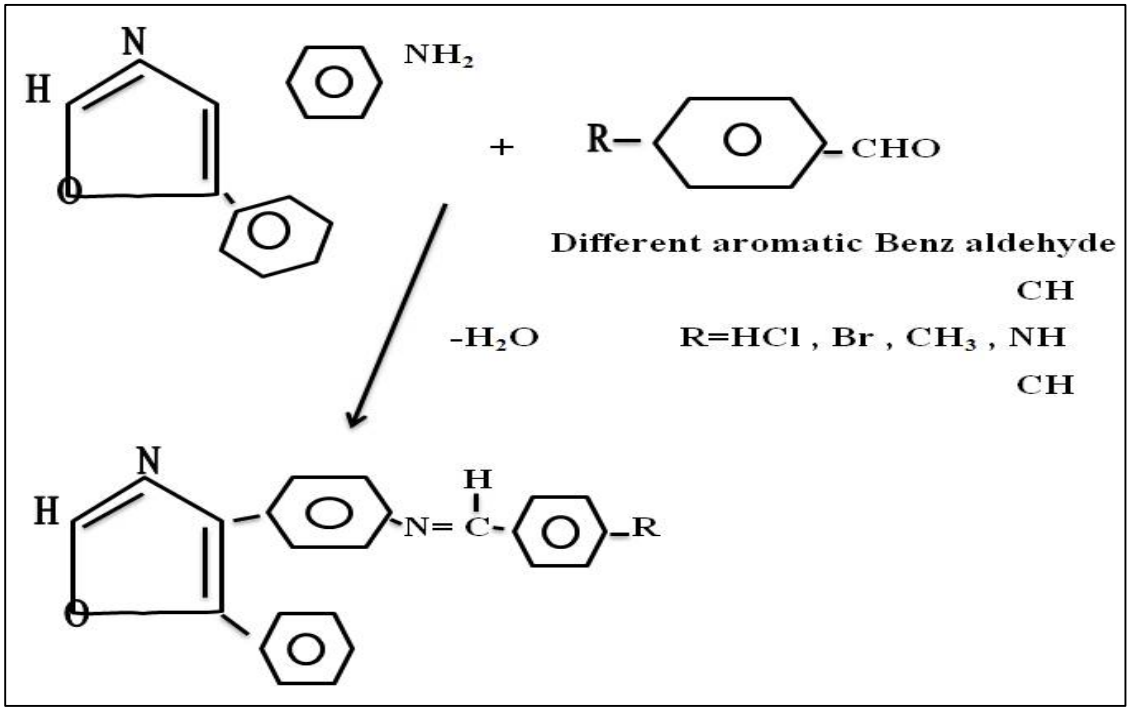

Fig 1.A study of biological activity

Indian Journal of Natural Sciences www.tnsroindia.org.in ©IJONS

Vol.9 /Issue 51 / December / 2018 *International Bimonthly* *ISSN: 0976 – 0997*

RESEARCH ARTICLE

Geochemical Indicator for Decipher the Paleoredox Environment of the Zubair Formation in Southern Iraq

Salih.M. Awadh[1]*, M. R. A. Al-Auweidy[1] and A.A.Al-Yaseri[2]

[1]Department of Geology, College of Science, University of Baghdad, Baghdad, Iraq.
[2]Ministry of Oil,Southern Oil Company, Basrah, Iraq.

Received: 19 Sep 2018 Revised: 21 Oct 2018 Accepted: 27 Nov 2018

***Address for Correspondence**
Salih.M.Awadh
Department of Geology,
College of Science, University of Baghdad,
Baghdad, Iraq.
Email: salihauad2000@yahoo.com

ABSTRACT

The main objective of this study is characterized the paleoredoxenvironment of the clastics Zubair Formation deposition.The Zubair Formation is deposited in L. Cretaceous under variable levels of oxygenation. Forty samples are analyzed to decipher oxic deposition conditions of the formation. They are included twenty- five samples of upper sandstone and fifteen samples of upper shale members. The trace elements (V, Mo, U, Cu, Ni, Cr, Co, and Th) which are utilizedas geochemical indicator to determine the environment of deposition. Trace element ratios such as U/Th, (Cu + Mo)/Zn, V/Cr, V/ (V+Ni)and Ni/Co in addition to authigenic uranium and Th/U are demonstrated the paleo-oxygenation of the Zubair Formation. The values of U/Th (0.31, 0.21), (Cu + Mo)/Zn (0.42, 0.45), V/Cr (0.55, 1.3), V/ (V+Ni) (0.75-0.80), authigenic uranium(-0.15, -1.79) and Ni/Co (2.87, 2.47).These results environment is most predominant mainly under oxic conditions.

Keywords: paleo-oxygenation, Zubair Formation,Trace elements.

INTRODUCTION

The L. Cretaceous (Barremian-Early Albian) Zubair Formationis a huge clastic deposit with more than 200 meters. It is a huge oil reservoir in Iraq.The trace elements (V, Mo, U, Cu, Ni, Cr, Co, and Th) are utilizedas indicator of oxic deposition conditions of the formation.Redox-sensitive trace element concentrationsor ratios are among the most widely used geochemical indicators ofredox conditions in modern and ancient sedimentary (4).

Geological setting

The present research deals with salinity that includes in the oilfields Ratawi (Rt), Luhais (Lu), Suba (Su), Rumaila North (R), Rumaila South (Ru), Zubair (Zb) and NahrUmer (NR) within Zubair reservoir. The selected part of the Zubair reservoir is located in Southern Iraq at Basra Governorate (Figure 1). It is boundaries restricted within the Zubair Formation.In Iraq, it extends from the Tharthar region in central Iraq toward the south extend passing the Iraqi-Kuwait border (9). It passes laterally into E and NE equivalent to Gadvan Formation in Iran, while toward the S and SW it is equivalent in both age and lithology to Biyadh Formation in KSA and Zubair in Kuwait (5).The Zubair Formation belongs to the L. Cretaceous; its age is Barremian-Early Albian (1) Formation thickness is ranging composed of 245 and 517m of (23), while in southern Iraq, the thickness is ranging from 301 to 381m in wells NR-9 in well Zb-47 respectively (2). In the south of Iraq and Kuwait, it is overlain by the Aptian Shuaiba limestone Formation and is underlain by the Valanginin-Hauterivian Ratwi limestone Formation, both formation contacts are gradational and conformable (15). In some parts of the Salman Zone in the south, the Zubair Formation is overlain unconformable the Sullay Formation (9).

The Zubair Formation is assumed to represent a prograding delta (25). After the uplifting in the west, deltaic sediments derived from the erosion of the Arabian Shield and the stable shelf (6). The uplifting results of the late Kimmerian movement (3) and thermal doming and rifting eastern Africa (12). The deposition contemporaneous with the opening Neo-Tethys Ocean in the east of Arabian plate in the Early Cretaceous. It's composed of flovio- deltaic, deltaic and huge amount of marine sandstones (7). The Zubair Formation is divided mainly, into five lithological units in southern Iraq (15), it composed of alternating sandstone, siltstone, and mudstone/shale units in southern and central Iraq. (23). Intraformation Zubair shale is the primary seal, which envelops the reservoirs from the same formation. In southern Iraq, the Zubair Formation overlies the Jurassic–Early Cretaceous formations which are included Sargelu, Najmah, Gotnia, SulaiyYamama and Ratawi (7) (Figure 2).

Study area location

The study area is approximately located between longitude (65 000- 78 000) Easting and Latitude (333 0000- 342 0000) Northing as shown in (Figure 1). The study area is relatively flat terrain with a gradient of less than 10 cm per kilometer. It is located tectonically in the southern part of the Near platform flank of Mesopotamian foredeep (10), within the Zubair subzone which is a part of the Stable Shelf (15). The fields in the Basra occur along N-S trending folds in the southern part of the basin. N-S striking, basement-cored anticlines in this part of the basin began forming in the Paleozoic, with continued but with more limited growth throughout the Mesozoic and Early Cenozoic (1). It is a result of the continental collision of the Arabian and Eurasian plates. Collision started during the Late Cretaceous and increased in intensity during the Paleogene/ Neogene (8).The stratigraphic section of formation of Zubair is showed in figure 2

MATERIALS AND METHODS

Geochemistry of the Zubair Formation was investigated in seven oil fields through total forty (40) core samples, 15 samples collected from upper shale member and 25 samples collected from upper sandstone member. These core samples were analyzed for trace elements (V, Mo, U, Cu, Ni, Cr, Co, and Th) using inductively coupled plasma-mass spectrometry (ICP-Ms) and inductively coupled plasma atomic emission spectroscopy (ICP-AES) instrument that were conducted at ALS Laboratory Group, Sl- Sevilla, Spain. The result of the analysesis tabulate in table (1).

Objectives

The targets of this study: Characterized thepaleoredox environment of the Zubair Formation deposition.

Paleo-oxygenation

For evaluating the paleoredox conditions, some specific trace elements and their ratios, such as V, Mo, U,Co, Zn, Cr and Cu, are powerful tool for evaluation and determination the paleoredox conditions (4 ,22 ,17 ,24).The redox conditions are mostly controlled some multi valence trace elements such as V, Mo, U, and Ni, affected in their mobilization, precipitation, and concentration and thus considered as redox-sensitive elements that are usually enriched in anoxic sediments (21).Theycharacterized by geochemical properties which have a solubility in oxidizing conditions and less soluble under reducing conditions,resulting in an authigenic concentration tend to precipitate in an oxygen-depleted environment (22).Trace element ratios such as U/Th, (Cu + Mo)/Zn, V/Cr, and Ni/Co are used to decipher depositional redox conditions of sediments (24). The basic fact is that Ni/Co and V/Cr ratios decrease with increasing oxygenation level in water columns (11). (18) demonstrated that U in a water column is oxidized to soluble U^{6+} under an oxidizing condition and results in the loss of U, while Th is generally present as insoluble Th^{4+} and stable under redox conditions. (20) demonstrated that U/Th ratios < 1.25 indicate an oxic condition, 1.25 to 1.50 reflect a dysoxic condition, and > 1.50 reveal an anoxic environment. The U/Th ratios of sand and shale from the Zubair Formations vary from 0.22 to 0.47; average 0.33, and 0.11 to 0.62; 0.25 respectively, reflecting oxic conditions (Table, 1). Another index of depositional conditions is the authigenic uranium content which calculated as (19):

$$(U_{authigenic}) = (U_{total}) - Th/3.$$

Values of authigenic U below 5 are thought to represent oxic depositional conditions, while values above 5 are indicative of suboxic and anoxic conditions. The authigenic U ratios of sand and shale from the Zubair Formations vary from -0.26 to 0.55; average -0.15, and -4.17 to 0.78; -1.79 respectively, confirming oxic depositional conditions (Table, 2). In addition, (13) believed that (Cu+Mo)/Zn ratios will increase under reducing environments (> 2) and decrease under oxic conditions (< 2). The (Cu + Mo)/Zn ratios of sand and shale from the Zubair Formations vary from 0.02 to 2.04; average 0.42, and 0.04 to 2.5; average 0.45 respectively, which are obviously lower than 2, indicating more oxidising conditions (Table,2). Vanadium in sediments also increases under anoxic conditions, and the V/Cr ratios usually used as an index of paleo-oxygenation (13). It increases with decreasing oxygenation in water columns. Cr is mainly derived from detrital, clastic components, while V is commonly linked to organic matter and accumulated in reducing conditions (22). Generally, V/Cr ratios < 2.0, 2.0 to 4.25, and > 4.25 reflect oxic, dysoxic, and anoxic conditions, respectively (16). The V/Cr ratios of sand and shale from the Zubair Formations fluctuate from 0.15 to 1.2; average 0.55, and 0.68 to 3.22; average 1.3 respectively, which are lower than the oxic-thresholds of 2.0 which imply that the Zubair clasts were deposited in an oxic depositional environment. (Table,2); Figure 3). (16) used Ni/Co ratios as a redox indicator and suggested if it < 5.0 inferred oxic environment, 5.0 to 7.0 reveal a dysoxic environment, whereas ratios > 7.0 indicate a reducing condition which related to low oxygen levelsduring the deposition. It is obtained for sand and shale of the Zubair Formations fluctuate from 1.0 to 8.0; average 2.87, and 1.33 to 7.0; average 2.47 respectively, which suggest an oxic environment (Table 5). As discussed above, the redox-sensitive trace element ratios, such as U/Th, (Cu + Mo)/Zn, V/Cr, and Ni/Co, indicate that the Zubair Formation clasts were deposited under well oxidizing conditions of their deposition. The Figure, 3 confirm the anoxic conditions of the Zubair Formation sedimentation.

CONCLUSION

This study has provided geochemical data to constrain thedepositional environmentconditions of the Zubair Formation in the southern Iraq. The clastic sediments ofthe formation were deposited mainly under oxic depositionalenvironments as evidenced by relationship ratios such as U/Th, (Cu + Mo)/Zn, V/Cr, and Ni/Co in addition to uranium.Accordingly, the oxicconditions are most predominant for the deposition of theZubair sandstones and shales.

ACKNOWLEDGEMENTS

The grateful from us to the Basrah Oil Company (BOC) for providing with the oilfield water samples and all the related data to complete this research. Our appreciation is also gone to the ALS Laboratory Group, Sl- Sevilla, Spain for conducting the analysis of core samples.

REFERENCES

1. Al-Ameri, T. K., Pitman J., Naser M. E., Zumberge J. and Al-Haydari H. A., 2011: Programed oil generation of the Zubair Formation, Southern Iraq oil fields: results from Petromod software modeling and geochemical analysis. Arabian Journal of Geosciences, Vol. 4, pp 1239-1259.
2. Ali, A. J., and Nasser, M. E., 1989: Facies analysis of the L. Cretaceous oil-bearing Zubair Formation in southern Iraq. Modern Geology, Vol. 13, pp. 225-242.
3. Al-Fares A. A., Bouman M. and Jeans P. A., 1998: New look at the Middle-Lower Cretaceous stratigraphy, offshore Kuwait. GeoArabia, Vol. 3, No. 4, pp. 543-560.
4. Algeo, T.J., Maynard, J.B., 2004: Trace element behavior and redox facies incore shales of Upper Pennsylvanian Kansas–type cyclothems. Chem. Geol. Vol. 206, pp. 289–318.
5. Al-Husseini, M., 2000: Preliminary Chronostratigraphic Chart of gulf region, http://www.gulfpetrolink.com.
6. Al-Sharhan, Abdulrahman S., Nairn A. E. M., 1997: Sedimentary basins and petroleum geology of the Middle East, Elsevier, Amsterdam, 843 p.
7. Aqrawi, A., Goff, J., Horbury, A. and Sadooni, F., 2010: The petroleum geology of Iraq, Scientific press ltd, UK 424 P.7
8. Beydoun Z. R., Hughes-Clark M.W. and Stoneley, R., 1992: Petroleum in the Mesopotamian Basin: A late Tertiary foreland basin overprinted onto the outer edge of a vast hydrocarbon-rich Paleozoic- Mesozoic passive-margin shelf, in R.W. Macqueen, and D.A. Leckie, (eds), Foreland Basins and Fold Belts: AAPG Memoir 55, AAPG, Tulsa, Oklahoma, USA, pp. 309-339.
9. Buday T. and Jassim S.Z., 1980: The regional geology of Iraq, stratigraphy and palaeogeography. State Organization for Minerals, Baghdad, Iraq, 445p.
10. Ditmar, V. and Iraqi–Soviet Team., 1971: Geological conditions and hydrocarbon prospects of the republic of Iraq (Northern and Central Parts). Manuscript report, INOC Library, Baghdad, Iraq.
11. Fu X., Wang J., Chen W., Feng X., Wang D., Song C. and Zeng S., 2016: Elemental geochemistry of the early Jurassic black shales in the Qiangtang Basin, eastern Tethys: constraints for paleoenvironment conditions. Geol. J., Vol. 51, pp 443-454.
12. Giraud R., and Maurin J. C., 1992: Early Cretaceous rifts of Western and Central Africa: an overview. Tectonophysics, Vol. 213, pp. 153- 168 Elsevier Science Publishers.
13. Hallberg, R.O.A., 1976: Geochemical method for investigation of paleoredox conditions in sediments. Ambio special report Vol. 4, pp. 139–147.
14. Jafar, M. S. A, 2010:Hydrocarbon source and oil accumulation in Cenomanian-Early Turonian Mishrif Formation reservoir, in selected fields, Southeastern Iraq. Ph.D. Thesis, University of Baghdad, 203P.
15. Jassim, S. Z., and Goff, J. C., 2006: Geology of Iraq. Published byDolin, Prague and Moravian Museum, Brno, 341 P.
16. Jones, B., Manning, D.A., 1994: Comparison of geochemical indices used for the interpretation of palaeo-redox conditions in ancient mudstones. Chem. Geol. Vol. 111, pp. 111-129.
17. Lézin, C., Andreu, B., Pellenard, P., Bouchez, J.L., Emmanuel, L., Fauré, P., Landrein, P., 2013: Geochemical disturbance and paleo-environmental changes during the Early Toarcian in NW Europe. Chem. Geol. Vol. 341, pp. 1–15.
18. Morford, J.L., Martin, W.R., Carney, C.M., 2009. Uranium diagenesis in sediments underlying bottom waters with high oxygen content. Geochim. Cosmochim. Acta, Vol. 73, pp. 2920-2937.
19. Nagarajan, R., Madhavaraju, J., Raghavendra N., Armstrong-Aldrin, J. S., Moutte, J., 2007: Geochemistry of Neoproterozoic shales of the Rabanpalli Formation, Bhima Basin, Northern Karnataka, southern India:

implications for provenance and paleoredox conditions. Revista Mexicana de CienciasGeologicas Vol. 24, pp 150-160.

20. Nath B. N., Kunzendorf H., and Pluger W. L, 2000: Influence of provenance, weathering, and sedimentary processes on the elemental ratios of the fine-grained fraction of the bedload sediments from the Vembanad lake and the adjoining continental shelf, Southwest coast of India. Journal of Sedimentary Research, Vol. 70, No. 5, pp. 1081–1094.
21. Tobia F. H., Mustafa B. H., 2016: Geochemistry and mineralogy of the Al-rich shale from Baluti formation, Iraqi Kurdistan region: implications for weathering and provenance. Arabian Journal of Geosciences, Vol. 9 Issue, 20, 23 P.
22. Tribovillard, N., Algeo, T.J., Lyons, T., Riboulleau, A., 2006: Trace metals as paleoredox and paleoproductivity proxies: An update. Chem. Geol. Vol. 232, pp. 12–32.
23. Van Bellen, R. C., Duningotn, H. V., Wetzel, R. and Moroton, D. M., 1959: Lexique stratgraphique international, Asia, Facicula; Tenth A. Iraq, Center National de la Recherché Scientifique, Paries, 333 P.
24. Zeng, S.Q., Wang, J., Fu, X.G., Chen, W.B., Feng, X.L., Wang, D., Song, C.Y., Wang, Z.W., 2015. Geochemicalcharacteristics, redox conditions, and organicmatter accumulation of marine oil shale from the Changliangmountainarea, Northern Tibet, China. Mar. Pet. Geol. Vol. 64: pp. 203-221.
25. Ziegler, M. 2001: LatePermian to Holocenepaleofaciesevolution of the Arabian plate and itshydrocarbon occurrence. GeoArabian, Vol. 6, No. 3, pp. 445-504.

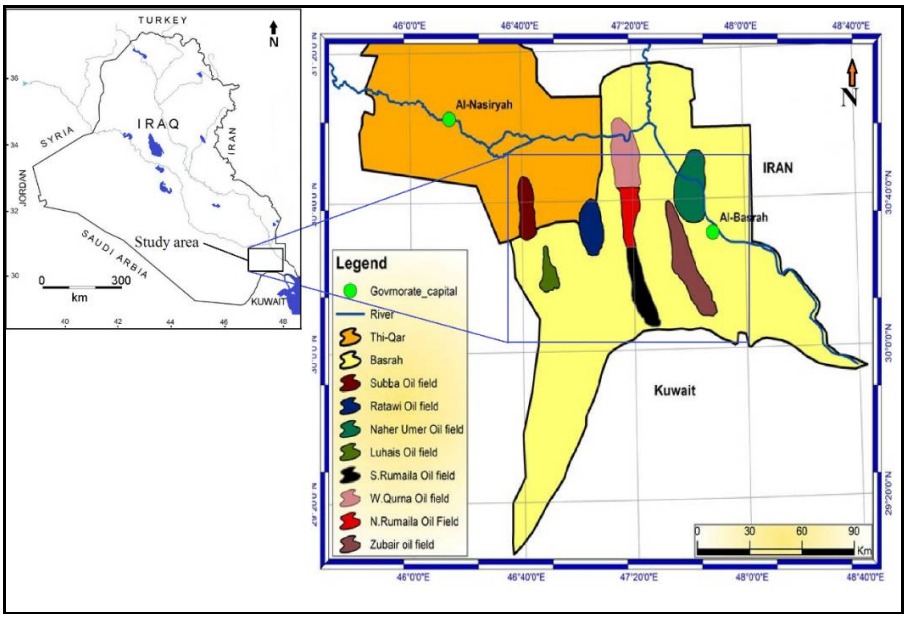

Fig. 1: Oil fields of study area

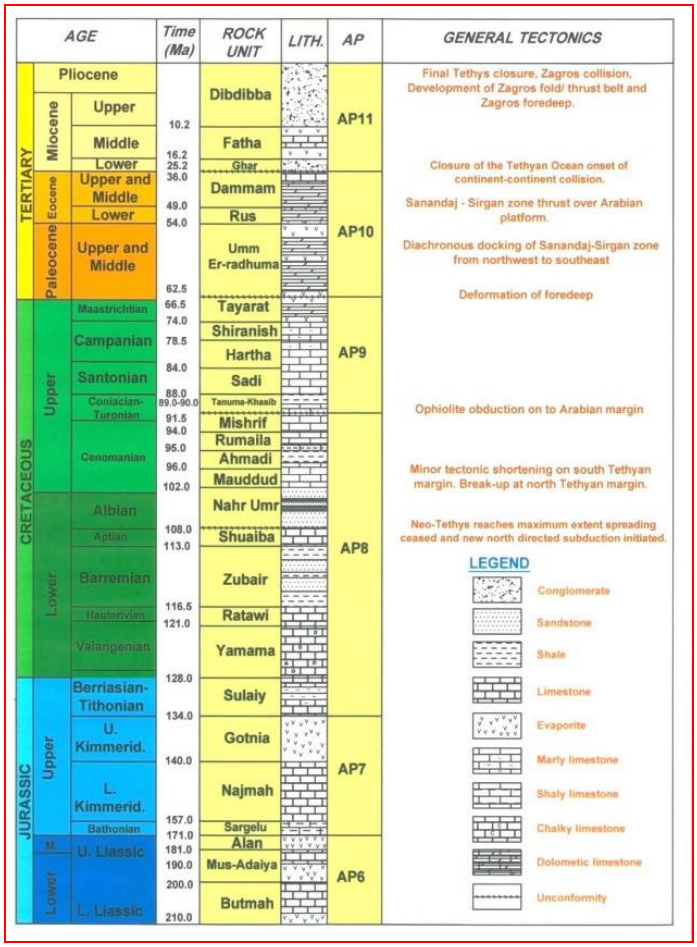

Fig. 2: Stratigraphic section of formation of Zubair oilfield after Jafar, 2010.

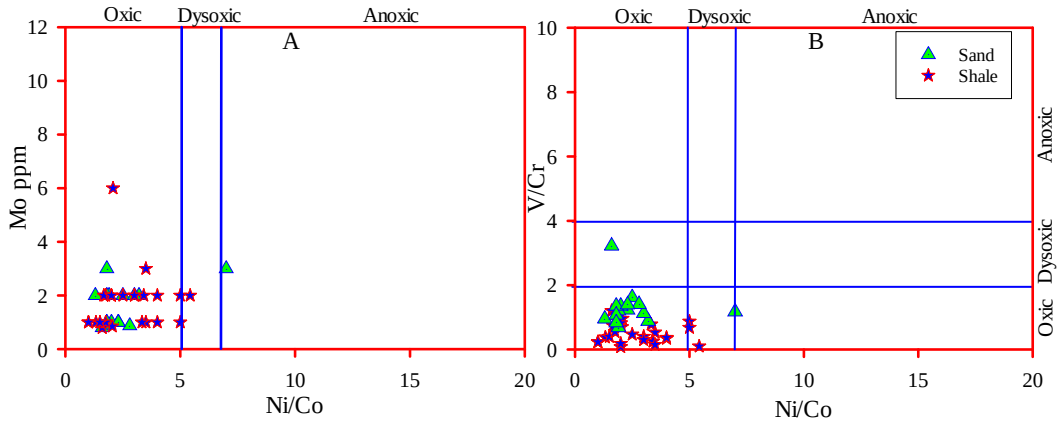

A. B.

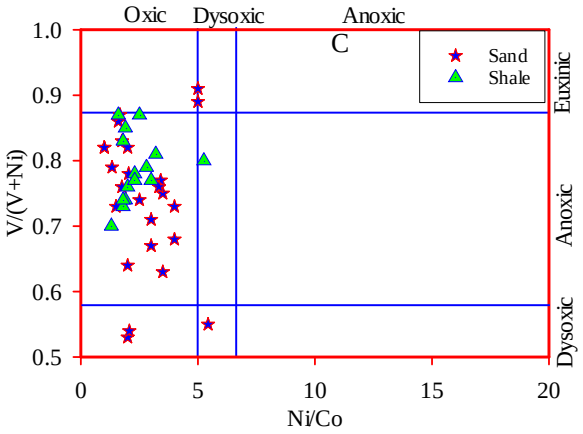

C

Figure 3:. Cross plots of trace element ratios used as palaeoredox proxies: (A) Moversus Ni/Co; (B) V/Cr versus Ni/Co and (C) after V/(V+Ni) versus Ni/Co (Fu et al., 2016)

Table 1: The geochemical analyses of the Zubair Formation samples

	Core Sample	Lito-logy	Co	Cu	Mo	Ni	Cr	Th	U	V
			Trace element (ppm)							
1	S- 1	Sandston member	1	35	0.87	2	10	0.99	0.37	7
2	S- 11		1	19	1	5	60	15.35	4.37	52
3	Rt- 2		2	17	2	4	60	2	0.71	4.5
4	Rt- 7		5	12	0.9	8	40	10.5	2.83	48
5	Rt- 13		3	12	1	4	40	6.17	1.98	15
6	L- 1		2	12	1	7	40	9.38	3.68	21
7	L- 5		1	9	2	3	40	2.43	0.79	10
8	L- 8		3	11	1	10	40	7.45	1.95	31
9	L- 10		2	9	2	6	30	4.48	1.44	12
10	L- 16		2	48	1	2	40	3.6	1.01	9
11	N- 1		2	10	1	8	50	1.81	0.56	17
12	N- 15		4	7	1	7	30	3.9	1.05	33
13	Z- 1		2	10	2	5	30	1.29	0.39	14
14	Z- 6		2	149	1	3	20	2.94	1.09	8
15	Z- 10		1	9	2	4	30	2.59	1.1	11
16	Z- 18		27	25	6	56	70	15.4	3.89	67
17	R- 1		8	13	2	16	90	10.65	2.29	74
18	R- 3		4	15	2	7	40	5.77	1.5	22
19	R- 6		2	13	1	2	40	2.3	1.02	9
20	R- 11		2	12	2	6	50	2.61	1.18	15

21	R- 13		6	9	2	10	90	32.7	10.25	67
22	R- 18		1	8	2	5	60	16	5.88	41
23	Ru- 1		2	7	2	4	40	1.87	0.88	7
24	Ru- 4		2	10	3	7	80	4.88	1.76	12
25	Ru- 11		1	6	2	5	60	0.88	0.3	6
26	S- 7	**Shale member**	12	18	2	23	190	16.65	3.57	130
27	Rt- 6		14	23	1	32	90	22.1	4.66	111
28	L- 3		10	13	2	25	100	19.9	4.15	162
29	N- 9		16	8	0.8	25	50	14.85	1.58	161
30	N- 10		22	16	1	43	100	15.7	2.21	135
31	N- 12		11	12	0.9	21	50	5.38	1.34	60
32	N- 18		17	210	2	30	60	11.7	2.24	81
33	Z- 11		6	48	2	8	20	2.69	1.68	19
34	Z- 23b		3	23	3	21	70	17.6	4.98	82
35	R- 5		5	11	2	16	80	21.1	5.65	70
36	R- 8		10	16	2	30	90	24.1	6.24	101
37	R- 25		15	17	0.87	42	110	19	2.54	154
38	Ru- 6		6	6	3	11	30	5.04	1.67	32
39	Ru- 9		4	6	1	7	40	3.65	1.3	33
40	Ru- 220		20	20	1	46	110	23.2	3.56	153

Table 2: Elemental ratios illustrate paleoredox conditions for Zubair Formation

Elemental ratio	**Paleoredox condition**			**Zubair Formation**		
	Oxic	**Dysoxic**	**Anoxic**	**Sand**	**Shale**	**Condition**
U/Th	< 1.25	1.25- 1.50	> 1.50	0.31	0.21	Oxic
(Cu+Mo)/ Zn	< 2.0	2.0	> 2.0	0.42	0.45	Oxic
V/Cr	< 2.0	2.0- 4.25	> 4.25	0.55	1.30	Oxic
Ni/ Co	< 5.0	5.0- 7.0	> 7.0	2.87	2.47	Oxic
V/ (V+Ni)	< 5.9	5.9- 8.8	> 8.8	0.75	0.80	Oxic
Authigenic U	< 5.0	-	>50	-0.15	-1.79	Oxic